IL
NUOVO CIMENTO
ORGANO DELLA SOCIETÀ ITALIANA DI FISICA
SOTTO GLI AUSPICI DEL CONSIGLIO NAZIONALE DELLE RICERCHE

VOL. XIX, N. 5 *Serie decima* 1° Marzo 1961

Search for a Neutral Meson of Zero I-Spin (*).

N. E. BOOTH, O. CHAMBERLAIN and E. H. ROGERS

Lawrence Radiation Laboratory, Department of Physics
University of California - Berkeley, Cal.

(ricevuto il 10 Ottobre 1960)

Summary. — A search has been made for a neutral meson of zero I-spin by means of the reaction $d+d \to {}^4He+\pi_0^0$. No evidence was found for the existence of the π_0^0 in the mass range zero to 1.8 times the $\pi^\pm$ mass. The upper limit of the cross section was $7 \cdot 10^{-32}$ cm^2 for $\pi_0^0 \simeq \pi^\pm$ mass. The reaction was studied by using 460 MeV deuterons from the Berkeley 184 in. cyclotron and a liquid deuterium target. α-particles produced at 0° in the laboratory system were selected by momentum analysis and by a counter telescope which measured time of flight, dE/dx, and differential range. The experiment may also set a limit on the validity of charge independence.

1. – Introduction.

Several authors [1-8] have postulated the existence of a neutral meson of isotopic spin zero (called the π_0^0 or ρ_0 meson) and suggested means of verifying its existence. Mass estimates vary from a few MeV less than the ordinary π^0

(*) Work done under the auspices of the U. S. Atomic Energy Commission.
(1) H. M. STEINER: private communication to O. CHAMBERLAIN (1955).
(2) A. BALDIN: *Nuovo Cimento*, **8**, 569 (1958).
(3) A. M. BALDIN and P. K. KABIR: *Nuovo Cimento*, **9**, 547 (1958).
(4) B. D'ESPAGNAT, J. PRENTKI and A. SALAM: *Nucl. Phys.*, **3**, 446 (1957).
(5) W. KROLIKOWSKI: *Nucl. Phys.*, **8**, 461 (1958); **10**, 213 (1959).
(6) W. HEISENBERG: in *Proc. of Geneva Conference CERN* (1958).
(7) L. B. OKUN: *Žurn. Éksp. Teor. Fiz.*, **34**, 469 (1958).
(8) IA. B. ZEL'DOVICH: *Žurn. Éksp. Teor. Fiz.*, **34**, 1644 (1958).

mass to about three times the $\pi^{\pm}$ mass (μ). At least one experimental test has been made [9]. The experiment described here is concerned with a search between the mass limits of 0 and 1.8 μ by means of a reaction first suggested to the authors by STEINER [1] and independently by BALDIN [2],

$$(1) \qquad d + d \rightarrow {}^4He + \pi_0^0 .$$

Since the three heavy particles in (1) all have I-spin zero, the ordinary π^0 meson cannot be produced in place of the π_0^0 in this reaction, at least to the extent that isotopic spin is conserved. The upper limit of 1.8 μ was set by the maximum kinetic energy of the deuterons available from the Berkeley 184 inch cyclotron, namely 460 MeV. No evidence was found for the existence of the π_0^0. The upper limit obtained for the cross-section of (1) depended upon the value of the π_0^0 mass assumed; it was $20 \cdot 10^{-32}$ cm^2 for zero mass and $0.2 \cdot 10^{-32}$ cm^2 for 1.8 times the $\pi^{\pm}$ mass (assuming isotropy in the center-of-mass system. See Fig. 3).

2. – Experimental arrangement.

2·1. *General.* – Reaction (1) was studied by searching for α-particles produced at zero degrees when a liquid deuterium target was bombarded with 460 MeV deuterons. The momentum of the α-particles depends of course upon the mass of the π_0^0, and for given mass is double-valued, corresponding to emission at both 0 and 180° in the barycentric system.

TABLE I. – *Spectrometer and counter telescope components indicated in Fig.* 1.

Item	Designation	Description
Magnets	Q_1, Q_2, Q_3	4 in. aperture three-element quadrupole focusing magnets
	M_1	24×36 in. analyzing magnet with 7 in. gap, 46° bend
	M_2	18×36 in. analyzing magnet with 8 in. gap, 51° bend
Counters	S_1	plastic scintillator, 1/16 in., 5 in. diam.
	S_2	plastic scintillator, 1/16 in., 3 in. diam.
	S_3	plastic scintillator, 1/4 in., 4 in. diam.
	S_4	plastic scintillator, 3/8 in., 5 in. diam.
Absorbers	A_1, A_2	variable thickness copper

(9) M. GETTNER, L. HOLLOWAY, D. KRAUS, K. LANDÉ, E. LEBOY, W. SELOVE and R. SIEGEL: *Phys. Rev. Lett.*, **2**, 471 (1959); see also B. PONTECORVO: *Report to* 1959 *International Conference on Physics of High-Energy Particles* (Kiev, July 1959).

The experimental arrangement is shown in Fig. 1 and details are given in Table I. The deuteron beam obtained by regenerative extraction from the 184 in. cyclotron was focused on the liquid D_2 target. The system of bending and focusing magnets selected particles of a certain effective momentum p/Z,

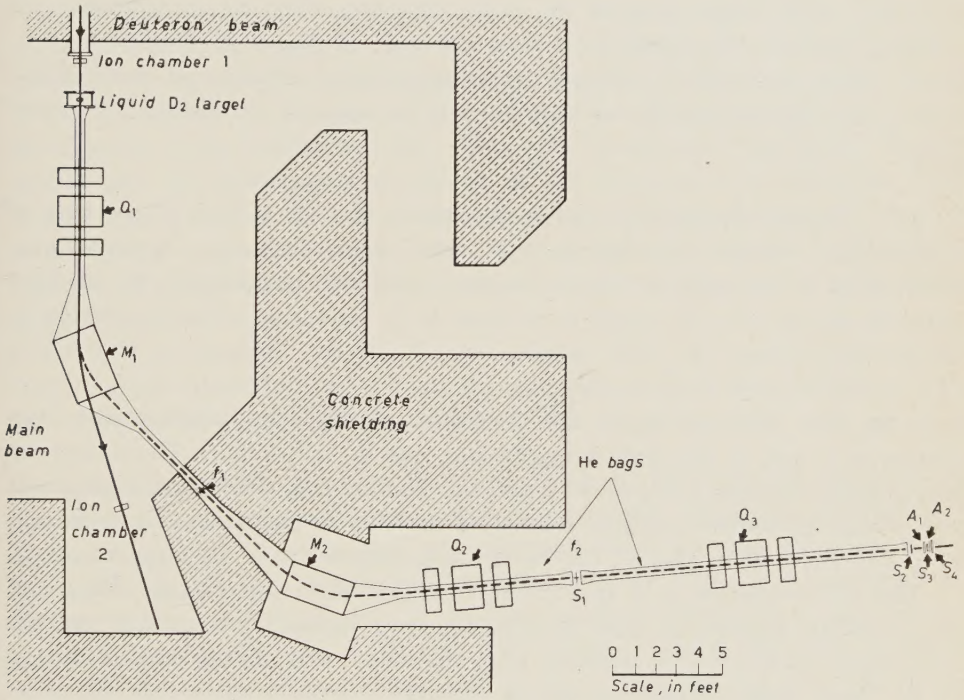

Fig. 1. – Experimental arrangement.

which came off at 0°, and delivered them outside the shielding into an area of relatively low background. A system of counters separated ^{4}He nuclei from the other components of this mono-momentum secondary beam. The momentum of the secondary beam was varied to cover the range of ^{4}He momentum from reaction (1) for any mass of π_0^0 between 0 and 1.8 μ.

2·2. *Deuteron beam and target.* – The external 460 MeV deuteron beam was collimated and focused to give a spot $1 \times 1\frac{1}{2}$ in. at the D_2 target. The beam position was checked periodically by exposing an X-ray film immediately behind the target. This ensured that the beam always passed cleanly through the target cylinder.

Two ion chambers were used to monitor the beam, one in front of the D_2 target and another after M_1. For some of the runs, after intercalibration, the first ion chamber was removed. The ion-chamber multiplication factor

was calculated from the calibration performed by CHAMBERLAIN, SEGRÈ, and WIEGAND [10] and the values of dE/dx for 345 MeV protons and 460 MeV deuterons. For most of the measurements the beam intensity was $1.5 \cdot 10^8$ to $5 \cdot 10^8$ deuterons per second.

The deuterium container was a cylinder 3 in. in diameter with a length of (0.94 ± 0.05) g cm^2 of D_2 in the beam direction. The target windows and vacuum chamber windows were each 0.010 in. Mylar. An aluminum heat shield 0.0015 in. thick surrounded the target cylinder. The target was equiped with a reservoir and heater so that it could be emptied or filled in a few minutes.

2·3. *Magnetic analysis.* – The spectrometer was set to accept particles of a particular effective momentum p/Z. The required magnet currents were determined beforehand by the wire-orbit method. Quadrupole Q_1 brought particles leaving the D_2 target to a focus at f_1. Because of the dispersion in the bending magnet M_1, only particles whose effective momentum was within $2\frac{1}{2}\%$ of the central value passed through the 4×4 in. collimator at f_1. These particles were deflected again and focused at f_2, and refocused at S_3. The images at f_2 and S_3 had unit magnification and no dispersion. The beam size was therefore approx $1 \times 1\frac{1}{2}$ in. at f_2 and S_3. Helium bags were used throughout the system to reduce multiple scattering in order to maintain sharp images at f_2 and S_3, and to reduce the energy loss between the D_2 target and S_3.

Two characteristics of a spectrometer are of prime importance. These are the fractional momentum bite $\Delta p/p$ transmitted through the system, and the solid angle $\Delta\Omega$ into which particles from the target must fall in order to arrive at S_3. Both these quantities can be calculated crudely from the geometry. In a production experiment such as we performed the product $(\Delta\Omega)(\Delta p/p)$ enters the analysis. This quantity was measured directly and found to be $1.16 \cdot 10^{-5}$. (See Appendix I.)

2·4. *Counters and electronics.* – The counter telescope was required to pick out ^{4}He nuclei from other particles with the same p/Z determined by the magnet settings. Time of flight between S_1 and S_2 fixed the velocity and therefore M/Z. Deuterons were then the only contamination. The differences in range and dE/dx for deuterons and α-particles were used to reject deuterons. The Cu absorbers A_1 and A_2 were chosen so that α-particles were counted in S_3 but not in S_4, while deuterons of this momentum had sufficient range to be counted in S_4. Alpha particles were selected by the coincidence $S_1S_2S_3\bar{S}_4$ [11].

---

[10] O. CHAMBERLAIN, E. SEGRÈ and C. WIEGAND: *Phys. Rev.*, **83**, 923 (1951).

[11] W. A. WENZEL: *Millimicrosecond coincidence circuit for high speed counting*, University of California Radiation Laboratory Report UCRL-8000 (Oct. 1957).

However, this system also counted a small fraction of the vast number of deuterons passing through the telescope, presumably those that underwent stripping or other nuclear reactions in S_3 or A_2 and did not give a pulse in S_4. These were eliminated by a second coincidence which required, in addition to the fast coincidence $S_1S_2S_3\bar{S}_4$, that the pulses in S_1, S_2, and S_3 be above a given height. This was accomplished by feeding pulses from the three counters into pulse-height discriminators ([12]) and placing the outputs in a slow coincidence ([13]) with the fast coincidence $S_1S_2S_3\bar{S}_4$. Differential range curves taken by varying the absorber A_1 showed that this system counted only α-particles at the beam intensities used. The entire system was thoroughly checked periodically by accelerating α-particles in the cyclotron and degrading them before the D_2 target. This procedure also measured the efficiency of the telescope at each momentum used. As a check on the electronics the pulses from the individual counters were photographed on moving film during part of the run.

3. – Production of α-particles in complex nuclei.

Although considerable care had been taken to minimize the thickness of the materials (other than liquid deuterium) in the beam, an unexpectedly large background of α-particles was observed from the ion chamber, target windows, etc., in the vicinity of the target. Their origin was confirmed by placing additional foils of various elements in the deuteron beam and measuring their production of α-particles. The results showed that the materials normally in the beam accounted (within the errors) for the observed yields of α-particles.

In order to calculate production cross-section it is useful to consider particle momentum as a function of range X, in g/cm^2 of Cu equivalent, particularly because the momenta of the α-particles change drastically from the point where they are produced to where they are detected. If we let $R(MT, p_s)$ be the observed rate for the D_2 target empty and the magnets set for momentum p_s at M_1, and let $R(MT+x, p_s)$ be the rate with an additional foil of thickness x, then we can write

$$(2) \qquad R(MT+x, p_s) - R(MT, p_s) = N_0\left(\frac{Nx}{A}\right)\left(\frac{\Delta p\,\Delta\Omega}{p}\right)_s p_s\left(\frac{\mathrm{d}^2\sigma}{\mathrm{d}p\,\mathrm{d}\Omega}\right)_p \frac{(\mathrm{d}p/\mathrm{d}X)_p}{(\mathrm{d}p/\mathrm{d}X)_s},$$

where N_0 is the number of incident deuterons, N is Avogadro's number, A is the atomic weight of the additional foil, and $(\mathrm{d}^2p/\mathrm{d}p\,\mathrm{d}\Omega)_p$ is the production

([12]) J. Mey: *Rev. Sci. Instr.*, **30**, 282 (1959).
([13]) R. L. Garwin: *Rev. Sci. Instr.*, **24**, 618 (1953).

cross-section at the momentum p. Fig. 2 shows the cross-section data for Cu. The yields per g/cm² from lighter elements (C and Al) were greater by a factor of about two.

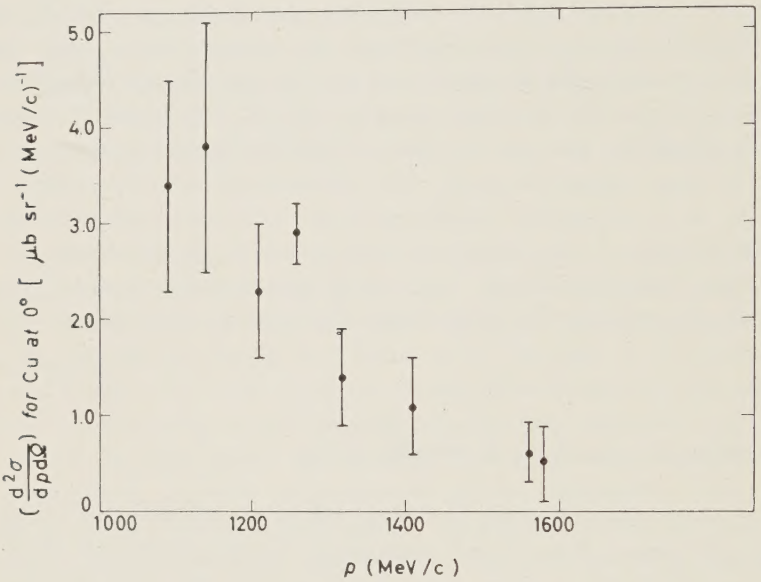

Fig. 2. – Production of α-particles from copper by 460 MeV deuterons.

4. – α-particles from deuterium.

The observed counting rates at various momenta are given in Table II. The observation of more α-particles with the target empty than with the target full is to be expected, if no α-particles are produced in the D_2, because of the

TABLE II. – *Observed counting rates* (*counts per* $1.15 \cdot 10^{11}$ *deuterons*).

Momentum at M_2 (MeV/c)	Target full	Target empty	$R(D_2, p_s)$ full-empty (corrected)
980	9.11 ± 0.78	17.00 ± 1.17	− 1.6 ± 1.5
1104	10.67 ± 0.55	17.90 ± 0.88	− 1.5 ± 1.5
1214	9.94 ± 0.58	15.29 ± 1.01	− 0.8 ± 1.4
1298	9.69 ± 0.69	13.70 ± 1.18	− 0.5 ± 1.4
1390	12.61 ± 0.72	17.43 ± 0.80	+ 0.2 ± 1.5
1440	11.00 ± 0.95	14.90 ± 1.20	+ 0.2 ± 1.7
1494	15.11 ± 0.70	19.70 ± 0.86	− 0.04 ± 1.9

α-particles produced in the foils ahead of the target. The following factors contribute:

a) Production of α-particles in complex nuclei is a sensitive function of the momentum of the produced α-particles, production being greater for lower momentum. The extra stopping power in the system when the target is full causes a significant increase in the momentum and decrease in the momentum spread with which α-particles must be produced if they are to enter the magnet system and be counted. In more quantitative terms we say the counting rate is reduced when the target is full because the quantity $(\mathrm{d}^2\sigma/\mathrm{d}p\,\mathrm{d}\Omega)\times(\mathrm{d}p/\mathrm{d}X)$ is a decreasing function of the momentum p of the produced α-particle.

b) Nuclear interactions in the deuterium also remove α-particles formed in the foils ahead of the target.

With these considerations, and a knowledge of the materials in the beam and their α-particle production cross-sections, we can correct the target full data to find the yield of α-particles from the deuterium, $R(D_2, p_s)$ given in the last column of Table II. Details of the calculation are given in Appendix II.

5. – Cross-section limits.

The laboratory-system differential cross-section for the production of α-particles at 0° is given by

$$R(D_2, p_s) = N_0 \left(\frac{\mathrm{d}\sigma}{\mathrm{d}\Omega}\right)_L \left(\frac{\Delta p\,\Delta\Omega}{p}\right)_s \frac{p_s}{(\mathrm{d}p/\mathrm{d}X)_s} \frac{N}{A} \frac{(\mathrm{d}E/\mathrm{d}x)_{\mathrm{Cu}}}{(\mathrm{d}E/\mathrm{d}x)_{\mathrm{D}_2}}. \tag{3}$$

The last factor corrects for the fact that we measure range in g/cm² Cu equivalent. A is the atomic weight of deuterium. The effective thickness of the D_2 target is determined by the momentum bite of the magnet system provided we have

$$\left(\frac{\Delta p}{p}\right)_s \frac{p_s}{(\mathrm{d}p/\mathrm{d}X)_s} \frac{(\mathrm{d}E/\mathrm{d}x)_{\mathrm{Cu}}}{(\mathrm{d}E/\mathrm{d}x)_{\mathrm{D}_2}} \leqslant 0.94 \text{ g/cm}^2 \text{ of } \mathrm{D}_2 .$$

This was true in all cases except at the highest momentum. The differential cross-section in the c.m. system is given by $(p^*/p)^2(\mathrm{d}\sigma/\mathrm{d}\Omega)_L$, where p^* is the momentum in the c.m. system. From the data of Table II we can calculate an upper limit for the differential cross-section of (1) as a function of the mass of the π_0^0. (In this calculation the upper limit on the observed rate,

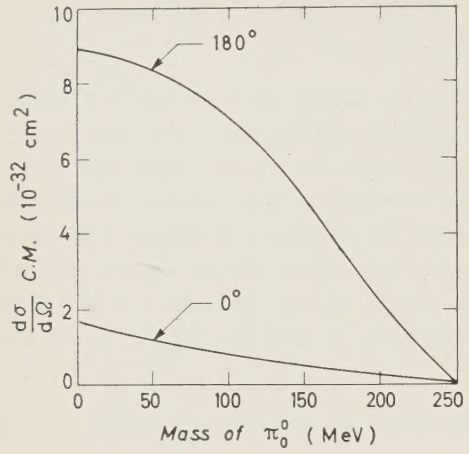

R is taken to be $R+1.7\Delta R$ when R is positive and $1.7\Delta R$ when R is negative.) Fig. 3 shows the way in which the upper limit depends upon the assumed mass. The cross-section limit is best near 1.8 $\pi^{\pm}$ masses, but is not to be taken seriously because here we are near threshold.

Fig. 3. – Upper limit on the differential cross-section of $d+d \to {}^4He+\pi_0^0$. The two curves are for production angles of the ^{4}He of 0° and 180° in the c.m. system.

6. – Charge independence.

The principle of I-spin conservation or charge independence forbids the reaction

$$d + d \to {}^4He + \pi^0 .$$

Our measurements set an upper limit on the cross-section for this reaction, assuming isotropy, of about $7 \cdot 10^{-32}$ cm^2. This result is a test of charge independence provided we can estimate what the cross-section should be if I-spin were not conserved.

Unfortunately it is not easy to make this estimate. However, we can compare our upper limit with the cross-section for the reaction

$$d + d \to {}^4He + \gamma .$$

Our data give an upper limit on the latter of about 10^{-31} cm^2. Measurements on the inverse ([14,15]) give, by detailed balacing, about 10^{-32} cm^2. Thus the π^0 production cross-section is at most only a few times the radiative capture at an energy well above the threshold for π^0 production.

([14]) E. R. GAERTTNER and M. L. YEATER: *Phys. Rev.*, **83**, 146 (1951).

([15]) A. GORBUNOV and V. SPIRIDONOV: *Žurn. Èksp. Teor. Fiz.*, **33**, 21 (1957); translation *Sov. Phys. JETP*, **6**, 16 (1958).

* * *

We wish to thank Mr. ROBERT B. BACASTOW for assistance throughout the course of the experiment, and Dr. JANICE BUTTON for help during the planning stage. We are also grateful to Mr. JAMES VALE and the cyclotron operating crew.

APPENDIX I

Acceptance of the magnet system.

The acceptance of a spectrometer such as the one used in this experiment is defined as the product of the solid angle and the fractional momentum bite. The acceptance of this magnet system was measured as follows.

The α beam from the cyclotron was degraded with copper, part of which was in the form of 45° wedges, at the position of the D_2 target. The momentum distribution of this degraded beam was flat over a region large compared with the momentum bite of the magnet system. The aperture of Q_1 was uniformly illuminated. A scintillation counter 6 in. wide was placed at f_1. This geometry defined a fractional momentum bite $(\Delta p/p)' = 0.0963$. The rate R_1' in this counter was measured as a function of the aperture of a collimator placed at the entrance of Q_1. From this measurement, the effective aperture of Q_1 without collimation was found to be $\Delta\Omega' = 4.36 \cdot 10^{-3}$ sr for this case. With the counter at f_1 removed, the rate R in the α-particle telescope was measured. Since

$$\frac{R'}{\Delta\Omega'}\left(\frac{p}{\Delta p}\right)' = \frac{R}{\Delta\Omega}\left(\frac{p}{\Delta p}\right),$$

we obtain $\Delta\Omega\,\Delta p/p = 1.16 \cdot 10^{-5}$, where p is defined at M_1.

APPENDIX II

Corrections.

To be more explicit, we write

$$R(MT, p_s) = N_0\left(\frac{\Delta p\,\Delta\Omega}{p}\right)_s p_s \left\{\left[\left(\frac{Nx}{A}\right)\left(\frac{\mathrm{d}^2\sigma}{\mathrm{d}p\,\mathrm{d}\Omega}\right)\left(\frac{\mathrm{d}p}{\mathrm{d}X}\right)\right]_f + \right.$$
$$\left. + \left[\left(\frac{Nx}{A}\right)\left(\frac{\mathrm{d}^2\sigma}{\mathrm{d}p\,\mathrm{d}\Omega}\right)\left(\frac{\mathrm{d}p}{\mathrm{d}X}\right)\right]_i\right\} \Big/ \left(\frac{\mathrm{d}p}{\mathrm{d}X}\right)_s,$$

where the subscript f refers to the foils behind the target and i to the foils in front of the target. With the target full we have

$$R(\text{full}, p_s) = R(D_2, p_s) + N_0 \left(\frac{\Delta p\, \Delta\Omega}{p}\right)_s p_s \left\{\left[(1 - A_{dd})\left(\frac{Nx}{A}\right)\left(\frac{d^2\sigma}{dp\, d\Omega}\right)\left(\frac{dp}{dX}\right)\right]_f + \right.$$
$$\left. + \left[(1 - A_{\alpha d})\left(\frac{Nx}{A}\right)\left(\frac{d^2\sigma}{dp\, d\Omega}\right)'\left(\frac{dp}{dX}\right)'\right]_i\right\} \Big/ \left(\frac{dp}{dX}\right)_s,$$

where $R(D_2, p_s)$ is the rate from the D_2, A_{dd} is the attenuation of the deuteron beam in the D_2, $A_{\alpha d}$ that of the α-particles in the D_2, and p' the momentum at which α-particles must be produced in front of the target such that they come down the magnet system. We can get a measure of $(d^2\sigma/dp\, d\Omega)'_i$ by setting the magnet system for a momentum p'_s such that we have

$$R\,(MT, p'_s) = N_0 \left(\frac{\Delta p\, \Delta\Omega}{p}\right)_s p'_s \left\{\left[\left(\frac{Nx}{A}\right)\left(\frac{d^2\sigma}{dp\, d\Omega}\right)'\left(\frac{dp}{dX}\right)'\right]_f + \right.$$
$$\left. + \left[\left(\frac{Nx}{A}\right)\left(\frac{d^2\sigma}{dp\, d\Omega}\right)'\left(\frac{dp}{dX}\right)'\right]_i\right\} \Big/ \left(\frac{dp}{dX}\right)'_s.$$

If we substitute

$$\varepsilon R(MT, p_s) = N_0 \left(\frac{\Delta p\, \Delta\Omega}{p}\right)_s p_s \left[\left(\frac{Nx}{A}\right)\left(\frac{d^2\sigma}{dp\, d\Omega}\right)\left(\frac{dp}{dX}\right)\right]_f \Big/ \left(\frac{dp}{dX}\right)_s,$$

where ε is the ratio of the detected α-particles that where produced behind the target to the total produced, behind and in front of the target, we have

$$R(D_2, p_s) = R(\text{full}, p_s) - R(MT, p_s) \cdot$$
$$\cdot \left\{\varepsilon(1 - A_{dd}) + (1 - \varepsilon')(1 - A_{\alpha d}) \frac{p_s}{p'_s} \frac{(dp/dX)'_i}{(dp/dX)_i} \frac{R(MT, p'_s)}{R(MT, p_s)}\right\}.$$

A_{dd} and $A_{\alpha d}$ were obtained by extrapolation of the results of MILLBURN *et al.* [16] on the inelastic cross sections of complex nuclei for high-energy deuterons and α-particles. The total cross sections in D_2 assumed were (200 ± 100) mb for deuterons and (400 ± 100) mb for α-particles. ε was determined from the production data. The quantity $R(MT, p'_s)/R(MT, p_s)$ was determined from straight lines through the raw data obtained with target empty. Values of $R(D_2, p_s)$ are given in the last column of Table II.

---

[16] G. P. MILLBURN, W. BIRNBAUM, W. E. CRANDALL and L. SCHECTER: *Phys. Rev.*, **95**, 1268 (1954).

RIASSUNTO (*)

Si è ricercato il mesone di spin isotopico zero per mezzo della reazione $d+d \to {}^4He+\pi_0^0$. Non si è trovata alcuna prova dell'esistenza del π_0^0 per una massa compresa nell'intervallo fra zero ed 1.8 volte la massa del $\pi^{\pm}$. Il limite superiore della sezione d'urto era $7 \cdot 10^{-32}$ cm^2 per la massa del $\pi_0^0 \ll \pi^{\pm}$. La reazione fu studiata servendosi di deutoni di 460 MeV del ciclotrone da 184 in. di Berkeley e di una targhetta di deuterio liquido. Le particelle α emesse a 0° nel sistema del laboratorio furono selezionate con l'analisi degli impulsi e con un contatore telescopico che misurava la durata di volo, dE/dx ed il range differenziale. L'esperimento può anche stabilire un limite alla validità della indipendenza della carica.

(*) *Traduzione a cura della Redazione.*

Fast Photo-Neutrons from Bismuth.

A. Wataghin, R. B. Costa and A. M. Freire

Centro Brasileiro de Pesquisas Físicas - Rio de Janeiro

J. Goldenberg

Dep. Física da Faculdade de Filosofia, Ciencias e Letras da Universidade - São Paulo

(ricevuto il 10 Ottobre 1960)

Summary. — The energy spectrum of the photo-neutrons emitted from a bismuth target irradiated with 22 MeV bremsstrahlung is studied at angles of 30°, 90° and 150° to the γ-beam, using nuclear emulsions. An excess of high energy neutrons over the evaporation spectrum exists at all angles measured. The angular distributions can be described by the formula $A+B\sin^2\theta+C\cos\theta$. The average value of the ratio B/A is 0.68–0.15 and the average value of $C/A=0.155\pm0.056$. The variation of B/A with energy was studied. Our data indicate a maximum value of the ratio B/A around 5.5 MeV.

1. – Introduction.

It has been known for some time ([1-4,8,9]), that some elements such as Bi, Cr, Ta, at betatron energies show an excess of high energy photo-neutrons over the numbers expected from evaporation theory ([5]). Angular distributions

([1]) H. L. Poss: *Phys. Rev.*, **79**, 539 (1950).

([2]) F. Ferrero, A. O. Hanson, R. Malvano and C. Tribuno: *Nuovo Cimento*, **4**, 418 (1956).

([3]) G. N. Zatsepina, L. E. Lazareva and A. N. Pospelov: *Soviet. Phys. J.E.T.P.* **5**, 21 (1957).

([4]) V. Emma, C. Milone and R. Rinzivillo: *Nuovo Cimento*, **14**, 1149 (1959).

([5]) V. F. Weisskopf and D. H. Ewing: *Phys. Rev.*, **57**, 472 (1940).

([6]) R. S. White: Section **2-D**, in *Fast Neutron Physics*, J. B. Marion and J. L. Fowler ed. (New York, 1960).

([7]) F. Tagliabue and J. Goldenberg: private communication.

([8]) G. A. Price: *Phys. Rev.*, **93**, 1279 (1954).

([9]) G. Cortini, C. Milone, A. Rubbino and F. Ferrero: *Nuovo Cimento*. **9**, 85 (1958).

for these high energy photo-neutrons show an asymmetry instead of the isotropy predicted by the evaporation theory.

The present work contributes to this problem for the case of ^{209}Bi. Energy spectra of the photo-neutrons emitted from the Bi target at angles of 30°, 90° and 150° to the γ beam were obtained by means of proton recoils in nuclear emulsions.

2. – Experimental procedure.

A cylindrical target of Bi (1.5 cm thickness, 1 cm diameter) was irradiated by a collimated γ-ray beam, from the betatron of the University of S. Paulo, running at (22.0 ± 0.1) MeV.

The total γ-ray dose at the Bi sample was 990 r, as measured by a victoreen thimble inside an 8 cm lucite cube.

The photo-neutrons emitted at angles of 30°, 90° and 150° to the photon beam were recorded by means of proton recoil tracks ([6]) in Ilford C_2 emulsions 400 μm thick. Fig. 1 shows the experimental arrangement. The scanned volumes at 30°, 90° and 150° were respectively 730, 988 and 774 mm^3.

The results of the scanning are summarized in Table I.

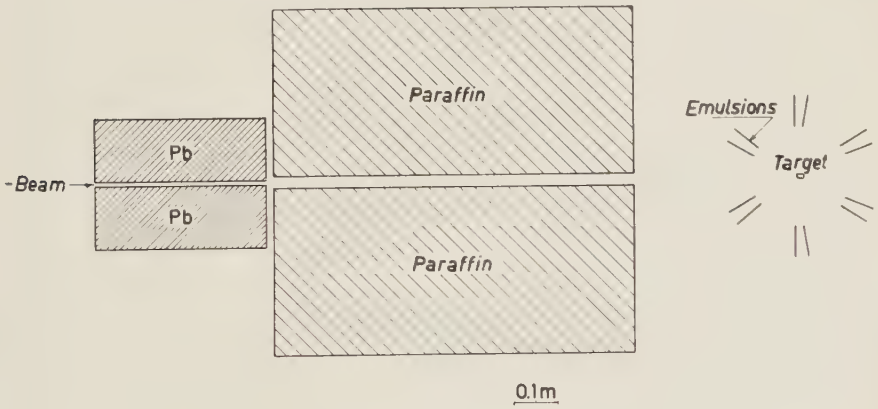

Fig. 1. – Experimental arrangement.

TABLE I. – *Number of events corrected and normalized.*

Energy interval (MeV)	B/A	C/A
3 ÷ 4	0.37 ± 0.13	0.14 ± 0.07
4 ÷ 5	0.99 ± 0.29	0.15 ± 0.11
5 ÷ 6	2.43 ± 0.86	-0.03 ± 0.20
6 ÷ 7	0.94 ± 0.55	0.37 ± 0.24
7 ÷ 8	1.62 ± 1.01	0.16 ± 0.30
8 ÷ 10	-0.17 ± 0.59	0.40 ± 0.40

These data must be normalized for equal scanned volumes and must be corrected (9) for *a*) efficiency of the scanners, *b*) back-ground, *c*) geometrical losses, *d*) variation of (n, p) cross-sections with energy.

In Table II a summary of the corrected data is presented.

The back-ground was measured with a carbon target of 1.9 cm thickness and 1 cm diameter in the place of the Bi target (3), since the same number

TABLE II. – *Measurements of B/A.*

E_{max}	Neutron energy interval (MeV)	B/A	Detector	Reference
22.0	> 3	0.86 ± 0.15	emuls.	This work
22.0	> 6	0.92 ± 0.41	emuls.	This work
18.9	> 4	2.0	emuls.	(3)
18.9	> 1.5	0.47	emuls.	(3)
20.0	> 6	0.9 ± 0.1	^{28}Si(n, p)^{28}Al	(2)
22	> 6	5.6	^{28}Si(n, p)^{28}Al	(8)
22	> 6	1.1 ± 0.15	^{28}Si(n, p)^{28}Al	(7)
30	> 6	1.0 ± 0.1	^{28}Si(n, p)^{28}Al	(2)
20	> 4	1.0 ± 0.5	^{27}Al(n, p)^{27}Mg	(1)
22	> 4	0.99 ± 0.10	^{27}Al(n, p)^{27}Mg	(8)
30	> 4	0.67 ± 0.1	^{27}Al(n, p)^{27}Mg	(2)
30	$4 \div 5$	~ 0.7	emuls.	(11)

of back-ground neutrons coming through the collimator is scattered by the 1.9 cm carbon target and by the 1.5 cm bismuth target.

The scanned volume was in this case 1117 mm^3.

The value of the back-ground varied from 20% to 10% of the total number of neutrons depending on the angle.

The efficiency of each scanner was measured by having a sample area scanned independently by a second scanner and by comparing the number of events found. Let us call N_1 and N_2 the total number of events found (for given energy interval) by scanners 1 and 2 respectively in the same sample area, and N_{12} the number of events which were found by both scanners. The efficiency α_1 of the first scanner will be N_{12}/N_2 and we have taken the possible statistical fluctuation in α_1 to be measured by a standard deviation $E(\alpha_1) = \alpha_1 \cdot \sqrt{1/N_{12} - 1/N_2}$, since the quantity N_{12}/N_2 is expected to follow a binomial distribution.

The efficiences of our scanners were of the order of 70%. In a few cases the efficiency was as low as 55%, but in each case the possible fluctuation was computed as shown above. The errors given in Table I are standard deviations which include the possible fluctuations in the factors α (we have used the law of propagation of errors).

In addition the procedure for measuring the efficiency was repeated for a given scanner after a given interval of time in order to check the constancy in time.

The proton recoils were accepted only inside given limits of angle with respect to the incident neutrons. The acceptance pyramid of the proton recoils was defined by $0 \leqslant |\varphi| \leqslant 30°$ and $0 \leqslant |\lambda| \leqslant 17°17'$, where φ is the projected angles of the proton on the emulsion surface and λ is the angle of dip *i.e.* the angle between the proton track and the emulsion surface.

3. – Results and discussion.

3·1. *Energy spectra.* – Fig. 2*a*, 2*b*, and 2*c* show the corrected spectrum obtained at 30°, 90° and 150°.

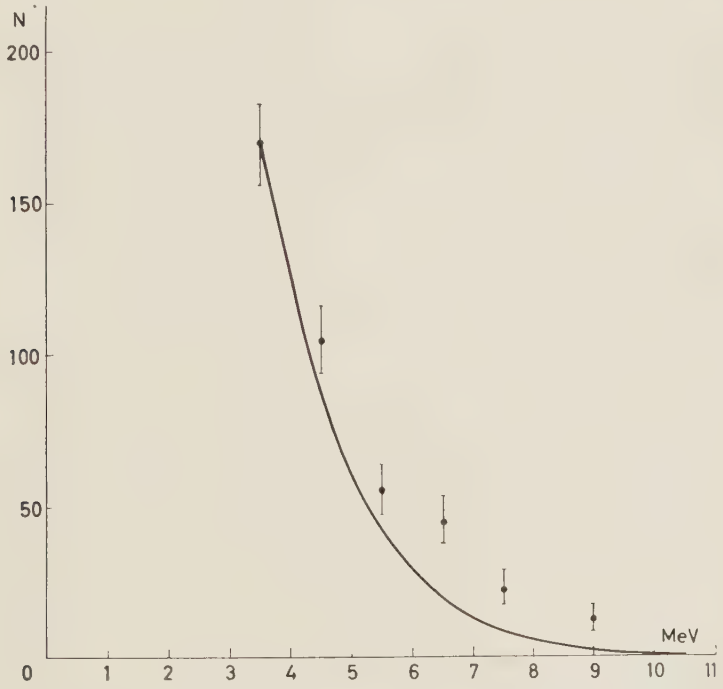

Fig. 2*a*. – Neutron energy spectrum for $\theta = 30°$. Full line is evaporation spectrum.

The solid curves are theoretical ([5]) for evaporation neutrons,

$$I(E_n) = C \cdot E_n \exp\left[2\sqrt{a(E_{max} - E_b - E_n)}\right],$$

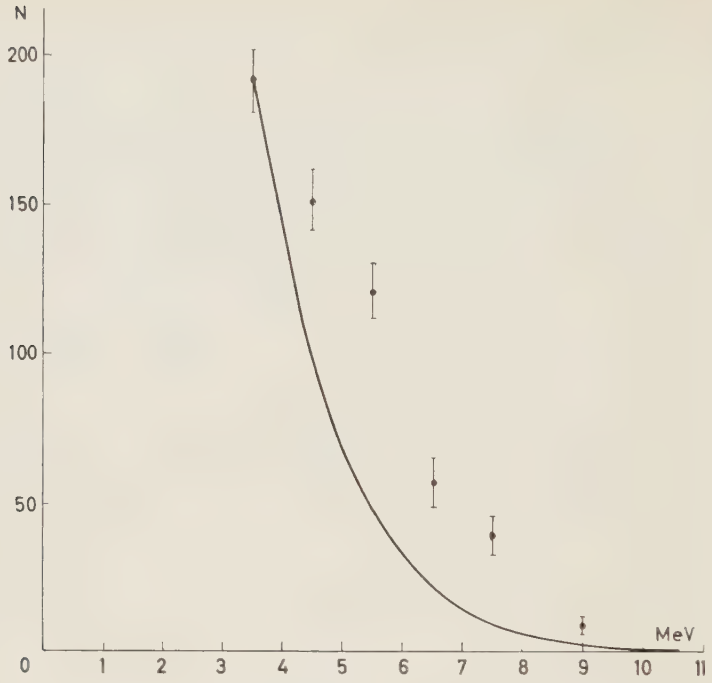

Fig. 2*b*. – Neutron energy spectrum for $\theta=90°$. Full line is evaporation spectrum.

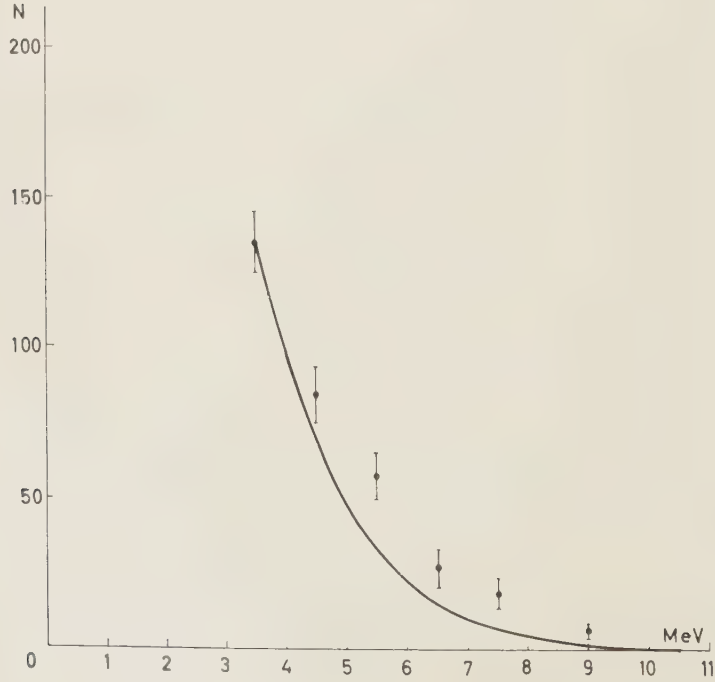

Fig. 2*c*. – Neutron energy spectrum for $\theta=150°$. Full line is evaporation spectrum.

where: $E_b = 7.44$ MeV $= \gamma - n$ threshold in Bi.

$a = 5$ (see text);

$E_{max} = 22$ MeV = maximum γ-ray energy;

E_n = neutron energy.

The theoretical curves were normalized at 3.5 MeV, to the experimental value.

One sees from Fig. 2 that there are more high energy neutrons than expected by the evaporation theory.

The parameter a depends on the level density of the residual nucleus.

The value of a given by other authors ([3,5,9-14]) for Bi are in the range from 5 to 25. Fig. 2 shows that even if we choose the lowest value ($a = 5$) the evidence for the excess neutrons is still clear.

3·2. *Angular distribution.* – If we fit our angular distribution (for all energies) with a formula (2) of the type $A + B \sin^2\theta + C \cos\theta$ we obtain $B/A = 0.86 \pm 0.15$ and $C/A = 0.155 \pm 0.056$.

Table II compares the B/A we obtain collecting our data in wider energy intervals with the results of other authors.

The average value calculated by FERRERO *et al.* ([2]) using a Wilkinson type model ([15]) is 0.90, also in very good agreement with our data.

The probability that the value of C is zero in view of our measurement is only 0.3%. We would like to point out that FERRERO *et al.* ([2]) and EMMA *et al.* ([11]), found some indication of a C term. FERRERO *et al.* give the value of 0.05 and 0.12 for the C term, with the Al(n, p) and Si(n, p) detectors respectively.

Fig. 3 gives B/A as a function of energy from our measurements. Our data indicate a maximum asymmetry for 5.5 MeV.

The drop in the value of B/A for lower energy can be understood because evaporation neutrons contribute appreciably in that region.

([10]) B. B. KINSEY: of *Encyclopedia of Physics*, ed. by S. FLÜGGE (Berlin, 1957), vol. **11** p. 296.

([11]) V. EMMA, C. MILONE, A. RUBBINO and R. MALVANO: private communication,

([12]) P. R. BYERLY jr. and W. E. STEPHENS: *Phys. Rev.*, **83**, 54 (1951).

([13]) S. A. MOSZKOWSKI: *Encyclopedia of Physics*, ed. by S. FLÜGGE (Berlin, 1957), vol. **39** p. 437.

([14]) J. HEIDMANN and H. A. BETHE: *Phys. Rev.*, **84**, 274 (1951).

([15]) P. H. WILKINSON: *Proc. of the Glasgow Conf. of Nuclear and Meson Physics*, (London, 1954).

It should be noticed the flux of photo-neutrons above 10 MeV is very small (of the order of the back-ground).

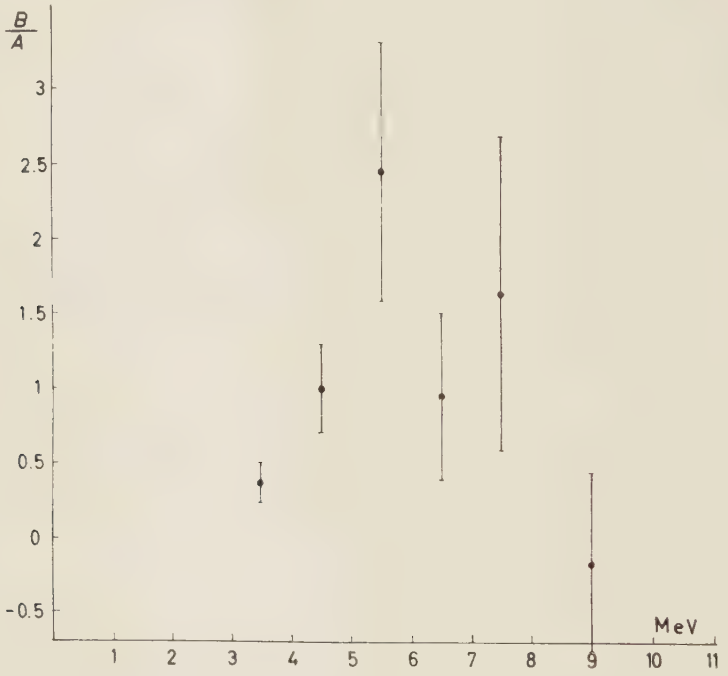

Fig. 3. – B/A as a function of the neutron energy on the assumption that the angular distribution $f(\theta)$ is described by the formula $f(\theta)=A+B\sin^2\theta+C\cos\theta$.

This raises the problem of consistency with the results expected from a direct photo-electric effect.

* * *

We thank Prof. C. G. M. Lattes and Prof. A. O. Hanson for useful discussions.

We thank the Conselho Nacional de Pesquisas of Brasil, and the Commissao Nacional de Energia Nuclear of Brazil for financial support, which made possible the realization of this work.

RIASSUNTO

Si studia in questo lavoro lo spettro di energia dei foto-neutroni emessi da un bersaglio di bismuto bombardato da radiazione di bremsstrahlung di energia massima di 22 MeV. Si usano come detettori dei neutroni 3 gruppi di emulsioni nucleari, collocati in modo tale che i neutroni provenienti dal bersaglio formino col fascio di raggi γ incidente angoli di 30°, 90° e 150° rispettivamente. In tutti e tre gli angoli sopraddetti si trovano più neutroni di alta energia di quanti siano previsti da uno spettro di evaporazione. Le distribuzioni angolari trovate sono in buon accordo colla formula $A+B\sin^2\theta+C\cos\theta$, con convenienti valori dei parametri. È stata studiata la variazione di questi parametri coll'energia dei neutroni emessi. Si trova un massimo del rapporto B/A a circa 5.5 MeV. I valori medi di B/A e di C/A sono rispettivamente 0.68 ± 0.15 e 0.155 ± 0.056.

IL NUOVO CIMENTO Vol. XIX, N. 5 1° Marzo 1961

On the Theory of Primary Specific Ionization in Helium.

R. T. Van de Walle (*) and C. C. Grosjean (**)

Interuniversitair Instituut voor Kernwetenschappen
Centrum van de Rijksuniversiteit te Gent - Gent

(ricevuto l'11 Ottobre 1960)

Summary. — It is the aim of the present paper to establish an improved formula for the non-relativistic primary specific ionization of electrons in helium, as a result of a carefully developed theory in which numerically computed helium wave functions are introduced instead of less accurate hydrogenic wave functions. Sect. **1** presents the calculation of the differential cross section for inelastic scattering of an incident electron by a helium atom on the basis of a well-known method for treating rearrangement collisions which makes use of the Born approximation. In Sect. **2**, the resulting formula is applied to the specific problem under consideration and it is first shown that the terms due to spin-exchange effects can be neglected under the prevailing conditions of validity. The various parts of the remaining simplified formula for the differential cross section are then calculated explicitly and in Sect. **3**, the necessary summations and integrations which ultimately lead to the primary specific ionization $S(\beta)$, are carried out. One of these integrations is studied in particular detail since it necessitates the introduction of additional simplifying approximations. The new final result for $S(\beta)$ is discussed and compared with a frequently adopted formula derived from the classical work of Bethe on primary specific ionization. A graphical representation also permits a comparison with some experimental data. The main conclusion is that the new formula is able to account for as much as 25% of the discrepancy between Bethe's formula and the experimental points. The remaining deviation can be physically understood. Finally, Sect. **4** is devoted to the velocity distributions of the secondary electrons ejected from the helium atoms during the process of primary ionization in various quantum states of angular momentum characterized by the non-negative integer l. The general behavior of

(*) On leave of absence to the Lawrence Radiation Laboratory, Berkeley 4, Cal.
(**) *Address*: Natuurkundig Laboratorium, Universiteit te Gent, Rozier, 6, Gent.

the cross sections per unit $\varkappa$-interval ($\varkappa$ being a convenient dimensionless velocity parameter) corresponding to $l=0$, 1 and 2 is discussed and physically interpreted. These cross sections are also compared with their respective analytic counterparts in which Coulomb wave functions are used to describe the final states of the ejected electrons approximately. It turns out that the agreement is excellent for $l=2$ as well as for all higher l-values.

Introduction.

It is the purpose of the present article to describe the derivation of a formula for the non-relativistic primary specific ionization of electrons in helium, endowed with a precision surpassing that attained by means of expressions based upon currently used hydrogen approximations.

This paper is connected with a previous article [1] in which the calculation of the needed more accurate helium wave functions, belonging to energies in the continuum part of the spectrum, was outlined in detail and can therefore be considered as an example of practical application of the results obtained there.

Primary specific ionization values calculated for a certain v/c-range of the incident electron by means of the mentioned final formula will be compared with earlier values which have been obtained treating the He-atom as a superposition of two hydrogen atoms for what its electron behavior is concerned.

Finally, some attention will be devoted to the related problem of the energy spectrum of the ejected secundary electrons for various values of their angular momentum quantum number.

Theoretical Development.

1. – Derivation of the basic formula for the differential cross section for inelastic scattering of an electron by a helium atom.

The calculation of the differential cross section for inelastic scattering of an incident electron by a helium atom can be carried through on the basis of a well-known method for treating rearrangement collisions [2], in which the

[1] C. C. Grosjean and R. T. Van de Walle: *Nuovo Cimento*, **19**, 696 (1961).
[2] L. I. Schiff: *Quantum Mechanics* (New York, 1949), pp. 230-239.

wave equation is transformed into an equivalent integral equation and use is made of the Born approximation. It has been shown that a calculation of this type can be largely executed as though the particles were distinguishable. It is only near the end that a proper symmetrization is carried out by forming a linear combination of the exchange-degenerate wave functions.

Neglecting an unimportant term due to the motion of the helium nucleus and all spin-dependent forces, the fundamental Schrödinger equation for the space part of the wave function which describes the phenomenon of primary ionization can be written as

$$(1.1)\qquad \left[-\frac{\hbar^2}{2\mu}(\nabla_1^2+\nabla_2^2+\nabla_3^2)- -\left(\frac{2e^2}{r_1}+\frac{2e^2}{r_2}+\frac{2e^2}{r_3}-\frac{e^2}{r_{12}}-\frac{e^2}{r_{13}}-\frac{e^2}{r_{23}}\right)\right]\psi(\boldsymbol{r}_1,\boldsymbol{r}_2,\boldsymbol{r}_3)=\mathscr{E}\psi(\boldsymbol{r}_1,\boldsymbol{r}_2,\boldsymbol{r}_3)\,,$$

in which

— $\boldsymbol{r}_1$, $\boldsymbol{r}_2$ and $\boldsymbol{r}_3$ can be chosen to represent respectively the position vectors of the incident electron and the two atomic electrons with respect to the nucleus as origin;

— $\mu = m_e M_{He}/(M_{He}+m_e)$ is the usual expression for the reduced mass of an electron in the presence of a helium nucleus;

— r_{12}, r_{13} and r_{23} symbolize the distances separating the various electron pairs which we can distinguish;

— $\mathscr{E}$ expresses the total energy of the three electrons.

Neglecting all spin-dependent interactions does not mean, however, that in what follows, we shall neglect spin effects, but this simplifying approximation will enable us to characterize all states by products of space wave functions and Pauli spin state vectors or by linear combinations of such products. Thus, if $u_0^{(s)}(\boldsymbol{r}_2,\boldsymbol{r}_3)$ is the normalized symmetric space function for the helium ground state, the total wave function for the latter is

$$(1.2)\qquad u_0^{(s)}(\boldsymbol{r}_2,\boldsymbol{r}_3)\left\{\frac{1}{\sqrt{2}}\left[\binom{1}{0}\binom{0}{1}-\binom{0}{1}\binom{1}{0}\right]\right\},$$

and the unperturbed wave functions describing the possible initial states of the system are given by

$$\exp\left[i\boldsymbol{k}_0\cdot\boldsymbol{r}_1\right]\cdot u_0^{(s)}(\boldsymbol{r}_2,\boldsymbol{r}_3)\left\{\frac{1}{\sqrt{2}}\binom{1}{0}\left[\binom{1}{0}\binom{0}{1}-\binom{0}{1}\binom{1}{0}\right]\right\},$$

or briefly

$$\exp[i\boldsymbol{k}_0\cdot\boldsymbol{r}_1]\cdot u_0^{(s)}(\boldsymbol{r}_2,\boldsymbol{r}_3)\left\{\frac{1}{\sqrt{2}}[(++-)-(+-+)]\right\}, \tag{1.3}$$

and, in the same abridged notation,

$$\exp[i\boldsymbol{k}_0\cdot\boldsymbol{r}_1]\cdot u_0^{(s)}(\boldsymbol{r}_2,\boldsymbol{r}_3)\left\{\frac{1}{\sqrt{2}}[(-+-)-(--+)]\right\}, \tag{1.4}$$

where $\boldsymbol{k}_0$ represents the propagation vector of the incident electron.

In what follows, we shall also need the wave functions describing all mutually independent excited states of the helium atom. Let us represent their normalized space parts symbolically by

$$u_n^{(s)}(\boldsymbol{r}_2,\boldsymbol{r}_3) \qquad \text{and} \qquad u_n^{(a)}(\boldsymbol{r}_2,\boldsymbol{r}_3), \tag{1.5}$$

(s) and (a) being abbreviations for symmetric and antisymmetric, and n being a shorthand notation for the set of quantum numbers characterizing each particular state. Let us point out that in certain cases similar to the ground state, where the two atomic electrons are spatially indistinguishable, $u_n^{(a)}$ vanishes identically. The total wave functions constructed with (1.5) are

$$u_n^{(s)}(\boldsymbol{r}_2,\boldsymbol{r}_3)\left\{\frac{1}{\sqrt{2}}[(+-)-(-+)]\right\}, \tag{1.6}$$

and

$$\begin{cases} u_n^{(a)}(\boldsymbol{r}_2,\boldsymbol{r}_3)(++), \qquad u_n^{(a)}(\boldsymbol{r}_2,\boldsymbol{r}_3)(--), \\ u_n^{(a)}(\boldsymbol{r}_2,\boldsymbol{r}_3)\left\{\frac{1}{\sqrt{2}}[(+-)+(-+)]\right\}. \end{cases} \tag{1.7}$$

Let us represent by E_n, the total energy of the two atomic electrons in the state designated by n.

Now, one can simply apply the entire mentioned formalism for dealing with rearrangement collisions to the present problem. This application is straightforward, but leads to quite lengthy calculations which we shall largely omit here. Still before antisymmetrization of the total wave function, one arrives at the following asymptotic forms of its first-order (perturbed) approximation, including spin and corresponding to the unperturbed wave function (1.3):

$$\Psi(1,2,3)\xrightarrow[r_1\to\infty]{}\left\{\exp[i\boldsymbol{k}_0\cdot\boldsymbol{r}_1]\cdot u_0^{(s)}(\boldsymbol{r}_2,\boldsymbol{r}_3)+\right.$$
$$\left.+\frac{1}{r_1}\sum_n f_n(\theta_1,\varphi_1)\exp[ik_nr_1]u_n^{(s)}(\boldsymbol{r}_2,\boldsymbol{r}_3)\right\}\left\{\frac{1}{\sqrt{2}}[(++-)-(+-+)]\right\} \tag{1.8}$$

$$\xrightarrow[r_2\to\infty]{} -\frac{1}{2}\cdot\frac{1}{r_2}\sum_n \exp\left[ik_n r_2\right]\left[g_n(\theta_2,\varphi_2)\,u_n^{(s)}(\boldsymbol{r}_3,\boldsymbol{r}_1)\left\{\frac{1}{\sqrt{2}}\left[(-++)-(++-)\right]\right\}-\right.$$

$$\left.-\sqrt{3}\,h_n(\theta_2,\varphi_2)\,u_n^{(a)}(\boldsymbol{r}_3,\boldsymbol{r}_1)\left\{\frac{1}{\sqrt{6}}\left[(-++)+(++-)-2(+-+)\right]\right\}\right]$$

$$\xrightarrow[r_3\to\infty]{} -\frac{1}{2}\cdot\frac{1}{r_3}\sum_n \exp\left[ik_n r_3\right]\left[g_n'(\theta_3,\varphi_3)\,u_n^{(s)}(\boldsymbol{r}_1,\boldsymbol{r}_2)\left\{\frac{1}{\sqrt{2}}\left[(+-+)-(-++)\right]\right\}+\right.$$

$$\left.+\sqrt{3}\,h_n'(\theta_3,\varphi_3)\,u_n^{(a)}(\boldsymbol{r}_1,\boldsymbol{r}_2)\left\{\frac{1}{\sqrt{6}}\left[(+-+)+(-++)-2(++-)\right]\right\}\right],$$

in which

$$k_n=\left[k_0^2-\frac{2\mu}{\hbar^2}\left(E_n-E_0\right)\right]^{\frac{1}{2}}, \tag{1.9}$$

$$f_n(\theta_1,\varphi_1)=\frac{\mu}{2\pi\hbar^2}\iiint\exp\left[-i\boldsymbol{k}_n\cdot\boldsymbol{r}_1\right]\cdot u_n^{(s)*}(\boldsymbol{r}_2,\boldsymbol{r}_3)\cdot$$

$$\cdot\left(\frac{2e^2}{r_1}-\frac{e^2}{r_{12}}-\frac{e^2}{r_{13}}\right)\exp\left[i\boldsymbol{k}_0\cdot\boldsymbol{r}_1\right]\cdot u_0^{(s)}(\boldsymbol{r}_2,\boldsymbol{r}_3)\,\mathrm{d}\boldsymbol{r}_1\,\mathrm{d}\boldsymbol{r}_2\,\mathrm{d}\boldsymbol{r}_3\,, \tag{1.10}$$

where $\boldsymbol{k}_n$ is a propagation vector of magnitude k_n that forms an angle θ_1 with $\boldsymbol{k}_0$; φ_1 represents an azimuth angle measured with respect to a conveniently chosen reference plane through $\boldsymbol{k}_0$ which we need not specify;

$$g_n(\theta_2,\varphi_2)=\frac{\mu}{2\pi\hbar^2}\iiint\exp\left[-i\boldsymbol{k}_n\cdot\boldsymbol{r}_2\right]\cdot u_n^{(s)*}(\boldsymbol{r}_3,\boldsymbol{r}_1)\cdot$$

$$\cdot\left(\frac{2e^2}{r_2}-\frac{e^2}{r_{21}}-\frac{e^2}{r_{23}}\right)\exp\left[i\boldsymbol{k}_0\cdot\boldsymbol{r}_1\right]\cdot u_0^{(s)}(\boldsymbol{r}_2,\boldsymbol{r}_3)\,\mathrm{d}\boldsymbol{r}_1\,\mathrm{d}\boldsymbol{r}_2\,\mathrm{d}\boldsymbol{r}_3\,, \tag{1.11}$$

$$h_n(\theta_2,\varphi_2)=\frac{\mu}{2\pi\hbar^2}\iiint\exp\left[-i\boldsymbol{k}_n\cdot\boldsymbol{r}_2\right]\cdot u_n^{(a)*}(\boldsymbol{r}_3,\boldsymbol{r}_1)\cdot$$

$$\cdot\left(\frac{2e^2}{r_2}-\frac{e^2}{r_{21}}-\frac{e^2}{r_{23}}\right)\exp\left[i\boldsymbol{k}_0\cdot\boldsymbol{r}_1\right]\cdot u_0^{(s)}(\boldsymbol{r}_2,\boldsymbol{r}_3)\,\mathrm{d}\boldsymbol{r}_1\,\mathrm{d}\boldsymbol{r}_2\,\mathrm{d}\boldsymbol{r}_3\,, \tag{1.12}$$

where $\boldsymbol{k}_n$ is a propagation vector of magnitude k_n, whose polar angles with respect to the direction of $\boldsymbol{k}_0$ are θ_2 and φ_2, this time;

and $g_n'(\theta_3,\varphi_3)$ and $h_n'(\theta_3,\varphi_3)$ represent two similar multiple integrals.

The first part in the asymptotic behavior of $\Psi(1,2,3)$ clearly corresponds to scattering of the incident electron by the helium atom without exchange. In contrast, the second and the third part imply an exchange collision between the incoming electron and one of the atomic electrons.

After complete antisymmetrization of the total wave function for the three electrons, its asymptotic form for large values of one of the radial co-ordinates, say r_1, is given by

$$\left\{\exp\left[i\boldsymbol{k}_0\cdot\boldsymbol{r}_1\right]\cdot u_0^{(s)}(\boldsymbol{r}_2,\boldsymbol{r}_3)+\frac{1}{r_1}\sum_n\left[f_n(\theta,\varphi)-g_n(\theta,\varphi)\right]\exp\left[ik_nr_1\right]u_n^{(s)}(\boldsymbol{r}_2,\boldsymbol{r}_3)\right\}\cdot$$

$$\cdot\left\{\frac{1}{\sqrt{2}}\left[(++-)-(+-+)\right]\right\}+$$

$$+\frac{\sqrt{3}}{r_1}\left[\sum_n h_n(\theta,\varphi)\exp\left[ik_nr_1\right]u_n^{(a)}(\boldsymbol{r}_2,\boldsymbol{r}_3)\right]\left\{\frac{1}{\sqrt{6}}\left[(++-)+(+-+)-2(-++)\right]\right\}.$$

From this and from an analogous result corresponding to the case that (1.4) describes the initial unperturbed state, it follows immediately that the differential cross section per unit solid angle $\mathrm{d}\sigma_n(\theta,\varphi)/\mathrm{d}\Omega$ for inelastic scattering of an electron in a direction characterized by the polar angles θ and φ with respect to the direction of incidence, while the helium atom is transferred from its initial ground state to some final excited state characterized by the index n, is

$$\frac{\mathrm{d}\sigma_n(\theta,\varphi)}{\mathrm{d}\Omega}=\frac{k_n}{k_0}\left[\left|f_n(\theta,\varphi)-g_n(\theta,\varphi)\right|^2+3\left|h_n(\theta,\varphi)\right|^2\right], \tag{1.13}$$

in which $f_n(\theta,\varphi)$, $g_n(\theta,\varphi)$ and $h_n(\theta,\varphi)$ are given by (1.10), (1.11) and (1.12) respectively. This is the basic formula on which all further calculations in this paper will be founded.

2. – Application to the specific problem under consideration and simplifying approximations for the differential cross section.

Returning more particularly to the problem of primary ionization, it appears useful to start by writing down the mathematical expressions for the space wave functions associated with the initial and final states of the helium atom. As we have already pointed out in our previous article, the ground state creates no difficulty, since it is described to within a sufficient degree of precision by the so-called normalized Hylleraas wave function, namely:

$$u_0^{(s)}(\boldsymbol{r}_2,\boldsymbol{r}_3)=\frac{\lambda^3}{\pi a_0^3}\exp\left[-\frac{\lambda}{a_0}(r_2+r_3)\right], \tag{2.1}$$

where $\lambda=27/16=1.6875$, and a_0 is the usual notation for the Bohr radius, but calculated with the reduced electron mass appearing in (1.1), *viz.*: $a_0=\hbar^2/\mu e^2$.

The corresponding total energy of the state is

$$E_0=-\lambda^2\frac{e^2}{a_0}. \tag{2.2}$$

As for the final state, in which one of the atomic electrons should be as strongly bound to the nucleus as quantum mechanics permits, whereas the other electron should have a positive energy, our preceding paper was entirely devoted to the problem of calculating accurate wave functions to describe such states. There, we arrived at the conclusion that the unsymmetrized space part of the wave functions under study can be approximated by

$$\frac{1}{\sqrt{\pi}}\left(\frac{2}{a_0}\right)^{\frac{3}{2}} \exp\left[-2\frac{r_2}{a_0}\right] R_{kl}(r_3)\, Y_{lm}(\theta_3, \varphi_3)\,, \qquad \begin{matrix}(m=-l, -l+1, \ldots, l;\\ l=0, 1, 2, \ldots),\end{matrix} \tag{2.3}$$

where l and m are the usual quantum numbers describing the angular momentum state of the ejected atomic electron with respect to the z-axis of the frame of reference, and where the radial wave function $R_{kl}(r)$ is the regular solution of the differential equation

$$\frac{1}{r^2}\frac{\mathrm{d}}{\mathrm{d}r}\left(r^2\frac{\mathrm{d}R_{kl}(r)}{\mathrm{d}r}\right) + \\ + \left\{k^2 - \frac{l(l+1)}{r^2} + \frac{2}{a_0 r}\left[1+\left(1+2\frac{r}{a_0}\right)\exp\left[-4\frac{r}{a_0}\right]\right]\right\} R_{kl}(r) = 0\,, \tag{2.4}$$

which satisfies the δ-function normalization condition in the k-scale:

$$\int_0^\infty R_{kl}(r) R_{k'l}(r) r^2\, \mathrm{d}r = \delta(k-k')\,. \tag{2.5}$$

The quantity k is the wave number associated with the ejected electron, so that the total energy of the latter in the electric field due to the nucleus and the charge cloud of the bound electron is

$$\frac{k^2\hbar^2}{2\mu}\,, \tag{2.6}$$

and the total energy of the excited state of the atom is

$$E_f = -\frac{2e^2}{a_0} + \frac{k^2\hbar^2}{2\mu}\,. \tag{2.7}$$

From this, we can construct the desired normalized symmetric and antisymmetric space functions:

$$\left.\begin{matrix}u_f^{(s)}(\boldsymbol{r}_2, \boldsymbol{r}_3)\\ u_f^{(a)}(\boldsymbol{r}_2, \boldsymbol{r}_3)\end{matrix}\right\} = \frac{2}{\sqrt{\pi a_0^3}}\left[\exp\left[-2\frac{r_2}{a_0}\right] R_{kl}(r_3)\, Y_{lm}(\theta_3, \varphi_3) \pm \right. \\ \left. \pm \exp\left[-2\frac{r_3}{a_0}\right] R_{kl}(r_2)\, Y_{lm}(\theta_2, \varphi_2)\right]\,. \tag{2.8}$$

To obtain the differential cross section, our first task consists in evaluating the multiple integrals (1.10), (1.11) and (1.12), after having introduced (2.1) and (2.8). This can of course not be carried through analytically, not only because of the mathematical difficulties involved, but also due to the fact that there exists no simple analytical expression for the radial function $R_{kl}(r)$. Nevertheless, from the particular form of (1.11) and (1.12), it can be seen that under the assumptions which permit the use of the Born approximation in the formalism outlined in Sect. **1**, $g_n(\theta, q)$ and $h_n(\theta, q)$ must be quite small in comparison with $f_n(\theta, q)$. Indeed, it is interesting to recall that the formalism giving rise to the result (1.13) is only valid under the condition that

$$\frac{\mu v_{at}}{\hbar} \ll k_0 \ll \frac{\mu c}{\hbar}, \tag{2.9}$$

where v_{at} represents the classical velocity of the planetary electrons on their normal Bohr orbits around the helium nucleus. The right-hand inequality guarantees that the whole problem remains thoroughly non-relativistic, whereas the left-hand inequality ensures that there is very little interaction between the impinging electron and the helium atom. This appears from the fact that the left-hand inequality is equivalent to

$$\frac{\mu v_{at}^2}{2} \ll \frac{k_0^2 \hbar^2}{2\mu}, \tag{2.10}$$

in which the classical kinetic energy of a planetary helium electron can be identified with the corresponding quantum mechanical expectation value namely $\lambda^2 e^2/2a_0$, so that (2.10) becomes

$$\frac{\lambda^2 e^2}{2a_0} \ll \frac{k_0^2 \hbar^2}{2\mu}. \tag{2.11}$$

Since the interaction energy of the incoming electron is certainly of the same order of magnitude as the left-hand side in (2.11), the inequality clearly expresses that it is small compared with the kinetic energy of the impinging electron, condition under which the Born approximation is known to yield meaningful results. In many experiments on primary ionization, but not in all of them, however, the energy of the used β-rays exceeds the kinetic energy of the atomic electrons by several orders of magnitude. The predictions of the present theory will be strictly comparable solely with the results of such experiments.

From (2.11), it also follows that

$$k_0^2 \gg \frac{\lambda^2 \mu e^2}{a_0 \hbar^2} = \frac{\lambda^2}{a_0^2} \quad \text{or} \quad k_0 a_0 \gg \lambda \simeq 1.69 . \tag{2.12}$$

Now, concerning $g_n(\theta, q)$ and $h_n(\theta, q)$, we observe that, regarded as integrals with respect to $\boldsymbol{r}_2$, these functions are of the form

$$\int \exp\left[-i\boldsymbol{k}_f \cdot \boldsymbol{r}_2\right] \cdot F(\boldsymbol{r}_2)\, \mathrm{d}\boldsymbol{r}_2 \,, \tag{2.13}$$

where $F(\boldsymbol{r}_2)$ contains the factor $\exp\left[-\lambda r_2/a_0\right]$ besides other decreasing functions of r_2. Here, k_f is our notation for the final wave number associated with the scattered electron. According to (1.9), (2.2) and (2.7), it has the value

$$k_f = \left\{k_0^2 - \frac{2\mu}{\hbar^2}\left[\frac{k^2\hbar^2}{2\mu} - \frac{2e^2}{a_0} + \frac{\lambda^2 e^2}{a_0}\right]\right\}^{\frac{1}{2}} = \tag{2.14}$$

$$= \left[k_0^2 - k^2 - \frac{2(\lambda^2 - 2)}{a_0^2}\right]^{\frac{1}{2}} = \left[k_0^2 - k^2 - \frac{1.695}{a_0^2}\right]^{\frac{1}{2}},$$

and since the incoming electron transfers only a very small fraction of its energy to the helium atom, we have that $k_f \cong k_0$. An integral of the type (2.13) is known to become small with respect to the value it takes around $\boldsymbol{k}_f = 0$ as soon as

$$\frac{k_f a_0}{\lambda} \gg 1 \,,$$

which is practically equivalent to $k_0 a_0 \gg \lambda$. According to (2.12), this is precisely the inequality which is very well satisfied here. The preceding argument cannot be applied to $f_n(\theta, q)$ because there, *both* complex exponentials are functions of $\boldsymbol{r}_1$ which cancel each other largely since $\boldsymbol{k}_f$ is mostly not very different from $\boldsymbol{k}_0$ and moreover, these functions are not coupled to a rapidly decreasing function of r_1. But this is not the sole reason for which $g_n(\theta, \varphi)$ and $h_n(\theta, q)$ turn out to be quite small compared to $f_n(\theta, q)$. Besides the integration with respect to $\boldsymbol{r}_2$ in (1.11) and (1.12), one should also consider the integration with respect to $\boldsymbol{r}_1$ in which, according to (2.8), the factor $\exp\left[i\boldsymbol{k}_0 \cdot \boldsymbol{r}_1\right]$ is either again coupled to an exponentially decreasing function of r_1 or combined with a spherical harmonic and a much more slowly oscillating function of r_1. All these considerations tend to strengthen the justification for the simplifying approximation which one customarily introduces in such problems and which we can undoubtedly adopt here, namely: we neglect the corrections due to exchange by putting

$$\frac{\mathrm{d}\sigma(\theta, \varphi)}{\mathrm{d}\Omega} = \frac{k_f}{k_0} |f(\theta, \varphi)|^2 \,, \tag{2.15}$$

equation in which we dropped the index n. The inaccuracy introduced in this way is certainly insignificant compared with the final correction on earlier evaluations of the cross section which we hope to find by the use of more precise helium wave functions.

Next, before proceeding with the calculation of $f(\theta, \varphi)$, let us remark that the formula (2.15) should undergo a slight change in notation on account of the fact that, strictly speaking, as it is actually written, it is only valid in the case that the final excited state of the helium atom is associated with an energy level belonging to the *discrete* part of the spectrum. When one deals with a continuum level, as we do in the present problem, one is always obliged to regard this level as belonging to a certain energy band whose extension depends on the particular δ-function normalization chosen for the corresponding wave function. In the case that the condition (2.5) is adopted, the width of the level band associated with the wave functions (2.8) is unity in the k-scale so that (1.13) and (2.15) actually yield a differential cross section, not only per unit solid angle, but also per unit interval in the k-scale in which the energy of the ejected secundary electron is characterized by means of expression (2.6). To indicate this feature explicitly, it is very convenient to introduce a supplementary differential and to write

$$\frac{\mathrm{d}^2\sigma(\theta, \varphi; k)}{\mathrm{d}\Omega\, \mathrm{d}k} = \frac{k_f}{k_0} |f(\theta, \varphi; k)|^2 , \tag{2.16}$$

in which, according to (1.10),

$$f(\theta, \varphi; k) = \frac{\mu e^2}{2\pi\hbar^2} \iiint (\exp [i(\boldsymbol{k}_0 - \boldsymbol{k}_f)\cdot \boldsymbol{r}_1]) \left(\frac{2}{r_1} - \frac{1}{r_{12}} - \frac{1}{r_{13}}\right) \cdot \cdot u_f^{(s)*}(\boldsymbol{r}_2, \boldsymbol{r}_3)\, u_0^{(s)}(\boldsymbol{r}_2, \boldsymbol{r}_3)\, \mathrm{d}\boldsymbol{r}_1\, \mathrm{d}\boldsymbol{r}_2\, \mathrm{d}\boldsymbol{r}_3 . \tag{2.17}$$

Let us now calculate the preceding multiple integral explicitly. Introducing the vector difference

$$\boldsymbol{K} = \boldsymbol{k}_0 - \boldsymbol{k}_f , \tag{2.18}$$

so that $\hbar\boldsymbol{K}$ is the commonly used momentum transfer in the collision, we can first subject the integral with respect to $\boldsymbol{r}_1$ to the following transformation:

$$\begin{aligned}
&\int \exp [i(\boldsymbol{k}_0 - \boldsymbol{k}_f)\cdot \boldsymbol{r}_1] \left(\frac{2}{r_1} - \frac{1}{r_{12}} - \frac{1}{r_{13}}\right) \mathrm{d}\boldsymbol{r}_1 = \\
&\quad = \int \exp [i\boldsymbol{K}\cdot \boldsymbol{r}_1] \left(\frac{2}{r_1} - \frac{1}{|\boldsymbol{r}_1 - \boldsymbol{r}_2|} - \frac{1}{|\boldsymbol{r}_1 - \boldsymbol{r}_3|}\right) \mathrm{d}\boldsymbol{r}_1 = \\
&\quad = 2\int \exp [i\boldsymbol{K}\cdot \boldsymbol{r}_1] \frac{\mathrm{d}\boldsymbol{r}_1}{r_1} - \exp [i\boldsymbol{K}\cdot \boldsymbol{r}_2] \int \exp [i\boldsymbol{K}\cdot (\boldsymbol{r}_1 - \boldsymbol{r}_2)] \frac{\mathrm{d}\boldsymbol{r}_1}{|\boldsymbol{r}_1 - \boldsymbol{r}_2|} - \\
&\quad - \exp [i\boldsymbol{K}\cdot \boldsymbol{r}_3] \int \exp [i\boldsymbol{K}\cdot (\boldsymbol{r}_1 - \boldsymbol{r}_3)] \frac{\mathrm{d}\boldsymbol{r}_1}{|\boldsymbol{r}_1 - \boldsymbol{r}_3|} = \\
&\quad = (2 - \exp [i\boldsymbol{K}\cdot \boldsymbol{r}_2] - \exp [i\boldsymbol{K}\cdot \boldsymbol{r}_3]) \int \exp [i\boldsymbol{K}\cdot \boldsymbol{r}] \frac{\mathrm{d}\boldsymbol{r}}{r} ,
\end{aligned}$$

in which we have twice gone over to a new origin of co-ordinate system in the $\boldsymbol{r}_1$-space. Further

$$\int \exp\left[i\boldsymbol{K}\cdot\boldsymbol{r}\right]\frac{\mathrm{d}\boldsymbol{r}}{r} = \int_0^\infty r\,\mathrm{d}r \int_0^\pi \int_0^{2\pi} \exp\left[i\boldsymbol{K}\cdot\boldsymbol{r}\right]\sin\theta\,\mathrm{d}\theta\,\mathrm{d}\varphi =$$

$$= 4\pi\int_0^\infty r\,\frac{\sin Kr}{Kr}\,\mathrm{d}r = \frac{4\pi}{K}\int_0^\infty \sin Kr\,\mathrm{d}r = \frac{4\pi}{K^2}\int_0^\infty \sin x\,\mathrm{d}x\,.$$

Strictly speaking, the resulting integral is not convergent, but this is a well-known characteristic difficulty arising whenever scattering is caused by long-range coulombic potential interactions. By the use of a form factor with a small screening constant which one lets approach to zero after the integration, or by the use of an adaptation of the Cesàro summation procedure to integrals, one arrives at the unequivocal result that the integral under study stands for unity. Thus

$$f(\theta,\varphi;k) = \frac{2\mu e^2}{\hbar^2 K^2}\iint \left(2 - \exp\left[i\boldsymbol{K}\cdot\boldsymbol{r}_2\right] - \exp\left[i\boldsymbol{K}\cdot\boldsymbol{r}_3\right]\right)\cdot \tag{2.19}$$

$$\cdot\, u_f^{(s)*}(\boldsymbol{r}_2,\boldsymbol{r}_3)\,u_0^{(s)}(\boldsymbol{r}_2,\boldsymbol{r}_3)\,\mathrm{d}\boldsymbol{r}_2\,\mathrm{d}\boldsymbol{r}_3\,.$$

This expression can undergo further simplifications in virtue of the following considerations:

— the functions $u_f^{(s)}(\boldsymbol{r}_2,\boldsymbol{r}_3)$ and $u_0^{(s)}(\boldsymbol{r}_2,\boldsymbol{r}_3)$ represent two space parts of helium wave functions corresponding to states of different energies, but with the same (antisymmetric) spin configuration. Thinking in terms of their exact expressions which are unknown, rather than in terms of their approximate expressions, we know that due to the orthogonality condition which they should rigorously satisfy, we can write

$$\iint u_f^{(s)*}(\boldsymbol{r}_2,\boldsymbol{r}_3)\,u_0^{(s)}(\boldsymbol{r}_2,\boldsymbol{r}_3)\,\mathrm{d}\boldsymbol{r}_2\,\mathrm{d}\boldsymbol{r}_3 = 0\,; \tag{2.20}$$

— due to the symmetry of the integrand in (2.19) with respect to $\boldsymbol{r}_2$ and $\boldsymbol{r}_3$, it can easily be shown that the two terms whose sum constitutes an approximation for $u_f^{(s)}(\boldsymbol{r}_2,\boldsymbol{r}_3)$ according to (2.8), give rise to equal contributions to $f(\theta,\varphi;k)$.

From these arguments, we conclude that $f(\theta,\varphi;k)$ can be rewritten as

$$f(\theta,\varphi;k) = -\frac{8\mu e^2}{\hbar^2 K^2}\cdot\frac{\lambda^3}{(\pi a_0^3)^{\frac{1}{2}}}\iint \left(\exp\left[i\boldsymbol{K}\cdot\boldsymbol{r}_2\right] + \exp\left[i\boldsymbol{K}\cdot\boldsymbol{r}_3\right]\right)\exp\left[-2\,\frac{r_2}{a_0}\right]\cdot \tag{2.21}$$

$$\cdot\, R_{kl}(r_3)\,Y_{lm}^*(\theta_3,\varphi_3)\exp\left[-\frac{\lambda}{a_0}\,(r_2+r_3)\right]\mathrm{d}\boldsymbol{r}_2\,\mathrm{d}\boldsymbol{r}_3\,,$$

where the radial wave function $R_{kl}(r_3)$ does not need an asterisk sign, since it is real. Carrying out the integrations which can be treated analytically, we find

$$(2.22)\qquad f(\theta, \varphi; k) = -\frac{8\mu e^2}{\hbar^2 K^2}\cdot\frac{\lambda^3}{(\pi a_0^3)^{\frac{1}{2}}}\cdot$$

$$\cdot\left[4\pi\int_0^\infty r_2^2 \exp\left[-(2+\lambda)\frac{r_2}{a_0}\right]\mathrm{d}r_2\cdot\int\exp\left[i\boldsymbol{K}\cdot\boldsymbol{r}_3\right]\cdot\exp\left[-\lambda\frac{r_3}{a_0}\right]R_{kl}(r_3)\,Y^*_{lm}(\theta_3,\varphi_3)\,\mathrm{d}\boldsymbol{r}_3+\right.$$

$$\left.+\int\exp\left[i\boldsymbol{K}\cdot\boldsymbol{r}_2\right]\cdot\exp\left[-(2+\lambda)\frac{r_2}{a_0}\right]\mathrm{d}\boldsymbol{r}_2\cdot\int\exp\left[-\lambda\frac{r_3}{a_0}\right]R_{kl}(r_3)\,Y^*_{lm}(\theta_3,\varphi_3)\,\mathrm{d}\boldsymbol{r}_3\right] =$$

$$= -\frac{8\mu e^2}{\hbar^2 K^2}\cdot\frac{1}{(\pi a_0^3)^{\frac{1}{2}}}\left(\frac{2\lambda}{2+\lambda}\right)^3\left[\int\exp\left[i\boldsymbol{K}\cdot\boldsymbol{r}_3\right]\cdot\exp\left[-\lambda\frac{r_3}{a_0}\right]R_{kl}(r_3)\,Y^*_{lm}(\theta_3,\varphi_3)\,\mathrm{d}\boldsymbol{r}_3+\right.$$

$$\left.+\frac{\sqrt{4\pi}\,\delta_{l0}\,\delta_{m0}}{\left[1+(K^2a_0^2/(2+\lambda)^2)\right]^2}\int_0^\infty\exp\left[-\lambda\frac{r_3}{a_0}\right]R_{k0}(r_3)\,r_3^2\,\mathrm{d}r_3\right|.$$

The fact that the last term in the preceding result vanishes identically except when $l = m = 0$ is rather surprising at first sight. However, it appears to be an indirect consequence of the approximations underlying the unsymmetrized space function for the excited helium state (2.3). Indeed, it is our proof that this function must be representable to within a high degree of precision by a product of two one-electron wave functions, which led to the possibility of separating the variables in the equation for the part describing the ejected electron. Thus, within this approximation, definite angular momentum quantum numbers l and m could be assigned to the latter, although this would not be possible in an exact treatment of the problem. In turn, it is the presence of only one spherical harmonic in (2.3) which causes the last term in the above result to vanish identically except for $l = m = 0$. This could be expected on the ground that a pure p, d, ... state is always orthogonal to a pure s-state. However, the appearance of the exception for $l = m = 0$ is directly connected with the lack of rigorous orthogonality between the approximate wave functions (2.1) and (2.8) in that case. When $l = m = 0$, the condition (2.20) still exists, but it is clearly something else than the presence of a spherical harmonic which should cause it to be satisfied. Introducing (2.1) and (2.8) under the integral signs in (2.20), one easily proves this condition to be equivalent to

$$(2.23)\qquad \int_0^\infty\exp\left[-\lambda\frac{r_3}{a_0}\right]R_{k0}(r_3)\,r_3^2\,\mathrm{d}r_3 = 0\,,$$

equality, which should be rigorously true. If this were so, there would evi-

dently not exist an exceptional ($l = m = 0$)-case. But, the integral in (2.23) cannot be expected to vanish identically, since the exponential function and $R_{k0}(r_3)$ do not satisfy the same wave equation. However, there are good reasons to believe that (2.23) is approximately valid and that the last integral in the previous formulas contributes very little to $f(\theta, \varphi; k)$. First, there is the logical argument that since (2.3) was shown to be a good approximation for the unsymmetrized space part of the wave function describing the final configuration of the atomic electrons, it can be expected to be nearly orthogonal to a good approximation for the space part of the ground state wave function such as (2.1), when $l = m = 0$. Secondly, the function $\exp[-\lambda r/a_0]$ can be regarded as the radial part of the ground state wave function for a hydrogenic atom with nuclear charge λe. In this way, it is the regular solution of the differential equation

$$\frac{1}{r^2}\frac{\mathrm{d}}{\mathrm{d}r}\left(r^2\frac{\mathrm{d}y(r)}{\mathrm{d}r}\right) + \left(\frac{2\mu E}{\hbar^2} + \frac{2\lambda}{a_0 r}\right) y(r) = 0\,, \tag{2.24}$$

corresponding to the lowest eigenvalue of E, namely

$$E = -\frac{\lambda^2 e^2}{2a_0}\,.$$

In contrast, $R_{k0}(r)$ is the regular solution of another differential equation, namely,

$$\frac{1}{r^2}\frac{\mathrm{d}}{\mathrm{d}r}\left(r^2\frac{\mathrm{d}R_{k0}(r)}{\mathrm{d}r}\right) + \left\{\frac{2\mu E}{\hbar^2} + \frac{2}{a_0 r}\left[1 + \left(1 + 2\,\frac{r}{a_0}\right)\exp\left[-4\,\frac{r}{a_0}\right]\right]\right\} R_{k0}(r) = 0\,, \tag{2.25}$$

with

$$E = \frac{k^2\hbar^2}{2\mu}\,. \tag{2.26}$$

Although the potential terms in (2.24) and (2.25) are formally quite different, it is nevertheless possible to regard λ ($=1.6875$) as some kind of average value replacing the function

$$1 + \left(1 + 2\,\frac{r}{a_0}\right)\exp\left[-4\,\frac{r}{a_0}\right],$$

in some neighborhood of $r = 0$. Therefore, $R_{k0}(r)$ must show a close resemblance to the regular solution of eq. (2.24) where we introduce the value of E given by (2.26). This regular solution is certainly perfectly orthogonal to $\exp[-\lambda r/a_0]$.

These arguments lead us to the proposition to drop the last term on the right-hand side of (2.22). Moreover, this new simplifying approximation is also justified by the fact that we have already made use of the exact orthogonality condition (2.20) to get rid of a term in (2.19). It would be inconsistent to carry out a simplification which includes (2.23), on the one hand, and to keep the same integral in another term as a factor different from zero, on the other hand. Hence

$$f(\theta, \varphi; k) = -\frac{8\mu e^2}{\hbar^2 K^2} \cdot \frac{1}{(\pi a_0^3)^{\frac{1}{2}}} \left(\frac{2\lambda}{2+\lambda}\right)^3 \cdot \cdot \int \exp\left[i\boldsymbol{K}\cdot\boldsymbol{r}_3\right] \exp\left[-\lambda \frac{r_3}{a_0}\right] R_{kl}(r_3)\, Y^*_{lm}(\theta_3, \varphi_3)\, \mathrm{d}\boldsymbol{r}_3 \,. \tag{2.27}$$

Finally, to reduce the remaining triple integral to its simplest form, let us integrate with respect to the polar angles θ_3 and φ_3, making use of the following spherical harmonics series expansion for $\exp\left[i\boldsymbol{K}\cdot\boldsymbol{r}_3\right]$:

$$\exp\left[i\boldsymbol{K}\cdot\boldsymbol{r}_3\right] = 4\pi \sum_{l'=0}^{\infty} \sum_{m'=-l'}^{l'} i^{l'} j_{l'}(Kr_3)\, Y_{l'm'}(\theta_3, \varphi_3)\, Y^*_{l'm'}(\xi, \zeta) \,, \tag{2.28}$$

in which K represents the magnitude of $\boldsymbol{K}$ and (ξ, ζ) are spherical angular co-ordinates describing the direction of this vector in the initially adopted reference system. We find

$$f(\theta, \varphi; k) = -\frac{32\pi^{\frac{1}{2}}\mu e^2}{\hbar^2 K^2 a_0^{\frac{3}{2}}} \left(\frac{2\lambda}{2+\lambda}\right)^3 i^l\, Y^*_{lm}(\xi, \zeta) \cdot \cdot \int_0^{\infty} \exp\left[-\lambda \frac{r_3}{a_0}\right] R_{kl}(r_3) j_l(Kr_3) r_3^2\, \mathrm{d}r_3 . \tag{2.29}$$

This function depends on θ, φ and k in an indirect manner through the vectorial relationship (2.18). In conclusion, we obtain the following result for (2.16):

$$\frac{\mathrm{d}^2\sigma}{\mathrm{d}\Omega\, \mathrm{d}k} = \frac{1024\pi\mu^2 e^4 k_f}{\hbar^4 K^4 a_0^3 k_0} \left(\frac{2\lambda}{2+\lambda}\right)^6 |\, Y_{lm}(\xi, \zeta)|^2 \cdot \cdot \left(\int_0^{\infty} \exp\left[-\lambda \frac{r}{a_0}\right] R_{kl}(r) j_l(Kr) r^2 \mathrm{d}r \right)^2 . \tag{2.30}$$

Let us recall that this expression represents the differential cross section per unit solid angle and per unit interval in the k-scale for the inelastic scat-

tering of an electron of momentum $\hbar \boldsymbol{k}_0$ impinging upon a helium atom in its ground state. After the scattering, the electron moves with a new momentum $\hbar \boldsymbol{k}_f = \hbar(\boldsymbol{k}_0 - \boldsymbol{K})$, characterized by angles (θ, φ) with respect to the direction of $\boldsymbol{k}_0$, and the helium atom is left in an ionized state, one of its planetary electrons having been transferred to the continuum part of the energy spectrum, whereas the other electron remains as strongly bound to the nucleus as possible. The ejected secondary electron is in a pure angular momentum state characterized by the quantum numbers l and m (with respect to the z-axis of the chosen co-ordinate system) and it has a total energy $k^2\hbar^2/2\mu$.

Before proceeding with the derivation of a total cross section from (2.30) in the next paragraph, let us subject this formula to a last useful transformation. From our preceding article [1], we know that there exists no simple analytical expression for the functions $R_{kl}(r)$ and that consequently they have to be calculated numerically. However, what we have actually computed for various values of certain parameters, are functions of the dimensionless distance co-ordinate ϱ $(= r/a_0)$ which we denoted by $f^{(n)}_{\varkappa l}(\varrho)$, satisfying the normalization condition

$$\int_0^\infty f^{(n)}_{\varkappa l}(\varrho) f^{(n)}_{\varkappa' l}(\varrho)\, \mathrm{d}\varrho = \frac{\pi}{2}\, \delta(\varkappa - \varkappa') \,, \tag{2.31}$$

where $\varkappa$ $(= ka_0)$ determines a dimensionless k-scale. This condition is equivalent to attributing a unit amplitude to these oscillating functions at $\varrho = +\infty$. For the purpose of later numerical evaluation, it is important to replace $R_{kl}(r)$ under the integral sign in (2.30) by the corresponding $f^{(n)}_{\varkappa l}(\varrho)$, reducing at the same time the integration with respect to r to one with respect to ϱ. Comparing (2.31) with the normalization condition (2.5), one easily sees that $R_{kl}(r)$ and $f^{(n)}_{\varkappa l}(\varrho)$ are interconnected by the following relationship:

$$R_{kl}(r) = \sqrt{\frac{2}{\pi}} \cdot \frac{f^{(n)}_{\varkappa l}(\varrho)}{a_0 \varrho} \,.$$

Carrying out the desired replacement of functions, one finds after a few additional manipulations

$$\frac{\mathrm{d}^2\sigma(\theta, \varphi; \varkappa)}{\mathrm{d}\Omega\, \mathrm{d}\varkappa} = \frac{2\,048 \mu^2 e^4 k_f}{\hbar^4 K^4 k_0} \left(\frac{2\lambda}{2+\lambda}\right)^6 |\, Y_{lm}(\xi, \zeta)\,|^2 \cdot \cdot \left(\int_0^\infty \exp\left[-\lambda\varrho\right] f^{(n)}_{\varkappa l}(\varrho)\, j_l(K a_0 \varrho)\, \varrho\, \mathrm{d}\varrho \right)^2 , \tag{2.32}$$

where the differential cross section is now expressed per unit interval in the $\varkappa$-scale.

3. – Calculation of the primary specific ionization.

The result (2.32) is much too detailed for our present purpose. Indeed, we are actually interested in finding an improved formula for the *total macroscopic* cross section for primary ionization produced by incident electrons in helium. Thus, both sides of (2.32) should be suitably summed and integrated with respect to the quantum numbers entering the description of the final state of the ejected electron and the angular co-ordinates characterizing the direction of scattering of the primary electron. In what follows, this program will be executed in several steps.

Let us start by successively summing with respect to m and to l, and integrating over all directions of scattering. Thus, we have to study the possibility of carrying out the various operations appearing on the right-hand side of the equality

$$(3.1)\qquad \frac{\mathrm{d}\sigma}{\mathrm{d}\varkappa} = \frac{2\,048\mu^2 e^4 k_f}{\hbar^4 k_0}\left(\frac{2\lambda}{2+\lambda}\right)^6 \int_0^{\pi}\int_0^{2\pi} \frac{\sin\theta\,\mathrm{d}\theta\,\mathrm{d}\varphi}{K^4} \sum_{l=0}^{\infty}\sum_{m=-l}^{l} |\, Y_{lm}(\xi,\zeta)\,|^2 \mathscr{I}^2_{\varkappa l}(Ka_0)\,,$$

where

$$\mathscr{I}_{kl}(Ka_0) = \int_0^{\infty} \exp\left[-\lambda\varrho\right] f^{(n)}_{\varkappa l}(\varrho)\, j_l(Ka_0\varrho)\,\varrho\,\mathrm{d}\varrho\,.$$

The summation with respect to m involves solely the spherical harmonics and can easily be carried out as an application of the well-known addition theorem for Legendre polynomials, *viz.*:

$$P_l(\cos\Theta) = P_l(\cos\xi)\,P_l(\cos\xi') + 2\sum_{m=1}^{l}\frac{(l-m)!}{(l+m)!}\,P^m_l(\cos\xi)\,P^m_l(\cos\xi')\cos m(\zeta-\zeta')\,,$$

or in its spherical harmonics notation which we need here:

$$(3.2)\qquad P_l(\cos\Theta) = \frac{4\pi}{2l+1}\sum_{m=-l}^{l} Y_{lm}(\xi,\zeta)\,Y^*_{lm}(\xi',\zeta')\,,$$

where

$$\cos\Theta = \cos\xi\cos\xi' + \sin\xi\sin\xi'\cos(\zeta-\zeta')\,.$$

In the special case that $\xi' = \xi$ and $\zeta' = \zeta$ (identical directions), one finds $\cos\Theta = 1$ and

$$P_l(1) = \frac{4\pi}{2l+1}\sum_{m=-l}^{l} Y_{lm}(\xi,\zeta)\;Y^*_{lm}(\xi,\zeta)\,,$$

so that

$$\sum_{m=-l}^{l} |Y_{lm}(\xi, \zeta)|^2 = \frac{2l+1}{4\pi}, \tag{3.3}$$

and

$$\frac{d\sigma}{d\varkappa} = \frac{512\mu^2 e^4 k_f}{\pi\hbar^4 k_0}\left(\frac{2\lambda}{2+\lambda}\right)^6 \sum_{l=0}^{\infty}(2l+1)\int_0^{\pi}\int_0^{2\pi}\mathscr{I}_{\varkappa l}^2(Ka_0)\frac{\sin\theta\, d\theta\, d\varphi}{K^4}. \tag{3.4}$$

The preceding summation not only introduces a simplification, but also has the interesting property of eliminating any φ-dependence in the remaining integrand. This corresponds to the well-known fact that summing with respect to a magnetic quantum number which enters the description of a group of final states generally destroys the preference connected with a certain direction which one customarily chooses as z-axis of the polar co-ordinate system. Here after summation with respect to m, there remains only one preferential direction in the problem, namely that of the propagation vector $\boldsymbol{k}_0$ of the incident particle. There is rotational symmetry around this direction and the differential cross section only depends on the angle of scattering θ. Therefore

$$\frac{d\sigma}{d\varkappa} = \frac{1024\mu^2 e^4 k_f}{\hbar^4 k_0}\left(\frac{2\lambda}{2+\lambda}\right)^6 \sum_{l=0}^{\infty}(2l+1)\int_0^{\pi}\mathscr{I}_{\varkappa l}^2(Ka_0)\frac{\sin\theta\, d\theta}{K^4}. \tag{3.5}$$

Note that this total cross section per unit $\varkappa$-interval ultimately depends on no more than two variables, namely k_0 and $\varkappa$.

Finally, since the integrand in the preceding result does not contain θ explicitly (except for $\sin\theta$), it is particularly convenient to pass from θ to a new integration variable, namely K. From the vector eq. (2.18), it follows that

$$K^2 = k_0^2 + k_f^2 - 2k_0 k_f \cos\theta.$$

Keeping k_0 and k_f fixed, we find the following relationship between the differentials dK and $d\theta$:

$$K\, dK = k_0 k_f \sin\theta\, d\theta,$$

so that

$$\frac{d\sigma(k_0, \varkappa)}{d\varkappa} = \frac{1024\mu^2 e^4}{\hbar^4 k_0^2}\left(\frac{2\lambda}{2+\lambda}\right)^6 \sum_{l=0}^{\infty}(2l+1)\int_{K_{\min}}^{K_{\max}}\mathscr{I}_{\varkappa l}^2(Ka_0)\frac{dK}{K^3}. \tag{3.6}$$

The new integration limits are, respectively,

$$K_{\max} = k_0 + k_f \simeq 2k_0 ,$$

$$K_{\min} = k_0 - k_f = \frac{k_0^2 - k_f^2}{k_0 + k_f} = \frac{k^2 + [2(\lambda^2 - 2)/a_0^2]}{k_0 + k_f} =$$

$$= \frac{\varkappa^2 + 2(\lambda^2 - 2)}{(k_0 + k_f)a_0^2} \simeq \frac{\varkappa^2 + 1.695}{2k_0 a_0^2} ,$$

in which we made us of (2.14). In view of the discussion which will follow, it is advisable to introduce a dimensionless K-scale by means of the linear transformation

$$K' = Ka_0 .$$

Going over to K' as new integration variable in (3.6), we find

$$\frac{\mathrm{d}\sigma(k_0, \varkappa)}{\mathrm{d}\varkappa} = \frac{1024}{k_0^2}\left(\frac{2\lambda}{2+\lambda}\right)^6 \sum_{l=0}^{\infty} (2l+1) \int_{K_1'}^{K_2'} \mathscr{I}_{\varkappa l}^2(K') \frac{\mathrm{d}K'}{K'^3} , \tag{3.7}$$

where

$$\left.\begin{aligned} K_2' &\simeq 2k_0 a_0 = 2\beta \frac{\hbar c}{e^2} = 274\beta , \\ K_1' &\simeq \frac{\varkappa^2 + 1.695}{2k_0 a_0} = \frac{\varkappa^2 + 1.695}{274\beta} \end{aligned}\right\} \text{ with } \beta = \frac{v_0}{c} ,$$

v_0 being the velocity of the incident electron.

This is as far as we can progress in simplifying the cross section without introducing further approximations, mainly because we do not dispose of an analytic expression for $f_{\varkappa l}^{(n)}(\varrho)$. The integration with respect to K' could in principle be carried out under the integral signs contained in $\mathscr{I}_{\varkappa l}^2(K')$, but this method would lead to much too complicated and impractical formulas. Instead, we prefer to proceed in the following manner.

Let us first study the general behavior of the functions $\mathscr{I}_{\varkappa l}(K')$ defined by

$$\mathscr{I}_{\varkappa l}(K') \equiv \int_0^{\infty} \exp\left[-\lambda\varrho\right] f_{\varkappa l}^{(n)}(\varrho) j_l(K'\varrho) \varrho \, \mathrm{d}\varrho . \tag{3.8}$$

In this integral, $f_{\varkappa l}^{(n)}(\varrho)$ and $\varrho j_l(K'\varrho)$ are two oscillating functions of ϱ converging more and more towards purely sinusoidal functions with amplitudes 1 and $1/K'$ respectively, as $\varrho \to +\infty$. On the basis of the theory of Fourier-Bessel integrals, we can conclude that when K' starts to exceed a quantity

roughly equal to the inverse of the range of the exponentially decreasing Hylleraas function, namely λ, $\mathscr{I}_{\varkappa l}(K')$ converges very rapidly to zero. Another more quantitative way to establish this fact consists in replacing $f^{(n)}_{\varkappa l}(\varrho)$ in (3.8) by its power series expansion given by formula (3.6) of our preceding article, *viz.*:

$$(3.9)\qquad f^{(n)}_{\varkappa l}(\varrho) = c_0 \varrho^{l+1}\left\{1 - 2\frac{2\varrho}{2l+2} + \right.$$
$$\left. + \left[2(l+3) - \frac{(l+1)\varkappa^2}{2}\right]\frac{(2\varrho)^2}{2!(2l+2)(2l+3)} - \ldots\right\},$$

and integrating term by term:

$$(3.10)\qquad \mathscr{I}_{\varkappa l}(K') = \frac{2^{l+1}(l+1)!\lambda K'^l c_0}{(\lambda^2+K'^2)^{l+2}}\left\{1 - \frac{2}{l+1}\cdot\frac{(2l+3)\lambda^2 - K'^2}{\lambda(\lambda^2+K'^2)} + \right.$$
$$\left. + \frac{(l+2)[2(l+3) - ((l+1)\varkappa^2/2)]}{(l+1)(l+\frac{3}{2})}\cdot\frac{(2l+3)\lambda^2 - 3K'^2}{(\lambda^2+K'^2)^2} - \ldots\right\},$$

where c_0 is an unknown normalization constant. From this, it appears that for large K',

$$\mathscr{I}_{\varkappa l}(K') \sim \frac{1}{K'^{l+4}}.$$

This, in turn, has as consequence that the integrand in (3.7) roughly behaves like $1/K'^{2l+11}$ for large K' and cannot contribute much to the integral as soon as K' starts to exceed the mentioned value λ. Thus, no appreciable inaccuracy will be introduced by writing

$$(3.11)\qquad \frac{\mathrm{d}\sigma(k_0,\varkappa)}{\mathrm{d}\varkappa} = \frac{1024}{k_0^2}\left(\frac{2\lambda}{2+\lambda}\right)^6 \sum_{l=0}^{\infty}(2l+1)\int_{K_1'}^{\lambda}\mathscr{I}^2_{\varkappa l}(K')\frac{\mathrm{d}K'}{K'^3},$$

but the substitution of K_2' by λ is essential for the kind of approximate integration with respect to K' which we shall perform. At this point, one could object that the choice of λ as new upper limit is somewhat arbitrary, since the integrand in (3.7) decreases sharply within an interval of *finite* extent whose average position is only roughly characterized by λ. However, it will turn out that this particular choice is not very critical and that, in reality, it is much more favourable than one would perhaps expect at first sight.

Comparing the value of λ, namely 1.6875, with a typical value of K_2', for example, for an electron with $\beta = 0.3$:

$$K_2' = 82.2,$$

we observe that K_2' appears to be an unnecessarily high upper limit. This is confirmed quite generally by the appropriate form in which the condition of validity (2.9) can be brought, namely,

$$\lambda = 1.6875 \ll k_0 a_0 \ll 137 ,$$

so that

$$3.375 \ll K_2' \ll 274 .$$

In contrast, λ is still much larger than the lower integration limit K_1', which is generally of the order 10^{-2} to 10^{-1}.

The importance of the tremendous reduction in the extension of the integration interval in (3.7) resides in the fact that it makes the substitution of the spherical Bessel function $j_l(K'\varrho)$ in (3.8) by the sum of only a very small number of terms of its power series expansion entirely sensible. Indeed, from the particular form of the integral in (3.8), it follows that the mentioned polynomial replacing $j_l(K'\varrho)$ should represent this function with sufficient precision up to a value of the order of K'/λ. Now, if the upper limit of K' were K_2' as in (3.7), the required number of terms would be enormous. But with the practical upper limit for K' reduced to λ, the maximum value of K'/λ is unity and we can be sure that only one or two terms of the expansion of $j_l(K'\varrho)$ will be important in calculating (3.8). This permits us to write

$$\mathscr{I}_{\varkappa l}(K') \simeq \frac{(2K')^l \cdot l!}{(2l+1)!}\left[I_{l,l+1}(\varkappa) - \frac{K'^2}{2(2l+3)} I_{l,l+3}(\varkappa)\right], \qquad (0 \leqslant K' \leqslant \lambda), \tag{3.12}$$

where

$$I_{lp}(\varkappa) \equiv \int_0^\infty \exp\left[-\lambda\varrho\right] f_{\varkappa l}^{(n)}(\varrho)\, \varrho^p \, \mathrm{d}\varrho .$$

Next, making use of (3.12) to calculate the sum of integrals in (3.11), another factor permitting a new simplification enters the picture, namely: the relative importance of the various integrands

$$\frac{\mathscr{I}_{\varkappa l}^2(K')}{K'^3} . \qquad (l = 0, 1, 2, \ldots).$$

It turns out that the curves $\mathscr{I}_{\varkappa l}(K')$ *vs.* K' converge so rapidly towards the K'-axis as l increases, that only the terms with $l = 0$, 1 and 2 in the sum on the right-hand side of (3.11) contribute significantly to the cross section and that for these l-values, the following approximations for $\mathscr{I}_{\varkappa l}(K')$ are suffi-

ciently accurate:

$$
\text{(3.13)}\qquad
\begin{cases}
\mathscr{I}_{\varkappa 0}(K') \simeq I_{01}(\varkappa) - \dfrac{K'^2}{6}\, I_{03}(\varkappa)\,, \\[2ex]
\mathscr{I}_{\varkappa 1}(K') \simeq \dfrac{K'}{3}\, I_{12}(\varkappa) - \dfrac{K'^3}{30}\, I_{14}(\varkappa)\,, \qquad (0 \leqslant K' < \lambda)\,. \\[2ex]
\mathscr{I}_{\varkappa 2}(K') \simeq \dfrac{K'^2}{15}\, I_{23}(\varkappa)\,.
\end{cases}
$$

In addition, we are obliged to put $I_{01}(\varkappa)$ equal to zero in order to remain consistent with an earlier approximation, since this integral is, apart from a proportionality factor, identical to the one in (2.23). This leads us to the following expression for $\mathrm{d}\sigma/\mathrm{d}\varkappa$ (up to the fourth power of K'):

$$
\text{(3.14)}\qquad \frac{\mathrm{d}\sigma(k_0, \varkappa)}{\mathrm{d}\varkappa} = \frac{1024}{k_0^2}\left(\frac{2\lambda}{2+\lambda}\right)^6 \cdot
$$

$$
\cdot \int_{K_1'}^{\lambda} \left\{ \frac{K'^4}{36} I_{03}^2(\varkappa) + \frac{1}{3}\left[K'^2 I_{12}^2(\varkappa) - \frac{K'^4}{5} I_{12}(\varkappa)\, I_{14}(\varkappa) \right] + \frac{K'}{45}\, I_{23}^2(\varkappa) \right\} \frac{\mathrm{d}K'}{K'^3} =
$$

$$
= \frac{1024}{k_0^2}\left(\frac{2\lambda}{2+\lambda}\right)^6 \left\{ \frac{1}{3} I_{12}^2(\varkappa) \ln \frac{2\lambda k_0 a_0}{\varkappa^2 + 2(\lambda^2 - 2)} + \right.
$$

$$
\left. + \left[\frac{1}{72} I_{03}^2(\varkappa) - \frac{1}{30} I_{12}(\varkappa) I_{14}(\varkappa) + \frac{1}{90} I_{23}^2(\varkappa) \right] \left(\lambda^2 - \frac{[\varkappa^2 + 2(\lambda^2 - 2)]^2}{4 k_0^2 a_0^2} \right) \right\}.
$$

The logarithmic term in this formula arises from the integration of the $1/K'$-term. That K'^{-1}, and not K'^{-3}, is the lowest power of K' appearing under the integral sign, is a rigorous result. This can most easily be established on the basis of form. (2.19). Indeed, replacing the two exponential functions in the multiple integral by their Maclaurin series expansion and characterizing the direction of $\boldsymbol{K}$ by the unit vector $\mathbf{1}_{\boldsymbol{K}}$, we find

$$
\text{(3.15)}\qquad f(\theta, q; k) = -\frac{2i\mu e^2}{\hbar^2 K} \iint [(\boldsymbol{r}_2 + \boldsymbol{r}_3)\cdot \mathbf{1}_{\boldsymbol{K}}]\, u_f^{(s)*}(\boldsymbol{r}_2, \boldsymbol{r}_3)\, u_0^{(s)}(\boldsymbol{r}_2, \boldsymbol{r}_3)\, \mathrm{d}\boldsymbol{r}_2\, \mathrm{d}\boldsymbol{r}_3 -
$$

$$
+ \frac{\mu e^2}{\hbar^2} \iint [(\boldsymbol{r}_2 \cdot \mathbf{1}_{\boldsymbol{K}})^2 + (\boldsymbol{r}_3 \cdot \mathbf{1}_{\boldsymbol{K}})^2]\, u_f^{(s)*}(\boldsymbol{r}_2, \boldsymbol{r}_3)\, u_0^{(s)}(\boldsymbol{r}_2, \boldsymbol{r}_3)\, \mathrm{d}\boldsymbol{r}_2\, \mathrm{d}\boldsymbol{r}_3 + \ldots,
$$

showing, actually *without* the use of any orthogonality arguments, that the lowest power of K in the series expansion of the amplitude function is rigorously K^{-1} and not K^{-2}. From this fact, one simply deduces the previous statement.

In order to make the right-hand side of (3.14) suitable for practical calculation of $d\sigma/d\varkappa$ and in view of carrying out the final integration with respect to $\varkappa$ to obtain the desired total cross section for ionization, we have evaluated the integrals $I_{03}(\varkappa)$, $I_{12}(\varkappa)$, $I_{14}(\varkappa)$ and $I_{23}(\varkappa)$ for various values of $\varkappa$, namely, 0.3, 0.5, 0.7, 0.8, 1.0, 1.5, 2.0, 3.0 and 4.0. These numbers together with $\varkappa = 0$, for which the mentioned integrals can be shown to vanish identically, form a sufficiently detailed set of abscissas to provide the complete knowledge of the variation of I_{03}, I_{12}, I_{14} and I_{23} as functions of $\varkappa$ in the interval where they are not exceedingly small compared with their maximum value. This explains why the functions $f_{\varkappa l}^{(n)}(\varrho)$ had to be calculated numerically for $l = 0$, 1 and 2, and for all the mentioned (non-vanishing) $\varkappa$-values, as we stated in Sect. **4** of our preceding article (1). The numerical integrations of I_{03}, I_{12}, I_{14} and I_{23} have been carried out on the basis of a simple trapezium quadrature formula, again using the IBM 650 ordinator. Integrating up to $\varrho = 8$ appeared to be more than sufficient, apart from a few exceptional cases. In some of these cases, where the $f_{\varkappa l}^{(n)}(\varrho)$-curves had been calculated to higher ϱ-values for normalization purposes (cfr. (1)), the integration could be pushed to a sufficiently high ϱ-value. For the remaining part of the exceptional cases, in which the $f_{\varkappa l}^{(n)}(\varrho)$-curves were not available above $\varrho = 8$, a correction was introduced on the basis of an extrapolation of the behavior of the latter. The relative precision attained was always of the order of $1‰$. The entire operation has covered about five hours of machine time.

Finally, integrating with respect to $\varkappa$ on both sides of (3.14), and characterizing the velocity of the incoming electron by β rather than by k_0, we obtain for the total cross section

$$\sigma_T(\beta) = \frac{1024}{\beta^2}\left(\frac{\hbar}{\mu c}\right)^2\left(\frac{2\lambda}{2+\lambda}\right)^6\left\{\frac{1}{3}(\ln\beta)\int_0^\infty I_{12}^2(\varkappa)\,d\varkappa + \right.$$

$$+\frac{1}{3}\int_0^\infty I_{12}^2(\varkappa)\ln\frac{2\lambda\hbar c}{\varrho^2[\varkappa^2+2(\lambda^2-2)]}\,d\varkappa+\lambda^2\int_0^\infty\left[\frac{1}{72}I_{03}^2(\varkappa)-\frac{1}{30}I_{12}(\varkappa)I_{14}(\varkappa)+\frac{1}{90}I_{23}^2(\varkappa)\right]d\varkappa -$$

$$\left.-\left(\frac{e^2}{2\beta\hbar c}\right)^2\int_0^\infty\left[\frac{1}{72}I_{03}^2(\varkappa)-\frac{1}{30}I_{12}(\varkappa)I_{14}(\varkappa)+\frac{1}{90}I_{23}^2(\varkappa)\right](\varkappa^2+2(\lambda^2-2))^2\,d\varkappa\right\},\tag{3.16}$$

in which the last term turns out to be negligible with respect to the sum of the other terms for all practical values of β. In this way, $\sigma_T(\beta)$ becomes

$$\sigma_T(\beta)\simeq\frac{89.781\cdot10^{-20}}{\beta^2}\left\{\frac{1}{6}(\ln\beta^2)\int_0^\infty I_{12}^2(\varkappa)\,d\varkappa+\frac{1}{3}\int_0^\infty I_{12}^2(\varkappa)\ln\frac{462.51}{\varkappa^2+1.695}\,d\varkappa+\right.$$

$$\left.+2.848\int_0^\infty\left[\frac{1}{72}I_{03}^2(\varkappa)-\frac{1}{30}I_{12}(\varkappa)I_{14}(\varkappa)+\frac{1}{90}I_{23}^2(\varkappa)\right]d\varkappa\right\}\ (\mathrm{cm}^2),\tag{3.17}$$

valid for

$$\lambda/137 = 0.0123 \ll \beta \ll 1 . \tag{3.18}$$

The integrals in this expression have been evaluated by plotting on millimeter paper, the values of the respective integrands for the ten $\varkappa$-abscissas in which I_{03}, I_{12}, I_{14} and I_{23} are known, connecting the various points by smooth curves and determining the area enclosed by these curves and the $\varkappa$-axis by planimetric integration. The results are

$$\int_0^\infty I_{12}^2(\varkappa)\,\mathrm{d}\varkappa = 0.0607 \pm 0.0002 , \qquad \int_0^\infty I_{12}^2(\varkappa) \ln \frac{462.51}{\varkappa^2 + 1.695}\,\mathrm{d}\varkappa = 0.337 \pm 0.003 ,$$

$$\int_0^\infty I_{03}^2(\varkappa)\,\mathrm{d}\varkappa = 0.0623 \pm 0.0002 , \qquad \int_0^\infty I_{12}(\varkappa) I_{14}(\varkappa)\,\mathrm{d}\varkappa = 0.0930 \pm 0.0010 ,$$

$$\int_0^\infty I_{23}^2(\varkappa)\,\mathrm{d}\varkappa = 0.2205 \pm 0.0004 .$$

Introducing these values in (3.17) and multiplying the resulting expression by N, the number of He-atoms per cubic centimeter, we obtain the following final formula for the primary specific ionization in helium:

$$S(\beta) = \frac{(0.908 \pm 0.003)\cdot 10^{-20} N}{\beta^2} \left[\ln \beta^2 + (11.2 \pm 0.2)\right] . \tag{3.19}$$

Concerning the dependence of this expression upon the particular upper limit of integration chosen to replace the unnecessarily high value K_2' in form. (3.7), let us point out that the first numerical factor in (3.19) is totally independent of this choice, and that the second factor is rather insensitive to permissible variations of the modified upper limit.

It is interesting to compare our final result with a frequently adopted formula derived from the classical work of BETHE [3]:

$$S_B = 2N \frac{2\pi e^4}{\mu v_0^2} \cdot \frac{0.285}{W_{1s}^{\mathrm{He}}} \ln \frac{2\mu v_0^2}{0.048\, W_{1s}^{\mathrm{He}}} , \tag{3.20}$$

in which the numerical factors were evaluated using the approximation of hydrogen-like wave functions, and W_{1s}^{He} is chosen to represent the experimental

[3] H. A. BETHE: *Ann. d. Phys.*, **5**, 325 (1930).

value of the first ionization potential in helium, *viz.*,

$$W_{1s}^{\mathrm{He}} = 24.58 \text{ eV} .$$

Brought in a form similar to our final result, S_B becomes

$$S_B(\beta) = \frac{0.591 \cdot 10^{-20} N}{\beta^2} (\ln \beta^2 + 13.7) . \tag{3.21}$$

Comparing formulas (3.19) and (3.21), one notices that the use of more accurate helium wave functions in the calculation of the primary specific ionization leads to a considerable modification of the values of the numerical coefficients involved. The largest change affects the first coefficient which undergoes an increase of roughly 50% with respect to its earlier value.

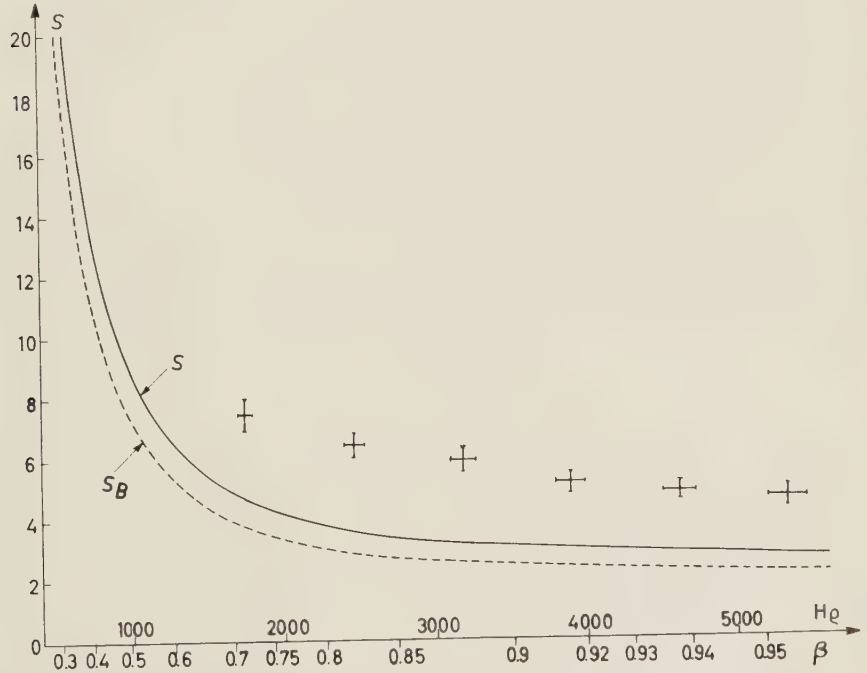

Fig. 1. - Comparison between two theoretical primary specific ionization curves and some experimental results in the case of helium at a pressure of one atmosphere and a temperature of 20 °C. $H\varrho$ is measured in oerstedt-cm. The full-line curve pictures our improved formula (3.19), whereas the dashed curve represents formula (3.21) deduced deduced from Bethe's theory.

In Fig. 1, we have made a graphical representation of the curves defined by (3.19) and (3.21), with N $(= 0.25039 \cdot 10^{20})$ corresponding to the case of

one atmosphere of helium gas pressure and a temperature of 20 °C, solely for the purpose of comparison with some experimental points obtained by one of us from cloud chamber measurements. As is customarily done, the abscissa scale is chosen linear in $H\varrho$, the product of the magnetic field (measured in oerstedt) which was applied in the cloud chamber to determine the momentum of the incident electrons and the resulting radius of curvature of the tracks, but we have also plotted the non-linear β-scale. Concerning the experimental points, we must admit that, unfortunately, they fall in a β-region which lies too close to unity to satisfy the condition (3.18). In other words, their abscissas are situated outside the β-interval in which the formulas (3.19) and (3.21) can certainly be expected to hold on strict theoretical grounds. From this point of view, one could be inclined to regard the possibility of any meaningful comparison between theory and experiment as dubious here. Yet, there is a good reason for which the comparison is nevertheless significant. It follows from the consideration of the case of atomic hydrogen. In this case, exact calculations carried out by BETHE [3] have led to a non-relativistic formula which is very similar to (3.20), namely:

$$S_B^{\mathrm{H}} = N\frac{2\pi e^4}{\mu v_0^2}\cdot\frac{0.285}{W_{1s}^{\mathrm{H}}}\ln\frac{2\mu v_0^2}{0.048\,W_{1s}^{\mathrm{H}}}, \tag{3.22}$$

where $W_{1s}^{\mathrm{H}} = 13.60$ eV. Later, the problem was treated relativistically, using Moller's method [4], and the difference between the resulting relativistic formula and its non-relativistic counterpart is the addition of the terms

$$-\ln\left(1-\frac{v_0^2}{c^2}\right)-\frac{v_0^2}{c^2},$$

to the logarithmic term in (3.22). A few evaluations show that unless v_0/c reaches a value of the order of 0.95 or higher, the relativistic correction to form. (3.22) is rather unimportant, as it raises the non-relativistic curve over a quantity varying from a fraction of a percent to a few percent only. This proves that Bethe's formula (3.22) remains physically meaningful up to much higher values of β than could be expected from purely theoretical considerations. The complete analogy between the mathematical treatments of the primary specific ionization of electrons in hydrogen and in helium certainly permits us to conclude that up to $\beta = 0.95$, say, relativity corrections to formulas such as (3.19) and (3.21) must also remain small, not only compared with $S(\beta)$ and $S_B(\beta)$ themselves, but also with respect to the difference $S(\beta) - S_B(\beta)$. Therefore, the comparison presented in Fig. 1 is really significant.

[4] C. MØLLER: *Zeits. f. Phys.*, **70**, 786 (1931).

As can be noticed on this figure, our more exact treatment results in an increase of as much as 20 to 25% with respect to the older primary specific ionization values. Nevertheless, the essential disagreement with the experimental values which was already pointed out in earlier papers [5,6] still exists. This conclusion confirms an assertion put forward in ref. [7], namely, that theoretical imperfections alone cannot be held responsible for the observed differences. In that same article, a plausible explanation hypothesis for the remaining discrepancy between theory and experiment was presented.

In conclusion, we should like to point out that with the aid of the computer results given above, calculations could also be performed along the same lines in order to obtain more accurate values for such quantities as, *e.g.*, stopping-power.

4. – Velocity distributions of the ejected secundary electrons.

The preceding calculations implicitly contain some additional information in connection with a problem related to the general subject, namely, that of the velocity distributions of the secundary electrons ejected from the helium atoms in some well-defined quantum state of angular momentum. Indeed, returning to form. (3.14), one readily observes that the cross section per unit $\varkappa$-interval can be split up in three distinct contributions respectively corresponding to the values 0, 1 and 2 of the angular momentum quantum number l of the ejected electrons. Again neglecting $K_1'^2$ with respect to λ^2 in the last term (as we did in passing from (3.14) to the total cross section (3.17)), these three contributions can be written as

$$(4.1)\qquad \frac{\mathrm{d}\sigma_0(\beta,\varkappa)}{\mathrm{d}\varkappa} = \frac{128\lambda^2}{9k_0^2}\left(\frac{2\lambda}{2+\lambda}\right)^6 I_{03}^2(\varkappa) = \frac{3.551\cdot 10^{-20}}{\beta^2} I_{03}^2(\varkappa)\,,$$

$$(4.2)\qquad \frac{\mathrm{d}\sigma_1(\beta,\varkappa)}{\mathrm{d}\varkappa} = \frac{1024}{3k_0^2}\left(\frac{2\lambda}{2+\lambda}\right)^6 I_{12}(\varkappa)\left[I_{12}(\varkappa)\ln\frac{2\lambda k_0 a_0}{\varkappa^2+2(\lambda^2-2)} - \frac{\lambda^2}{10} I_{14}(\varkappa)\right] =$$

$$= \frac{29.927\cdot 10^{-20}}{\beta^2} I_{12}(\varkappa)\left[I_{12}(\varkappa)\ln\frac{462.51\beta}{\varkappa^2+1.695} - 0.2848\, I_{14}(\varkappa)\right],$$

$$(4.3)\qquad \frac{\mathrm{d}\sigma_2(\beta,\varkappa)}{\mathrm{d}\varkappa} = \frac{512\lambda^2}{45k_0^2}\left(\frac{2\lambda}{2+\lambda}\right)^6 I_{23}^2(\varkappa) = \frac{2.841\cdot 10^{-20}}{\beta^2} I_{23}^2(\varkappa)\,.$$

[5] J. Allewaert, R. Van de Walle and J. Verhaeghe: *Comp. Rend. Acad. Sci. Paris*, **245**, 1611 (1957).

[6] R. Van de Walle and J. Verhaeghe: *Compt. Rend. Acad. Sci. Paris*, **248**. 3292 (1959).

[7] R. Van de Walle and J. Verhaeghe: *Compt. Rend. Acad. Sci. Paris*, **245**, 1721 (1957).

As an illustration of the general behavior of these partial cross sections as functions of $\varkappa$ and l, we have represented in Fig. 2, the right-hand sides of (4.1), (4.2) and (4.3) for such a typical value of β as 0.2, corresponding to a kinetic energy of 10.22 keV. As expected, it appears that there is a strong preference

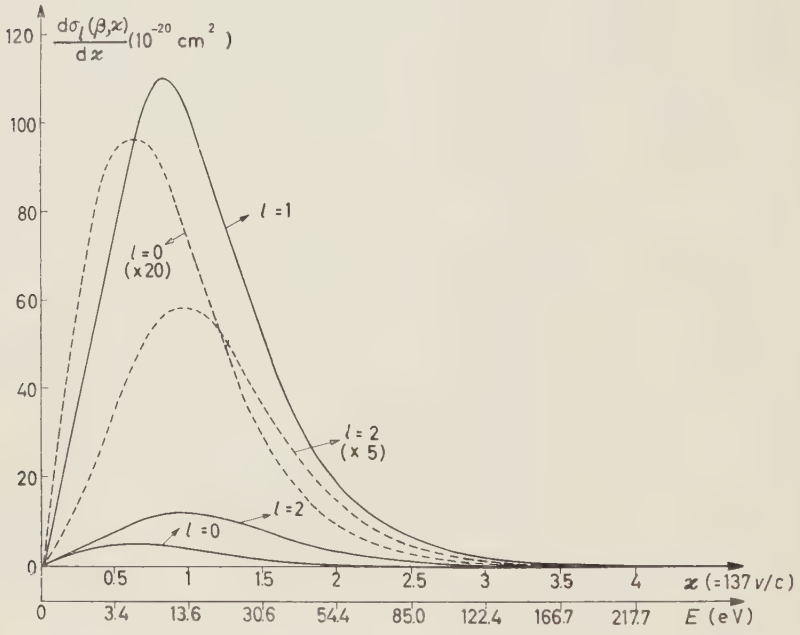

Fig. 2. – Behavior of the partial cross sections $d\sigma_l(\beta, \varkappa)/d\varkappa$ as functions of $\varkappa$ for $l=0$, 1 and 2, in the case of $\beta=0.2$. Dashed curves represent the $l=0$ and $l=2$ cross sections with suitable magnification.

for the secundary electrons to be ejected with an angular momentum characterized by $l=1$ with respect to the nucleus left behind. This can most easily be understood by looking upon the electric interaction between the incident and the atomic electron in terms of the familiar image of the exchange of virtual quanta. In this picture, the mentioned preference results from the fact that in the multipole radiation « emitted » by the primary particle, the dipole component is predominant.

Concerning the partial cross sections corresponding to $l=0$ and $l=2$, Fig. 2 also shows that their values are generally quite small with respect to those of $d\sigma_1/d\varkappa$, so that they contribute very little to the total cross section. This result supports the statement previously made about the possibility of neglecting all angular momentum contributions of higher order. One also

notices that the abscissas of the maxima of the three curves in Fig. 2 are in ascending order. This merely reflects the fact that an electron leaving the atom on a D-wave possesses a velocity which, on the average, is greater than that of an electron leaving it on a P-wave. The same statement holds for the relative behavior of P-electrons as compared to S-electrons.

Finally, we have also found it interesting to make numerical comparisons between the three previously obtained partial cross sections (pictured in Fig. 2) and their respective counterparts resulting from formulas in which only hydrogenic wave functions are used, so that their calculation can be performed analytically. Leaving the description of the ground state unaltered, but replacing systematically, in the entire preceding theoretical development, each encountered $f_{\varkappa l}^{(n)}(\varrho)$-function by the corresponding Coulomb wave function $F_{\varkappa l}(\varrho)$ for an effective nuclear charge with $Z = 1$ (cfr. [1]), one arrives at the following formulas, in one-to-one correspondence with (4.1-3):

$$(4.4)\qquad \frac{\mathrm{d}\sigma_0'(\beta,\varkappa)}{\mathrm{d}\varkappa} = \frac{16\,384\pi\lambda^2}{9\beta^2}\left(\frac{\hbar}{\mu c}\right)^2\left(\frac{2\lambda}{2+\lambda}\right)^6 \frac{\varkappa \exp\left[-(4/\varkappa)\,\mathrm{arctg}\,(\varkappa/\lambda)\right]}{(\lambda^2+\varkappa^2)^8(1-\exp\left[-2\pi/\varkappa\right])}\cdot$$

$$\cdot\left[(3\lambda-2)\varkappa^2-(3\lambda^3-9\lambda^2+6\lambda-1)\right]^2 =$$

$$= \frac{1427.905\cdot 10^{-20}}{\beta^2}\,\frac{\varkappa \exp\left[-(4/\varkappa)\,\mathrm{arctg}\,0.5926\varkappa\right]}{(2.8477+\varkappa^2)^8(1-\exp\left[-2\pi/\varkappa\right])}\,(3.0625\varkappa^2++2.0876)^2,$$

$$(4.5)\qquad \frac{\mathrm{d}\sigma_1'(\beta,\varkappa)}{\mathrm{d}\varkappa} = \frac{32\,768\,\pi}{3\beta^2}\left(\frac{\hbar}{\mu c}\right)^2\left(\frac{2\lambda}{2+\lambda}\right)^6 \frac{(2\lambda-1)^2\varkappa(1+\varkappa^2)\exp\left[-(4/\varkappa)\,\mathrm{arctg}\,(\varkappa/\lambda)\right]}{(\lambda^2+\varkappa^2)^6(1-\exp\left[-2\pi/\varkappa\right])}\cdot$$

$$\cdot\left[\ln\frac{2\lambda\hbar c\beta}{e^2[\varkappa^2+2(\lambda^2-2)]}+\frac{\lambda^2[(18\lambda-7)\varkappa^2-(30\lambda^3-45\lambda^2+18\lambda-2)]}{5(2\lambda-1)(\lambda^2+\varkappa^2)^2}\right] =$$

$$= \frac{16\,970.33\cdot 10^{-20}}{\beta^2}\cdot\frac{\varkappa(1+\varkappa^2)\exp\left[-(4/\varkappa)\,\mathrm{arctg}\,0.5926\varkappa\right]}{(2.8477+\varkappa^2)^6(1-\exp\left[-2\pi/\varkappa\right])}\cdot$$

$$\cdot\left[\ln\frac{462.51\beta}{\varkappa^2+1.695}+\frac{0.2398\,(23.375\varkappa^2-44.393)}{(2.8477+\varkappa^2)^2}\right],$$

$$(4.6)\qquad \frac{\mathrm{d}\sigma_2'(\beta,\varkappa)}{\mathrm{d}\varkappa} = \frac{65\,536\,\pi\lambda^2}{45\beta^2}\left(\frac{\hbar}{\mu c}\right)^2\left(\frac{2\lambda}{2+\lambda}\right)^6\cdot$$

$$\cdot\frac{(3\lambda-1)^2\varkappa(1+\varkappa^2)(1+4\varkappa^2)\exp\left[-(4/\varkappa)\,\mathrm{arctg}\,(\varkappa/\lambda)\right]}{(\lambda^2+\varkappa^2)^8(1-\exp\left[-2\pi/\varkappa\right])} =$$

$$= \frac{18\,852.89\cdot 10^{-20}}{\beta^2}\cdot\frac{\varkappa(1+\varkappa^2)(1+4\varkappa^2)\exp\left[-(4/\varkappa)\,\mathrm{arctg}\,0.5926\varkappa\right]}{(2.8477+\varkappa^2)^8(1-\exp\left[-2\pi/\varkappa\right])},$$

in which we have marked the partial cross sections with a prime to distinguish them from those calculated numerically on the basis of (4.1-3). Replacing

each $f_{\varkappa l}^{(n)}(\varrho)$-function by the corresponding Coulomb wave function $F_{\varkappa l}(\varrho)$ is physically equivalent to neglecting the effect of the *finite* extension of the charge cloud due to the atomic electron which remains bound to the helium nucleus, in the evaluation of the effective potential acting upon the ejected electron. As we have seen in our preceding article [1], the effect of the mentioned finite extension is the presence of a short-range attractive potential superimposed on a pure $1/r$-potential with $Z = 1$ in the approximate one-particle Schrödinger equation for the secundary electron. This reflects a slight imperfection in the screening of the nuclear charge by the remaining bound electron. But, since the short-range potential is practically damped out at a distance of one atomic unit ($r = a_0$), and since the wave functions describing the ejected electrons are very extended, neglecting the imperfection of the screening and using pure Coulomb wave functions with $+e$ as effective nuclear charge to characterize the secundary electrons is certainly the most logical approximation that can be introduced over and above those which were already made in the theory, if one wishes to arrive at final results such as (4.4-6) that are analytically expressible.

Putting $\beta = 0.2$ and evaluating the right-hand sides of (4.4-6) for the appropriate $\varkappa$-values, we can set up the following table of comparison:

$\varkappa$	$d\sigma_0/d\varkappa$ (4.1)	$d\sigma_0'/d\varkappa$ (4.4)	$d\sigma_1/d\varkappa$ (4.2)	$d\sigma_1'/d\varkappa$ (4.5)	$d\sigma_2/d\varkappa$ (4.3)	$d\sigma_2'/d\varkappa$ (4.6)
0	0	0	0	0	0	0
0.3	3.44	1.03	45.9	57.3	3.64	3.62
0.5	4.65	1.71	76.8	86.8	6.97	6.94
0.7	4.79	2.21	103.8	102.8	10.02	9.99
0.8	4.55	2.34	109.5	104.8	11.04	11.00
1.0	3.66	2.32	102.1	98.5	11.62	11.57
1.5	1.50	1.38	51.5	55.7	7.36	7.37
2.0	0.467	0.557	18.5	22.9	3.01	3.04
3.0	0.035	0.067	2.05	3.12	0.343	0.375
4.0	0.000	0.009	0.212	0.482	0.044	0.051

$\times 10^{-20}$ cm^2 .

From this table, it readily follows that $d\sigma_0'/d\varkappa$ is a rather poor approximation of the more accurate partial cross section resulting from (4.1) and our numerical calculations. On the contrary, the agreement between the $l = 1$ cross sections is much better, and for $l = 2$, it can be called excellent. This confirms a statement which we have already expressed in the beginning of Sect. 4 of our preceding article, namely, that the perturbation of a radial Coulomb wave function caused by the presence of the short-range attractive

potential in the Hartree potential which we obtained in ref. (1), must steadily diminish with increasing l. This was to be expected on the ground that, as l becomes larger, a radial wave function shows the tendency of growing more and more slowly as ϱ increases from zero on, so that the probability to find the described particle in the vicinity of the origin becomes smaller and smaller. Our table of comparison has the advantage of providing a more quantitative idea of the magnitude of the errors resulting from the replacement of helium wave functions by hydrogenic wave functions in the description of the final state. The fact that $\mathrm{d}\sigma_2/\mathrm{d}\varkappa$ and $\mathrm{d}\sigma_2'/\mathrm{d}\varkappa$ agree to within better than one percent over almost the entire $\varkappa$-range in which they are not negligibly small, not only proves the high accuracy of our numerical integration procedures expounded in (1), but also shows that at least for $0 \leqslant \varkappa < 3$, say, the normalized Coulomb wave function $F_{\varkappa 2}(\varrho)$ must be a very good approximation of the corresponding « perturbed » radial wave function $f_{\varkappa 2}^{(n)}(\varrho)$. This permits us to assert that for higher l-values, the difference between $F_{\varkappa l}(\varrho)$ and $f_{\varkappa l}^{(n)}(\varrho)$ must be quite negligible in the mentioned $\varkappa$-range, so that carrying out the numerical computation of $f_{\varkappa l}^{(n)}(\varrho)$ as we described in ref. (1) for $l = 0$, 1 and 2, would really be senseless for $l > 2$. This has as consequence that if, for some reason or another, it became necessary to calculate a partial cross section $\mathrm{d}\sigma_l(\beta, \varkappa)/\mathrm{d}\varkappa$ for a value of l larger than 2, one could simply use the appropriate Coulomb wave function with $Z = 1$ to describe the final state of the ejected electron and still be sure to find a result endowed with a much better accuracy than 1%.

* * *

The authors are indebted to the Institut Interuniversitaire des Sciences Nucléaires and to the Fonds National de la Recherche Scientifique for their financial support. They also express their gratitude towards the IBM of Belgium for the computational facilities offered to them. Finally, they wish to thank Prof. Dr. J. L. Verhaeghe for his interest in this work.

RIASSUNTO (*)

Scopo del presente lavoro è di stabilire una formula migliorata per la ionizzazione specifica primaria non relativistica degli elettroni in elio, come risultato di una teoria accuratamente sviluppata in cui vengono introdotte le funzioni d'onda dell'elio calcolate accuratamente invece delle meno accurate funzioni d'onda dell'idrogeno. La Sezione 1 presenta il calcolo della sezione trasversale differenziale per lo scattering

(*) *Traduzione a cura della Redazione.*

anelastico di un elettrone incidente su un atomo di elio in base al ben noto metodo per trattare le collisioni di riassestamento, che fa uso dell'approssimazione di Born. Nella Sezione 2 la formula risultante viene applicata al problema specifico considerato e si mostra in primo luogo che i termini dovuti ad effetti di scambio di spin possono essere trascurati nelle condizioni di validità prevalenti. Le varie parti della restante formula semplificata per la sezione d'urto differenziale vengono poi esplicitamente calcolate e, nella Sezione 3, vengono eseguite le sommatorie e gli integrali necessari, che infine conducono alla ionizzazione specifica primaria $S(\beta)$. Una di queste integrazioni viene studiata in modo particolarmente dettagliato in quanto necessita della introduzione di ulteriori approssimazioni semplificatrici. Si discute il nuovo risultato finale per $S(\beta)$, che viene messo a raffronto con una formula frequentemente usata derivata dal classico lavoro di Bethe sulla ionizzazione specifica primaria. Una rappresentazione grafica permette pure un confronto con alcuni dati sperimentali. La conclusione principale è che la nuova formula può spiegare sino al 25% del disaccordo fra la formula di Bethe ed i punti sperimentali. Il resto della differenza può essere compreso fisicamente. Infine la Sezione 4 è dedicata alle distribuzioni delle velocità degli elettroni secondari emessi dagli atomi di elio durante il processo di ionizzazione primaria in vari stati quantici del momento angolare caratterizzati dall'intero non negativo l. Si discute e si interpreta fisicamente il comportamento generale delle sezioni d'urto per intervalli $\varkappa$ unitari (essendo $\varkappa$ un conveniente parametro della velocità adimensionale) corrispondenti a $l=0$, 1 e 2. Queste sezioni d'urto sono anche confrontate con le corrispondenti espressioni analitiche in cui si usano le funzioni d'onda di Coulomb per descrivere approssimativamente gli stati finali degli elettroni emessi. Ne risulta che la concordanza è eccellente per $l=0$ e per tutti i valori di l maggiori.

IL NUOVO CIMENTO Vol. XIX, N. 5 1° Marzo 1961

I prodotti adimensionali caratteristici della magnetofluidodinamica.

A. M. Pratelli

Istituto di Matematica del Politecnico - Milano

(ricevuto il 12 Ottobre 1960)

Riassunto. — Mediante un'analisi dimensionale diretta (senza cioè far uso del sistema di equazioni che governa la m.f.d.) si cercano i parametri di forma in senso lato e i prodotti adimensionali caratteristici della m.f.d. Per rendere l'analisi più profonda e fruttuosa si scelgono sei grandezze come fondamentali (lunghezza L, densità materiale ϱ, velocità V, temperatura assoluta θ, induzione magnetica B e costante universale c' delle equazioni di Maxwell). Si costruiscono, oltre ai classici prodotti della meccanica dei fluidi, quelli già noti in m.f.d. ed altri prodotti che sono indipendenti dai precedenti e che inoltre non hanno avuto occasione di esser messi in luce. Si illustra il significato fisico dei parametri e dei prodotti e si mostra che i numeri costruiti in conformità di particolari sistemi di misura (gaussiano, elettrostatico, elettromagnetico, Giorgi) sono casi particolari di quelli qui trovati. Infine i prodotti trovati si applicano per verificare ed estendere la similitudine di T. Kihara.

1. – Introduzione.

Non appena fu affrontato, col nome di « Hg-dynamics », lo studio [1] delle interazioni tra un fluido conduttore in moto e il campo elettromagnetico ad esso collegato, vennero introdotti alcuni numeri adimensionali, cui fu dato successivamente il nome di « numero di Hartmann » e numero di « Reynolds

[1] J. Hartmann: *Kgl. Dan. Vid. Sels. Math. Fis. Medd.*, **15**, n. 6 (1937); J. Hartmann e I. Lazarus: *Kgl. Dan. Vid. Sels. Math. Fis. Medd.*, **15**, n. 7 (1937).

magnetico » [2]. Altri numeri si son mostrati utili allo studio delle applicazioni astrofisiche della magnetoidrodinamica e, più recentemente ancora, allo studio delle applicazioni all'aerodinamica ipersonica: ad esempio, il « numero di Alfvén » [3,4] o numero di « Mach magnetico » [5].

Benchè siano stati messi in evidenza altri numeri oltre quelli citati sopra (« altri » nel senso di indipendenti da questi), il sistema dei prodotti adimensionali finora noto non può dirsi completo; ciò è presumibilmente dovuto al fatto che la complessità matematica del sistema di equazioni suggerisce di adottare talune ipotesi semplificatrici (che verranno richiamate in seguito, e che sono più o meno direttamente collegate con l'ipotesi che la velocità del fluido sia di gran lunga minore di quella della luce nel vuoto e che la conducibilità del fluido sia alta).

E dal momento che i numeri caratteristici della classica meccanica dei fluidi, aggiunti a quelli utili allo studio della propagazione del calore, a quelli che si incontrano nel campo elettromagnetico e a quelli citati all'inizio non sono sufficienti per tutte le necessità della magnetofluidodinamica così come è intesa oggi, mi sembra interessante cercare di predisporre una tabella di prodotti adimensionali fin dove possibile completa. Ciò potrà essere utile sia per meglio caratterizzare il significato delle ipotesi semplificatrici già adottate, sia per rendersi conto dell'ordine delle approssimazioni, sia in vista di similitudini magnetofluidodinamiche.

Procedimenti e considerazioni di natura dimensionale sono stati già applicati da Elsasser [6,7], da Landshoff [8] e da Grad e Rose [9] senza che il problema possa dirsi esaurito.

In casi del genere, le strade mi sembra che siano essenzialmente due. Si può scrivere in forma adimensionale il sistema di equazioni che reggono la magnetofluidodinamica (che d'ora innanzi indicherò brevemente m.f.d.) cosicchè i prodotti adimensionali cercati vengono messi in evidenza sotto forma di coefficienti di taluni addendi delle equazioni. Questo procedimento si segue, ad esempio, nello studio delle equazioni della meccanica dei fluidi [10] ed è stato

---

[2] T. G. Cowling: *Magnetohydrodynamics* (New York, 1957).

[3] I. Imai: *Proc. 2nd Int. Congr. Aer. Scien.* (Zurigo, 1960), (in corso di stampa).

[4] W. R. Sears e E. L. Resler jr.: *Proc. 2nd Int. Congr. Aer. Scien.* (Zurigo, 1960), (in corso di stampa).

[5] T. von Kármán: *Proc. 9th Int. Astr. Congr. Amsterdam* 1958, vol. 2 (Wien, 1959), p. 644.

[6] W. M. Elsasser: *Phys. Rev.*, **95**, 1 (1954).

[7] W. M. Elsasser: *Magnetohydrodynamics, A Symposium* (Stanford, 1957), p. 16.

[8] R. K. M. Landshoff: *Magnetohydrodynamics, A Symposium* (Stanford, 1957), p. 69.

[9] H. Grad e M. H. Rose: *Dimensional considerations*, NYO-0486; *Notes on Magnetohydrodynamics* - II, Inst. Mat. Sc. NYU (Aug. 7, 1956).

[10] Cfr. ad es. B. Finzi: *Lezioni di aerodinamica* (Milano, 1960), pp. 18, 76.

già seguito, in m.f.d. da S. I. Pai [11] e L. G. Napolitano [12], i quali hanno messo in luce alcuni numeri (il « numero di Reynolds magnetico » e quello cui darò il nome di « numero Cauchy magnetico), rinunciando però implicitamente a metterne in luce altri, che in conformità alle ipotesi semplificatrici venivano assunti eguali a zero o a uno; poichè tuttavia manca un sistema di equazioni unanimemente accettato dagli studiosi di m.f.d., ritengo opportuno seguire l'altra strada, cioè procedere mediante un'analisi dimensionale pura e semplice.

Una volta precisato il numero n delle grandezze determinanti indipendenti, e il numero m delle grandezze scelte come fondamentali, il numero dei prodotti caratteristici π_i ci viene indicato in $n - m$ dal teorema « π », così denominato per la difficoltà di citarne tutti gli autori [13].

La costruzione effettiva dei prodotti caratteristici π_i (o « rapporti », o « invarianti », o « numeri ») è possibile mediante vari procedimenti [14] che presuppongono la conoscenza delle dimensioni delle grandezze determinanti rispetto a quelle di carattere, dirò così, basilare, come lunghezza, tempo e massa per la meccanica. Senonchè è facile constatare che tali procedimenti sono in varia misura rapidi ed eleganti quando si ha a che fare con un ristretto campo di ricerca (ad esempio un problema di propagazione del calore o un problema di meccanica dei fluidi nel senso stretto della parola) mentre risultano un po' macchinosi e pesanti (sia pure in varia misura) quando si vogliano applicare alla m.f.d., col grave inconveniente di dover rifare gran parte dei calcoli se a un certo momento ci si trova nella necessità di aggiungere, all'elenco delle n grandezze determinanti, una $n+1$-esima grandezza.

In merito al numero m delle grandezze indipendenti assunte come fondamentali, è ben noto che le considerazioni dimensionali sono tanto più fruttuose quanto più m è grande [15].

Nel campo della meccanica, è pacifico che se ne debbono scegliere tre, ad esempio, lunghezza L, massa M e tempo T. Se sono in gioco fenomeni termici, potrebbero ancora bastare tre grandezze, ricordando che la temperatura è una densità d'energia; in conformità a quanto detto sopra conviene invece intro-

---

[11] S. I. Pai: *Introduction to the Theory of Compressible Flow* (Princeton, 1959), p. 358.

[12] L. G. Napolitano: *Missili* **1**, 15 (1959).

[13] A. Signorini: *I modelli della tecnica*, in *Atti del Convegno di Venezia*, 1955 vol. **1** (Roma, 1956), pp. XI-XXIV.

[14] Nella comunicazione presentata dallo scrivente al VI Congresso dell'U.M.I. (Napoli, 1959) (in corso di stampa negli Atti di tale congresso) le grandezze scelte come fondamentali erano quattro (L, V, ϱ, H) e veniva seguito il procedimento di identificazione diretta di Lord Raileigh: *Proc. Roy. Soc. London*, **66**, 74 (1899-1900).

Per altri procedimenti cfr. L. Brand: *Arch. Rat. Mech.*, **1**, 35 (1957-58); W. J. Duncan: *Physical Similarity and Dimensional Analysis* (London, 1955); D. C. Ipsen: *Units, Dimensions and Dimensionless Numbers* (New York, 1960).

[15] A proposito dei valori di m si veda E. Fues: *Zeits. Phys.*, **107**, 662 (1937).

durre una quarta grandezza fondamentale, ad esempio la temperatura assoluta θ [16].

Per lo studio di fenomeni elettromagnetici, potrebbero sempre bastare tre grandezze fondamentali (cioè sostanzialmente potremmo valerci del sistema di unità gaussiane o di quello elettrostatico o di quello elettromagnetico); meglio introdurre una quarta unità indipendente dalle tre meccaniche (cioè sostanzialmente valerci del sistema di unità di Giorgi); ma è più opportuno ancora valerci della libertà concessa quando si tratta di decidere in merito a un sistema di misura [17] scegliendo due grandezze fondamentali in aggiunta alle tre meccaniche, cosicchè in totale $m = 5$.

In m.f.d., ove alle grandezze meccaniche si aggiungono quelle termiche e quelle elettromagnetiche, conviene quindi che il numero delle grandezze scelte come fondamentali, sia $m = 6$.

Qualunque siano le grandezze fondamentali scelte (come, ad esempio, L, M, T, θ, la carica elettrica Q e il flusso magnetico Φ) non si trovano già pronte e tabellate le dimensioni delle grandezze determinanti rispetto alle sei scelte come fondamentali, cosicchè i procedimenti citati, che nella quasi totalità comportano la risoluzione di m equazioni algebriche lineari in n incognite, non sono applicabili.

Per questo costruisco i prodotti mediante un procedimento diverso [18]:

1) elencate le grandezze determinanti, scelgo le sei grandezze fondamentali;

2) successivamente valuto le dimensioni di tutte le grandezze rispetto alle sei fondamentali. Se due o più grandezze han le stesse dimensioni, una verrà scelta come determinante, e i rapporti tra grandezze di egual natura, cioè di eguali dimensioni, assumono l'aspetto di parametri o fattori di forma (fattori di forma intesi in senso lato, come ad esempio, il rapporto tra la velocità del fluido e la velocità del suono, cioè il « numero di Mach »);

3) i prodotti caratteristici π_i si ottengono allora dividendo per la grandezza in esame le grandezze fondamentali prese con gli esponenti corrispondenti alle dimensioni della grandezza stessa.

Nella Sezione **2** elenco tutte le grandezze determinanti, e nella successiva

---

[16] È noto che nei problemi di propagazione del calore conviene addirittura prendere anche la quantità di calore come grandezza fondamentale: qui non è il caso perchè hanno luogo trasformazioni tra una forma e un'altra di energia; cf. Lord Rayleigh: *Nature*, **95**, 66 e 664 (1915).

[17] Vedi anche più oltre, Sez. **3** e nota [23].

[18] Non mi risulta fino a qual punto il procedimento qui seguito sia usato altrove; la letteratura sull'analisi dimensionale è talmente vasta che questo procedimento potrebbe anche esser già noto.

costruisco la tabella con i parametri di forma e i prodotti caratteristici. Nella Sezione **4** illustro il significato fisico dei λ_j e dei π_i ed espongo i legami tra i prodotti trovati e i numeri già noti.

Dando poi a c' particolari valori trovo (nella Sezione **5**) i legami tra i π_i da me presentati e quelli che si otterrebbero usando particolari sistemi di misura.

I risultati si basano, ripeto, su ipotesi e procedimenti di natura strettamente dimensionale: ove si introducano altre ipotesi (ad esempio, che la trasformazione sia isentropica o il gas sia perfetto) i numeri possono venir presentati diversamente.

Da ultimo mostro che il criterio di similitudine che T. KIHARA ([19]) deduce dall'esame del suo sistema di equazioni, è soddisfatto ed esteso dall'esame dei prodotti π_i.

2. – Elenco delle grandezze determinanti e loro simboli.

È opportuno, appunto perchè non scrivo il sistema di equazioni, delimitare la sfera di competenza della m.f.d., la quale al presente si occupa più dei gas ionizzati che dei metalli liquidi. Il fluido conduttore verrà qui considerato come un continuo; siffatta descrizione, detta anche macroscopica ([20]) o fenomenologica, costituisce una buona approssimazione quando il cammino libero delle particelle è piccolissimo in confronto a lunghezze aventi interesse fisico ([21]).

Le grandezze di cui la m.f.d. si occupa di solito nello schema precisato sono (comprendendo nell'elenco anche quelle che non sono indipendenti):

$a = \sqrt{\mathrm{d}p/\mathrm{d}\varrho}$ velocità del suono nel fluido considerato;

B, B_c induzione magnetica (o densità di flusso magnetico) del fluido o del corpo immerso nel fluido;

c velocità della luce nel vuoto;

([19]) T. KIHARA: *Journ. Phys. Soc. Japan*, **13**, 473 (1958).

([20]) Per la distinzione tra impostazione *macroscopica* e impostazione *microscopica* cf. ad es. H. ALFVÉN: *Rendiconti S.I.F.* Corso XIII (Bologna, 1960), p. 7.

([21]) In altre parole resta escluso quanto può interessare la dinamica dei gas rarefatti o superaerodinamica; ciò equivale a considerare praticamente nullo il numero di Knudsen (rapporto tra il cammino libero delle molecole ed una lunghezza caratteristica). Parimenti il trattare come « continuo » un gas ionizzato significa trascurare il fatto che in realtà si tratta di una miscela di elettroni (aventi carica $-e$) e di ioni (aventi carica $+e$); si rinuncia quindi a introdurre un coefficiente di diffusione e in conseguenza non si trova nè il numero di Schmid nè quello di Lewis: per questi numeri cf. P. S. LYKOUDIS: *Proc. 9th Int. Astr. Congr. Amsterdam*, 1958 (Wien, 1959), p. 169 e L. G. NAPOLITANO: *Proc. 9th Int. Astr. Congr. Amsterdam*, 1958 (Wien, 1959), p. 570.

c_n velocità di fase della luce nel fluido;

c' costante universale delle equazioni di Maxwell;

c_p, c_v calore specifico (dell'unità di massa) a pressione o a volume costante;

D spostamento elettrico;

E campo elettrico;

f frequenza caratteristica;

F risultante (resistenza o portanza) delle forze di origine strettamente meccanica che agiscono sul solido immerso nel fluido;

g accelerazione di gravità;

H campo magnetico;

K densità di corrente elettrica superficiale (rotore superficiale della differenza tra il campo magnetico del fluido e quello del corpo);

J densità di corrente elettrica (definita tenendo presente che J^2/σ è il calore dissipato per effetto Joule per unità di volume e di tempo);

L lunghezza caratteristica del fenomeno in esame;

M momento delle forze di origine strettamente meccanica che agiscono sul corpo immerso nel fluido;

m momento del dipolo magnetico del solido immerso (integrale triplo della magnetizzazione);

$n = c/c_n$ indice assoluto di rifrazione;

p pressione;

Q carica elettrica;

$R = c_p - c_v$ costante dei gas;

T tempo;

V valore caratteristico della velocità del fluido nel fenomeno in esame;

$\overline{v}$ media quadratica delle fluttuazioni di velocità della turbolenza isotropica;

α coefficiente di dilatazione lineare;

$\gamma = c_p/c_v$ rapporto tra i calori specifici (esponente dell'adiabatica);

γ_s tensione superficiale (su eventuali superfici libere del fluido);

$\varepsilon = \varepsilon_r \varepsilon_0$ permettività o costante dielettrica del fluido (ε_r relativa, ε_0 nel vuoto);

$\eta = \varrho\nu$ viscosità dinamica;

θ, θ_c temperatura assoluta del gas, e del solido immerso;

λ conducibilità termica o interna;

Λ scala della turbolenza;

$\mu = \mu_r \mu_0$ permeabilità magnetica del fluido (μ_r relativa, μ_0 nel vuoto);

ν viscosità cinematica;

ϱ densità materiale (massa/cubo della lunghezza caratteristica);

ϱ_e densità di carica elettrica;

σ conducibilità elettrica (reciproco della resistenza specifica);

σ_s densità di carica elettrica superficiale (divergenza superficiale della differenza tra lo spostamento elettrico del fluido e quello del solido immerso);

$\chi = \lambda/\varrho c_p$ conducibilità termometrica o diffusività termica.

3. – Scelta delle sei grandezze fondamentali. Costruzione dei λ_j e dei π_i.

Secondo la tradizione della meccanica dei fluidi, scelgo come fondamentali una lunghezza L (e se nella corrente è immerso un solido, L potrà essere una lunghezza del solido stesso), un valore V della velocità del fluido e un valore ϱ della densità materiale.

Come quarta grandezza fondamentale indipendente assumo la temperatura assoluta θ; questa convenzione è confortata dal fatto che è lecito cambiare l'unità di misura della temperatura senza dover necessariamente modificare le unità di misura per le grandezze meccaniche ([22]). In vista degli scambi di energia che hanno luogo in m.f.d., una quantità di calore (come, del resto, una quantità di energia elettrica o magnetica) è espressa in unità meccaniche e quindi ha le dimensioni $[\varrho L^3 V^2]$.

Resta da decidere in merito alle grandezze fondamentali indipendenti di natura elettromagnetica: a tale scopo giova rammentare che ([23]) le unità di

---

([22]) È del resto noto che nella similitudine aerodinamica si trova comodo prendere come grandezze fondamentali L, ϱ, V, θ; cf. ad es. E. Pistolesi: *I modelli della tecnica* in *Atti del Convegno di Venezia* 1955, vol. 1 (Roma, 1956), p. 481.

([23]) Ricordo, per comodità del lettore, come si giunge al legame tra ε_0, μ_0, c e c': si cerchino in primo luogo i legami tra le dimensioni di E, B, ε, μ, c', esaminando le equazioni di Maxwell

$$\text{(I-}a\text{)} \quad -\frac{1}{c'}\frac{\partial \boldsymbol{B}}{\partial t} = \operatorname{rot} \boldsymbol{E}; \qquad \text{(I-}b\text{)} \quad \frac{1}{c'}\frac{\partial \varepsilon \boldsymbol{E}}{\partial t} = \operatorname{rot} \frac{\boldsymbol{B}}{\mu}.$$

Le corrispondenti equazioni dimensionali sono

$$\text{(II-}a\text{)} \quad [c'^{-1} B T^{-1}] = [E L^{-1}]; \qquad \text{(II-}b\text{)} \quad [c'^{-1} \varepsilon E T^{-1}] = [B \mu^{-1} L^{-1}];$$

moltiplicando membro a membro (II-a) e (II-b), con ovvie semplificazioni, risulta

$$\text{(III)} \qquad [c'^2 \varepsilon^{-1} \mu^{-1}] = [L^2 T^{-2}] = Sr^2[V^2],$$

misura in elettromagnetismo debbono obbedire al legame

$$c^2 = c'^2/\varepsilon_0\mu_0 .$$

Quindi due delle tre grandezze al secondo membro possono venir scelte ad arbitrio e la terza risulta determinata in conseguenza.

Il sistema di Gauss, che suppone ε e μ adimensionali, e quindi D, E, B, H, aventi tutt'e quattro le medesime dimensioni, è il meno felice ai fini di una analisi dimensionale diretta, perchè non ci permette di trovare nessun numero contenente ε o μ.

Il sistema elettrostatico, in cui ε è considerato numero puro, mentre $\mu_0 = 1/c^2$, non presenta interesse se si debbono effettuare misure di grandezze magnetiche, ma è invece utile se si vuol fare dell'analisi dimensionale perchè il considerare ε numero puro costringe a rinunciare *a priori* a trovare la per-

ove Sr è il numero di Strouhal; nei successivi passaggi supporremo $Sr=1$ per semplicità. Dividendo invece membro a membro (II-*a*) e (II-*b*) e ricordando le dimensioni della densità d'energia, troviamo

$$[B^2/\mu] = [\varepsilon E^2] = [\rho V^2] . \qquad \text{(IV)}$$

Le (III) e le (IV) sono in tutto tre equazioni dimensionali che legano le 5 grandezze E, B, ε, μ, c' alle ϱ, L, V. Possiamo fare varie scelte:

a) se assumiamo ε e μ numeri puri, c' ha le dimensioni d'una velocità: si ottiene il sistema gaussiano, in cui $c'=c$ e $\varepsilon_0=\mu_0=1$;

b) se assumiamo ε e c' numeri puri, le dimensioni di μ sono date da $[\mu]=[V^{-2}]$; otteniamo il sistema elettrostatico, in cui $\mu_0=c^{-2}$, $\varepsilon_0=1$, $c'=1$;

c) se assumiamo μ e c' numeri puri, le dimensioni di ε son date da $[\varepsilon]=[V^{-2}]$; otteniamo il sistema elettromagnetico, in cui $\varepsilon_0=c^{-2}$, $\mu_0=1$, $c'=1$;

d) se supponiamo che tanto ε quanto μ abbiano le dimensioni del reciproco d'una velocità e solo c' sia numero puro, otteniamo il sistema suggerito da Hertz;

e) se supponiamo ancora che solo c' sia numero puro, permettendo alla permeabilità magnetica e alla permettività elettrica di avere dimensioni diverse da quelle prese dalla meccanica, ε e μ rimangono legate da $[\varepsilon\mu]=[V^{-2}]$; allora anche nel vuoto $[E]\neq[D]$, $[B]\neq[H]$; posto $c'=1$, $\varepsilon_0\mu_0c^2=1$, abbiamo il sistema di Giorgi, in cui alle tre grandezze meccaniche aggiungiamo una quarta grandezza (in questa sede non ci interessa se si tratta della carica elettrica o altro);

f) se infine tutte e tre le grandezze ε, μ, c' son considerate dimensionate, sempre però in obbedienza alla (III), allora alle tre grandezze meccaniche aggiungiamo *due* grandezze elettromagnetiche (in questa sede non ci interessa quali) e otteniamo in sostanza il sistema ideato da Cohn.

Per i casi *a*), *b*), *c*) cf. G. Maggi: *Teoria fenomenologica del campo elettromagnetico* (Milano, 1931), p. 184; per il caso *d*) cf. H. Hertz: *Gesammelte Werke*, **2**, 215 (1894); per altri sistemi di unità che non introducono altre dimensioni all'infuori di quelle della meccanica cf. J. Palacios: *Analyse Dimensionelle* (Paris, 1960), p. 150; per il sistema a cinque unità cf. E. Cohn: *Das elektromagnetische Feld* (Leipzig, 1901); cf. anche A. Sommerfeld: *Elektrodynamik* (Wiesbaden, 1948).

mettività in qualche numero caratteristico, ma il danno è limitato se si accetta l'ipotesi che in via di massima le grandezze elettriche sono trascurabili in m.f.d.

Invece il sistema elettromagnetico, di indubbia utilità se si debbono effettuare delle misurazioni in m.f.d. ed ivi usato da parecchi autori ([24]), è meno fruttuoso ai fini della nostra analisi dimensionale, perchè μ è considerato numero puro e quindi rinunciamo *a priori* a trovarlo in numeri caratteristici.

Il sistema di Giorgi, in cui ε e μ sono due grandezze dimensionali, è più fruttuoso dei precedenti.

Però i numeri caratteristici « classici » (come ad esempio, il numero di Reynolds) mettono d'accordo lo sperimentatore che compie misure facendo uso del sistema metrico decimale con lo sperimentatore che compie misure in yarde e in libbre, perchè tali numeri non recano traccia del sistema di misura usato; e per mettere d'accordo lo sperimentatore che usa il sistema di Gauss con quello che usa il sistema di Giorgi mi par opportuno far rientrare tali sistemi come casi particolari del sistema che considera come fondamentali (cioè dimensionalmente indipendenti) B e c'; ciò non significa che B e c' debbano venir prese come unità di misura, ma solo che è fruttuoso sceglierle come grandezze fondamentali ai fini della nostra analisi dimensionale ([25]): cosicchè complessivamente abbiamo, oltre alla temperatura assoluta, cinque grandezze.

Poichè stiamo facendo considerazioni strettamente dimensionali, tutti i prodotti risulteranno privi di coefficienti numerici.

La tabella ([26]) che segue espone nella prima colonna le grandezze determinanti, nelle successive gli esponenti delle sei grandezze fondamentali, nella penultima i parametri di forma in senso lato e nell'ultima i numeri caratteristici.

([24]) Per il fluido, ma non per il corpo immerso nella corrente, l'inconveniente è mitigato dalla considerazione che il fluido è non-ferromagnetico, cosicchè il valore della permeabilità magnetica μ coincide con buona approssimazione con quello del vuoto μ_0, vale a dire $\mu_r \simeq 1$; cf. E. L. Resler e W. R. Sears: *Journ. Aero-space Sc.*, **25**, 235 (1958).

([25]) Una volta stabilite le dimensioni di μ, ε, E, le dimensioni di H e di K si ottengono da $[H]=[B/\mu]$; quelle di D e di σ_s da $[D]=[\varepsilon E]$; quelle della densità spaziale di carica elettrica dalla sua definizione $\rho_e = \mathrm{div}\, D$; le dimensioni della densità di corrente elettrica da $[J]=[\rho_e V]$ oppure da $[J]=[\partial D/\partial t]$; le dimensioni della conducibilità σ da $[J]=[\sigma E]=[\sigma(E+V/c'\wedge B)]$ oppure da $[J^2/\sigma]=[\rho V^2/T]$. Le dimensioni del momento magnetico m si ottengono ricordando che tale grandezza è l'integrale triplo, esteso al corpo, della magnetizzazione, che a sua volta ha le dimensioni del campo H.

([26]) L'elenco della prima colonna della tabella cerca di esser completo nei confronti delle grandezze di diverse dimensioni, rinunciando a elencare tutte le grandezze che hanno eguali dimensioni e il cui rapporto è un fattore di forma in senso lato.

TABELLA I.

	L	V	ϱ	θ	B	c'	λ_j	π_i
A	1	—	—	—	—	—	$\lambda_1 = L/A$	
$\left\{\begin{matrix} a, \bar{v} \\ c, c_n \end{matrix}\right\}$	—	1	—	—	—	—	$\left\{\begin{matrix} \lambda_2 = V/a;\ \lambda_3 = \bar{v}/V \\ \lambda_4 = V/c;\ \lambda_5 = V/c_n \end{matrix}\right\}$	
$\theta_c, 1/\alpha$	—	—	—	1	—	—	$\lambda_6 = \theta/\theta_c;\ \lambda_7 = \theta\alpha$	
B_c	—	—	—	—	1	—	$\lambda_8 = B/B_c$	
$T, 1/f$	1	−1	—	—	—	—	$\lambda_9 = Tf$	$\pi_1 = L/VT;\ \lambda_9\pi_1 = Lf/V$
ν	1	1	—	—	—	—		$\pi_2 = L V/\nu$
p	—	2	1	—	—	—		$\pi_3 = \varrho V^2/p$
g	−1	2	—	—	—	—		$\pi_4 = V^2/gL$
γ_s	1	2	1	—	—	—		$\pi_5 = \varrho L V^2/\gamma_s$
F	2	2	1	—	—	—		$\pi_6 = \varrho L^2 V^2/F$
M	3	2	1	—	—	—		$\pi_7 = \varrho L^3 V^2/M$
λ	1	3	1	−1	—	—		$\pi_8 = \varrho L V^3/\lambda\theta$
c_p, c_v	—	2	—	−1	—	—	$\lambda_{10} = c_p/c_v$	$\pi_9 = V^2/\theta c_p$
μ	—	−2	−1	—	2	—		$\pi_{10} = B^2/\mu\varrho V^2$
ε	—	—	1	—	−2	2		$\pi_{11} = \varrho c'^2/\varepsilon B^2$
E	—	1	—	—	1	−1		$\pi_{12} = VB/Ec'$
H, K	—	2	1	—	−1	—	$\lambda_{11} = H/K$	$\pi_{13} = \varrho V^2/KB$
D, σ_s	—	1	1	—	−1	1	$\lambda_{12} = \sigma_s/D$	$\pi_{14} = \varrho V c'/\sigma_s B$
J	−1	2	1	—	−1	1		$\pi_{15} = \varrho V^2 c'/JLB$
σ	−1	1	1	—	−2	2		$\pi_{16} = \varrho V c'^2/\sigma L B^2$
ϱ_e	−1	1	1	—	−1	1		$\pi_{17} = \varrho V c'/\varrho_e LB$
m	3	2	1	—	−1	—		$\pi_{18} = L^3\varrho V^2/mB$

4. – Significato fisico dei λ_j e dei π_i e legami con numeri noti.

Il parametro $\lambda_1 = L/\Lambda$ è noto e non ha particolare nome;

» $\lambda_2 = V/a = Ma$ è il « numero di Mach »;

» $\lambda_3 = v/V = i$ prende il nome di « indice di turbolenza »;

» $\lambda_4 = V/c$ (rapporto tra la velocità caratteristica del fluido e la velocità della luce nel vuoto) è di solito indicato in relatività con β; ma β ha anche altri significati in aerodinamica e per questo preferisco denominarlo « numero di Lorentz » e indicarlo con $Lo = V/c$.

Il parametro $\lambda_5 = V/c_n = (V/c)(c/c_n) = Lo \cdot n$ è eguale al prodotto del numero di Lorentz per l'indice assoluto di rifrazione. Poichè nella m.f.d. ordinaria Lo si considera praticamente nullo (o almeno lo si considera tale nelle applicazioni astrofisiche) non si usa distinguere tra V/c e V/c_n; ma la distinzione ha motivo d'esser chiara in m.f.d. relativistica e in quelle regioni in cui l'indice assoluto di rifrazione è sensibilmente diverso da 1.

Evito di esaminare uno per uno tutti i rimanenti parametri di forma, trattandosi in genere del rapporto tra il valore d'una grandezza relativa al fluido e il valore della stessa grandezza di eguali dimensioni riferita al solido immerso nel fluido; il parametro $\lambda_{10} = c_p/c_v = \gamma$ è ben noto.

Il numero $\pi_1 = L/TV$ è il reciproco del « numero di Thomson » $Th = TV/L$; se al posto del tempo sostituiamo il reciproco di una frequenza caratteristica f, o meglio se eseguiamo il prodotto $\pi_1 \lambda_9$, allora troviamo il « numero di Strouhal » $Sr = Lf/V$.

Il numero $\pi_2 = (LV/\nu) = (LV\varrho/\eta) = Re$ è « il numero di Reynolds »; scritto nella forma $Re = \varrho L^2V^2/\eta LV$ tale numero si presenta come rapporto tra due forze: la forza d'inerzia e la forza viscosa.

Il numero $\pi_3 = \varrho V^2/p = (\varrho V^2/2)/(p/2) = Ca$ è il « numero di Cauchy »; esso esprime il rapporto tra la cosiddetta pressione dinamica e la metà della pressione, cioè il rapporto tra la densità d'energia cinetica e la metà della pressione.

Il numero $\pi_4 = V^2/gL = Fr$ è il « numero di Froude o di Reech » ([27]); scritto nella forma $Fr = \varrho L^2V^2/\varrho L^3 g$ esprime il rapporto tra la forza d'inerzia e il peso totale del solido immerso nella corrente fluida.

Il numero $\pi_5 = \varrho LV^2/\gamma_s = \varrho L^2V^2/\gamma_s L = We$ è il « numero di Weber », anch'esso interpretabile come rapporto tra due forze (forza d'inerzia e forza di tensione superficiale).

Il reciproco del numero $\pi_6 = \varrho L^2V^2/F$ è noto come coefficiente di portanza o di resistenza, a seconda che F esprima la portanza o la resistenza (di natura strettamente meccanica) che si esercitano tra solido e fluido.

([27]) R. COMOLET: *Introduction à l'analyse dimensionelle et aux problèmes de similitude en mécanique des fluides* (Paris, 1958), p. 76.

Infine il reciproco del numero $\pi_7 = \varrho L^3 V^2/M$ prende il nome di « coefficiente del momento » (anche qui converrà precisare che si tratta del momento dovuto alle azioni meccaniche che si esercitano tra solido e fluido).

I numeri π_8 e π_9, come tali, non hanno un nome particolare. Essi si riconducono facilmente a numeri noti, perchè possiamo scrivere

$$\pi_8 = \frac{L\varrho V^3}{\lambda\theta} = \frac{\varrho\nu c_p}{\lambda}\,\frac{c_v}{c_p}\,\frac{LV}{\nu}\,\frac{\varrho V^2}{\varrho\theta c_v},$$

ove il primo fattore, cioè

$$Pr = \frac{\nu}{\chi} = \frac{\eta c_p}{\lambda} = \frac{\varrho\nu c_p}{\lambda},$$

è il classico « numero di Prandtl »; l'ultimo fattore invece esprime il rapporto tra il doppio della densità d'energia cinetica e la densità dell'energia interna del fluido supposto perfetto, numero che chiamerei « numero di Cauchy interno » $Ci = \varrho V^2/\varrho\theta c_v$; cosicchè possiamo scrivere

$$\pi_8 = \frac{Pr\,Re\,Ci}{\gamma}.$$

Analogamente si può scrivere

$$\pi_9 = \frac{V^2}{\theta c_p} = \frac{\varrho V^2}{\varrho\theta c_v}\,\frac{c_v}{c_p} = \frac{Ci}{\gamma}.$$

Quanto sopra è sostanzialmente noto ([28]), e mi son permesso richiamarlo solo perchè ci sarà utile per i legami con i « nuovi » numeri.

Il numero $\pi_{10} = B^2/\mu\varrho V^2 = (B^2/2\mu)/(\varrho V^2/2)$ esprime il rapporto tra la densità d'energia magnetica e la densità d'energia cinetica o, se si preferisce, tra la pressione magnetica e la pressione dinamica della corrente. Il suo reciproco, per analogia col numero di Cauchy, mi sembra giusto indicarlo come « numero di Cauchy magn tico » Cm ponendo ([29])

$$Cm = \frac{\mu\varrho V^2}{B^2} = \frac{1}{\pi_{10}}.$$

Poichè d'altra parte la velocità di propagazione delle onde di Alfvén è

([28]) Per i legami con i numeri di Nusselt e di Fourier si veda ad es. W. I. Duncan: l. c. ([14]) e G. Bozza: *Rend. Sem. Mat. Fis. Milano*, 7, 13 (1933).

([29]) Il numero qui indicato con Cm è indicato con R_H da S. I. Pai: l. c. ([11]) e con Pm da L. G. Napolitano: l. c. ([12]).

$V_A = B/\sqrt{\mu\varrho}$, possiamo denominare « numero di Alfvén » Al il numero [30]

$$Al = V/V_A = V\sqrt{\mu\varrho}/B$$

e in tal caso avremo $\pi_{10} = Al^2 = 1/Cm$.

Il numero Al è anche denominato « numero di Alfvén-Mach » [31] o « numero di Mach magnetico » [32].

Il numero π_{11} può scriversi

$$\pi_{11} = \frac{c'^2}{\varepsilon\mu V^2}\frac{\varrho\mu V^2}{B^2} = \frac{c_n^2}{c^2}\frac{c^2}{V^2}\frac{\mu\varrho V^2}{B^2} = \frac{Cm}{n^2 Lo^2},$$

tale numero è praticamente infinito nell'ordinaria m.f.d.; è significativo il suo legame con π_{16}, che vedremo in seguito.

Il numero π_{12} può venir variamente interpretato; il rapporto $B/Ec' = v_s$ ha le dimensioni di una velocità ed esprime la velocità di una trasformazione di Lorentz in cui scompare la componente di E perpendicolare alla velocità stessa. Il numero $\pi_{12} = VB/Ec' = V/v_s$ potrebbe venir chiamato « numero di scorrimento » [33]; nell'ordinaria m.f.d. viene supposto $\pi_{12} \simeq 1$.

Mi sembra utile far osservare che si può scrivere

$$\pi_{12} = \frac{B/\sqrt{\mu}}{\sqrt{\varepsilon}E}\frac{V\sqrt{\varepsilon}\sqrt{\mu}}{c'} = \sqrt{\frac{B^2}{\mu\varrho V^2}}\sqrt{\frac{\varrho V^2}{\varepsilon E^2}}\frac{c}{c_n}\frac{V}{c};$$

se denominiamo « numero di Cauchy elettrico » il rapporto tra l'energia cine-

---

[30] I. Imai: l. c. [3].

[31] W. R. Sears e E. L. Resler jr.: l. c. [4].

[32] T. von Kármán: l. c. [5], p. 648. La denominazione di numero di Mach magnetico non sembra del tutto felice, anche pensando al legame tra il numero di Mach Ma e il numero di Cauchy Ca nel caso dei gas perfetti, in condizioni isentropiche. In conseguenza di tali ipotesi semplificatrici, estranee all'analisi dimensionale, la velocità del suono è data da $a = \sqrt{p\gamma/\varrho}$: ciò modifica il numero delle grandezze indipendenti, e in tali circostanze si trova il noto legame tra Ma e Ca:

$$Ma = \frac{V\sqrt{\varrho}}{\sqrt{p\gamma}} = \sqrt{\frac{\varrho V^2}{p\gamma}} \qquad \text{ossia} \qquad Ca = \gamma\, Ma^2.$$

Analogamente, essendo $p = \varrho(c_p - c_v)\theta$, si trova facilmente il legame tra π_9 e il numero di Mach Ma.

È superfluo elencare tutte le conseguenze che le suddette ipotesi, o altre analoghe, recano all'elenco dei numeri caratteristici della m.f.d.

[33] Questo nome mi è suggerito dall'interpretazione che R. K. M. Landshoff: l. c. [8] dà al rapporto B/Ec'; vedi anche L. Spitzer jr.: *Physics of Fully Ionized Gases* (New York, 1956).

tica e l'energia elettrica, cioè se poniamo $Ce = \varrho V^2/\varepsilon E^2$, allora possiamo scrivere

$$\pi_{12} = n\, Lo \sqrt{\frac{Ce}{Cm}}.$$

In armonia con l'ipotesi $\pi_{12} \simeq 1$ e con l'ipotesi $Lo \simeq 0$, Ce è grandissimo di fronte a Cm, cioè l'energia elettrica è trascurabile di fronte all'energia magnetica.

Il numero $\pi_{13} = \varrho V^2/KB$ esprime il rapporto tra la pressione dinamica del fluido e la pressione dovuta al campo magnetico e alla corrente elettrica superficiale e lo indico con $Cs = \pi_{13}$, « numero di Cauchy di corrente elettrica superficiale ».

Il numero $\pi_{14} = \varrho V c'/\sigma_s B = V/(B\sigma_s/\varrho c')$ può venir interpretato come rapporto tra due velocità e come tale lo indico con As, « numero di Alfvén di carica elettrica superficiale ».

Il numero

$$\pi_{15} = \frac{\varrho V^2 c'}{JLB} = \frac{\varrho L^2 V^2}{L^3 JB/c'},$$

esprime il rapporto tra la forza d'inerzia del solido e il risultante delle forze ponderomotrici che la corrente elettrica esercita sul corpo stesso. Si osservi che si può scrivere (tornando a π_{10})

$$Cm = \frac{L^2 \varrho V^2}{L^2 B^2/\mu},$$

e il denominatore della frazione rappresentata da Cm (cioè L^2B^2/μ) spesso equivale praticamente [34] al denominatore della frazione rappresentata da π_{15} (cioè L^3JB/c'); ma non mi sembra motivo sufficiente per confondere con il reciproco di π_{10} il numero π_{15}.

Il numero $\pi_{16} = \varrho V c'^2/\sigma LB^2$ è stato usato per la prima volta da T. G. Cowling [35] col simbolo $1/N$, cosicchè potrebbe chiamarsi « numero di Cowling » $N = Co = 1/\pi_{16}$; esso può scriversi

$$\pi_{16} = \frac{\varrho V^2}{B^2/\mu} \frac{c'^2}{\sigma\mu LV} = \frac{Cm}{Rm} = \frac{1}{Co},$$

[34] In armonia con le consuete ipotesi della m.f.d. (e in particolare se la conducibilità elettrica è altissima e se la velocità è limitata, in modo da porre $Lo \simeq 0$) la corrente elettrica di convezione e quella di spostamento sono trascurabili di fronte a J; cosicchè può scriversi c' rot $\boldsymbol{B}/\mu \simeq \boldsymbol{J}$ da cui segue $c'B/\mu L \simeq J$.

[35] Cf. T. G. Cowling: l.c. [2], p. 11, eq. (1.25).

ove il numero Rm sta a indicare il « numero di Reynolds magnetico » in quanto al posto della viscosità cinematica ν del numero di Reynolds Re troviamo la viscosità « magnetica » $\xi = c'^2/\sigma\mu$; esso può anche scriversi

$$Rm = \frac{\varrho L^2 V^2}{\varrho L V c'^2/\mu\sigma},$$

e in tal modo esprime il rapporto tra la forza d'inerzia e la forza dovuta alla viscosità magnetica ([36]).

Il numero π_{17} può presentarsi come prodotto di due frazioni

$$\pi_{17} = \frac{\varrho V c'}{\varrho_e L B} = \frac{c' B}{\varrho_e \mu L V} \frac{\mu \varrho V^2}{B^2};$$

poichè $c'B/\varrho_e\mu$ (che ha manifestamente le dimensioni d'una viscosità cinematica) esprime la viscosità dovuta alle cariche elettriche, il rapporto $Re = \varrho_e \mu L V/c'B$ può denominarsi « numero di Reynolds di carica elettrica »; cosicchè $\pi_{17} = Cm/Re$. In conseguenza delle ipotesi dell'ordinaria m.f.d. π_{17} risulta grandissimo.

È interessante rilevare che π_{17} può scriversi

$$\pi_{17} = \frac{\varrho V^2 c'}{\varrho_e L B} = \frac{\varrho V^2 L^2}{\varrho_e E L^3} \frac{E c'}{B V} = \frac{\varrho V^2 L^2}{\varrho_e E L^3} \frac{1}{\pi_{12}}.$$

La prima frazione esprime il rapporto tra la forza d'inerzia del corpo immerso nel fluido e il risultante delle forze di natura elettrostatica che si esercitano tra il fluido e il corpo immerso nel medesimo; tale denominatore è spesso trascurabile nell'ordinaria m.f.d., ed è forse per questo motivo che il numero π_{17} non ha trovato occasione d'esser messo in luce.

Da ultimo il numero $\pi_{18} = \varrho L^3 V^2/MB$ esprime il rapporto tra il momento delle forze d'inerzia e quello dovuto al momento del dipolo magnetico; anch'esso non mi risulta sia stato ancora messo in luce.

([36]) Il numero che si ottiene mediante il reciproco del prodotto di π_{10} e π_{11}, cioè

$$\frac{1}{\pi_{10}\pi_{11}} = \frac{\mu\varrho V^2}{B^2} \frac{\varepsilon B^2}{\varrho c'^2} = \frac{\varepsilon\mu V^2}{c'^2} = V^2/c_n^2,$$

era già noto (pur senza aver un nome particolare) nella similitudine dei campi elettromagnetici, nella forma $\varepsilon\mu L^2/c'^2T^2$; altrettanto dicasi del numero di *Reynolds magnetico*, nella forma $\mu\sigma L^2/c'^2T$; si veda in proposito, nel caso $c' = 1$, T. A. Stratton: *Electromagnetic Theory* (New York, 1941), p. 488; E. Bottani: *I modelli della tecnica*, in *Atti del Convegno di Venezia* 1955, vol. 2 (Roma, 1956), p. 12.

Immediata è la ricerca del legame con altri numeri classici in m.f.d. Il « numero di Hartmann » (37) può scriversi:

$$Ha = \frac{BL}{c'}\sqrt{\frac{\sigma}{\varrho\nu}} = \sqrt{\frac{B^2/\mu}{\varrho V^2}\,\frac{LV}{\nu}\,\frac{LV\sigma\mu}{c'^2}} = \sqrt{\frac{Rm\,Re}{Cm}} = \sqrt{\pi_2/\pi_{16}}\,.$$

Il rapporto tra la « viscosità magnetica » $c'^2/\sigma\mu$ e la viscosità cinematica ν (rapporto che, se non vado errato, è usato per la prima volta in una Nota di Elsasser (37')) potrebbe denominarsi « numero di Elsasser » El ponendo

$$El = \frac{c'^2}{\sigma\mu\nu} = \frac{c'^2}{\sigma\mu LV}\,\frac{LV}{\nu} = \frac{Re}{Rm} = \pi_2\cdot\pi_{10}\cdot\pi_{15}\,.$$

Recentemente è stato usato col nome di « numero di Prandtl magnetico » (38) il reciproco del numero citato, cioè il rapporto

$$Pm = \frac{Rm}{Re}\,.$$

Analogamente potrebbe chiamarsi « numero di Naze » Na il parametro (usato da J. Naze col simbolo di h) (39):

$$Na = \frac{B/\sqrt{\mu}}{a\sqrt{\varrho}} = \frac{B}{V\sqrt{\mu\varrho}}\cdot\frac{V}{a} = \frac{Ma}{Al}\,.$$

Il rapporto $\pi_{11}/\pi_{16} = \sigma L/V\varepsilon = \sigma/f\varepsilon$ è legato al « decadimento elettrico », e il suo significato è stato già messo in luce da Elsasser (40).

Se indichiamo con θ' una differenza caratteristica tra due temperature, e con $\lambda_7' = \alpha\theta'$ il corrispondente fattore di forma, il « numero di Grashof » Gr si esprime

$$Gr = \lambda_7'\pi_2^2/\pi_4 = \alpha\theta'\,\frac{\varrho^2L^2V^2}{\varrho^2\nu^2}\,\frac{gL}{V^2} = \frac{g\alpha\theta'L^3\varrho}{\varrho\nu^2}\,,$$

ed è il rapporto tra la forza ascensionale ed una forza che si collega al risultante delle forze viscose (41).

Chiudo questo elenco, inevitabilmente incompleto perchè i π_i e i λ_j pos-

(37) W. M. Elsasser: l. c. (7); T. G. Cowling: l. c. (2).

(37') W. M. Elsasser: l. c. (6).

(38) H. Hashimoto: *Proc. 10th Int. Congr. Appl. Mech.* (Stresa, 1960) (in corso di stampa); W. R. Sears: *Proc. 10th Int. Congr. Appl. Mech.* (Stresa, 1960) (in corso di stampa).

(39) J. Naze: *Compt. Rend.*, **246**, 3316 (1958).

(40) W. M. Elsasser: l. c. (6).

(41) Superfluo aggiungere che se inoltre supponiamo il gas perfetto, α eguaglia, a meno del segno, il reciproco d'una temperatura caratteristica, cosicchè λ_7' può venir sostituito da $\lambda_7'' = (\theta - \theta_\infty)/\theta_\infty$. Cf. G. Bozza: l.c. (28), p. 35.

sono combinarsi in tanti modi, avvertendo che potrebbe chiamarsi « numero di Lykoudis » Ly il rapporto, da lui indicato con Z, tra il quadrato del numero di Hartmann e la radice del numero di Grashof ([41']), cioè

$$Ly = \frac{Ha^2}{\sqrt{Gr}} = \frac{\sigma B^2 L^2}{c'^2 \varrho \nu} \frac{\nu \varrho^{\frac{1}{2}}}{\sqrt{\alpha \theta' g \varrho L^3}} = \frac{\sqrt{\pi_4}}{\pi_{16} \sqrt{\lambda_7'}} .$$

5. – Legami tra i prodotti trovati e quelli ottenuti in particolari sistemi di unità di misura.

Rinuncio ad esaminare fino a qual punto l'assumere c' come grandezza dimensionalmente autonoma o no possa portare a una discussione che ha qualche analogia con quella sorta attorno al paradosso di Lord Rayleigh ([42]) nell'analisi dimensionale in termologia.

Se invece di accettare il sistema di Gauss, o quello elettrostatico, o quello elettromagnetico, o quello di Giorgi assumiamo (come appunto è stato fatto nelle sezioni precedenti) come grandezze dimensionali tanto B quanto c', ignoriamo (ai soli fini dell'analisi dimensionale e in conformità della natura convenzionale di questa) ad esempio, l'ipotesi di Ampère, secondo cui il magnetismo è elettricità in moto; oppure ignoriamo che nello spazio-tempo le componenti delle due grandezze vettoriali $\boldsymbol{E}c'/c$ e $\boldsymbol{B}$ diventano le componenti del tensore $F_{\varkappa\lambda}$ (tensore « campo ») e analogamente con le componenti delle grandezze $\boldsymbol{D}c/c'$ e $\boldsymbol{H}$ si costruisce il tensore $f_{\varkappa\lambda}$ (tensore « induzione ») ([43]). Si suppone in altri termini che grandezze elettriche e grandezze magnetiche siano

([41']) P. S. Lykoudis: *Proc. 10th Int. Congr. Appl. Mech.* (Stresa, 1960) (in corso di stampa); cf. anche Report A-60-1 (Aug. 1960) Purdue University (Lafayette, Ind.): ivi, $c'=1$, è presentato come numero di Hartmann un rapporto diverso dal nostro Ha, e λ_7' è sostituito da λ_7''.

([42]) Lord Rayleigh: *Nature*, **95**, 66, 644 (1915); D. Riabouchinsky: *Nature*, **95**, 591 (1915); cf. anche G. Supino: *Rend. Sem. Mat. Fis. Milano*, **30**, 250 (1960).

([43]) Nello spazio-tempo di metrica

$$ds^2 = g_{\alpha\beta} dx^\alpha dx^\beta ,$$

(ove $\alpha, \beta = 0, 1, 2, 3$; $g_{00} = -g_{11} = -g_{22} = -g_{33} = 1$, $g_{\alpha\beta} = 0$ per $\alpha \neq \beta$) si ponga:

$$F_{0i} = -F_{i0} = -E_i c'/c ; \qquad F_{i+1,\, i+2} = -F_{i+2,\, i+1} = B_i$$

$$f_{0i} = -f_{i0} = -D_i c/c' ; \qquad f_{i+1,\, i+2} = -f_{i+2,\, i+1} = H_i .$$

In unità gaussiane, $c'=c$, e nel vuoto $f_{\alpha\beta}=F_{\alpha\beta}$; in unità del sistema Giorgi, $c'=1$, e nel vuoto

$$f_{\alpha\beta} = \frac{1}{\mu_0} F_{\alpha\beta} = c \sqrt{\frac{\varepsilon_0}{\mu_0}} F_{\alpha\beta} .$$

Per il primo caso, cf. ad es., B. Finzi: *Ann. Mat.*, **50**, 319 (1960); per il secondo caso J. I. Horváth: *Nuovo Cimento*, **7**, 628 (1958).

di natura del tutto diversa (e di ciò ci si rende conto ancor meglio se assumiamo come fondamentali B ed E [44] invece di B e c').

Nella tabella II sono esposti nella prima colonna i prodotti ora trovati (limitatamente alle grandezze elettromagnetiche), nella seconda l'espressione degli stessi prodotti se viene usato il sistema di Gauss, nella terza l'analoga espressione se viene usato il sistema elettrostatico, nella quarta se viene usato il sistema elettromagnetico, nell'ultima se viene usato il sistema di Giorgi [45].

TABELLA II.

	Gauss	Es.	Em.	Giorgi
$\pi_{10}=\frac{B^2}{\mu\varrho V^2}$	$\frac{B^2}{\varrho V^2}\left(\frac{1}{\mu}\right)$	$\frac{B^2}{\mu\varrho V^2}$	$\frac{B^2}{\varrho V^2}\left(\frac{1}{\mu}\right)$	$\frac{B^2}{\mu\varrho V^2}$
$\pi_{11}=\frac{\varrho c'^2}{\varepsilon B^2}$	$\frac{\varrho c^2}{B^2}\left(\frac{1}{\varepsilon}\right)$	$\frac{\varrho}{(\varepsilon)B^2}$	$\frac{\varrho}{\varepsilon B^2}$	$\frac{\varrho}{\varepsilon B^2}$
$\pi_{12}=\frac{VB}{Ec'}$	$\frac{VB}{Ec}$	$\frac{VB}{E}$	$\frac{VB}{E}$	$\frac{VB}{E}$
$\pi_{13}=\frac{\varrho V^2}{KB}$	$\frac{\varrho V^2}{KB}$	$\frac{\varrho V^2}{KB}$	$\frac{\varrho V^2}{KB}$	$\frac{\varrho V^2}{KB}$
$\pi_{14}=\frac{\varrho Vc'}{\sigma_s B}$	$\frac{\varrho Vc}{\sigma_s B}$	$\frac{\varrho V}{\sigma_s B}$	$\frac{\varrho V}{\sigma_s B}$	$\frac{\varrho V}{\sigma_s B}$
$\pi_{15}=\frac{\varrho V^2 c'}{JLB}$	$\frac{\varrho V^2 c}{JLB}$	$\frac{\varrho V^2}{JLB}$	$\frac{\varrho V^2}{JLB}$	$\frac{\varrho V^2}{JLB}$
$\pi_{16}=\frac{\varrho Vc'^2}{\sigma LB^2}$	$\frac{\varrho Vc^2}{\sigma LB^2}$	$\frac{\varrho V}{\sigma LB^2}$	$\frac{\varrho V}{\sigma LB^2}$	$\frac{\varrho V}{\sigma LB^2}$
$\pi_{17}=\frac{\varrho Vc'}{\varrho_e LB}$	$\frac{\varrho Vc}{\varrho_e LB}$	$\frac{\varrho V}{\varrho_e LB}$	$\frac{\varrho V}{\varrho_e LB}$	$\frac{\varrho V}{\varrho_e LB}$
$\pi_{18}=\frac{\varrho L^3 V^2}{mB}$	$\frac{\varrho L^3 V^2}{mB}$	$\frac{\varrho L^3 V^2}{mB}$	$\frac{\varrho L^3 V^2}{mB}$	$\frac{\varrho L^3 V^2}{mB}$

[44] In tal caso infatti le grandezze elettriche contengono B con esponente nullo, le grandezze magnetiche contengono E con esponente nullo, e solo c' contiene E e B con esponente non nullo.

$[\varepsilon]=[\rho V^2 E^{-2}]$; $[\rho_e]=[L^{-1}V^2\rho E^{-1}]$; $[J]=[L^{-1}V^3\rho E^{-1}]$; $[\sigma]=[L^{-1}V^3\rho E^{-2}]$; $[D]=[\sigma_s]=[V^2\rho E^{-1}]$; $[\mu]=[B^2\rho^{-1}V^{-2}]$; $[H]=[K]=[V^2\rho B^{-1}]$; $[m]=[\rho L^3 V^2 B^{-1}]$; $[c']=[VBE^{-1}]$.

[45] Il sistema gaussiano è usato ad es. da R. W. TRUITT: *Hypersonic Aerodynamics* (New York, 1959), p. 409; il sistema elettrostatico non mi risulta sia stato usato da nessun Autore in m.f.d.; il sistema elettromagnetico da L. G. NAPOLITANO: l. c. [12],

Vengono indicate tra parentesi quelle grandezze che sono considerate adimensionali in particolari sistemi di misura, e che quindi sarebbero rimaste escluse dal quadro dei prodotti alla stregua dei coefficienti numerici.

Esaminando i prodotti della 1ª colonna, è facile osservare che le grandezze B e c' non intervengono mai separatamente: invece vi intervengono le grandezze $\overline{B} = B/c'$, $\overline{H} = Hc'$, $\overline{\mu} = \mu c'^2$ e potremmo eliminare c' da tutti i prodotti della prima colonna facendo appunto queste sostituzioni: in tal modo otterremmo i prodotti della quinta colonna. L'aver considerato c' dimensionalmente indipendente non significa che si debba assumere c' come unità di misura, nè che si debba far uso di un sistema a cinque unità, quale ad esempio, era stato introdotto da COHN [46]. Il vantaggio d'aver scelto c' sta nel poter considerare i prodotti adimensionali che nascono corrispondentemente ai vari sistemi di misura come casi particolari dei prodotti della prima colonna.

In modo analogo nessuno pensa di costruire un sistema meccanico generale di misura prendendo come unità fondamentali una lunghezza L, un tempo T e la costante universale gravitazionale k: ma ha invece significato un'analisi dimensionale o un'applicazione del teorema π in cui si scelgono come fondamentali L, T, k. Se in tale sistema si ponesse $k = 1$, l'analisi dimensionale diverrebbe quella della meccanica celeste [47] (in cui le sole grandezze fondamentali sono L e T), proprio così come ponendo $c' = 1$ si passa dalla 1ª alla 5ª colonna della tavola precedente.

6. – La legge di similitudine di T. Kihara.

È ovvio che la realizzazione di una similitudine completa in m.f.d. è praticamente impossibile, in quanto dovrebbe rimanere invariato un numero troppo grande di prodotti adimensionali. Tuttavia giova ricordare che T. KIHARA [48] ha enunciato una legge di similitudine per la m.f.d. nella seguente forma: se s è un numero positivo, tutte le equazioni della m.f.d. sono invarianti di fronte alla trasformazione (tradotta nei nostri simboli)

$$(L, T) \to s^{-1}(L, T)\,,$$

$$(\varepsilon, \mu, V) \to s^{0}\ (\varepsilon, \mu, V)\,,$$

$$(E, B, D, H, g) \to s^{1}\ (E, B, D, H, g)\,.$$

da E. L. RESLER e W. R. SEARS: l. c. [24] e da T. VON KÁRMÁN: l. c. [5]; il sistema Giorgi da S. I. PAI: l. c. [11], H. GRAD e M. H. ROSE: l. c. [9], da V. M. ELSASSER: l. c. [7] e dallo scrivente: l. c. [14].

[46] E. COHN: l. c. [23].

[47] Cf. ad es. H. L. LANGHAAR: *Dimensional Analysis and Theory of Models* (New York, 1951), p. 9.

[48] T. KIHARA: l. c. [19], § 3.

L'esame dei prodotti π_i e dei parametri di forma λ_j permette di verificare ed estendere la similitudine citata. I π_i e i λ_i rimangono invariati di fronte alla trasformazione

$$(c_p, c_v, R, m, \alpha) \to s^{-2}(c_p, c_v, R, m, \alpha) ,$$

$$(\lambda, L, M, T, \nu) \to s^{-1}(\lambda, L, M, T, \nu) ,$$

$$(\varepsilon, \mu, V, a, c, c_n, c', F, \gamma) \to s^0 \ (\varepsilon, \mu, V, a, c, c_n, c', F, \gamma) ,$$

$$(B, D, E, H, K, \sigma_s, f, \gamma_s, \sigma, g) \to s^1 \ (B, D, E, H, K, \sigma_s, f, \gamma_s, \sigma, g) ,$$

$$(p, J, \varrho, \varrho_e, \theta, \eta) \to s^2 \ (p, J, \varrho, \varrho_e, \theta, \eta) .$$

SUMMARY

In this paper by means of a direct dimensional analysis, without employing all the equations of the magnetofluiddynamics, the author finds the generalized shape factors or parameters λ_j (ratios between two equidimensional quantities only) and the characteristic dimensionless products π_i (or ratios or numbers or invariants) of m.f.d. In the macroscopic approach (in conformity with the statement that a dimensional analysis is the more successful the greater is the number of fundamental independent quantities) the author choses six quantities as fundamental: a length L, a velocity V, a material density ϱ, an absolute temperature θ, a magnetic induction B and the universal constant c' of the Maxwell equations. The author finds eighteen products π_i, including the classical products of fluid mechanics, the products already employed in m.f.d. (the Reynolds magnetic number, the Alfvén number and so on) and also new products, independent of the products quoted above. The author illustrates the physical meaning of such products showing how to particular values of c' correspond numbers obtained in the field of particular measure-systems: if $c'=c$ (where c is the velocity of light in vacuum) the numbers are given in the gaussian system; if $c'=1$ the numbers are given in the e.s.u. or e.m.u. or Giorgi system. The products are also employed to verify and generalize T. Kihara's law of similitude.

Estudio mediante placas fotográficas, de la fisión ternaria del ^{235}U bombardeado con neutrones térmicos (*) (**).

J. Català, V. Domingo y J. Casanova

Centro de Física Fotocorpuscular (***), - Facultad de Ciencias - Valencia

(ricevuto il 14 Ottobre 1960)

Summary. — The results are presented of a study of 1 000 fission events in ^{235}U in which a light particle was emitted. Nuclear emulsions were used. Because of the large number of events analysed, it was possible to obtain data of good statistical accuracy on the frequency of emission of light particles, on their angular distribution and the upper limit of their energy spectrum. Also determined were the mean ranges, masses and energies of the light particles and of the heavy fragments.

1. – Introduccion.

Desde su descubrimiento en 1944, la fisión ternaria del ^{235}U ha sido estudiada por diversos investigadores ([1-17]), la mayor parte de los cuales emplea

(*) Presentato al XLVI Congresso della Società Italiana di Fisica, Napoli, 29 Settembre - 5 Ottobre 1960.

(**) Este trabajo ha sido subvencionado por una Ayuda de Investigación del Patronato de la Fundación « Juan March ».

(***) Este Centro está subvencionado por la Junta de Energía Nuclear.

(1) L. L. Green y D. L. Livesey: *Phil. Trans. Roy. Soc.*, A **241**, 323 (1948).

(2) Tsien San Tsiang, Ho-Zah-Wei, R. Chastel y L. Vigneron: *Journ. Phys. Rad.*, I, **8**, 165 (1947); II, **8**, 200 (1947).

(3) P. Demers: *Phys. Rev.*, **70**, 974 (1946).

(4) E. O. Wollan, C. D. Moak y R. B. Sawyer: *Phys. Rev.*, **72**, 447 (1947).

(5) L. Marshall: *Phys. Rev.*, **75**, 1339 (1949).

(6) E. W. Titterton: *Nature*, **168**, 590 (1951).

(7) N. A. Perfilov: *Trans. Radium. Inst. Acad. Sci. U.R.S.S.*, VII, 5 (1956).

(8) G. Farwell, E. Segré y C. Wiegand: *Phys. Rev.*, **71**, 327 (1957).

(9) K. V. Allen y J. T. Dewan: *Phys. Rev.*, **80**, 181 (1950).

la técnica fotográfica nuclear, y algunos la cámara de ionización; ésta última proporciona mayor número de medidas, pero en cambio la técnica fotográfica permite un estudio más completo de los sucesos individuales. Sin embargo los resultados obtenidos en las experiencias realizadas con emulsión fotográfica están basadas, con excepción de las realizadas por TITTERTON [6] y PERFILOV [7] en un corto número de sucesos medidos. Por ello hemos preparado nuestra experiencia para obtener resultados con mayor validez estadística.

2. – Parte experimental.

Las placas han sido preparadas por dos procedimientos distintos; unas han sido cargadas por inmersión en una disolución diluída de nitrato de uranilo, permitiendo así el estudio de las trazas completas que producen en la misma los tres fragmentos de la trifisión; otras placas han sido cargadas con tubos microcapilares de vidrio llenos de disolución concentrada de nitrato de uranilo; en ellas la emulsión no ha sufrido ninguna desensibilización y permite hacer medidas del índice de ionización para el reconocimiento de las partículas. Las dos series de placas han sido irradiadas con neutrones térmicos en la columna térmica del reactor BR-1 de Mol (Bélgica).

Se han medido 1000 de los sucesos registrados en las placas cargadas por inmersión. En cada uno de ellos se han determinado los alcances de los tres fragmentos y los ángulos que forman entre sí, y por aplicación de los principios de conservación de la masa y energía[16] se han calculado las masas de los tres fragmentos. En la selección de los sucesos se ha prescindido de aquéllos en que el fragmento es menor de 30 micras pues de este modo evitaba la posibilidad de medir sucesos que aparentemente eran trifisiones y podían ser debidos a meras coincidencias de fisiones binarias y emisión de una partícula α de la radiactividad natural; por otra parte los trabajos de LABOULAYE y col. [12]

---

[10] D. L. HILL: *Phys. Rev.*, **87**, 1046 (1952).

[11] C. B. FULMER y B. L. COHEN: *Phys. Rev.*, **108**, 770 (1957).

[12] H. LABOULAYE, J. OLKOWSKY y C. TZARA: *Compt. Rend. Acad. Sci. Paris*, **327**, 155 (1953).

[13] S. P. DUTTA: *Indian. Journ. Phys.*, **27**, 547 (1953).

[14] U. I. MOSTOVOI, T. A. MOSTOVAYA, M. SOVINSKII y YU. S. SALTYKOV: *Atommaya Energya*, **7**, 372 (1959).

[15] V. F. APALIN, YU. P. LOBRYNIN, V. F. ZAKHAROVA, I. E. KUTIKOV y L.A. MIKAELYAN: *Atomnaja Energija*, **7**, 375 (1959).

[16] J. CATALÁ, V. DOMINGO, J. CASANOVA, F. SENENT y A. LLEÓ: *An. Real. Soc. Esp. Fís. y Quím.*, **56** a, 19 (1960).

[17] N. PERFILOV y Z. SOLOV'EVA: *Trans. Radium. Inst. Acad. Sci. U.R.S.S.*, **9**, 5 (1959).

y PERFILOV (7) ponen de manifiesto que el fenómeno de la fisión ternaria con emisión de una partícula ligera de corto alcance no tiene lugar al menos con frecuencia medible.

3. – Resultados.

Los cálculos expuestos en (16) han sido aplicados a los 1000 sucesos medidos, dando lugar a los siguientes resultados:

a) *Frecuencia del suceso*: Hemos encontrado una frecuencia relativa de la fisión ternaria a la fisión binaria de 1:550, valor algo más bajo de los encontrados por otros autores.

b) *Fragmentos de masa intermedia*: Los alcances de los fragmentos de las fisiones ternarias medidas aparecen agrupados alrededor de los valores medios 10.7 y 13.6 micras (Fig. 1).

A partir de los alcances, con la relación alcance-energía de MATTIEU y DEMERS (18), fueron calculadas las energías de los fragmentos pesados, siendo la energìa media para los fragmentos mayor y menor de (56 ± 11) MeV y (85.4 ± 13) MeV respectivamente, valores que son algo más bajos que los que se presentan en la fisión ordinaria, de acuerdo con el resultado reciente de MOSTOVOI y col. (4).

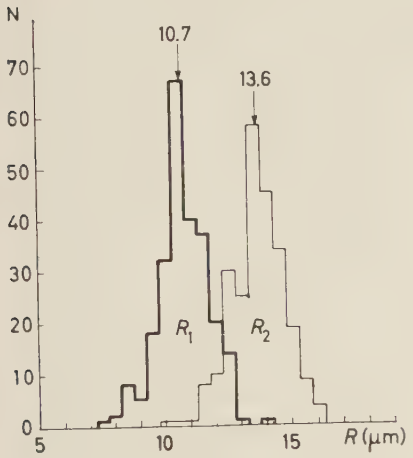

Fig. 1.

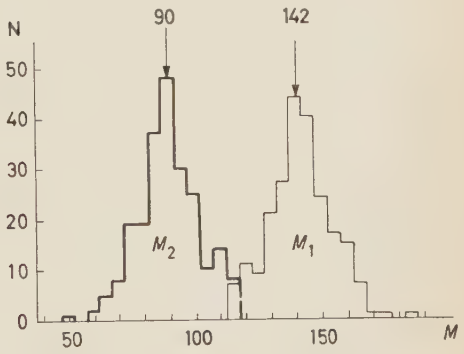

Fig. 2.

Las masas obtenidas para los fragmentos pesados presentan una distribución que viene representada en la Fig. 2, siendo los valores más probables 90 y 142 u.a.m., los mismos que tienen lugar en la fisión ordinaria, aunque

(18) R. MATTIEU y P. DEMERS: *Can. Journ. Phys.*, **31**, 97 (1953).

en nuestro caso el número de fisiones simétricas encontrado es superior al que se encuentra en la fisión ordinaria. No obstante este resultado puede venir afectado por la dispersión que tienen nuestros valores, debido al straggling de los alcances de los fragmentos en la emulsión.

c) *Estudio de la partícula ligera*: Aunque después de la experiencia de FULMER y COHEN [11] en la que analizan la naturaleza de las partículas ligeras emitidas en la fisión, parece definitivo que se trata de partículas α, nosotros hemos obtenido la masa del fragmento ligero en cada suceso como si aquélla fuera desconocida. Ahora bien, la masa que se calcula depende del ángulo que forman entre sì los fragmentos pesados y éste se mide con un gran error relativo en la zona que presenta un valor medio que corresponde a las partículas α. La medida de los índices de ionización no es aplicable a las placas cargadas por inmersión, porque la desensibilización que produce el uranio hace que la ionización sea irregular en profundidad. Por ello estas medidas se han hecho en las placas cargadas con tubos. En estas placas se encuentran junto a las trazas de partículas ligeras de la trifisión saliendo de los tubos, otro grupo de trazas de alcance hasta 100 μm, debidas a los protones de retroceso que producen las partículas α del uranio en el agua del interior de los tubos. La medida del espesor medio de las trazas de las partículas procedentes de la trifisión da como resultado (0.37 ± 0.03) μm, mientras que la de las trazas de los protones da el espesor medio de (0.26 ± 0.02) μm, de acuerdo con la relación que debe existir entre la ionización producida por las partículas α y los protones.

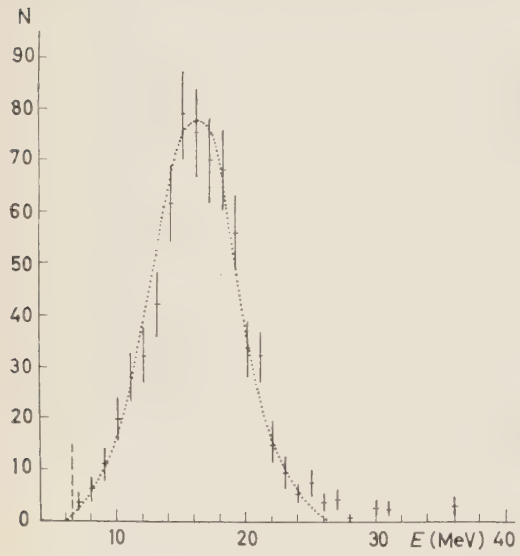

Fig. 3.

Por otra parte se ha medido el índice de indentificación llamado « radio de curvatura » [19] de algunas de las trazas de fragmentos ligeros dando los valores correspondientes a las partículas α.

Se han medido los alcances de todas aquellas partículas ligeras que están totalmente comprendidas en el seno de la emulsión y a partir de ellos las energías cuya distribución (Fig. 3) corresponde a una curva de forma aproxima-

[19] F. SENENT, E. VILLAR, R. FONT, L. MIRALLES, A. GARCIA y J. CATALÁ: *An. Real. Soc. Esp. Fís. y Quím.*, **54** A, 251 (1959).

damente gaussiana, a la que le hemos calculado su ecuación, que resulta ser

$$N = 78 \cdot \exp\left[-0.433\,(E-16)^2\right],$$

y cuyo valor más probable se presenta para los 16 MeV de energía de la partícula α emitida.

d) *Distribución angular*: Habiendo observado que parece existir una relación entre el alcance de la partícula ligera y el ángulo que ésta forma con el fragmento pesado de mayor alcance, hemos representado, en la Fig. 4, dichos ángulos, agrupando en tres histogramas los sucesos correspondientes a tres intervalos de energías de emisión de la partícula ligera. De este modo se confirma la observación hecha por PERFILOV y SOLOV'EVA [17] de que existe una correlación entre el ángulo de emisión de la partícula α y la energìa de la misma. Resulta ser que mientras para partículas que tienen energías relativamente bajas hay un marcada preferencia para los ángulos próximos a los 83° y casi ninguna partícula supera los 90°, para energías mayores la distribución tiende a hacerse isotrópica.

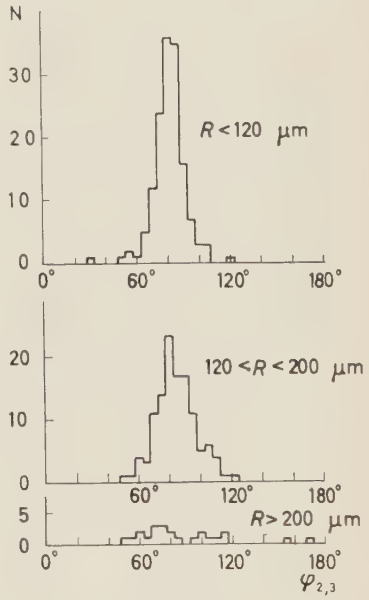

Fig. 4.

e) *Energía cinética total del suceso*: Despreciando la energía que puedan poseer los neutrones emitidos durante el proceso, la energía cinética total se obtiene sumando la de los tres fragmentos. El histograma de la Fig. 5 contiene los valores obtenidos para todos los sucesos completos medidos por nosotros. El valor medio, 157 MeV es algo mayor que el de la fisión binaria de acuerdo con lo obtenido por TSIEN SAN TSIANG y col. [2].

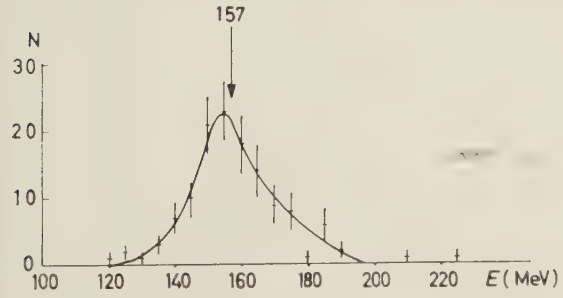

Fig. 5.

f) *Sucesos en los que el tercer fragmento tiene masa superior a cuatro*: En la observación de las placas cargadas por inmersión se han encontrado dos sucesos comple-

tos en los que las masas de los fragmentos son: 150 ± 13, 74 ± 13, y 12 ± 2 para uno y 169 ± 13, 55 ± 13 y 11 ± 2 para el otro. Un estudio detallado de estos sucesos se ha publicado anteriormente ([20]). Posteriormente se han encontrado dos sucesos más en los que el ángulo que forman los fragmentos pesados permite suponer que ha sido emitido un tercer fragmento de masa superior a cuatro, pero en ambos la tercera partícula escapa por el fondo, haciendo imposible el cálculo.

([20]) J. CATALÁ, J. CASANOVA y V. DOMINGO: *Nature*, **184**, 1057 (1959).

RIASSUNTO (*)

Si presentano i risultati dello studio di 1 000 fissioni in ^{235}U in cui veniva emessa una particella leggera. Si sono usate emulsioni nucleari. Per il grande numero di eventi analizzati, è stato possibile ottenere con buona precisione statistica dati sulla frequenza di emissione di particelle leggere, sulla loro distribuzione angolare e sul limite superiore del loro spettro di energia. Si sono pure determinati i percorsi medi, le masse e le energie delle particelle leggere e dei frammenti pesanti.

(*) *Traduzione a cura della Redazione.*

IL NUOVO CIMENTO Vol. XIX, N. 5 1° Marzo 1961

Emploi, à la température ambiante, de chambres d'ionisation remplies d'un diélectrique liquide.

D. Blanc, J. Mathieu et J. Boyer

Centre de Physique Nucléaire, Faculté des Sciences - Toulouse

(ricevuto il 24 Ottobre 1960)

Summary. — We examine the properties of ionization chambers with parallel plane electrodes, filled with hexane, highly purified. At 26 °C, the remanent current (background) is $2 \cdot 10^{-14}$ A/cm² when an electric field of 8 200 V/cm is applied. A source of ^{60}Co (12 millicuries) being disposed in the middle of one of the electrodes, the ionization current is a hundred times greater than the remanent current. The Jaffé theory can be applied up to fields of 20 000 V/cm. Above, an amplification effect happens; that effect can be compared to the multiplication process in gaseous fillings. We have shown the pulses given by α particles (5.3 MeV) in the region where this amplification effect exists. For electric fields from 25 600 V/cm to 65 600 V/cm, the amplitudes of impulsions are between 2.5 and $25 \cdot 10^{-5}$ V and the rise times between 5 and 20 μs.

1. – Introduction.

L'augmentation de la conductibilité électrique de liquides isolants placés dans des faisceaux de rayons X a été notée, pour la première fois, en 1896 par J. J. Thomson. P. Curie [1] confirma l'existence d'un phénomène analogue sous l'irradiation des particules émises par des sources radioactives. Les premières déterminations quantitatives furent effectuées par Jaffé [2], qui mesura la variation du courant obtenu I en fonction de l'intensité E du champ électrique appliqué. D'après lui:

$$I = f(E) + CE \tag{1}$$

[1] P. Curie: *Compt. Rend. Acad. Sci.*, **134**, 420 (1902).

[2] G. Jaffé: *Journ. Phys.*, **5**, 263 (1901); *Ann. Phys.*, **25**, 274 (1908); *Le Radium*: **10**, 126 (1913).

la fonction $f(E)$ devenant constante au dessus d'une valeur déterminée de E; la constante C est différente de zéro: I n'atteint pas la valeur de saturation, comme c'est le cas pour les gaz.

Partant de ces mesures, JAFFÉ a établi une théorie dont l'hypothèse fondamentale est la suivante [3]: l'ionisation d'un certain volume de liquide diélectrique par des particules ionisantes n'est pas homogène; les ions produits s'accumulent dans un cylindre entourant la trajectoire de la particule pour former une « colonne » ionisée de faible rayon. Cette distribution varie en fonction du temps sous l'effet de l'agitation thermique, de la recombinaison, de l'action du champ électrique appliqué. Tenant compte de ces divers paramètres, JAFFÉ a calculé quelle est la fraction des ions produits qui doit atteindre les électrodes. La mesure des courants d'ionisation dans les liquides diélectriques, à la température ambiante et la vérification de la théorie de JAFFÉ, ont fait l'objet d'un certain nombre de publications [4]. Les travaux les plus récents sont ceux de RICHARDS [5] et de GIBAUD [6]. Dans tous les cas, les champs électriques ne dépassaient pas 15 000 V/cm.

A partir de 1948, on a essayé de mettre en évidence les impulsions créées par des particules individuelles. A la température ambiante, les tentatives ont été négatives; ces impulsions n'ont pu être décelées que dans l'argon liquide [7,8].

Nous avons repris ce problème pour examiner la validité de la théorie de JAFFÉ dans le cas de champs appliqués intenses (jusqu'à 100 000 V/cm), pour tenter de mettre en évidence, à la température ambiante, les impulsions dues à des particules α, enfin pour définir les conditions d'emploi pratique de tels détecteurs.

L'hexane présente l'avantage d'avoir une conductivité théorique nulle, d'être facile à distiller (point d'ébullition, 68 °C) et à purifier chimiquement.

Enfin, du point de vue nucléaire, le pouvoir d'arrêt d'un liquide est beaucoup plus grand que celui d'un gaz; un tel détecteur doit trouver des applications dans la mesure de l'intensité absolue de sources radioactives, dans la détection des particules très rapides, enfin dans la détection des neutrons rapides, à cause du grand nombre des atomes d'hydrogène dans la molécule.

---

[3] G. JAFFÉ: *Ann. Phys.*, **22**, 303 (1913).

[4] I. ADAMCZEWSKI: *Acta Polon.*, **3**, 235 (1934); A. ROGOZINSKI: *Phys. Rev.*, **60**, 148 (1941); H. J. PLUMBEY: *Phys. Rev.*, **59**, 200 (1941); C. S. PAO: *Phys. Rev.*, **64**, 60 (1943).

[5] E. W. T. RICHARDS: *Proc. Phys. Soc.*, **66** A, 631 (1953).

[6] R. GIBAUD: *Journ. Phys. Rad.*, **19**, 175 (1958).

[7] N. DAVIDSON et A. E. LARSH: *Phys. Rev.*, **77**, 705 (1950).

[8] G. W. HUTCHINSON: *Nature*, **162**, 610 (1948).

2. – Dispositif expérimental.

2·1. *Chambres d'ionisation utilisées.* – On trouvera sur la Fig. 1 le schéma de la chambre: la distance d des électrodes est réglable entre 0 et 5 mm, et le champ électrique est pratiquement uniforme dans tout le volume utile de la chambre. Il faut que les courants de fuite à travers les passages isolants soient très inférieurs au courant qui traverse le liquide, pour que les mesures électrométriques soient valables. Nous avons adopté des passages de téflon, dont la résistivité naturelle est voisine de $10^{19}\ \Omega\cdot$cm à la température ambiante; on sait que, sous irradiation intense, cette résistivité peut tomber à $10^{14}\ \Omega\cdot$cm [9]. Enfin, la valeur maximale du potentiel de l'électrode collectrice par rapport à la masse est 1 V; le courant de fuite est alors maximal.

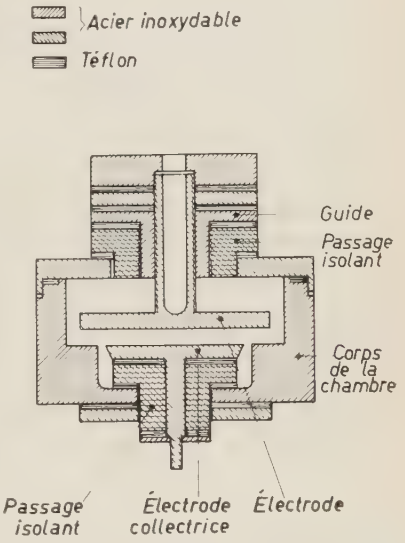

Fig. 1. – Schéma de la chambre d'ionisation.

Dans de telles conditions, le courant de fuite, sans irradiation, ne peut pas dépasser $0.6\cdot10^{-19}$ A/cm^2, et, sous irradiation intense, $0.6\cdot10^{-14}$ A/cm^2 [9]. Comme nous le verrons plus loin, ce courant est, dans les deux cas, négligeable devant celui qui traverse le liquide.

L'hexane à employer est traité par l'oléum, séché sur sodium, enfin distillé très soigneusement. Avant d'introduire le liquide à l'intérieur de la chambre, cette dernière est lavée à l'éthanol, étuvée à 60 °C, lavée par de l'hexane purifié, étuvée une seconde fois à 60 °C.

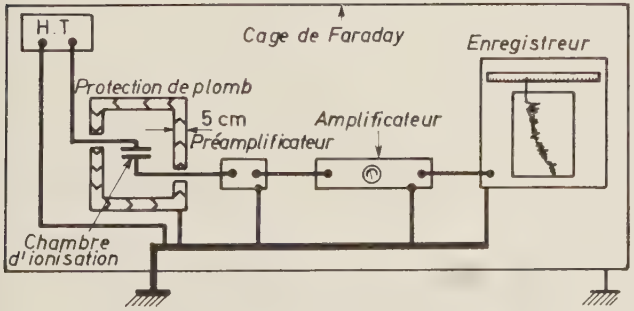

Fig. 2. – Dispositif de mesure du courant d'ionisation et du courant résiduel.

2·2. *Appareils de mesure et de comptage.* – Pour mesurer le courant d'ionisation et le courant résiduel, nous

(9) R. A. Mayer, F. L. Bouquet et R. S. Alger: *Journ. Appl. Phys.*, **27**, 1012 (1956).

utilisons un électromètre à condensateur vibrant, équipé de résistances d'entrée égales à 10^8, 10^{10} et $10^{12}\,\Omega$; les résultats sont recueillis sur un enregistreur graphique dont la vitesse maximale de déroulement est de 16 cm/h (Fig. 2).

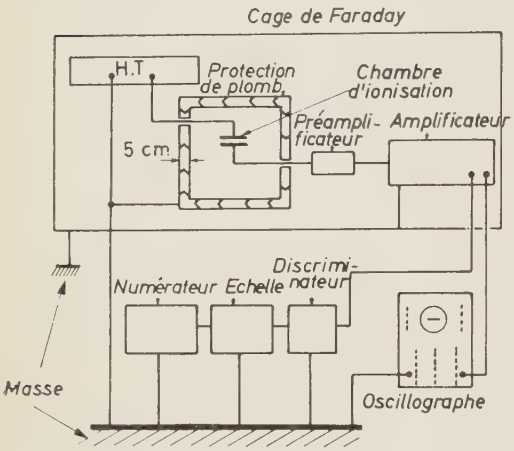

Fig. 3. – Système de mesure et de comptage des impulsions produites dans le liquide.

Pour mettre en évidence et compter les impulsions, nous employons un amplificateur linéaire de gain maximal égal à 200 000, suivi d'un système classique de mise en forme et de numération; en parallèle, est disposé un oscillographe cathodique, équipé d'un système photographique.

La haute tension de la chambre est constituée par une batterie de piles sèches permettant d'atteindre 5 000 V par échelons successifs de 90 V; la stabilité est excellente.

Les perturbations électriques venant de l'extérieur sont éliminées par une cage de Faraday entourant l'ensemble des appareils.

3. – Courant résiduel dans le liquide.

Il définit le bruit de fond du détecteur; c'est pourquoi nous avons étudié sa variation avec le temps, le champ électrique appliqué, la température.

3·1. *Variation en fonction du temps.* – Immédiatement après l'application de la haute tension entre les bornes de la chambre, le courant résiduel subit des variations rapides à partir de sa valeur moyenne: les fluctuations peuvent atteindre 10 fois la valeur moyenne; elles s'atténuent progressivement en même temps que leur fréquence diminue. Après plusieurs heures de fonctionnement, les variations sont inférieures à 5 pour cent de la valeur moyenne. La Fig. 4 est un enregistrement de ces fluctuations au bout de 50 h de fonctionnement: on remarquera la régularité du phénomène.

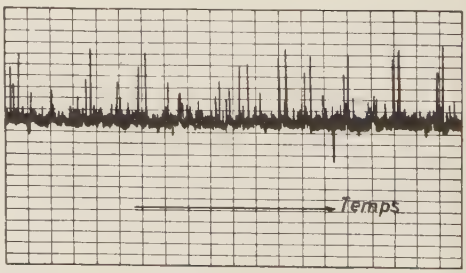

Fig. 4. – Fluctuations du courant résiduel au bout de 50 h de fonctionnement ($E = 20\,000$ V/cm).

La valeur moyenne i du courant résiduel décroît en fonction du temps (courbe 1 de la Fig. 5) pour atteindre une valeur presque constante au bout de 10 à 15 h. Lorsque l'on supprime la haute tension et qu'on la rétablit au bout de quelques minutes, i reprend une valeur initiale plus grande pour diminuer à nouveau en fonction du temps. On peut expliquer ce phénomène par la présence d'impuretés de caractère ionique, qui s'éliminent par purification électrolytique (voir plus loin).

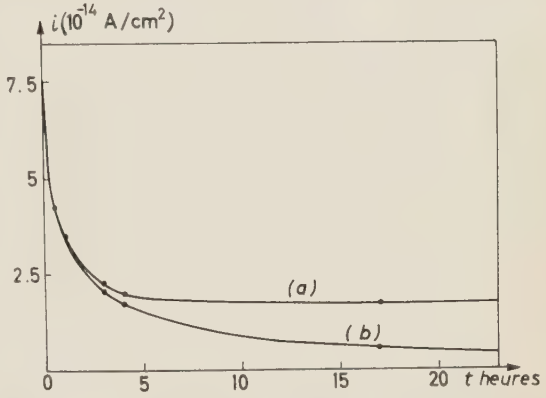

Fig. 5. – Variation du courant résiduel moyen en fonction du temps ($E = 8\,200$ V/cm, 26 °C); a) courbe expérimentale; b) variation théorique.

3·2. *Variation en fonction du champ E appliqué.* – On trouvera sur la Fig. 6 la variation de i en fonction de E pour $d = 1$ mm: la courbe (a) a été construite 6 h après mise sous tension, la courbe (b) au bout de 12 h, la courbe (c) au bout de 60 h: au dessus d'une certaine valeur du champ, i se met à augmenter rapidement; pour l'échantillon utilisé (Fig. 6), la résistivité, de $10^{15}\ \Omega$ pour E inférieur à 20 000 V/cm, atteint $1.3 \cdot 10^{18}\ \Omega$/cm pour $E = 50\,000$ V/cm.

On assiste à un phénomène d'amplification ionique à l'intérieur du liquide.

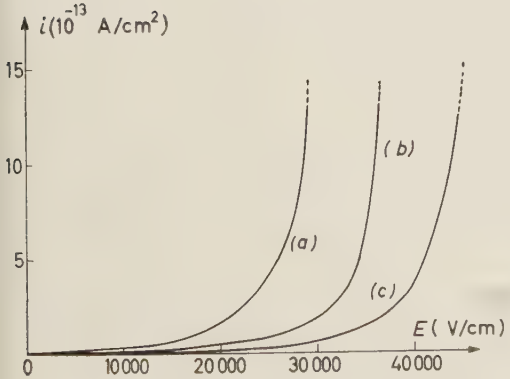

Fig. 6. – Variation du courant résiduel moyen en fonction du champ appliqué ($d = 1$ mm, 26 °C).

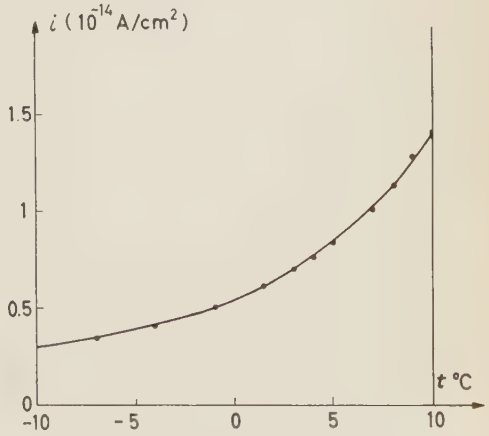

Fig. 7. – Variation du courant résiduel en fonction de la température ($E = 8\,200$ V/cm).

3·3. *Variation avec la température.* – La Fig. 7 donne les résultats obtenus pour $E = 8\,200$ V/cm, le liquide ayant été maintenu au préalable sous tension pendant 72 h, pour que le courant résiduel soit très stable. Le cycle thermique a été décrit en 72 h afin que le refroidissement, très lent, soit bien homogène. A -10 °C, i, qui est environ 5 fois plus faible qu'à 10 °C, possède une stabilité remarquable, et les fluctuations sont très peu nombreuses.

3·4. *Interprétation des résultats obtenus.* [10] – Les impuretés ioniques, même en de très faibles proportions, ont une influence considérable sur le comportament électrique du liquide; elles peuvent expliquer la variation du courant résiduel avec le temps (Fig. 5): supposons en effet que i soit, à chaque instant, une fonction linéaire du pourcentage M de ces impuretés, supposé constant dans tout le volume utile:

$$i(t) = aM(t)$$

a étant une constante, et que seule la purification électrolytique intervienne. D'après la loi de FARADAY:

$$i(t) = \frac{i_0}{1 + bt}, \tag{2}$$

i_0 étant l'intensité initiale du courant résiduel et b une constante.

Il faut remarquer qu'il ne s'agit là que d'une première approximation: au fur et à mesure de la purification, M devient plus grand près des électrodes que dans la partie centrale du volume utile.

La courbe b de la Fig. 5 traduit graphiquement la formule (2), pour $E = 8\,200$ V/cm. La confrontation à la courbe expérimentale a montre que la purification électrolytique n'est pas le seul processus qui intervienne. Enfin, l'écart entre la courbe expérimentale et la courbe théorique est d'autant plus grand que le champ électrique est plus intense. Pour $E = 20\,000$ V/cm, la différence devient sensible après une mise sous tension de vingt minutes. On peut expliquer cet écart par la formation, sous l'effet du champ, d'ions à partir de molécules à caractère non électrolytique.

Nous avons vu plus haut que i se met à augmenter rapidement au dessus d'une certaine valeur du champ: cette valeur est d'autant plus élevée que la purification électrolytique est plus poussée (voir les courbes de la Fig. 6). Il en est de même pour la variation du courant d'ionisation en fonction de E (Fig. 10).

La valeur limite du courant résiduel est différente de zéro: ce fait peut être dû à une émission thermo-ionique depuis la cathode; cette hypothèse s'accorde avec la diminution du courant résiduel avec la température (Fig. 7).

[10] D. BLANC, G. GIRON, J. MATHIEU, M. PONSAN et T. PUJOL: *Compt. Rend. Acad. Sci.*, **249**, 2546 (1959).

4. – Fonctionnement de la chambre en courant.

Nous avons utilisé une source de ^{60}Co de 12 mC, émettrice de rayons γ de 1.17 et 1.33 MeV, placée en position invariable à l'intérieur de la cavité ménagée dans l'électrode supérieure (Fig. 1). Avant les mesures, la chambre était maintenue sous tension assez longtemps pour que le courant résiduel puisse atteindre sa valeur limite. Les résultats obtenus avec une source de rayons α sont analogues à ceux donnés ici.

La Fig. 8 présente le phénomène produit par l'introduction de la source: le courant passe de sa valeur résiduelle i ($2.5 \cdot 10^{-13}$ A/cm² dans l'exemple choisi) à une valeur I beaucoup plus élevée ($2.8 \cdot 10^{-11}$ A/cm²), très stable ($E = 20\,000$ V/cm). Le courant résiduel est négligeable par rapport au courant dû à l'ionisation du liquide.

Nous avons vérifié que le courant d'ionisation est bien proportionnel à l'intensité du rayonnement qui traverse la chambre en modifiant la position de la source dans la cavité (Fig. 1): le fonctionnement du détecteur est donc correct.

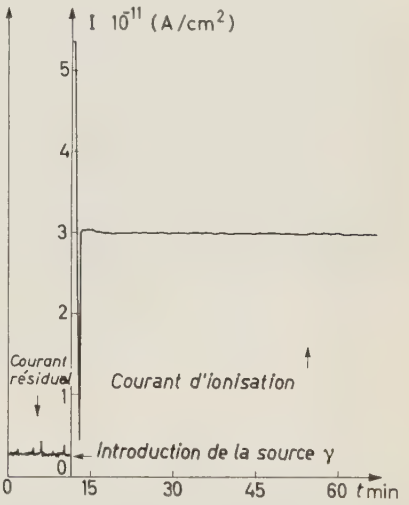

Fig. 8. – Enregistrement du courant traversant la chambre après introduction d'une source de ^{60}Co de 12 mC ($E = 20\,000$ V/cm).

4·1. *Comparaison a la théorie de Jaffe.* – Lorsque l'intensité E du champ électrique est inférieure à une valeur critique, comprise entre 10 000 et 30 000 V/cm selon l'état de pureté du liquide, le courant total I, pratiquement égal au courant d'ionisation, est une fonction linéaire de E (Fig. 9): la formule (1) est bien vérifiée. De plus, l'ordonnée à l'origine de la droite obtenue est pro-

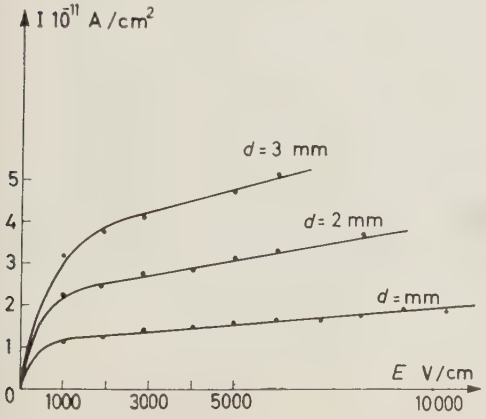

Fig. 9. – Variation du courant d'ionisation en fonction du champ électrique, au dessous de la région de multiplication.

portionnelle à la distance d séparant les électrodes, ce qui confirme le bon fonctionnement du détecteur.

La forme de la courbe $I = f(E)$ montre que l'on n'atteint pas la valeur de saturation du courant d'ionisation dans le liquide.

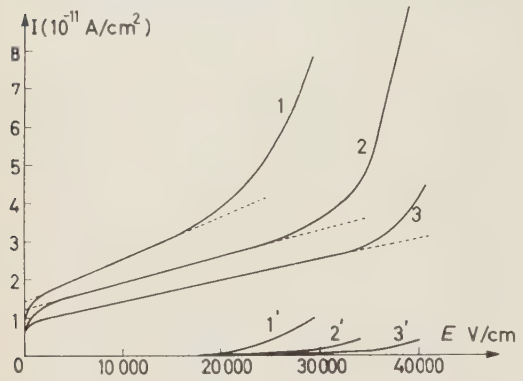

Fig. 10. – Variation de I et i en fonction de E pour des remplissages d'hexane de diverses puretés ($d = 1$ mm).

4·2. *Région de multiplication ionique.* – Lorsque E dépasse la valeur critique, I cesse d'être une fonction linéaire de E, tout en restant proportionnel à l'intensité du rayonnement qui traverse la chambre: il augmente d'autant plus vite que E est plus élevé (Fig. 10) et on voit sur la Fig. 11 que la courbe obtenue est une exponentielle, tout au moins jusqu'à 80 000 V/cm.

Ce phénomène, que les auteurs précédents n'ont pas signalé parce qu'ils employaient des valeurs de E trop faibles, prouve qu'il existe un processus de multiplication ionique à l'intérieur du liquide (10); ce processus se déclanche avant que I ne puisse atteindre la saturation, contrairement à ce que pensait JAFFÉ.

Les courbes de la Fig. 10 ont été prises dans les conditions suivantes: la chambre est maintenue 24 h sous tension ($E = 15\,000$ V/cm); on trace alors les caractéristiques donnant I (courbe 1) et i (courbe 1′) en fonction de E. Après avoir maintenu à nouveau la chambre 24 h sous tension, on obtient les courbes 2 et 2′; enfin, après un séjour de 48 h supplémentaires sous tension, les courbes sont 3 et 3′.

Cette expérience montre que, pour E donné, le courant d'ionisation dans l'hexane est d'autant plus faible que el liquide est plus pur, et que le seuil d'amplification augmente avec le degré de pureté. Ceci confirme l'importance des impuretés dans le mécanisme de fonctionnement d'un tel détecteur.

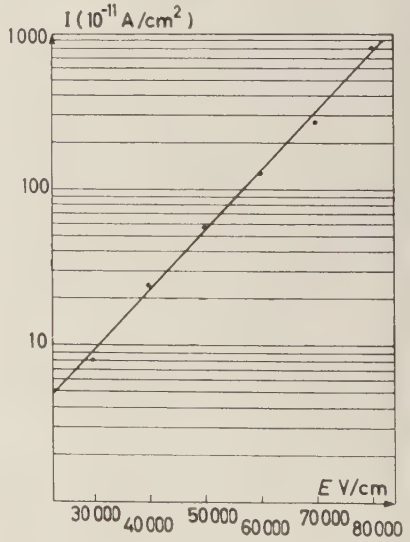

Fig. 11. – Variation de I en fonction de E dans la région d'amplification ($d = 0.5$ mm),

Fig. 12. – Série d'impulsions α produites dans l'hexane liquide (vitesse de balayage: 0.5 cm/ms, $E = 330$ V/cm).

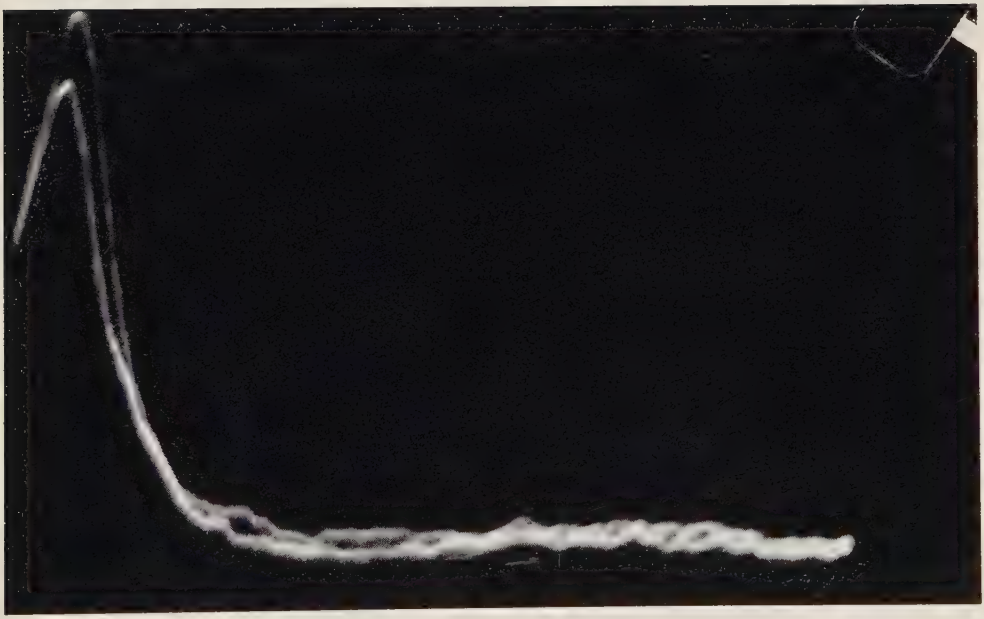

Fig. 13. – Deux impulsions successives produites dans l'hexane liquide par des particules α du ^{210}Po (vitesse de balayage: 160 cm/ms, $E = 44\,000$ V/cm).

5. – Fonctionnement de la chambre en impulsions.

Nous avons déposé une source de ^{210}Po (rayons α de 5.3 MeV) au centre de la face interne d'une cathode spéciale en argent; l'intensité de la source est très faible (inférieure à 60 particules α par seconde), pour que le temps qui sépare deux impulsions successives soit supérieur à la constante de temps du circuit d'entrée.

5·1. *Existence des impulsions.* – L'existence d'impulsions dans l'hexane à la température ambiante n'ayant jamais pu être mise en évidence antérieurement, nous avons choisi une source de particules α, très ionisantes, pour nous placer dans les conditions optimales permettant d'isoler les impulsions individuelles.

Nous avons maintenu la chambre plusieurs jours sous tension avant de faire les mesures et nous avons réglé la distance entre les électrodes à une valeur voisine du parcours des rayons α dans l'hexane, parce que les mobilités ioniques y sont très faibles. Moyennant ces précautions, nous avons obtenu des impulsions pour les valeurs de E correspondant à la région d'amplification; les impulsions ont des amplitudes suffisantes pour être comptées par le circuit de la Fig. 3 et être photographiées sur l'écran de l'oscillographe cathodique. On trouvera sur la Fig. 12 la succession des impulsions obtenues avec une vitesse de balayage de 0.5 cm/ms (temps de pose: 0.1 s): elles sont très supérieures au bruit de fond.

5·2. *Caractéristiques des impulsions.* – On trouvera sur la Fig. 13 deux impulsions successives prises en balayage déclenché, la vitesse de la base de temps étant de 160 cm/ms. L'une a une amplitude de 160 μV et un temps de montée de 20 μs, la seconde une amplitude de 140 μV et un temps de montée de 18 μs.

Les impulsions ne sont pas de hauteur uniforme (Fig. 12): la variation de leur amplitude maximale en fonction du champ est donnée sur la courbe 2 de la Fig. 14; la courbe 1 (courant d'ionisation sous irradiation γ) montre que ces impulsions ne deviennent détectables que dans la région d'amplification: c'est pour cette raison qu'aucun auteur n'était jusqu'alors parvenu à les mettre en

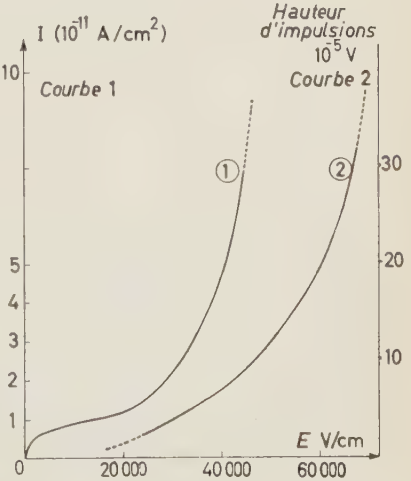

Fig. 14. – Variation, en fonction de E: 1) du courant d'ionisation I sous irradiation γ; 2) de la hauteur maximale des impulsions dues aux particules α de ^{210}Po.

évidence. Enfin, pour E donné, le temps de montée de l'impulsion est d'autant plus grand que son amplitude est plus élevée.

6. – Conclusion.

Nos expériences montrent que, moyennant une purification très poussée du liquide, les chambres d'ionisation à hexane fournissent des résultats stables et reproductibles; de plus, elles sont utilisables en courant comme en impulsions.

Nous avons mis en évidence un phénomène de multiplication ionique, non signalé jusqu'alors; cet effet est à rapprocher de celui qui se produit dans les gaz et dans les fonctions (p-n) de semi-conducteurs.

* * *

Nous remercions vivement M. G. Giron qui a construit la chambre d'ionisation utilisée dans cette étude.

Ces recherches on été effectuées dans les laboratoires mis aimablement à notre disposition par Monsieur le Professeur Blaizot, Directeur de l'Institut de Physiologie de l'Université de Toulouse.

RIASSUNTO (*)

Si esaminano le proprietà delle camere di ionizzazione con elettrodi piani paralleli, riempite con esano purissimo. A 26 °C la corrente residua (fondo) è di $2 \cdot 10^{-14}$ A/cm^2, quando è applicato un campo di 8 200 V/cm. Ponendo nel centro di uno degli elettrodi una sorgente di ^{60}Co (12 millicurie), la corrente di ionizzazione è 100 volte maggiore della corrente residua. La teoria di Jaffé può essere applicata per campi sino a 20 000 V/cm. Oltre questo valore si ha un effetto di amplificazione; questo processo può essere paragonato al processo di moltiplicazione nei riempimenti gassosi. Si sono mostrati gli impulsi dati dalle particelle α (5.3 MeV) nella regione in cui esiste questo effetto di amplificazione. Per campi elettrici compresi fra 25 600 e 65 600 V/cm, le ampiezze degli impulsi sono comprese fra 2.5 e $25 \cdot 10^{5}$ V ed il tempo di salita fra 5 e 20 μs.

(*) *Traduzione a cura della Redazione.*

IL NUOVO CIMENTO Vol. XIX, N. 5 1° Marzo 1961

A Proof of the Mandelstam Representation in Perturbation Theory (*).

P. V. Landshoff
St. John's College - Cambridge

J. C. Polkinghorne
Trinity College - Cambridge

J. C. Taylor (**)
Imperial College - London

(ricevuto il 26 Ottobre 1960)

Summary. — The Mandelstam representation is proved in each finite order in perturbation theory for processes for which forward scattering dispersion relations have been proved. A continuation in the external masses is then made so that the proof is extended to all processes for which there is no anomalous threshold in lowest order.

1. – Introduction.

Mandelstam (1) conjectured that the scattering amplitude is an analytic function in the product of the cut complex planes of the energy and momentum transfer variables. This seems a difficult result to establish rigorously from the general axioms of field theory. Therefore in this paper we shall be content with showing its validity to every finite order of perturbation theory, under the condition that no anomalous thresholds exst. This condition is the same

(*) An outline of this work was given as an invited paper at the Tenth International Conference on High Energy Physics, Rochester, 1960.

(**) Present address: Peterhouse, Cambridge.

(1) S. Mandelstam: *Phys. Rev.*, **112**, 1344 (1958).

as requiring that there be none in fourth order. In physical terms this means that the representation certainly holds for processes with only pions or nucleons as initial and final particles, but it may not when deuterons or Λ and Σ particles are involved.

Only the incurably optimistic would suppose that perturbation theory is convergent for strong interactions. However, we believe that it provides a guide for the physical and mathematical consistency of a conjecture, a guide which is the more welcome because the simplest physical intuition is unreliable in the complex plane. It has already, in the discovery of anomalous thresholds ([2]), shown the existence of singularities whose physical nature was only later realized ([3]). Moreover it has become clear that there is an intimate connection between the results of perturbation theory and deductions from general axioms ([4]). Therefore we believe that our result strengthens faith in the Mandelstam representation. Unfortunately, however, it does not seem immediately to suggest the form of a proof from the general axioms. This is because it depends on the interlocking structure of perturbation theory singularities, as is discussed in detail below.

2. – General theory.

It is known ([5]) that the singularities corresponding to a given Feynman graph must lie on certain real algebraic curves whose implicit equations were given by LANDAU ([6]). Each of these Landau curves is associated with putting some of the lines of the graph on the mass shell and short-circuiting the remainder. The curve corresponding to putting all the lines on the mass shell will be called the *leading curve* for the graph, while the others will be called *lower-order curves*. Whether these curves are in fact singular on the physical sheet is the subject of our investigation.

The equations of the Landau curves are functions of the complex variables z_1 and z_2 which are selected from the three linearly related Mandelstam invariants s, t, u. Each curve Σ is a two dimensional surface in the four-dimensional (z_1, z_2) space. Since it is a real curve its form may be deduced, using real searchlines, from the form of Γ, the one-dimensional real section of Σ lying in the real (z_1, z_2) plane. This is illustrated in Section 3.

([2]) R. KARPLUS, C. M. SOMMERFIELD and E. H. WICHMANN: *Phys. Rev.*, **111**, 1187 (1958).

([3]) R. OEHME: *Nuovo Cimento*, **13**, 778 (1959).

([4]) G. KÄLLÉN and A. S. WIGHTMAN: *Dan. Vid. Selsk. Mat.-fys. Skr.*, **1**, no. 6 (1958).

([5]) J. C. POLKINGHORNE and G. R. SCREATON: *Nuovo Cimento*, **15**, 289 and 925 (1960).

([6]) L. D. LANDAU: *Nuclear Physics*, **13**, 181 (1959).

We now consider how a given Landau curve can have one part singular and another non-singular, concentrating for definiteness on the leading curve. This discussion is a multi-dimensional version of previous work [5] on the analytic properties of perturbation theory.

The Feynman integration corresponding to an $(n+1)$-th order graph is made over an n-dimensional « hypercontour » $\boldsymbol{A}$ in the $2n$-dimensional complex space of Feynman parameters α. For a given value of (z_1, z_2) there is a $(2n-2)$-dimensional manifold $\boldsymbol{D}$ on which the Feynman denominator vanishes. As z_1 and z_2 vary the analytic continuation of the Feynman function is obtained by distorting $\boldsymbol{A}$ so that it never intersects $\boldsymbol{D}$. A singularity occurs only when the possibility of this distortion ceases. This can happen when there is a point of $\boldsymbol{D}$ at which $\boldsymbol{D}$ degenerates and so is locally cone-like. The singularity is actually present if $\boldsymbol{A}$ is pinched between the two halves of the cone. The curve Σ is the collection of points in z-space for which this locally cone-like behaviour occurs somewhere on $\boldsymbol{D}$.

Suppose that we are at a point of Σ which is singular and that we now move around in z-space, *remaining always on* Σ. $\boldsymbol{A}$ was originally pinched between two parts of $\boldsymbol{D}$. As we move on Σ the manifold $\boldsymbol{D}$ in α-space remains locally cone-like and the vertex of the cone moves, dragging $\boldsymbol{A}$ with it. Consequently we are still at a singular point. The only way that this situation can change is for the vertex of the cone to fall off an edge of $\boldsymbol{A}$. Such an edge is in a subspace in which at least one α is zero. Therefore the critical points are those in which Σ meets a lower order curve, Σ', in such a way that Σ, Σ' give common values of the α's at their intersection. We call this an *effective intersection*.

We remark that the intersection of Σ with any next lowest-order Landau curve (only one $\alpha = 0$) is necessarily effective, but that intersections with lower order curves corresponding to more than one vanishing α are not necessarily effective. It is easy to see that Σ, Σ' must touch at an effective intersection (*).

Since the intersections of Σ and Σ' are just a zero-dimensional set of points, the effective intersections themselves are not sufficient to divide Σ into singular and non-singular sections. A path on Σ may always be chosen to connect any two points on Σ and not pass through any effective intersection. However, such a path may cross a cut and so leave the physical sheet. Since our concern is with physics we must in fact not cross cuts but go round the singularities generating them (**). Alternatively, if we cross a cut we must ensure that we cross back again later on to the physical sheet. (We may think

(*) This follows from eq. (A.2) of Appendix I.

(**) If we do cross a cut and insist on remaining on the physical sheet the resulting discontinuity in $\boldsymbol{A}$ may cause a transition from singularity to non-singularity.

of this procedure as being equivalent to temporarily pushing back the cut, whose precise location is in any case arbitrary, except for its branch point.) If both these alternatives fail we are forced to go through an effective intersection and so may change from singularity to non-singularity. A simple illustration of this is given in Section 3.

Our conclusion is that the singular and non-singular parts of Σ are divided from each other by cuts due to lower-order singularities and that effective intersections with lower-order curves which are not singular at the intersection (and so have no cuts attached to them) need not concern us.

3. – The fourth order graph.

TARSKI (7) has already shown that the Mandelstam representation holds for the fourth order graphs under certain conditions which include the case when there are no anomalous thresholds. Our method is, in a sense, a generalization of this approach, but since we do not have detailed knowledge of the Landau curves our result is only one of sufficiency, not necessity. In this section we briefly restate Tarski's results, both to illustrate the nature of real algebraic curves and to put the argument in a form more suitable for generalization.

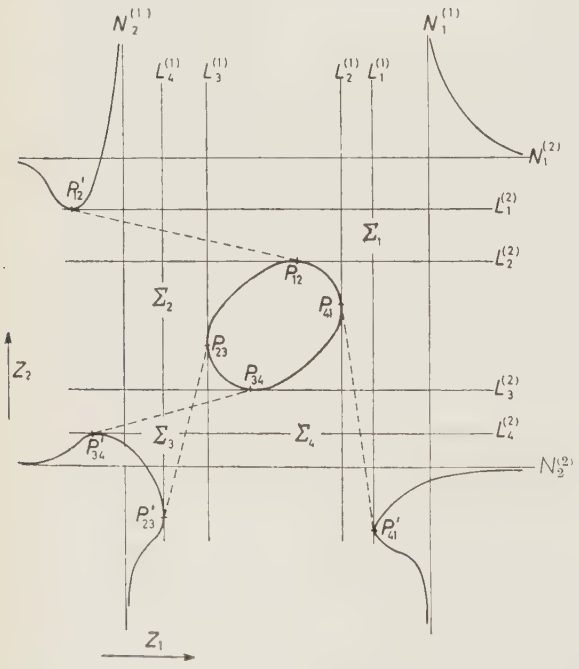

Fig. 1.

The leading curve Σ associated with the fourth order graphs has a real section Γ of the general form (7) sketched in Fig. 1. The lower-order curves are the lines labelled L and N, which correspond respectively to contractions of the Feynman graph into vertex and self-energy graphs. They are tangents and asymptotes respectively to Γ. The details of which line L touches

(7) J. TARSKI: *Journ. Math. Phys.*, **1**, 154 (1960).

which arc of Γ are not always as shown in the figure, but this is immaterial for our purposes.

Any point in complex z-space lies on a real line

$$z_1 = \lambda z_2 + \mu\,, \qquad \lambda,\ \mu \text{ real}, \tag{1}$$

for some λ, μ. Therefore drawing all such lines finds all points of Σ. Σ is given by a real polynomial equation and so its intersections with (1) are given by a real equation in z_2 whose roots give either real points or conjugate complex pairs of points. If the parameters λ and μ are varied continuously the transition from a real pair to a complex conjugate pair takes place at a coincident real pair, that is where (1) touches Γ. Thus complex conjugate portions of Σ sprout out of Γ as the moving searchline is successively a tangent to Γ and then fails to cut it. For Fig. 1 these complex surfaces join the central loop to the asymptotic arcs and form a sort of twisted torus.

If $\lambda > 0$ z_1 and z_2 have the same sign of their imaginary parts, while if $\lambda < 0$ their imaginary parts have opposite sign. Thus the sections Σ_2 and Σ_4 of Σ sprouting from the arcs $P_{12}P_{23}$ and $P_{34}P_{41}$ (of positive slope) contain only points for which $\operatorname{Im} z_1$ and $\operatorname{Im} z_2$ are of the same sign, and the sections Σ_1 and Σ_3 sprouting from the arcs $P_{41}P_{12}$ and $P_{23}P_{34}$ (of negative slope) give opposite signs. The divisions between these sections (indicated schematically in the figure by the broken lines) correspond to intersections of Σ with $z_1 =$ real or $z_2 =$ real.

The searchline method is applicable to any real algebraic curve. This is indeed fortunate for it enables the form of the curve to be adequately represented by drawing its real section.

We now consider which parts of Σ may be singular. The particular form of the Feynman denominator in this case implies that for $\operatorname{Re} z_1$ and $\operatorname{Re} z_2$ below certain values it does not vanish for real positive α. The integral is thus well-defined in this region by integrating over a part of α-space in which the α's are real and positive. The continuation to the rest of the physical sheet is made from this region. It is also found that the denominator does not vanish when $\operatorname{Im} z_1$, $\operatorname{Im} z_2$ are of the same sign and the α are real and positive. Therefore Σ_2 and Σ_4 are always non-singular. This proof of the existence of so extensive a non-singular region is a simplifying circumstance that does not generalize.

To find out whether Σ_1 and Σ_3 are singular we consider whether we can reach them from Σ_2 or Σ_4 without crossing a cut. The normal thresholds $N_1^{(1)}$ and $N_1^{(2)}$ are always singular on the physical sheet and $N_2^{(1)}$ and $N_2^{(2)}$ are always non-singular. The normal thresholds are not sufficient to generate boundaries between singular and non-singular parts of Σ: for this, anomalous thresholds are needed. There are four distinct possibilities ([7]):

i) No anomalous thresholds. There are no cuts dividing Σ_1 and Σ_3 from Σ_2 and Σ_4, so that all are non-singular and the Mandelstam representation holds.

ii) Either $L_1^{(1)}$ or $L_1^{(2)}$ (or both) is singular. Again there are no dividing cuts.

iii) $L_2^{(1)}$ and $L_2^{(2)}$ are singular (and maybe also $L_1^{(1)}$, $L_1^{(2)}$). The resulting cuts $P_{12}P_{12}'$ and $P_{41}P_{41}'$ divide Σ_1 from Σ_2 and Σ_4 and force us to pass through one of the effective intersections P_{12}, P_{41} on going from Σ_2 or Σ_4 to Σ_1. Thus we cannot say that Σ_1 is non-singular. In fact it is singular ([7]) and the Mandelstam representation does not hold. No cuts exist across $P_{23}P_{32}'$ or $P_{34}P_{34}'$ so that Σ_3 is still non-singular.

iv) $L_3^{(1)}$ and $L_3^{(2)}$ are singular (and maybe also $L_1^{(1)}$, $L_1^{(2)}$). The situation is similar to that in iii).

We remark that the trouble in cases iii) and iv) is caused by the coincidence of a singularity in z_1 with a double point in the mapping $z_1 \to z_2$ generated by Σ.

4. – Reality properties.

Naturally not all the properties which make the fourth order graph comparatively simple continue to hold to all orders. One that does is that a point on Σ and its complex conjugate (also on Σ) are either both singular or both non-singular. This comes about in the following way.

Majorisation techniques ([8]) imply that there is a region $\mathscr{R}$ of the real (z_1, z_2) plane for which the Feynman denominator does not vanish for real positive values of the α's. Here the resulting Feynman integral F is real and non-singular. As we continue from $\mathscr{R}$ to some point (z_1, z_2) along some route in z-space we end up with a certain configuration in α-space of the hypercontour $\boldsymbol{A}$ and the manifold of zeros of the denominator. If we continue instead to $(\bar{z}_1, \bar{z}_2)$ along the complex conjugate route we end up with the complex conjugate configuration. This proves the stated property.

This branch of F defines for us the physical sheet. It is a simple corollary of the analytic properties which we shall deduce for this branch that this definition agrees with the Feynman prescription in the physical scattering regions ([5]).

The general perturbation theory function for a Feynman graph with four external lines has normal threshold cuts corresponding to each of the three

([8]) K. SYMANZIK: *Prog. Theor. Phys.*, **20**, 690 (1957). Note that the parameters α used by SYMANZIK are essentially the inverse of our Feynman parameters.

Mandelstam channels. However, at any point in the real subspace at most two of these cuts overlap. The corresponding invariants are the most convenient variables for discussing the behaviour at the point. The reality property implies that there are at most two distinct limits ont o the real section I' of Σ at this point: that in which $\mathrm{Im}\, z_1$, $\mathrm{Im}\, z_2$ are of the same sign and that in which they are opposite. On I' the limit defined by approach in the same sense as the attached complex part of Σ will be called the *appropriate* limit. At points where there is only one cut both limits must be equal, since the way in which the limit is taken for the variable not having a cut is immaterial.

5. – Method of proof.

In order to use the ideas of Section 1 it is desirable that there be as few cuts as possible. The normal threshold cuts are always present, but we use an induction procedure on the order of the Feynman graph to remove the others. The absence of anomalous thresholds (see Appendix 2) permits the induction procedure to start. Then, in considering the behaviour of any leading Landau curve, we may suppose the Mandelstam representation to hold for each of the contracted graphs for which the lower order curves are themselves the leading curves.

This induction is not quite trivial in that it supposes that the behaviour of a given curve is the same when it is a lower-order curve as when it is the leading curve. To see that this is so we consider the permissible distortion of the hypercontour $\boldsymbol{A}$. In the neighbourhood of one of its interior points $\boldsymbol{A}$ may be distorted arbitrarily, but at an edge the distortion is arbitrary only in the subspace of the non-zero α's. The resulting sub-contour in the edge subspace is therefore the same as that obtained for the actual hypercontour of the corresponding contracted Feynman graph. Note, however, that there may be intrusions into the edge subspace from the interior of $\boldsymbol{A}$ (Fig. 2).

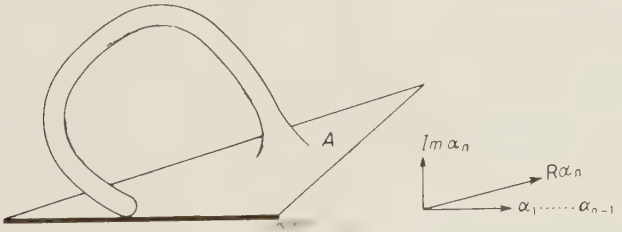

Fig. 2.

The intrusions need not concern us, as they do not correspond to true edges where a pinch can slip off the hypercontrour, but they do provide the explanation of an apparent paradox occurring, for example, in case iv) of the fourth

order graph discussed in Section 3. Here the lower-order curve $L_2^{(1)}$ is not singular, but the point P_{41} regarded as belonging to the leading curve Σ, is singular when approached with $\mathrm{Im}\, z_1$, $\mathrm{Im}\, z_2$ opposite in sign.

The proof is in two parts. In the first (Section 6) it is shown that the Landau curve can be divided into a number of sections, each of which is either wholly singular or wholly non-singular. In the second part (Section 7) a point is chosen from each section and it is shown that if this point were singular then known properties of the Feynman amplitude would be violated. Consequently each section, and so the whole of Σ, is non-singular.

6. – Normal thresholds.

It may seem surprising that the existence of normal threshold singularities is less of an embarrassment than the existence of anomalous thresholds. The reason for this is the important property that Landau curves for normal threshold graphs (which consist of a number of parallel straight lines) can only have effective intersection with the leading curve Σ at infinity. The proof is as follows.

If Σ has effective intersection with a normal threshold it simultaneously has effective intersection with some curves corresponding to vertex graphs (*). But the latter are also parallel straight lines, so that this can only happen at infinity.

Σ will now be divided into a number of sections having three properties.

A) Each complex point of Σ lies in one of the sections.

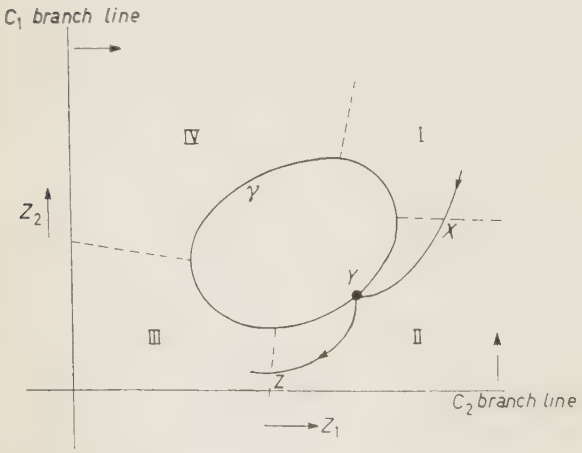

Fig. 3.

B) All points of a section behave in the same way, that is, all are singular or all non-singular.

C) It is possible to find points in any given section for which $\mathrm{Re}\, z$ belongs to the Symanzik region $\mathscr{R}$.

In this condition z is any one of the Mandelstam invariants. The considerations of Section 7 determine the most convenient choice of z in a given problem.

(*) This can be seen from dual diagrams. It is not necessarily true for self-energy parts other than normal thresholds.

The analysis of Section 2 shows that the *primitive* sections into which Σ is divided by the normal cuts have the properties A and B. However, they need not have the property C because of the sort of situation illustrated in Fig. 3. Here γ is a loop which is part of the real section Γ of Σ, lying in the region where two cuts C_1 and C_2 overlap. From it sprouts a complex part of Σ which is divided by C_1 and C_2 into four primitive sections I ... IV. To satisfy condition C it is necessary to link I to III and II to IV using paths *lying in* Σ.

This can be done by following the type of path P sketched in Fig. 3. At X we cross C_1. At Y we cross γ and move on to the complex conjugate half of II. In so doing we recross C_1 and also cross C_2. At Z we recross C_2. Between X and Z we have left the physical sheet and we are in a neighbouring unphysical sheet, but at Z we re-enter the physical sheet and so arrive at III on the physical sheet. The projections of P on the complex z_1 and z_2 planes are shown in Fig. 4. No change in behaviour on P will have occurred unless we have encountered a lower-order singularity between X and Z. At first sight this possibility cannot be discounted since the induction hypothesis refers only to the physical sheet. However, since we need only just enter the neigh-

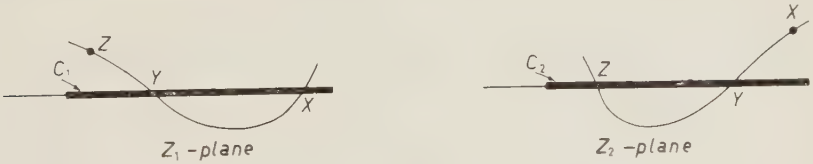

Fig. 4.

bouring unphysical sheet and can in fact *skim* along γ we need only encounter an effective intersection with such a singularity Γ' if its relevant arc γ' is singular in the inappropriate sense. We then call γ' an arc of *virtual singularity*: we know from the induction hypothesis that it is not singular in the appropriate sense.

For the path P sketched, joining I to III, this point is easily resolved. This follows from the fact that virtual singularities can only occur on a part of a curve having negative slope. This is shown in the next section. However, the joining of II to IV requires a special argument (*), which is given in Appendix I.

The situation considered in Fig. 3 provides the general method of linking together primitive sections. The more complicated cases can always be re-

(*) This point was raised and resolved in discussions with Dr. R. J. Eden. It also affects his proof [9].

[9] R. J. Eden: preprint (Cambridge).

duced to the problem of joining successive pairs of primitive sections such as I and III. This suffices to construct sections satisfying condition C unless the final primitive section is joined to an infinite arc still lying in the crossed outs. (See Fig. 6 of Appendix I.) In these circumstances a modified technique may be required to join the section in question to a neighbouring section which does satisfy C. This technique is described in Appendix I.

It now remains to show that each section is non-singular rather than singular.

7. – Non-singularity.

Dispersion relations for forward scattering have been proved, either from general principles ([10]) or in perturbation theory ([8,9]), in cases where there is no unphysical region. If the type of process in which we are interested possesses a channel for which this is true we fix the appropriate variable z at z_0 to give forward scattering in this channel and consider possible singularities in the complex plane of the other variable z'. By construction, each of our sections either has at least one complex point (z_0, z') or determines the behaviour (from the appropriate limit, which here is equal to the inappropriate limit since we are not in the crossed cuts) at a real point (z_0, z'). The only way such a point can be singular and not violate the dispersion relation is if it lies in the cuts along the real z'-axis. Since we have said that these cuts lie wholly in physical regions this possibility can be excluded, for unitarity ([11]) requires that the only singularities in the physical region correspond to normal thresholds. Thus each section is non-singular and the Mandelstam representation holds.

Although there are no complex singularities, arcs of the real part of Σ which lie in overlapping cuts may be virtual singularities, that is singular in the inappropriate sense. These arcs cannot have horizontal or vertical tangents, for the inappropriate behaviour to one side of such a tangent is, as is seen by skimming round the point of tangency, the same as the appropriate behaviour on the other side. They must not lead to regions where appropriate and inappropriate limits are equal, and so they lie wholly in the crossed cuts. Moreover, this last property implies that their asymptotes must be the singular normal thresholds. This is seen by considering the problem using as variables z_1 and $\zeta = 1/z_2$, say. (When using these variables, we must remember that $\zeta = 0$ is a line of singularities.) Our conclusion is, therefore, that an arc of virtual singularity must be an open arc asymptotic to normal thresholds.

([10]) See, for example, H. LEHMANN: *Suppl. Nuovo Cimento*, **14**, 153 (1959).
([11]) R. J. EDEN: *Phys. Rev.*, **119**, 1763 (1960).

It is necessary that such arcs exist, as they are the boundaries of the Mandelstam spectral functions. An illustration of their existence is provided in cases i) and ii) for the fourth order graph discussed in Section **3**, where (Fig. 1) the open arc lying in the crossed cuts is singular in the inappropriate limit. This shows, incidentally, that the Mandelstam representation does not hold in the first unphysical sheet.

These observations complete the discussion of those cases which have wholly physical cuts in forward scattering. Other cases can be obtained starting from a fictitious process with this property and continuing from this in the external masses, keeping the internal masses fixed. This procedure is discussed in the next section. A suitable fictitious case from which continuation may be made is a theory of π-π scattering in which no baryon or strangeness selection rules are imposed. Having proved the Mandelstam representation for each graph in this theory we can then perform our mass continuation on each of a subset of these graphs so as to obtain a proof for each permitted graph occurring in the process under consideration.

8. – Continuation in the masses.

We start with Σ non-singular at its intersections with the plane $z = z_0$ and are required to show that it remains so as each external mass in turn is increased from its fictitious to its actual value. This is exactly the same type of problem as we have already considered in Section **5** and **6** except that our variables are now z' and M instead of z' and z. It is simpler in detail, however, as we are only performing our continuation over a small region of the (M, z')-space which is, moreover, free from overlapping cuts. The only way that Σ can become singular is for it to have an effective intersection with a normal threshold (*). In this event a Landau curve for a vertex graph must also have an effective intersection at the same point and become singular. Thus we can continue in the external masses quite harmlessly up to the limit for the appearance of the first anomalous threshold. We may, of course, be able to continue even further.

9. – Discussion.

The foregoing arguments present sufficient conditions for the validity of the Mandelstam representation to each order of perturbation theory. For the fourth order case TARSKI ([7]) was also able to give necessary and sufficient

(*) This need not take place at infinity since the vertex curves are not straight lines in the (M, Z')-space.

conditions, permitting in certain cases the existence of not more than one anomalous threshold in each variable. It is not known how this generalizes (*). To investigate this it is necessary to know more details of the effective intersection of Landau curves with anomalous thresholds.

EDEN ([9]) has also given a proof of the Mandelstam representation in perturbation theory. In essence his proof and that given here are the same. They depend on the following three basic properties:

i) Effective intersections of Landau curve with normal thresholds are always at infinity.

ii) The hierarchical and interdependent structure of perturbation theory singularities permits the skimming procedures of Section 6 and so provides a link between behaviour on different parts of a curve. This is the most involved part of either proof and is the same for both.

iii) The existence of single variable dispersion relations in certain basic regions implies non-singularity in these regions.

A difference in the two proofs appears in the method of connection between the basic region and the rest of the complex space. We use ii) to travel to the basic region, while EDEN uses ii) to travel from the basic region. Thus schematically one proof is the other in reverse order.

* * *

One of us (J.C.T.) wishes to thank Dr. R. E. MARSHAK for hospitality received at the Department of Physics and Astronomy in the University of Rochester during part of the time this paper was being prepared. Another (P.V.L.) is grateful to the D.S.I.R. and the Amy Mary Preston Read Bequest for grants.

APPENDIX I

We here resolve the problem of virtual singularities, raised in Sect. 6.

Since we may choose to skim from IV to II (Fig. 3) either via I or III we only fail when both these paths are blocked by virtual singularities γ_1' and γ_2', as shown in Fig. 5.

(*) *Note added in proof*: The general necessary and sufficient conditions are given in a paper by R. I. EDEN, P. V. LANDSHOFF, J. C. POLKINGHORNE and J. C. TAYLOR, to be published.

If the Feynman denominator has the form [8]

$$f_1 z_1 + f_2 z_2 + K, \tag{A.1}$$

then it is a trivial consequence of the Landau equations that the slope of a Landau curve is given by

$$\frac{\mathrm{d}z_2}{\mathrm{d}z_1} = -\frac{f_1}{f_2}. \tag{A.2}$$

It is important to note that the values of the α's corresponding to points in the real section are real. This follows from the reality of the Landau equations in these circumstances together with the uniqueness of the α's for given z_1, z_2.

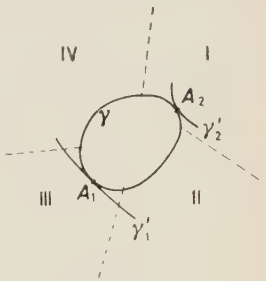

Fig. 5.

When two curves have effective intersection they have the same values of f_1 and f_2. Tracing round from A_1 to A_2 on λ we find that both f_1 and f_2 change sign once on the way (assuming that they do not vanish simultaneously). Since γ_1' (or γ_2') is an open arc of negative slope f_1 and f_2 must have the same sign all over γ_1'. In particular, the sign of f_1, f_2 at A_1 is the same as their sign at the effective intersection of γ_1' with the normal thresholds which are its asymptotes. It is known from the structure [8] of f_1 and f_2 that at such an effective intersection one is zero and the other is just equal to the product of the non-zero α's and hence positive. Thus the situation shown in Fig. 5 does not occur.

The arguments we have presented are sufficient to deal with the problem of virtual singularities, even in an apparently exceptional case such as illustrated in Fig. 6. Here the region I forms a self-contained primitive section which does not fulfil condition C of Sect. **6**. We have shown that there cannot be effective intersections with virtual singularities on both the arcs γ_1 and γ_2. If there is none on γ_1 then the whole arc γ_1 is singular in the inappropriate sense if I is singular. However, a part of γ_1 lies outside the overlapping cuts and so cannot be singular since appropriate and inappropriate limits then must coincide. The case in which γ_1 has effective intersection with a

Fig. 6.

virtual singularity, but not γ_2 can be cast in the same form by working with z_1 and $1/z_2$ as variables.

We note that a similar consideration of the signs of f_1 and f_2 prevents γ_1, say, from having effective intersection with a virtual singularity and at the same time γ_2 being asymptotic to a normal threshold.

RIASSUNTO (*)

Si dimostra la validità della rappresentazione di Mandelstam in ogni ordine finito nella teoria di perturbazione per processi pei quali sono state dimostrate relazioni di dispersione per lo scattering in avanti. Si fa poi una estensione alle masse esterne cosicchè la dimostrazione diviene valida per tutti i processi in cui non si hanno soglie anomale nell'ordine più basso.

(*) *Traduzione a cura della Redazione.*

A Bubble Chamber Experiment to Measure the Polarization of the Recoil Proton in the Photoproduction of π^0 Mesons from Hydrogen (*).

L. Bertanza, P. Franzini, I. Mannelli and G. V. Silvestrini

Istituto di Fisica dell'Università - Pisa
Istituto Nazionale di Fisica Nucleare - Sezione di Pisa

V. Z. Peterson

California Institute of Technology
Istituto di Fisica dell'Università - Roma

(ricevuto il 27 Ottobre 1960)

Summary. — A rapid cycling bubble chamber is used to measure the polarization of the recoil proton from the reaction $\gamma + p \to \pi^0 + p$. The experimental setup and the method of analysis of the events are described. We give a preliminary result of the polarization for a mean photon energy $k = 725$ MeV and a center of mass angle of 87°.

An experiment is in progress at the Frascati electron synchrotron to measure the polarization of the recoil proton in π^0 photoproduction using a propane-ethane bubble chamber and magnetic selection. The use of a visual method makes it possible to observe each scatter; this reduces the chances for systematic errors due to uneven flux of protons through the scatterer and the finite size of both hydrogen target and scatterer. In addition, an examination of the complete angular distribution of single-scattering events enables one to evaluate, within the data of this same experiment, the contribution of inelastic

(*) Comunicato al XLVI Congresso della Società Italiana di Fisica, Napoli (Settembre - Ottobre 1960).

scatters to the sample selected for measurement of the polarization. The contamination of inelastic scatters is not small, even for proton energies as low as 135 MeV, and the asymmetry in scattering essentially vanishes for excitation energies of 30 MeV or more [1]. When a range telescope is used, a good resolution measurement of the energy loss in the scattering is difficult because of the continuous energy spectrum of the incident protons. This results in a corresponding difficulty in the evaluation of the inelastic contribution.

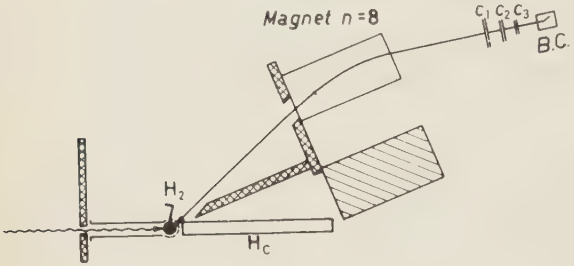

Fig. 1.

Our experimental arrangement is shown in Fig. 1. A strong focusing magnet selects protons at an angle of $(43 \pm 4)°$ from a liquid hydrogen target and focuses them upon the window of the bubble chamber. The magnetic field is greater for wider angle protons entering the magnet; the correlation between proton momentum and angle is such as to select protons produced by a nearly constant photon energy. This tends to improve the photon resolution of the experiment, at the expense of a wider spread of the center-of-mass angles. Another advantage of magnetic selection is that only protons in the momentum-angle interval of interest fall upon the scatterer; thus higher energy protons which could produce inelastic and elastic « background » scatters are excluded.

A counter telescope selects protons by pulse height discrimination, and the coincidence triggers the flash for the chamber. The bubble-chamber [2] (volume approx. 1.5 liter) is expanded 4 times/second (every 5th synchrotron pulse) in synchronism with the accelerator. Thus 1 proton in 5 which enters the chamber is photographed. With normal collimated beam intensity (10^{11} Q/min) there are 12 photographs/minute.

The bubble-chamber contains approximately equal parts by weight of ethane gas dissolved in propane, and operates at room temperature with tap-water cooling.

For the initial results reported here, a mean photon energy near 700 MeV, and a center-of-mass angle of 90° were desired. At 43° (lab.) the resulting proton has a kinetic energy of 190 MeV and momentum of 630 MeV/c in the magnet, and is reduced to 165 MeV at the center of the bubble-chamber.

[1] A. JOHANSSON, G. TIBELL and P. HILLMAN: *Nuclear Physics*, **11**, 540 (1959).

[2] L. BERTANZA, P. FRANZINI, I. MANNELLI and G. V. SILVESTRINI: *A rapid cycling bubble chamber*, to appear in *Nuclear Instruments and Methods*.

Range measurements were made by inserting copper absorbers between counters C-2 and C-3, to determine the actual mean proton energy and energy spread from the full aperture, of the magnet and from the two half-apertures $39° \div 43°$ (« *I* ») and $43° \div 47°$ (« *O* ») separately. It was found that the proton flux was far from uniform, the flux ratio between the two halves being $I/O = 1.4$ at the entrance of the magnet (and 1.7 at the chamber, due to magnet optics). Taking into account the proper weighting factors, the experiment accepts a mean photon energy of 725 MeV with a photon energy spread of about ± 80 MeV (70% of photons included).

We have not used a Čerenkov counter to detect the π^0 in coincidence with the proton because of the reduction in counting rate this would entail. The range curves show that our proton telescope selects protons (2.2 minimum or above) with less than 5% charged pion or electron contamination. In addition we can be sure we have a proton by the chamber photographs. Hence we have accepted a 20% background from the empty target, and subtract its effect statistically. The background contribution can be evaluated in a short time with good statistics by means of the counter telescope, without requiring the proton to be photographed or to scatter in the bubble chamber. The background asymmetry is measured by replacing the hydrogen target with a mylar target, in order to have a high counting rate.

At this date we have analysed 20000 single view photos containing 13550 incident protons. Each proton has an average path length in the chamber of 12 cm. In this sample we see 474 single scatters without visible recoil or associated prong, 153 p-p scatters in which the recoil prong is visible, and 102 stars (mostly 2-prong). The 474 single scatters include events up to 90° projected angle of scatter, and the known angular distribution of elastic and inelastic scattering in this proton energy range makes it clear that essentially all events beyond 30° are inelastic scatters from carbon. A few of the events at small angles are p-p scatters in which we cannot see the recoil proton (less than two millimeters projected range). The total spread of proton energies in the bubble-chamber, taking into account the spread in incident momentum and the finite length of the chamber is (120 ÷190) MeV. Since elastic scattering is more probable at lower energy, while inelastic scattering is less strongly energy dependent, we have chosen the Harwell 135 MeV elastic scattering results ([3]), and the inelastic scattering data of Harvard ([4]) at 96 MeV and Uppsala ([5]) at 185 MeV (which nearly coincide). The comparison between predicted yields and that observed by us is shown in Table I.

The p-p events are the ones with non-visible recoils; the predicted total

([3]) J. M. Dickson and D. C. Salter: *Nuovo Cimento*, **6**, 235 (1957).
([4]) K. Strauch and F. Titus: *Phys. Rev.*, **104**, 191 (1956).
([5]) H. Tyren and Th. A. J. Maris: *Nuclear Physics*, **3**, 52 (1957).

TABLE I. – *Yields for* 13550 *protons in* 12 cm *ethane propane.*

Projected-angle	Predicted				Observed
	Elastic	inelastic	p-p	Total	
$6° \div 12°$	95	19	14	128	165
$12° \div 20°$	40	60	0	100	118
$20° \div 30°$	11	53	0	64	63
$30° \div 40°$	2	32	0	34	40
$40° \div 60°$	1	39	0	40	39

of 14 events agrees with the missing number in an angular distribution plot of the 153 visible events. The inelastic events in Table I do not include stars; the inelastic predictions include only excitation energy $(10 \div 50)$ MeV, and we have assumed that an inelastic encounter of 50 MeV or more will produce a star in carbon. The plot of the angular distribution in Fig. 2 shows that the shape and magnitude of the observed distribution is in good agreement with the predicted yields at large angles, while the yield observed at small angles is slightly high.

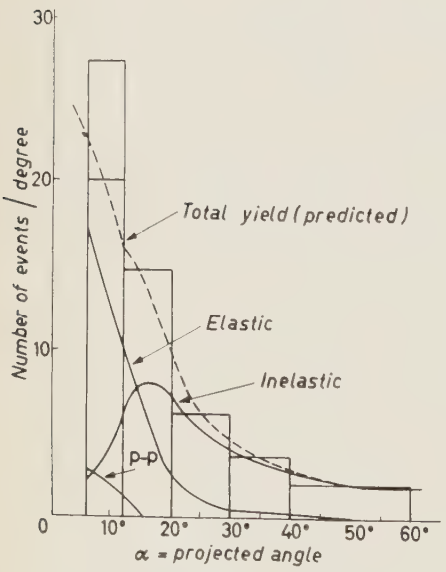

Fig. 2.

It is necessary to make substantial corrections to the 283 scatters (173 left, 110 right) in the $(6 \div 20)°$ interval in order to obtain the polarization. A small asymmetry applies to the p-p scattering, and to a few of the inelastic scatters; the result is that we subtract 9 L and 7 R p-p scatters, and 42 L and 37 R inelastic scatters. The 20% background (which has been measured to be symmetric) is then subtracted from the remaining 188 elastic events, yielding carbon elastic scatters of $L/R = 103/47 = 2.19 \pm .43$. Using the Harwell polarization data at 135 MeV for carbon [3], we obtain the preliminary result (*).

$$P = +\,0.78 \pm .27 \text{ (in the direction } \boldsymbol{k} \times \boldsymbol{p} \text{ (proton))}$$

(*) The proper factor to have the polarization from the asymmetry is going to be recalculated using a computing machine.

for a mean photon of 725 MeV and pion c.m. angle of 87°. 16600 more photos have been taken up to now with two stereoscopic views, and are going to be analysed. Further runs are anticipated both at the same and at higher photon energies (wider laboratory angles).

* * *

We are indebted to the Synchroton staff for continuos assistance and help during the machine runs.

One of us (V.Z.P.) wishes to acknowledge the support of a Fulbright Research Fellowship and of a Guggenheim travel grant for the period of this research.

Thanks are due to Prof. C. Franzinetti for several valuable discussions.

RIASSUNTO

Una camera a bolle a ciclo rapido è stata adoperata per misurare la polarizzazione del protone di rinculo della reazione $\gamma+p \rightarrow \pi^0+p$. Vengono descritte la disposizione sperimentale e il metodo di analisi degli eventi. Si dà il risultato preliminare per la polarizzazione a un'energia media dei fotoni $k=725$ MeV e ad un angolo di emissione nel sistema del baricentro di 87°.

Velocity Dependence of Track Density in Propane and Hydrogen Bubble Chambers.

A. Ahmadzadeh and N. N. Biswas

Lawrence Radiation Laboratory University of California - Berkeley, Cal.

(ricevuto il 31 Ottobre 1960)

Summary. — A study of ionization data for charged particles has been made in an underexpanded propane and a normally operated hydrogen bubble chamber. The gap-length distribution is found to be exponential over a wide range of velocity intervals, and the coefficient of this distribution gives a measure of the true track density, g; g is proportional to β^{-n}, where $n=1.71\pm0.11$ for propane and $n=1.86\pm0.37$ for hydrogen. The density of gaps, G, or of blobs, B, defined with good objective criteria, shows a dependence on g, namely $G(\varepsilon)=g\exp[-g(\alpha+\varepsilon)]$; it passes through a maximum value, the position of which is related to the minimum resolvable gap distance (approximately the the average diameter of individual bubbles). The mechanisms of energy loss or δ-ray formation for the process of bubble nucleation have been discussed in view of these measurements. We find the track density g to be approximately proportional to the rate of energy loss, $\mathrm{d}E/\mathrm{d}X$; this would indicate that the bubble nucleation process may not be as simple as has been considered so far.

1. – Introduction.

The ionization data on the charged particles passing through bubble chambers have rarely been used in the track evalutation because of the large variation of the operating conditions. It nevertheless has been helpful in some cases, such as in the identification of rare events (1). However, the

(1) F. S. Crawford Jr., M. Cresti, M. L. Good, G. R. Kalbfleisch, M. L. Stevenson and H. K. Ticho: *Phys. Rev. Lett.*, **1**, 377 (1958).

operating conditions have been improving, and the track evaluation by this method seems to be more promising. Therefore a systematic study of the problem under the present operating conditions would be worth while.

2. - Track-density evaluation.

In referring to ionization, the following nomenclature is relevant: (*a*) true bubble density, (*b*) blob or gap density. The « true bubble density » is defined as having a one-to-one correspondence to the density of the « thermal spikes » produced by the ionizing particle, which would lead to the formation of bubbles. Blobs are the isolated islands of bubble images separated by a minimum resolvable distance, and may have different sizes due to clogging of a number of bubbles. Also the gaps are counted only when they exceed a resolvable unit of length.

A number of observers [2] have used the method of counting bubbles per unit lenght as a measurement of specific ionization. This would underestimate the true bubble density because of losses due to limited optical resolution and possible bubble coalescence. Moreover, this method is somewhat subjective and involves the problem of reproducibility of the measurements. A really objective method is needed. The least subjective method seems to be the determination of the mean gap length from its distribution, which is extensively used in nuclear emulsion technique.

In nuclear emulsion, it was experimentally shown by O'Ceallaigh [3] that the gap distribution is exponential. The gap distribution was subsequently studied by Fowler and Perkins [4] in a systematic way. This distribution has been theoretically derived by Barkas [5], who finds that the gap-length coefficient is to be identified with the true grain density in emulsion. In bubble chambers, the same distribution has been observed by us and previously by Willis *et al.* [6] and Blinov *et al.* [7], namely

$$N(l) = N(0) \exp [-gl] , \tag{1}$$

---

[2] D. A. Glaser, D. C. Rahm, and C. Dodd: *Phys. Rev.*, **102**, 1653 (1956); W. J. Willis, E. C. Fowler and D. C. Rahm: *Bull. Am. Phys. Soc.*, **2**, 6 (1957).

[3] C. O'Ceallaigh: *Measurement of ionization in photographic emulsion by the technique of mean gap length*, Dublin Institute for Advance Studies, School of Cosmic Physics, Report NP-5372 (CERN Report BS-11, 1954).

[4] P. H. Fowler and D. H. Perkins: *Phil. Mag.*, **46**, 587 (1955).

[5] W. H. Barkas: *The theory of emulsion track structure*, Lawrence Radiation Laboratory Report UCRL-9181, (April 1960).

[6] W. J. Willis, E. C. Fowler and D. C. Rahm: *Phys. Rev.*, **108**, 1046 (1957).

[7] G. A. Blinov, I. S. Krestnikov and M. F. Lomanov: *Žurn. Eksp. Teor. Fiz.*, **31**, 761 (1956) (translation: *Sov. Phys., J.E.T.P.*, **4**, 661 (1957).

where $N(l)$ is the number of gaps exceeding length l and g is a constant depending on the velocity β of the particle.

From this distribution, the average separation between the « true bubbles » — that is between the « thermal spikes » — is $\bar{l} = 1/g$, which means that g is equal to the number of « true bubbles » per unit lenght. We can write the number of gaps between two successive « thermal spikes » exceeding lenght l per unit length as

$$n(l) = g \exp [-gl] . \tag{2}$$

Now, assuming that the distance between two successive « thermal spikes » has to be greater than α in order to resolve gap lengths greater than zero measured between the successive edges of « bubbles », one has the gap density, G, or the blob density, B, as defined before,

$$B = G = g \exp [-g\alpha] . \tag{3}$$

All the above formulae have been theoretically treated by BARKAS ([5]) for emulsion.

3. – Experimental results.

3·1. *General.* – We have measured track density in the 30 in. Powell propane chamber and the 15 in. Alvarez hydrogen bubble chamber of the Lawrence Radiation Laboratory. All measurements have been made on the film under microscopes using magnification of 100 to 200. Pictures usually taken for the investigation of the physical problems have rather high bubble density to facilitate observation on the projection table. Hence at the ends of their ranges the number of gaps is too small to make any practical measurement. For this and for the other reasons to be mentioned, high statistical accuracy could not be obtained in the case of the hydrogen bubble chamber; extensive measurements have been feasible in the case of the propane chamber, and we shall therefore report on these data in detail and briefly mention the results with the hydrogen bubble chamber.

3·2. *Propane bubble chamber.* – With the kind cooperation of Dr. WILSON POWELL and his group, a special run of the chamber exposed to a proton beam of the Bevatron was possible under special operating conditions. The chamber was underexpanded to reduce considerably the bubble size as well as bubble density, and a parallel beam of protons was selected to stop in the chamber; the operating conditions were kept uniform as far as possible.

Some data on the proton beam are shown in Figs. 1 and 2; the fractional height distribution of the tracks at the entrance end of the chamber is shown solid in Fig. 1 and that at the stopping end dotted. The beam at entrance is quite peaked at a region slightly higher than the middle point of the chamber (from the bottom); the end points of the tracks, however, show a wider spread as is expected from Coulomb scattering. The change in depth between the entrance and the stopping ends for the same sample of tracks is shown in Fig. 2. These distributions would be used in estimating the correction factor in the measurements for the dip of the tracks and for the variation of the ionization with the depth of the chamber.

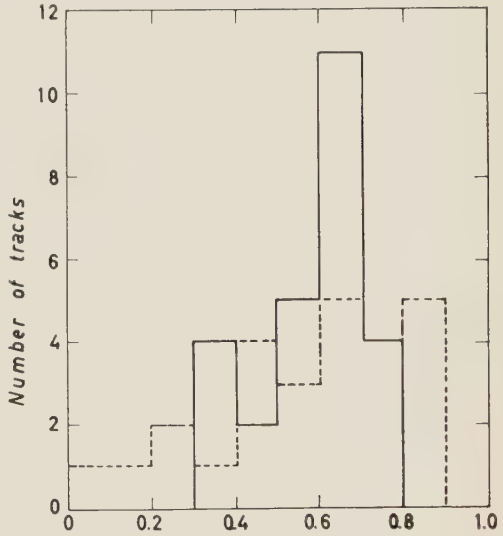

Fig. 1. – Height distribution of proton tracks in propane chamber at the entrance end (solid) and the stopping end (dotted); the heights are expressed in fractional units assuming the total height from bottom to top (6 inches) to be unity.

The gap lengths have been measured on the films with a microscope under 100× magnification. Two sets of measurements have been made (each set included about 100 tracks) — one with the help of an eyepiece with calibrated scale and the other with the help of a filar micrometer; in the latter case a line moved along the eyepiece scale and the gap length could be read more accurately from a micrometer scale fitted to the eyepiece. In fact, we did not need

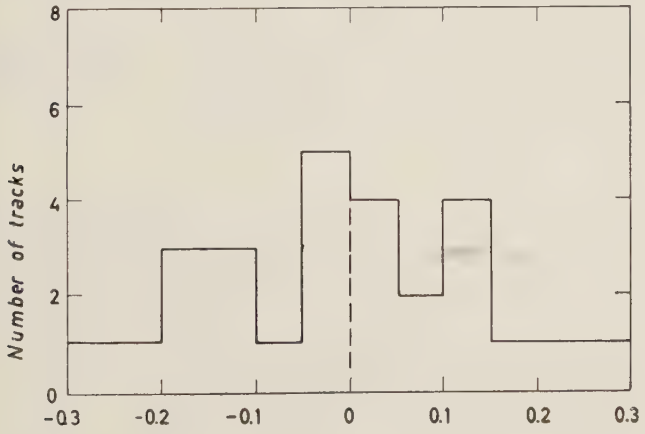

Fig. 2. – Distribution of the variation of height, Δh, between the points of entrance and stopping of the tracks. Δh is in fractional units, positive for a track moving towards the top of the chamber and negative in the reverse direction.

to measure the gaps accurately. It was sufficient to know to which interval in the differential distribution the gap belonged. The data have been combined to plot the integral distribution. The bubble images are not sharply defined, and this introduces some subjectivity in the measurements. The boundary of the image is defined to where the light intensity first matches the background of the film; we found that the measurements following this convention can be reproduced and do not appreciably vary with different observers.

For the high-velocity interval (at which $\beta = v/c$ is large), the number of counts per track is reasonably large (about 300), so that g can be evaluated for each track with statistical significance; the individual values of g agree within the statistical errors. This indicates that the chamber was working under reasonably uniform operating conditions during the run and that the pictures used for the measurements are of the same quality. Consequently, the combined data from all tracks can readily be used for evaluating g with higher statistical accuracy.

Counts from about 20 tracks in the high-β and about 200 in the low-β

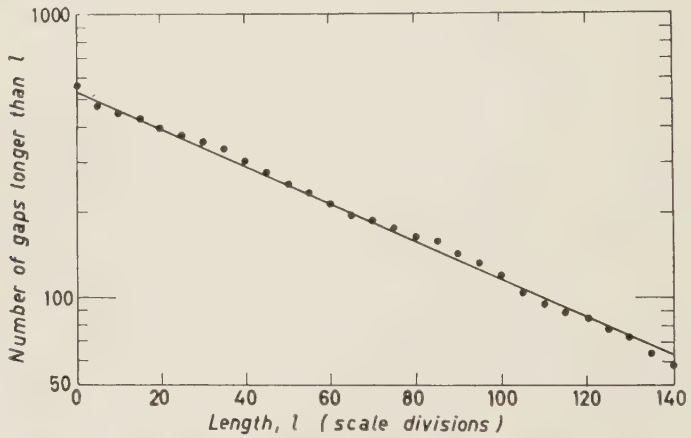

Fig. 3. – Integral distribution of gaps exceeding a length l *vs.* l; the lengths shown are in scale division of the eyepiece vernier as measured on the film; one scale division corresponds to 7.18 μm in the chamber.

intervals have been obtained to determine g. A typical distribution of gap lengths over a velocity interval for proton tracks in this chamber is shown in Fig. 3. The distribution is found, within our statistical accuracy, to be exponential over all ranges of the tracks we have measured, both in propane and in hydrogen bubble chambers.

To determine g, a least-squares fit to the semilog plot of $N(l)$ *vs.* l was obtained by using a suitable IBM 650 program. The program fits the

points to a straight line, giving proper weights to the corresponding points, and calculates the slope of the curve and its associated statistical error.

We report the values of g simply as obtained for the high-β interval, and introduce corrections to those at low velocities. The following correction factors to be used at the stopping end of the track compared to that at the entrance (correction factor = 1) can be readily evaluated:

3·2.1. Correction for foreshortening of the tracks due to distortion. – Measurements on the fiducial marks on the chamber reveal that for a horizontal track, g at the stopping end has to be multiplied by a factor 0.986.

3·2.2 Correction due to depth variation. – WILLIS *et al.* [6] report strong temperature dependence of g (about 50% change in g per °C). However, other causes, such as hydrodynamical conditions and the optical system, may introduce some effects also.

To investigate this, we have measured the gap distribution of fast steep tracks passing through the chamber and also of the proton tracks entering at different depths in the chamber. The variation of g with depth is found to be quite small; in individual measurements, the values of g at the bottom and at the top agree within the statistical errors. From the over-all measurements we may say that the fractional change in g, $\Delta g/g$, over the whole height of the chamber is no more than 20%. As mentioned before, we normalize our measurements to those of the proton beam at entrance, and therefore the variation of height at the stopping end with respect to its height at the entrance is relevant in the estimate of the correction factor. From Fig. 2 the average value of Δh is $\overline{\Delta h} = -0.011 \pm 0.002$, where Δh is expressed as fractional height (total height = 1); over this depth $\Delta g/g$ would vary at most by $\pm 0.2\%$. This small variation can therefore be neglected

During the operation of the chamber, no device for measuring the temperature gradient was used; it is believed, however, that this should not exceed 0.5 °C. Comparison of our data on $\Delta g/g$ with those of WILLIS *et al.* [6] indicates that the temperature gradient over the height of the chamber (6 in.) was less than 0.5 °C.

3·2.3. Correction for dip angle. – This can be readily made from the mean value of $|\Delta h|$, and the average correction factor is 0.985.

The correction factor when combined is then 0.97 at the end of the track, compared to unity at the entrance point, and would lie between these limits for the intermediate parts of the track.

The variation of g with velocity β thus evaluated is shown in Fig. 4. The lengths hereafter refer to the actual dimension in the chamber. The

values of β have been obtained from the range-energy relation, and the average value of β over the interval of measurements has been calculated, with proper weight given to each value of β according to the energy loss at that point. A least-squares fit of the points to a straight line gives $g = g_0\beta^{-n}$, where $g_0 = (5.92 \pm 0.33)$ cm^{-1}, $n = 1.71 \pm 0.11$. The errors correspond to statistical accuracy.

It is of interest how the gap density G varies with the track density g. In Fig. 5 we present the number of gaps per unit length (only gaps greater than 0.1 mm have been counted to ensure objectivity) versus the experi-

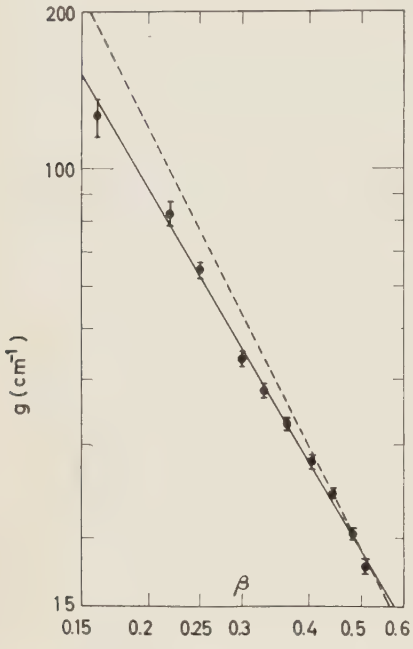

Fig. 4. – Track-density dependence on the velocity β in propane chamber; the lengths refer to chamber dimensions. The solid line corresponds to the least-squares fit of experimental data with slope $n = 1.71 \pm 0.11$. Plot of normalized dE/dX *vs.* β has a slope $n = 1.68$ and almost coincides with this line. For comparison, $1/\beta^2$-dependence of g normalized at $\beta = 0.5$ is shown dotted.

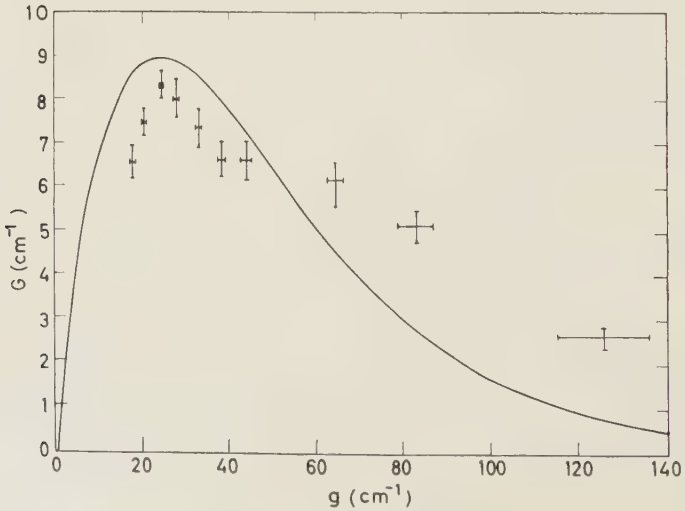

Fig. 5. – Density of gaps larger than 0.1 mm *vs.* the track density g in propane. The curve corresponds to $G = g \exp[-g(\alpha + 0.1)]$, $\alpha = 0.31$ mm.

mentally determined values of g. According to eq. (3), G should have a maximum at a g value given by

$$g = 1/(\alpha + \varepsilon) . \tag{4}$$

G indeed passes through a maximum; the position of the maximum may be used to determine the value of α. With $\varepsilon = 0.1$ mm, we obtain $\alpha \approx 0.31$ mm, which agrees very well with the measured average bubble diameter $D = (0.305 \pm 0.030)$ mm; α should, indeed, be identified with the average bubble diameter, as has been shown by BARKAS [5] for emulsion.

Though there seems to be qualitative agreement between eq. (3) and the plot in Fig. 5, the experimental data indicate some complexity. For example, the curve shown in Fig. 5 as calculated from eq. (3) by using the value of α from the position of the maximum in G gives a poor fit to the data. The fit can obviously be obtained by varying α with g; in Fig. 6, we show the behavior of α with g which would satisfy the relation (3).

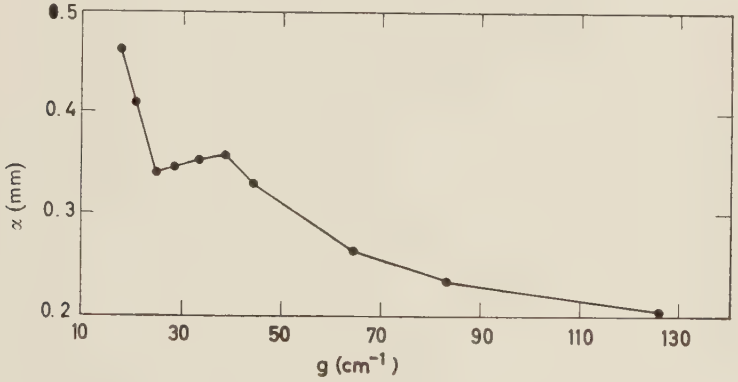

Fig. 6. – Variation of α with g in propane, if G follows the expected g dependence.

The optical system of the chamber might impair the resolution of measurement in a complex fashion in different parts of a track and also from track to track, this may be a reason for the variation of α with g. However direct determination of bubble diameter along the track length did not reveal such a drastic variation.

3·3 *Hydrogen bubble chamber.* – The original idea was to measure the ionization of protons and pions originating from the decay of Λ's produced by K^- capture in the chamber. In this way, a direct comparison of track density of protons and pions is possibile, since they have the same age. However, the protons from the decays were found to be slow to give gap

distribution of statistical significance; only the measurements on the pions are reported in this case. The tracks had to satisfy the following criteria:

(i) dip angle $\leqslant 10°$;

(ii) depth of the point of Λ-decay approximately halfway between the top and the bottom of the chamber.

Since the events were distributed over a large number of photographs, for consistency of measurement the fast beam tracks were used for calibration.

Here the measurements have been done in the same way as before, but under 210 × magnification. The variation of g with β for pions and a few electrons is shown in Fig. 7. The momentum of the particles is determined from the kinematics of the decay of Λ.

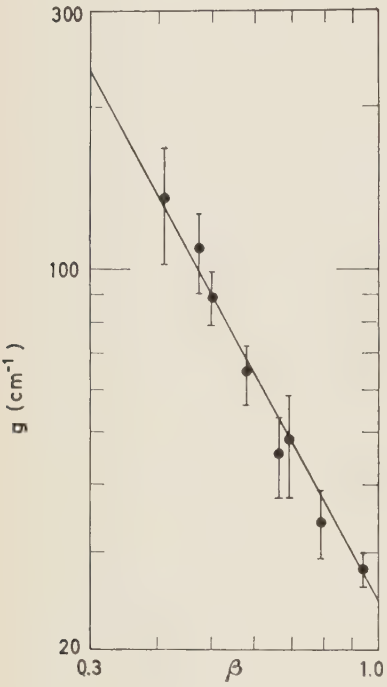

Fig. 7. – Dependence of track density g in hydrogen chamber on β; the lengths here also refer to the original dimensions of the chamber.

The statistical accuracy is rather poor in this case owing to the small number of measurable events. A least-squares fit of the data to a relation $g = g_0\beta^{-n}$ yields $g_0 = (24.4 \pm 5.9)$ cm^{-1}, $n = 1.86 \pm 0.37$. No detailed analysis of the data, as in the case of the propane chamber, is possible. KENNEY [8] in a recent investigation, in a hydrogen bubble chamber, has observed the same β-dependence of g as ours.

4. – Discussion.

The mechanism of bubble nucleation is not yet well understood. BUGG has discussed the problem in a recent review article [9]. If the energy is imparted to the bubbles by the stopping δ-rays, then the track density g should be well represented by a $1/\beta^2$-dependence; the number of δ-rays per unit length produced by a heavy particle colliding with electrons at rest (hard-collision approximation) between the limits of energy E_1 and E_2, which

[8] V. P. KENNEY: *Phys. Rev.*, **119**, 432 (1960).
[9] D. V. BUGG: *Progress in Nuclear Physics*, Vol. **7** (London, 1959), p. 1.

is assumed to lead to bubble formation, is

$$n = \frac{k}{\beta^2}\left[\frac{1}{E_1} - \frac{1}{E_2}\right]; \qquad k = 37.13 \text{ keV/cm}. \tag{5}$$

The collision cross section involves some other terms which can be neglected for all β. This mechanism would not lead to a relativistic rise in the track density.

Another mechanism of bubble formation would be the « storage » of energy from the energy loss of the passing particle; if an amount of energy exceeding Δ is to be stored in a dimension x for the nucleation process, then the β-dependence of g would be somewhat different from the δ-ray mechanism. It has been pointed out to us by Dr. W. H. BARKAS that Landau's treatment of ionization loss may be appropriate in this case. We have

$$g = (1/x)\psi\left(\frac{\Delta - \Delta_0}{\xi}\right), \tag{6}$$

where ψ is the universal function given by LANDAU [10]; and

$$\Delta_0 = \xi\left(\ln\left(\frac{2mc^2}{I^2}\,\xi\gamma^2\beta^2\right) - \beta^2 + 0.37\right),$$

$$\xi = x\,\frac{2\pi N e^4 \varrho}{mc^2\beta^2}\,\frac{\sum Z}{\sum A} = \frac{kx}{\beta^2}; \qquad k = 37.13 \text{ keV/cm}.$$

I is the ionization potential, 50 eV in propane.

In our case of an underexpanded chamber, $(\Delta - \Delta_0)/\xi$ is quite large, and $\psi(\eta)$ can be represented by $1/\eta$, as shown by LANDAU. Then eq. (6) can be written as

$$\frac{1}{g} = \frac{\beta^2\Delta}{37.13} - x\ln x - 16.91\,x = \beta^2\Delta' - \alpha\,, \tag{7}$$

$$\Delta' = \frac{\Delta}{37.13}\,, \qquad \alpha = x\ln x + 16.91\,x\,.$$

In the numerical values put into the equations, energy has been expressed in keV and lengths in cm. We note that β-dependence of g in this case would not necessarily follow the $1/\beta^2$ law.

[10] L. LANDAU: *Journ. Phys. U.S.S.R.*, **8**, 201 (1944).

For the purpose of comparison with experimental results, few systematic measurements are available. Consistent methods similar to ours have been used by BLINOV *et al.* [7] for track-density evaluation. Expressing g as $g = g_0\beta^{-n}$, they obtain $n = 2.07 \pm 0.17$, which is consistent with the δ-ray mechanism. However, they observe a relativistic rise of g for fast electrons contrary to the δ-ray formation mechanism due to hard collisions. Our value of $n = 1.71 \pm 0.11$ seems to be somewhat less than 2. We also find that g is practically a linear function of the relative ionization loss I_{rel}. Assuming the range-energy relation to be essentially correct, we can evaluate the relative ionization $I_{\text{rel}} = I_\beta / I_{\beta=0.5}$ from the equation

$$I_\beta = (\mathrm{d}E/\mathrm{d}X)_\beta = \frac{k}{\beta^2}\left[\ln\left(\frac{2mc^2}{I}\beta^2\gamma^2\right) - \beta^2\right]. \tag{8}$$

Our plot of g versus I_{rel} for the propane chamber is shown in Fig. 8; a straight-line fit to the data is quite good. We note in this connection, GLASER *et al.* [2] have reported that the bubble density is not a linear function I_{rel}. However, their method of evaluating bubble density is the conventional bubble counting, with greater possibility of loss of bubbles with the increase of the density.

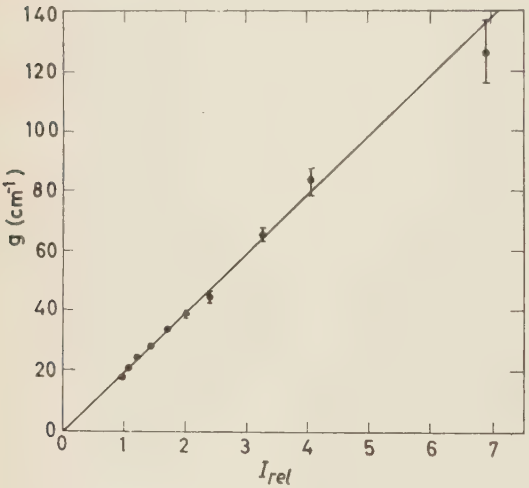

Fig. 8. – Dependence of track density g in propane chamber on the relative energy loss I_{rel} of protons.

On the basis of Landau's treatment, our data gave $\Delta \approx 8$ keV and $\alpha = -0.0026 \pm \pm 0.00245$; this value of α gives the β-dependence as observed in our case, but x has no physical solution.

Over the β interval 0.1 to 0.9, the β-dependence of $\mathrm{d}E/\mathrm{d}X$ can be well approximated by a β^{-n} law, with $n = 1.68$. Our value of n as obtained from the experimental data is in good agreement with this; also the relativistic rise observed by BLINOV *et al.* would favor the assumption that g is proportional to $\mathrm{d}E/\mathrm{d}X$. However, if this is really the case, it would be difficult to visualize the bubble-nucleation mechanism as a simple process, such as immediate generation of a « thermal spike » by a single δ-ray, or by storage over its dimension of energy exceeding a certain amount.

5. – Conclusions.

Our investigation shows that the gap-length distribution for a given β is exponential within our statistical accuracy over the entire range of the measurements. The mean gap length determined from this distribution gives a measure of the ionization of the particle. For practical purposes, we feel this method to be the least subjective one. Another advantage of this technique is that it can be consistently used over a wide range of velocities, provided sufficient counts are obtained with well-defined objective criteria. In bubble counts, the subjectivity of the observer would affect the consistency of measurement, particularly for heavy tracks; an attempt to determine the number of « bubbles » in a blob is difficult and somewhat unreliable, more so for dense tracks.

We find that g, the track density dependence on β, is well represented by $g = g_0\beta^{-n}$, where n is very near 2. The blob or gap density seems to be related to g in the same way as in emulsion, namely

$$\frac{B(\varepsilon)}{G(\varepsilon)} = g \exp\left[-g(\alpha + \varepsilon)\right] .$$

As required by this relation, G indeed passes through a maximum with the variation of g, and the position of this maximum determines a value of α which is in excellent agreement with the average diameter of the bubbles. However, in our case the above relation would hold if α were varied with g. B or G would be as sensitive a function of β as g if $g\alpha$ were very small; for low values of β, $g\alpha$ tends to be appreciable and B and G become less sensitive functions of β. Therefore for particle identification, g would be more advantageous.

We may remark that the method of evaluating g is not a too slow and time-consuming process, as may be thought. Even without having some highly mechanized system for channeling the distribution of gaps, the method may compete with the straightforward bubble counting. In a momentum-analyzed beam, if the βs of different particles are reasonably separated, a fast evaluation of g can be made to estimate the proportion of different particles. In this situation, the data on gap distribution need not be recorded in as many intervals as we have done; with a mechanical counter assembly having three or four push buttons to register three or four groups of gaps within rather long intervals, one can register the distribution by pressing appropriate keys. If the tracks are aligned along a certain axis of the microscope stage, one hand can be used to pass the track under the eyepiece rather rapidly and the other for pressing the buttons while the observer is looking through the microscope. Then a plot of the observed values of $N(l)$ *vs.* l

may be made on semilog paper and the slope of the straight line visually fitted would determine g; with a reasonable number of counts (more than 100), we find that the visual fit is quite good as compared to a least squares fit. In this way, the speed and the reliability in the evaluation of g are found to be quite satisfactory.

* * *

We are indebted to Dr. WILSON M. POWELL and his group for the trouble of running the propane bubble chamber under special conditions for our purpose, and for many helpful suggestions. We are thankful to the hydrogen chamber group for allowing us to make measurements on their films and furnishing us with the kinematical data of the events. This work was initiated with the suggestion of Dr. WALTER H. BARKAS, who contributed significantly to many discussions and criticism. We also had the privilege of having profitable help from a number of individuals of our group in some phases of the work.

This work was done under the auspices of the U. S. Atomic Energy Commission.

RIASSUNTO (*)

In una camera a bolle a propano sottoespansa ed in una ad idrogeno fatta funzionare normalmente si sono studiati i dati di ionizzazione delle particelle cariche. Si è trovato che la distribuzione delle lunghezze di gap è esponenziale per una vasta gamma di intervalli di velocità, ed il coefficiente di questa distribuzione dà una misura della vera densità delle tracce, g; g è proporzionale a β^{-n}, in cui $n=1.71\pm0.11$ per il propano ed $n=1.86\pm0.37$ per l'idrogeno. La densità dei gap, G, o dei blob, B, definita con buoni criteri obiettivi, mostra una dipendenza da g, precisamente $G(\varepsilon)-g\exp[-g(\alpha+\varepsilon)]$; essa passa per un valore massimo, la cui posizione è in rapporto alla minima ampiezza di gap risolvibile (approssimativamente il diametro medio delle singole bolle). Si è discusso in vista di queste misurazioni il meccanismo di perdita di energia e di formazioni di raggi δ nel processo di formazione dei nuclei delle bolle. Troviamo che la densità di tracce g è circa proporzionale al rapporto di perdita di energia, dE/dX; questo indicherebbe che il processo di formazione dei nuclei delle bolle non può essere così semplice come si è ritenuto sinora.

(*) *Traduzione a cura della Redazione.*

Interdomain Symmetry in the Reversible Phase Transformation of Potassium Cyanide.

A. Cimino and G. S. Parry

Istituto di Chimica Generale ed Inorganica dell'Università, e Centro per la Chimica Generale del Centro Nazionale Ricerche - Roma
Department of Chemical Engineering, Imperial College - London

(ricevuto il 7 Novembre 1960)

Summary. — The orientation of domains in transformed single crystals of KCN is considered in detail by means of stereographic projections. It is shown how the elements of point group symmetry of the high temperature phase divide on transformation into the intradomain symmetry elements that are preserved in the new crystal structure and the interdomain symmetry elements that relate individual domains possessing this new structure. A method of deriving the number of independent domain orientations is given in terms of these concepts and is applied to the alternative transformation schemes of KCN. Consideration is also given to the physical aspects of domain coexistence in KCN. The lattice changes which take place on transformation are considerable and it is shown that although « invariant » lattice planes common to two domain orientations do exist in some case, such a continuous transformation mechanism cannot account for all the domain orientations observed experimentally and an earlier conclusion that discontinuous processes must also occur is confirmed.

1. – Introduction.

Phase changes in solids may be divided into two classes, either continuous or discontinuous (1). In the latter case, the new phase bears no structural relation to the parent phase and therefore there is no specific relation between the orientation of different nuclei of the new phase with respect to the parent

(1) A. R. Ubbelohde: *Quart. Rev.*, **11**, 246 (1957).

phase. In other words, a single crystal of the first phase must transform into a randomly oriented polycrystalline mass which may or may not have the same external profile as the original crystal. A continuous phase transformation on the other hand is realized by some deformation of the original lattice so that a definite relation exists between the lattice orientation in the initial and final structures.

Typical examples of continuous transformations are the martensitic transformation in metals and the ferroelectric transitions in inorganic and organic salts. The lattice distortions that occur during ferroelectric transitions are usually small so that there are no serious angular or dimensional discontinuities at domain boundaries. For instance, in ferroelectric potassium dihydrogen phosphate, the transformation implies an angular misfit between neighbouring domains of only 27′ of arc. On the other hand, in the martensitic transformations, the dimensional and orientational changes are much greater so that although the metal is better able to withstand the stresses involved, nevertheless these stresses usually accumulate so as to prevent the whole of the parent phase transforming to the new structure.

It has been pointed out in a previous paper ([2]) that the reversible transformation of single crystals of KCN into the low temperature phase involves much larger dimensional and orientational changes than are found to occur in the ferroelectric transitions of ionic crystals so that this transformation is better considered as a simple example of a martensitic transformation. It is the purpose of this paper to consider in some detail the domain orientations in a transformed single crystal of potassium cyanide and to see what can be inferred about its domain texture.

2. – X-ray diffraction for the KCN transformation.

The experimental evidence, both for the structure of the low temperature phase of KCN and of the mutual orientation of domains having this structure, has been obtained through the interpretation of X-ray diffraction photographs of transformed single crystals ([2,3]). It has been found that KCN is cubic at temperature down to about — 106 °C and orthorhombic below this temperature (*). When discussing the mutual orientation of the cubic and orthorhombic lattices however, the low temperature form is best described by a monoclinic cell which can be directly derived by a homogeneous defor-

([2]) A. CIMINO, G. S. PARRY and A. R. UBBELOHDE: *Proc. Roy. Soc.*, A **252**, 445 (1959).

([3]) J. M. BIJVOET and J. A. LELY: *Rec. Trav. Chim. Pays Bas*, **59**, 908 (1940).

(*) The transformation temperature is approximate as hysteresis is present.

mation of the cubic cell together with small but significant dimensional changes. (According to BIJVOET and LELY [3] the dimensions of the cubic and monoclinic unit celles are: $a_c = 6.42$ Å; $a_m = c_m = 6.61$ Å, $b_m = 6.14$ Å $\beta = 100°$.) The orientation of this monoclinic cell with respect to the cubic phase has been deduced from the distribution of the « split » reflexions on the diffraction photographs, and as was shown in our previous investigation [2], the transformation to the orthorhombic phase can be accomplished through two distinct sets of orientation relationships, the more common one being the same as that found by BIJVOET and LELY, hereafter referred to as transition R, the other being different, R'.

Both schemes involve one plane and one zone whose orientation does not change on transformation. Because of the symmetry of the high temperature form, these orientation relations can be satisfied in more than one way, all equally probable. All allowed orientation relations are given below in terms of the monoclinic representation of the low temperature form.

$C \rightarrow R$	$C \rightarrow R'$
$(001)_R \parallel \{001\}_C$	$(001)_{R'} \parallel (001)_C$
$[100]_R \parallel \langle 100 \rangle_C$	$[110]_{R'} \parallel [110]_C$ or $[1\bar{1}0]_C$

The crystallographic *form* symbol is used to suggest the random selection of *one* member of the form to define the specific orientation of *one* domain in $C \rightarrow R$, and to emphasize that the orientation relations in $C \rightarrow R'$ are non random. As $[010]_R$ is perpendicular to $[100]_R$ and lies in $(001)_R$, $[010]_R$ is also parallel to one of the cubic axes. Therefore only one axis, namely [001], changes its orientation on transformation, being rotated through an angle $(\beta - 90°) = 10°$. Likewise in the transformation $C \rightarrow R'$, the axis with greatest divergence from its position in the cubic lattice is taken as $[001]_{R'}$.

In the same investigation [2] it was found that on going back to room temperature, the cubic single crystal was reformed so that the transformation cycle was repeatable. Evidence was found also that domains of both low and high temperature forms could coexist within the transformation region. It was shown that this result could not be explained solely on the basis of a homogeneous deformation of the cubic lattice but that some concurrent process such as slip or twinning must also occur in order to minimize the strain energy.

3. – Use of stereographic projection to specify domain orientation.

A complete description of the « splitting » of a cubic reflexion is possible only by a consideration of the composite reciprocal lattice of all domains in the transformed crystal. However, if we are interested particularly in the

directions rather than the *magnitudes* of the reciprocal lattice vectors, they can be conveniently represented by a stereographic projection. It should of course be noted that lattice planes from different domains which coincide in their absolute angular setting, will give rise to poles that are coincident in the stereographic projections, but will correspond to distinct reciprocal lattice points if the interplanar distance is different (see for instance poles 001 and 010 in Fig. 3).

A stereographic projection of one particular option of each of the two transformations $C \rightarrow R$ and $C \rightarrow R'$ are shown in Fig. 1*b* and 1*c* respectively. For the sake of clarity, a corresponding projection of the cubic cell is also reproduced (Fig. 1*a*). R rotates by an angle φ about [001] to give R', where $\varphi = \text{arctg}\,(a/b) - 45^\circ \simeq 2^\circ$. A second option, which simply reverses the direc-

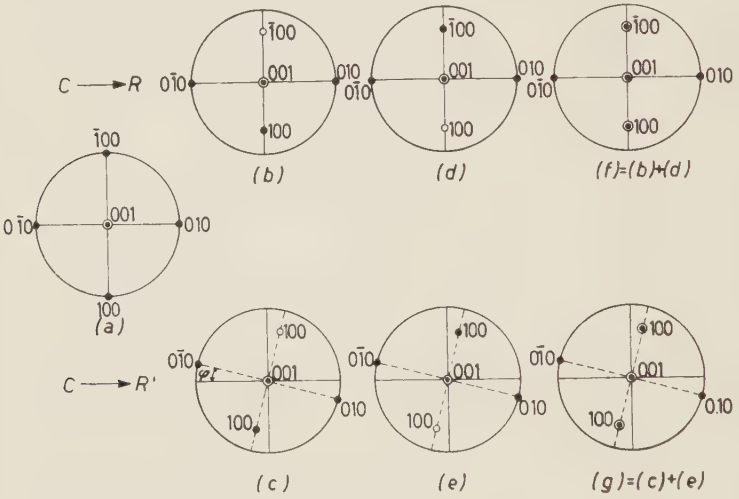

Fig. 1. – Stereographic projections of particular options for the transformations $C \rightarrow R$ (b, d, f) and $C \rightarrow R'$ (c, e, g). (Angles not drawn to scale).

tion of divergence of the c axis is shown in Fig. 1*d* and 1*e*. It can be seen that a combination of (1*b*) and (1*d*) leads to a splitting of the original pole $(100)_c$, one new pole lying above and one below the plane of the paper. When X-ray diffraction techniques are used, such a situation will be indicated by a « splitting » of reflexions.

4. – Symmetry operations relating individual domain orientations (interdomain symmetry).

The two options, represented in Fig. 1*b* and 1*d*, when considered together as in Fig. 1*f*, are seen to be related by a mirror symmetry plane which was

originally present in the point group of the high temperature form, but which is not in either (1*b*) or (1*d*). The same consideration would apply to the transformation $C \to R'$ (Fig. 1*c*, 1*e*, 1*g*) and, in fact, to any choice of two different options in either scheme of transformation. Therefore all possible options are related by point group symmetry elements originally present in the high temperature form and hence all domain orientations can be generated if these point group symmetry operators operate on *one* domain in its correct orientation relative to the axes of the original crystal.

We can therefore limit ourselves to consider one domain orientation only (*i.e.* one « option » of the transforming crystal), and subsequently generate the complete pattern of all options by applying the point group operator of the high symmetry form. This operator is therefore subsequently referred to as the *interdomain symmetry operator*.

If point group symmetry operations present in the original crystal are preserved throughout the transformation, then no new domain orientations are produced when they are applied to a standard domain. To illustrate the point, let us consider Fig. 1*b* once again. Whereas the operation of the mirror plane m_z (in the plane of the paper) which had been lost in the transformation leads to a new domain orientation, the application of the mirror plane m_y, which is preserved in the transformation does not. In the case of the transition $C \to R'$, on the other hand, m_y is also lost, and consequently its application does lead to a new domain orientation. The symmetry preserved in the two transitions is $2/m$ for $C \to R$ and $\bar{1}$ for $C \to R'$, and is shown in Fig. 2*a* and 2*b*. (It is assumed that (hkl) and $(\bar{h}\bar{k}\bar{l})$ are equivalent.)

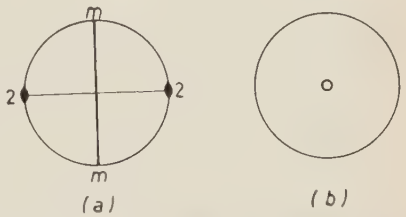

Fig. 2. – Elements of point group symmetry preserved in the transformation: *a*) $C \to R$: $2/m$; *b*) $C \to R'$: $\bar{1}$.

5. – Number of independent domain orientations.

A development of the considerations given above leads directly to a rigorous derivation of the number of independent domain orientations. Thus suppose that a transformation from a high to low symmetry takes place in such a way that some of the symmetry operations originally present in the group are lost. Let the point group of high symmetry be called G and that of low symmetry be g. Then g is a subgroup of G. If in G there are s elements, and in g there are r elements, then r is a submultiple of s, *i.e.* $s = qr$, where q is an integer (Theorem of Lagrange, see for instance ref. [4]). We can now tabu-

[4] M. J. Burger: *Elementary Crystallography* (New York, 1956), p. 483.

late all the elements of G (s in number) as an expansion of G in *cosets* of g:

$$\left.\begin{array}{lllll} g = a_1(=I), & a_2, & a_3, & \ldots & a_r \\ B_2 g = B_2 a_1, & B_2 a_2, & B_2 a_3, & \ldots & B_2 a_r \\ \ldots \quad \ldots & \ldots & \ldots & \ldots & \ldots \\ B_q g = B_q a_1, & B_q a_2, & B_q a_3, & \ldots & B_q a_r \end{array}\right\} = G$$

We have noted before that all domain orientations are obtained if we allow symmetry operations, which have been lost in the transformation, to operate on one single domain. The number of distinct domain orientations is then fixed by demand that by the time that all distinct domain orientations are obtained, all symmetry operations must be present as in the original group, and those only, either as interdomain symmetry, or intradomain symmetry. In other words, we can now solve the problem of the number of distinct domain orientations by looking for the number of distinct operations acting on g, which generate the whole of symmetry operations of G. It is apparent from the expansion table of G that there are q such operations, and q only, and that by allowing these operations to act on g, all and only elements of G are obtained. It is also quite obvious that each one of these q operations, except the identity (B_1), leads to a new domain orientation, since the elements B (except the identity) do not belong to g.

There are therefore $q = s/r$ distinct domain orientations. This number q can be obtained in the following way. We can notice that the number of poles of a point group corresponds to the number of distinct symmetry operations of the group, *i.e.* to its *order*. It follows that the number of distinct domain orientations is equal to the number of poles in the general form of the original point group divided by the number of poles in the general form of the point group which is preserved throughout the transformation. Before calculating these numbers the effect to the non-random selection of options in the transformation $C \rightarrow R'$ must be considered. KCN is cubic, point group $m3m$, and the presence of the 3-fold axes leads to the equivalence of (100), (010), and (001). Hence a situation in which the behavior of (001) is unique is incompatible with this point group. If the 3-fold axes are removed from the point group $m3m$, then the tetragonal point group $4/mmm$ remains. Although the high temperature form in this case was indistinguishable from a cubic crystal, it must be assumed that for the purpose of transformation its point group symmetry was tetragonal. The number of different domains orientations is therefore

$$C \rightarrow R': \quad 48/4 = 12 \qquad C \rightarrow R': \quad 16/2 = 8 .$$

To illustrate these different domain orientations when averaged over the whole volume of the crystal, we can consider the case of $\{100\}_c$ in some detail. The composite stereographic projection for all domains in the two cases $C \to R$ and $C \to R'$ is given in Fig. 3.

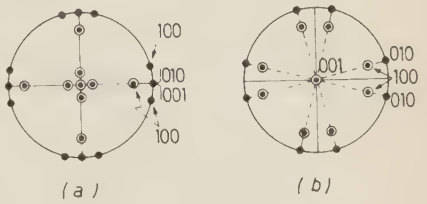

Fig. 3. – Composite stereographic projections for alla domain orientations in the two cases *a*) $C \to R$, and *b*) $C \to R'$.

6. – Physical implications of the coexistence of domains.

So far we have been concerned with the number of distinct domain orientations which arise in consequence of a transformation from high to low symmetry. Such an approach is purely geometrical and in particular describes only the average results of a transformation. When describing a transformation from the physical point of view however, we must consider how adjacent domains of different orientation might coexist without introducing stresses that would lead to break up the crystal. Thus suppose that one region of the high symmetry crystal transform to a domain of a certain orientation selected from q possible orientations, then it might appear from the treatment given above, that the orientation of a neighbouring domain could be selected at random from the $(q-1)$ domain orientations that remain. However this would completely ignore the need to minimize the energy of the internal surface that separates the different domains and so would be physically unrealistic ([5]).

The need for maximum coherency and minimum strain between adjacent domains of different orientation, can best be satisfied if there are sets of lattice planes having closely related orientation and dimensions in both domains. In other words the same problem exists as in the case of the transition from one crystal structure into another. In the latter case, at any instant, one of these « invariant » planes (also called « habit » planes), can be thought to define the interface between the parent and transformed crystal ([6]): by translating this interface within the crystal, the relative proportions, of each phase can be varied, thus enabling the transformation of each phase from one crystal structure to the other to be achieved in a continuous manner. In the former

([5]) See for instance the article by D. Turnbull, particularly Chapt. IV. 9, in *Solid State Physics*, Vol. **3** (F. Seitz and D. Turnbull Editors) (New York, 1956).

([6]) M. A. Jaswon: *Studies in Crystal Physics* (London, 1959), p. 23.

case, where a domain of one crystal structure changes into another domain with the same structure but different orientation, then the mutual orientation of these two domains imposes certain restrictions on the orientation of the invariant plane. As alternative domain orientations arise through the loss of symmetry elements from the parent lattice, it follows that adjacent domains must be related by one of these lost elements of symmetry and as both domains have the same crystal structure, *the pole of the invariant plane must lie in the element of symmetry concerned.*

To take a concrete example, consider the transformation scheme $C \rightarrow R'$ where, because of the smaller number of domains, the number of possibilities is reduced. The only possible interdomain symmetries relating the orientation of domains in pairs are as shown in Fig. 4.

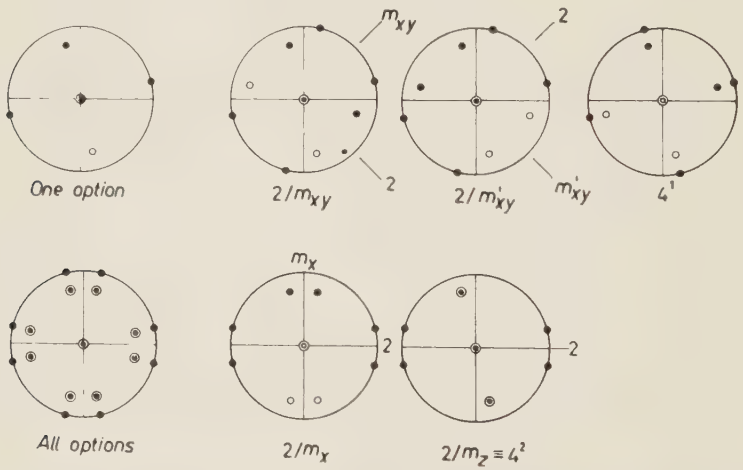

Fig. 4. All possible interdomain symmetries in the transformation $C \rightarrow R'$ that relate domain orientation in pairs.

To generate all domain orientations we require some but not necessarily all of these symmetry operations. Thus for instance repeated application of the following sequences would suffice:

$$4^1 \times 2/m_x \times 2/m_z \; ; \quad 2/m_{xy} \times 2/m_x \times 2/m_z \, .$$

The interdomain symmetry $2/m_z$ can be satisfied extremely simply by rotation of (001) through 180° which satisfies the 2-fold axis. The other symmetries however require more careful consideration. The symmetry $2/m_{xy}$ is particularly interesting because the orientation relations ensure that the es-

sential condition for there to be a single invariant plane between the two domains is automatically satisfied. As the zone $[1\bar{1}0]$ remains in the same orientation, the poles of lattice planes belonging to the zone (hkl with $h = k$) will after transformation still lie in the mirror plane m_{xy} of the cubic lattice, which has now become the mirror plane of interdomain symmetry. Hence the invariant plane must have indices $11l$ where l may be non-integral. An examination of the lattice dimensions suggests that an invariant plane in this orientation is possible if l is approximately equal to $\bar{3}$ (Fig. 5).

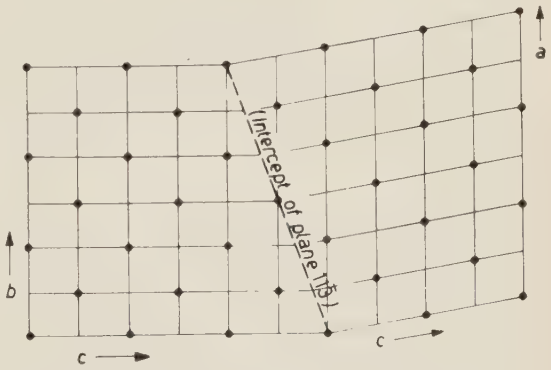

Fig. 5 – A 2-dimensional representation of a continuous transformation of one domain into another related by the interdomain symmetry operation $2/m_{xy}$ using the invariant plane $11\bar{3}$. For clarity only the potassium lattice sites are shown.

By a combination of the interdomain symmetries $2/m_{xy}$ and $2/m_z$ it is possible to obtain, in a linear array, one half of the observed domain orientations. To obtain all domain orientations, the interdomain symmetries $2/m_x$ or 4^1 must occur. On the other hand, an examination of the lattice geometries involved suggests that this is not possible by means of invariant planes so that it would appear that these symmetries can only be produced discontinuously.

The possibility of changing the domain orientation through an invariant plane does therefore exist. It appears however that it is not possible to realize all domain orientations by this means. As the problem is essentially three dimensional it is extremely complex but one is tempted to conclude that once a specific orientation is realized by a specific domain, it will in general restrict the choice of adjacent domain orientations. In an extreme case it may well be that some domain orientations cannot in fact be realized because of the above restrictions. Examples of such restricted options are in fact known and could well be explained along these lines.

In addition to the above considerations, the possibility that regions in which the crystal structure is disturbed may exist between domains, must also be considered. The extent to which such disturbed regions would be tolerated without impairing the ability of the crystal to undergo the reverse transformation will, of course, depend on the mechanical properties of the crystal. That such regions may well exist in the case of potassium cyanide is shown by the fact that if a certain cycle of temperature variation is fol-

lowed ([2]) then the transformation follows an abnormal course in which domains of a new crystal structure appear before the crystal attains the stable low temperature form.

RIASSUNTO

Le possibili orientazioni dei domini formati nella trasformazione di fase di un cristallo singolo di KCN vengono esaminate mediante proiezioni stereografiche. Si dimostra così che gli elementi di simmetria di gruppi di punti della fase stabile ad alta temperatura si dividono tra gli elementi di simmetria mantenuti nella nuova struttura cristallina e quindi esistenti all'interno di ciascun dominio, e gli elementi di simmetria che pongono in relazione tra loro i diversi domini. Viene dato un metodo per calcolare il numero delle orientazioni indipendenti dei domini, e tale metodo viene applicato nel caso dei due possibili schemi di trasformazione trovati per KCN. Vengono anche presi in esame alcuni aspetti fisici della coesistenza di differenti domini in KCN. Le variazioni reticolari che hanno luogo nella trasformazione sono notevoli. Si fa vedere che benchè esistano in alcuni casi piani reticolari invarianti, comuni a due orientazioni differenti, un simile meccanismo continuo di trasformazione non potrebbe rendere conto di tutte le orientazioni osservate sperimentalmente. Viene così confermato che debbono avere anche luogo processi discontinui.

π-$\mathcal{N}$ Forward Dispersion Relations with Electromagnetic Corrections.

A. Minguzzi

CERN - Geneva

(ricevuto il 10 Novembre 1960)

Summary. — Meson-nucleon dispersion relations with e.m. correction to e^2 order are proved, and a conjecture about the unphysical range absorptive part is discussed together with a comment about the Chew-Low extrapolation procedure.

1. – Introduction.

Meson-nucleon dispersion relations, disregarding electromagnetic correction, have been proved for momentum transfer $\Delta^2 < 3\mu^2$, and according to H. Lehmann (1) the absorptive part of the amplitude in the unphysical energy range, can be obtained from an extrapolation of π-$\mathcal{N}$ experimental data. The existence of forward π-$\mathcal{N}$ dispersion relations when electromagnetic interactions are taken into account has been conjectured (2), and analyticity properties of the absorptive part of the amplitude in the energy variable, in order to fill the unphysical energy range, have been postulated. Here we discuss the same problem and we prove that these dispersion relations follow from microcausality and spectrum conditions at least in the lowest e.m. order, and also discuss a conjecture about the unphysical range contribution. The conjecture applies to the general forward elastic dispersion relations, in which the threshold of the absorptive part is lower than the physical threshold.

A comment on the Chew-Low (3) continuation procedure is given at the end.

(1) H. Lehmann: *Nuovo Cimento*, **10**, 579 (1958).
(2) A. Agodi and M. Cini: *Nuovo Cimento*, **6**, 686 (1957); **5**, 1256 (1957).
(3) G. F. Chew and F. E. Low: *Phys. Rev.*, **115**, 1460 (1959).

2. – π^0-N dispersion relation with e.m. correction in lowest order.

In order to avoid infra-red divergences, we allow the photon to have a mass ε as small as one likes and we restrict ourselves to forward π^0-n elastic scattering. In terms of a negative ξ^2 (1), the square of the π^0-mass, we can write the dispersion relation

$$T(W, \xi^2) = \frac{1}{2\pi} \int_{(M+\varepsilon)^2}^{\infty} \mathrm{d}W'^2 A(W', \xi^2) \left\{ \frac{1}{W'^2 - W^2} + \frac{1}{W'^2 - 2(M^2 + \xi^2) + W^2} \right\} + \\ + \text{Bound state},$$

where the absorptive part $A(W', \xi^2)$, from unitarity can be written as

$$(1) \qquad A(W', \xi^2) = 2\pi \int \mathrm{d}x_1 \mathrm{d}x_2 \exp\left[i \frac{k' - p'}{2} x + i \frac{k - p}{2} x_2 \right] \cdot \\ \cdot \sum_{\alpha} \langle 0 | \theta(x_1) \left[J\left(\frac{x_1}{2}\right), \psi\left(-\frac{x_1}{2}\right) \right] | \alpha \rangle \langle \alpha | \theta(x_2) \left[J\left(\frac{x_2}{2}\right), \psi^+\left(-\frac{x_2}{2}\right) \right] | 0 \rangle ,$$

When $M + \varepsilon \leqslant W' < M + \mu$ the state $\alpha\rangle$ contains only one nucleon and one photon (states with more than one photon being disregarded); when $W' \geqslant M + \mu$ mesons and photons can be both present. From the Dyson integral representation (5) and rotation invariance around the axis defined by the meson momentum, we can write

$$A(W', \xi^2) = \int \mathrm{d}z_i \, \mathrm{d} |\boldsymbol{u}_i| \, \mathrm{d}u_{0,i} \, \mathrm{d}\chi_i \, \frac{\Phi(W', z_i, |\boldsymbol{u}_i|, u_{i\,0}, \chi_i)}{(x_1^2 - k^{2\prime} z_1^2)(x_2^2 - k^{2\prime} z_2^2)} , \qquad i = 1, 2$$

with

$$x_{1,2} = \frac{k'^2 + |\boldsymbol{u}^2|_{1,2} + \chi_{1,2}^2 - \left(u_{0,12} - \dfrac{M^2 - \xi^2}{2W'} \right)^2}{2k' |\boldsymbol{u}|_{1,2}} , \qquad k'^2 = \left(\frac{W'^2 + \xi^2 - M^2}{2W'} \right)^2 - \xi^2 ,$$

and Φ has the support

$$0 \leqslant |\boldsymbol{u}_i| \leqslant \frac{W'}{2} ; \qquad -\frac{W'}{2} + |\boldsymbol{u}_i| \leqslant u_0 \leqslant \frac{W'}{2} - |\boldsymbol{u}_i| ; \qquad 0 \leqslant z_i \leqslant 1 ;$$

$$\chi_i \geqslant \mathrm{Max} \left\{ 0, \, m_1 - \sqrt{\left(\frac{W'}{2} + u_{0i} \right)^2 - |\boldsymbol{u}_i|^2}, \qquad m_2 - \sqrt{\left(\frac{W'}{2} - u_{0,i} \right)^2 - |\boldsymbol{u}_i|^2} \right\} .$$

(1) N. N. Bogoljubov and D. V. Shirkov: *Introduction to the Theory of Quantized Fields* (New York, 1959); H. Lehmann: *Suppl. Nuovo Cimento*, **14**, 153 (1959); H. J. Bremermann, R. Oehme and J. G. Taylor: *Phys. Rev.*, **109**, 2178 (1958).

(5) F. J. Dyson: *Phys. Rev.*, **110**, 1460 (1958).

(1) is equivalent to the corresponding quantity in ref. (1), even if the denominators are not the same. One can show that

$$\text{Min } x_{1,2}^2 = k'^2 + \frac{(m_1^2 - \xi^2)(m_2^2 - M^2)}{W'^2 - (m_2 - m_1)^2} ,$$

where, when

$$M + \varepsilon \leqslant W' < M + \mu ; \qquad m_1 = 3\mu \qquad m_2 = M + \mu$$

and when

$$W' \geqslant M + \mu ; \qquad m_1 = \mu + \varepsilon \quad m_2 + M + \varepsilon$$

this, with the condition $0 \leqslant z_i \leqslant 1$ is sufficient to guarantee that the denominators never vanish, whatever is W', when ξ^2 from a negative value goes to its physical value μ^2. The existence of a neighbourhood of the real ξ^2-axis uniform in W' follows and from this theorem forward dispersion relation.

The $\pi^{\pm}$-$\mathcal{N}$ dispersion relations, in which the π^0-$\pi^{\pm}$ mass difference is taken into account, cannot be proved by this method. Only if one moreover assumes that the π^0-$\pi^{\pm}$ mass difference is only of electromagnetic origin, the $\pi^{\pm}$-$\mathcal{N}$ dispersion relations follow.

3. – Unphysical range contribution.

The absorptive part of the amplitude for both physical and unphysical energies is defined by (1). But the comparison of a dispersion relation with the experimental data cannot be accomplished until one knows the absorptive part in the unphysical energy range. To this aim, in ref. (2), one has postulated analyticity properties of $A(W')$ in the energy variable: unfortunately nothing can be predicted from the definition of non-retarded commutator or from (1). But even if analytical properties of $A(W', \xi^2)$ in W' could be proved, one ought to prove also analyticity properties of A in the variables W' and ξ^2 simultaneously, in order to justify this extrapolation procedure. H. LEHMANN (1) and R. F. STREATER (6) have examined unphysical range contribution in cases which are not so general to cover the case we are discussing. (Incidentally, we notice that all that will be said from now on, which applies each time a

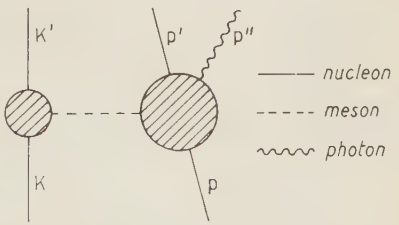

Fig. 1.

(6) R. F. STREATER: *Nuovo Cimento*, **13**, 57 (1959).

dispersion relation for forward elastic scattering of two particles A, B, can be proved and that $A(W')$ is different from zero for $W' < m_A + m_B$). We consider the square of the amplitude of the Feynman graph Fig. 1 integrated over the phase space of the three outgoing particles. In terms of $\Delta^2 = -\frac{1}{4}(K - K')^2$ and $w^2 = (p' + p'')^2$ we have

$$\frac{\mathrm{d}^2\sigma_1}{\mathrm{d}\Delta^2\,\mathrm{d}w^2} = \frac{g^2(\Delta^2)}{(4\Delta^2 + \mu^2)^2}\,\Psi(w, -4\Delta^2) \tag{2}$$

and, apart from a coefficient, $\Psi(w, -4\Delta^2)$ is the quantity (1), when w is identified with W', and $-4\Delta^2$ is identified with ξ^2; in fact $-4\Delta^2$ is the « mass » of the virtual meson in Fig. 1 and from the very fact that the π^0-$\mathcal{N}$ forward dispersion relations exist, $\Psi(W', \xi^2)$ is, whatever is $W > M + \varepsilon$ analytic in a strip around the real axis

$$S : \left\{ \xi_1^2 + i\xi_2^2 \,;\; -R^2 < \xi_1^2 \leqslant \mu^2 + \delta^2 \,;\; 0 \leqslant \xi_2^2 \leqslant \left(\frac{4W'^2}{W'^2 + M^2}\right)^2 \frac{8\mu^2(2M\mu + \mu^2)}{W'^2}\,[k'^2 + \mu^2 + 2M\mu] \right\}.$$

$g^2(-\xi^2/4)$ from the properties of the meson-nucleon vertex is analytic inside S, so that the analytic continuation of

$$\frac{(4\Delta^2 + \mu^2)^2}{g^2(-(\mu^2/4))}\,\frac{\mathrm{d}^2\sigma_1}{\mathrm{d}\Delta^2\,\mathrm{d}w^2}$$

to $\Delta^2 = -\mu^2/4$ gives the required π^0-$\mathcal{N}$ unphysical range absorptive part (*).

One has to know a prescription how to select the term (2) from the $\mathcal{N} + \mathcal{N} \to \mathcal{N} + \mathcal{N} + \gamma$ cross-section. Ascoli and myself (7) have shown that

$$\frac{\mathrm{d}^2\sigma(\mathcal{N} + \mathcal{N} \to \mathcal{N} + \mathcal{N} + \gamma)}{\mathrm{d}\Delta^2\,\mathrm{d}w^2}$$

in Δ^2 is analytic in a small Lehmann ellipse. The intersection between the Lehmann ellipse and S is the region of analyticity of the difference

$$\frac{\mathrm{d}^2\sigma_1}{\mathrm{d}\Delta^2\,\mathrm{d}w^2} - \frac{\mathrm{d}^2\sigma(\mathcal{N} + \mathcal{N} \to \mathcal{N} + \mathcal{N} + \gamma)}{\mathrm{d}\Delta^2\,\mathrm{d}w^2}$$

and this intersection is too small to justify the required continuation in Δ^2

(*) The form of the strip (3) suggests to perform the analytical continuation through a Neumann development in Legendre polynomials.

(7) R. Ascoli and A. Minguzzi: *Phys. Rev.*, **118**, 1435 (1960).

we need. If the conjecture of Chew-Low [3] how to get the cross-section for a process involving $\mathcal{N}$-particle from an experiment in which $N+1$ particles are involved proves to be true, the analytical continuation of

$$\frac{(4\Delta^2+\mu^2)^2}{g^2(-(\mu^2/4))}\,\frac{\mathrm{d}^2\sigma[\mathcal{N}+\mathcal{N}\to\mathcal{N}+\mathcal{N}+\gamma]}{\mathrm{d}\Delta^2\,\mathrm{d}w^2}$$

up to $\Delta^2=-(\mu^2/4)$ gives the required unphysical amplitude.

4. – A remark on the Chew-Low continuation procedure.

The analyticity properties embodied in (1) in terms of ξ^2 are useful to prove in general one of the hypotheses on which the Chew-Low procedure rests: *i.e.* the analyticity properties of the residue of the Born term in the neighbourhood of the pole (*). Let us consider the Feynman graph of Fig. 2 in connection with the calculation of the cross-section $\mathrm{A}+\mathrm{B}\to\mathrm{C}+\mathrm{D}+\ldots$.

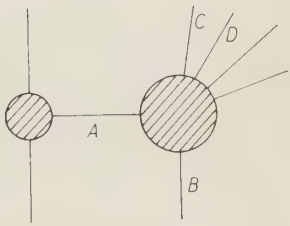

Fig. 2.

The state $\mathrm{C}+\mathrm{D}+\ldots$ will be one of the possible end channels araising from $\mathrm{A}+\mathrm{B}$. If the forward dispersion $\mathrm{A}+\mathrm{B}\to\mathrm{A}+\mathrm{B}$ can be proved we fall in the case we have already discussed; the only generalization we need is that in the previous case the $\mathcal{N}+\gamma$ state was the only open channel; in the general case one expects that various channels are open; now, the theorem predicting analytic properties of the absorptive part holds when in (1) one sums over the total phase space (we have disregarded spin) of outgoing particles, even if one does not sum over the particle number.

If the forward $\mathrm{A}+\mathrm{B}\to\mathrm{A}+\mathrm{B}$ dispersion relation cannot be proved, this means that $A(\xi^2, W')$ is not analytic in a uniform strip in ξ^2 when W' goes from the threshold value to infinity.

But $A(\xi^2, W')$ is analytic in S, if one is interested only in the W' values ranging from $m_\Lambda+m_\mathrm{B}$ up to infinity (and not in the W' values ranging from the threshold of the absorptive part up to infinity as is the case in the prove of the dispersion relations).

(*) The other hypothesis is that

$$(4\Delta^2+\mu^2)\left|\frac{\mathrm{d}^2\sigma_1}{\mathrm{d}\Delta^2\,\mathrm{d}w^2}\quad\frac{\mathrm{d}^2\sigma(\mathcal{N}+\mathcal{N}\to\mathcal{N}+\mathcal{N}+\gamma)}{\mathrm{d}\Delta^2\,\mathrm{d}w^2}\right|$$

is analytic in a neighbourhood of the real axis $-R^2<\Delta^2\leqslant(\mu^2/4)+\delta^2$.

For $W' \geqslant m_A + m_B$ the conditions

$$\min x_{1,2}^2 > (0, K'^2)$$

with the actual masses of the elementary particles, is satisfied, which guarantees the analyticity of the absorptive part in S.

And so we have shown that the Chew-Low hypothesis that the residue of the Born term is analytic in a neighbourhood of the real ξ^2 axis is true.

RIASSUNTO

In questo lavoro si dimostrano le relazioni di dispersione pione-nucleon includendo le correzioni elettromagnetiche nell'ordine più basso e si discute una ipotesi relativa al calcolo della parte assorbente dell'ampiezza nella regione non fisica dell'energia. In connessione colle proprietà analitiche nella massa della parte assorbente dell'ampiezza, si esamina la congettura di Chew-Low.

Sulla cattura nucleare dei muoni negativi con emissione di elettroni (*).

M. Conversi, L. di Lella, A. Egidi, C. Rubbia e M. Toller

Istituto di Fisica dell'Università - Roma
Istituto Nazionale di Fisica Nucleare - Sezione di Roma

(ricevuto l'11 Novembre 1960)

Riassunto. — Dopo aver accennato agli aspetti teorici che, nel quadro delle interazioni deboli, giustificano l'importanza di uno studio sperimentale accurato del processo di cattura nucleare del mesone μ^- accompagnato dall'emissione di un elettrone (invece che di un neutrino), si riferisce su di un primo esperimento effettuato recentemente, su tale soggetto, al sincrociclotrone del CERN. Questo esperimento — eseguito frenando i mesoni μ^- in una targhetta di rame — ha consentito di migliorare per oltre un fattore 20 il limite superiore più accurato finora ottenuto per il « branching ratio » del processo detto rispetto alla cattura ordinaria del mesone μ negativo.

1. – Il fatto che i processi

$$\mu^+ \to e^+ + \gamma \tag{1}$$

$$\mu^+ \to e^+ + e^- + e^+ \tag{2}$$

$$\mu^- + \mathcal{N} \to \mathcal{N} + e^- \tag{3}$$

siano stati finora ricercati sperimentalmente senza successo, non ha trovato ancora una soddisfacente interpretazione. Nessuno dei tre processi in questione risulta in effetti proibito dalle leggi generali di conservazione che sono a fondamento di ogni attuale teoria delle particelle elementari; cosicchè si è indotti a pensare che ad interdirli intervengano delle regole di selezione che hanno

(*) Comunicato al XLVI Congresso della S.I.F. in una seduta del 3 Ottobre 1960.

origine in qualche particolare caratteristica della struttura dell'interazione che li governa. Se, per esempio, l'interazione è rigorosamente locale, sembra potersi giustificare [1] l'assenza delle reazioni (1), (2), (3). Per il carattere universale dell'interazione di Fermi la mancata osservazione di tali reazioni interessa l'intero campo delle interazioni deboli, anche se si manifesta in processi che coinvolgono segnatamente il mesone μ. Già di qui si comprende l'importanza di misurare il « grado di proibizione » dei processi (1), (2), (3), stabilendo attraverso misure di grande accuratezza limiti superiori quanto più possibile piccoli per i rapporti (o « branching ratios ») tra le loro probabilità e le probabilità dei corrispondenti processi ordinari (decadimento $\mu \to e + \nu + \bar{\nu}$ nel caso dei processi (1) e (2), cattura $\mu^- + p \to n + \nu$ nel caso del processo (3)).

Per tali limiti superiori si sono ottenuti valori dell'ordine di 10^{-6} nel caso della reazione (1) [2] e dell'ordine di 10^{-5} nel caso della reazione (2) [3]. Il processo (3) è stato dapprima ricercato, con esito negativo, utilizzando i mesoni μ^- della radiazione cosmica [4]. Successivamente, in un esperimento circa 100 volte più sensibile del precedente, STEINBERGER e WOLFE lo hanno ricercato frenando in una targhetta di rame i mesoni μ^- prodotti artificialmente al ciclotrone di Nevis [5]. Questi autori hanno potuto così stabilire un limite superiore dell'ordine di 10^{-3} per il « branching ratio ».

$$R = \frac{\text{Frequenza del processo } \mu^- + \text{Cu} \to \text{Cu} + e^-}{\text{Frequenza del processo } \mu^- + \text{Cu} \to \text{Ni} + \nu} \qquad (4)$$

A prescindere dal fatto che lo stato attuale della teoria delle interazioni deboli richiede un esame quanto più accurato possibile di tutti i modi di decadimento e di cattura del mesone μ, l'utilità di una ricerca ulteriore del processo (3) appare dalle considerazioni seguenti. I processi (1), (2), (3) si possono far risalire ad uno stesso ipotetico diagramma di Feynman come quello disegnato nella Fig. 1, ove la « scatola » racchiude le proprietà strutturali dell'interazione. Tale diagramma rappresenta in effetti il processo (1) se il quanto γ emesso è reale. Dallo stesso diagramma si può far

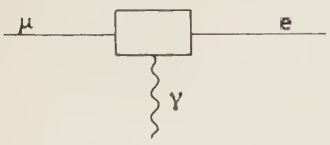

Fig. 1. – Diagramma di Feynman per il processo $\mu \to e + \gamma$.

(1) M. GELL-MANN: *Rev. Mod. Phys.*, **31**, 834 (1959).

(2) D. BERLEY, J. LEE and M. BARDON: *Phys. Rev. Lett.*, **2**, 357 (1959); J. ASHKIN, T. FAZZINI, G. FIDECARO, N. H. LIPMAN, A. M. MERRISON e J. PAUL: *Nuovo Cimento*, **14**, 1266 (1959).

(3) J. LEE e N. P. SAMIOS: *Phys. Rev. Lett.*, **3**, 55 (1959).

(4) A. LAGARRIGUE e C. PEYROU: *Compt. Rend.*, **234**, 1873 (1952).

(5) J. STEINBERGER e H. B. WOLFE: *Phys. Rev.*, **100**, 1490 (1955).

scaturire la reazione (2) se il quanto γ emesso è virtuale e si converte internamente in una coppia elettrone-positone. Il caso del processo (3) corrisponde infine ad un quanto γ virtuale assorbito dal nucleo che cattura il mesone μ^-. Come è stato mostrato da WEINBERG e FEINBERG [6] e indipendentemente da CABIBBO e GATTO [7], gli elementi di matrice relativi ai processi in questione si possono scrivere su base fenomenologica, senza cioè entrare nel merito delle proprietà strutturali dell'interazione contenute nella « scatola » di Fig. 1. Questi autori hanno così rilevato che il meccanismo dell'interazione può essere tale da interdire la produzione di fotoni reali, e quindi il processo (1), pur restando aperta la possibilità che i processi (2) e (3), nei quali intervengono dei fotoni virtuali, esistano ad un livello accessibile sperimentalmente. Da uno studio più dettagliato della questione risulta inoltre che agli effetti di una possibile loro rivelazione è più vantaggioso ricercare il processo (3) che non il processo (2).

A differenza di quanto accade nel caso della cattura ordinaria, il processo (1) lascia invariato il numero atomico Z del nucleo di partenza. Quest'ultimo si identifica con il nucleo finale se, nell'assorbire il fotone virtuale del diagramma di Fig. 1, resta nello stato fondamentale. In tal caso si ha un modo « coerente » di cattura, con partecipazione dell'intero nucleo, e l'elettrone è emesso sempre con la stessa energia, che nel caso di un nucleo di rame è lievemente superiore a 100 MeV. Se invece il nucleo viene eccitato a seguito dell'assorbimento del fotone, il modo di cattura è « incoerente » e l'elettrone è emesso con una energia che dipende dallo stato finale del nucleo. Lo spettro in energia degli elettroni da cattura incoerente è stato calcolato da STEINBERGER e WOLFE [5] sulla base del modello nucleare di Chew e Goldberger [8]. Esso presenta un massimo intorno ai 93 MeV di energia e fornisce un'energia media di circa 85 MeV.

Il peso relativo dei due possibili modi di cattura è stato calcolato per diversi nuclei [6,7] tenendo conto dei fattori di forma elettromagnetici. Il rapporto tra le probabilità del modo « coerente » e del modo « incoerente » di cattura ha un valore massimo di almeno 6 per Z prossimo al valore $Z = 29$ che compete al rame. Questo fatto costituisce una prima ragione per la scelta del rame come materiale della targhetta di frenamento dei mesoni μ^-. È infatti chiaro che, sperimentalmente, una ricerca accurata del processo (3) è resa difficile dalla presenza di elettroni di decadimento di mesoni μ^- sfuggiti alla cattura nucleare. A parte effetti trascurabili connessi al moto del mesone μ^- nell'orbita di Bohr [9], tali elettroni hanno un'energia massima di circa 53 MeV

[6] S. WEINBERG e G. FEINBERG: *Phys. Rev. Lett.*, **3**, 111, 244 (1959).
[7] N. CABIBBO e R. GATTO: *Phys. Rev.*, **116**, 1334 (1959).
[8] G. F. CHEW e M. L. GOLDBERGER: *Phys. Rev.*, **77**, 471 (1950).
[9] L. TENAGLIA: *Nuovo Cimento*, **13**, 284 (1959); H. ÜBERALL: *Nuovo Cimento*, **15**, 163 (1960).

e possono più facilmente simulare elettroni da cattura incoerente che non elettroni monoenergetici da circa 105 MeV come quelli emessi nel caso della cattura coerente. Una ulteriore ragione nel considerare felice la scelta del rame come materiale di frenamento dei mesoni μ sta nel compromesso, che con tale scelta si realizza, tra l'opportunità di avere un'elevata probabilità di cattura dei mesoni μ^- e, al tempo stesso, una probabilità relativamente piccola per processi di irraggiamento da parte degli elettroni.

La ricerca del processo (3) è stata da noi effettuata al sincrociclotrone del CERN in due stadi successivi corrispondenti a due esperimenti condotti in condizioni sensibilmente diverse. Il primo dei due esperimenti sarà descritto nel seguito di questa comunicazione; il secondo nella comunicazione successiva, ove i nostri risultati saranno posti a confronto anche con quelli di un analogo esperimento eseguito a Berkeley indipendentemente e contemporaneamente al nostro ([10]).

2. – L'esperimento qui descritto è stato effettuato, con il dispositivo di Fig. 2 esposto al fascio di pioni da 80 MeV, in condizioni di « parassitaggio » (ossia in parallelo ad altri esperimenti) sfruttando la possibilità di proiettare simultaneamente più fasci nell'area sperimentale del sinclociclotrone del CERN.

Come indicato nella Fig. 2 il fascio di pioni da 80 MeV è ulteriormente analizzato da un magnete deflettore allo scopo di eliminare la componente neutra. Il fascio di 170 MeV/c così ottenuto contiene circa un mesone μ^- e tre elettroni per ogni 10 pioni negativi. Dato che i pioni da 170 MeV/c hanno un percorso residuo di 28 g/cm^2 di Cu, essi vengono eliminati dal moderatore di Cu il cui spessore è scelto sperimentalmente in modo da ottenere il massimo numero di mesoni μ^- frenati nella targhetta. Quest'ultima è una lastrina di Cu da 12×17 cm^2, dello spessore di 5 mm, opportunamente inclinata rispetto al fascio dei mesoni incidenti. L'intensità media dei mesoni μ^- in essa frenati durante le misure corrispondeva a ~ 500 particelle/s (pari a circa la metà dei mesoni μ^- incidenti). Lo « stop » di un mesone μ nella targhetta è identificato dalla anticoincidenza $1.2.3.\bar{4}$ tra gli scintillatori plastici 1.2.3 (in coincidenza) e 4 (in anticoincidenza).

La Fig. 3 mostra in maggior dettaglio la parte dell'apparato destinata alla rivelazione degli elettroni di cattura. Sei scintillatori plastici di coincidenza (5, 6, ..., 10) ed uno (11) di anticoincidenza, fanno parte del « telescopio elettronico » (che indicheremo per brevità con TE) usato per distinguere gli elettroni del processo ricercato da quelli provenienti dalla disintegrazione dei mesoni μ^- frenati nella targhetta e nel materiale circostante. Allo scopo di escludere un eventuale fondo di particelle lente, e di ridurre in tal modo il numero delle coincidenze casuali tra uno « stop » nella targhetta ed una particella non

([10]) R. D. Sard, K. M. Crowe e H. W. Kruger: in corso di pubbl. su *Phys. Rev.*

correlata in TE, sono inseriti in prossimità dei due estremi di TE anche due contatori di Čerenkov di plexiglass (*) (C_1, C_2). I sei scintillatori ed i due con-

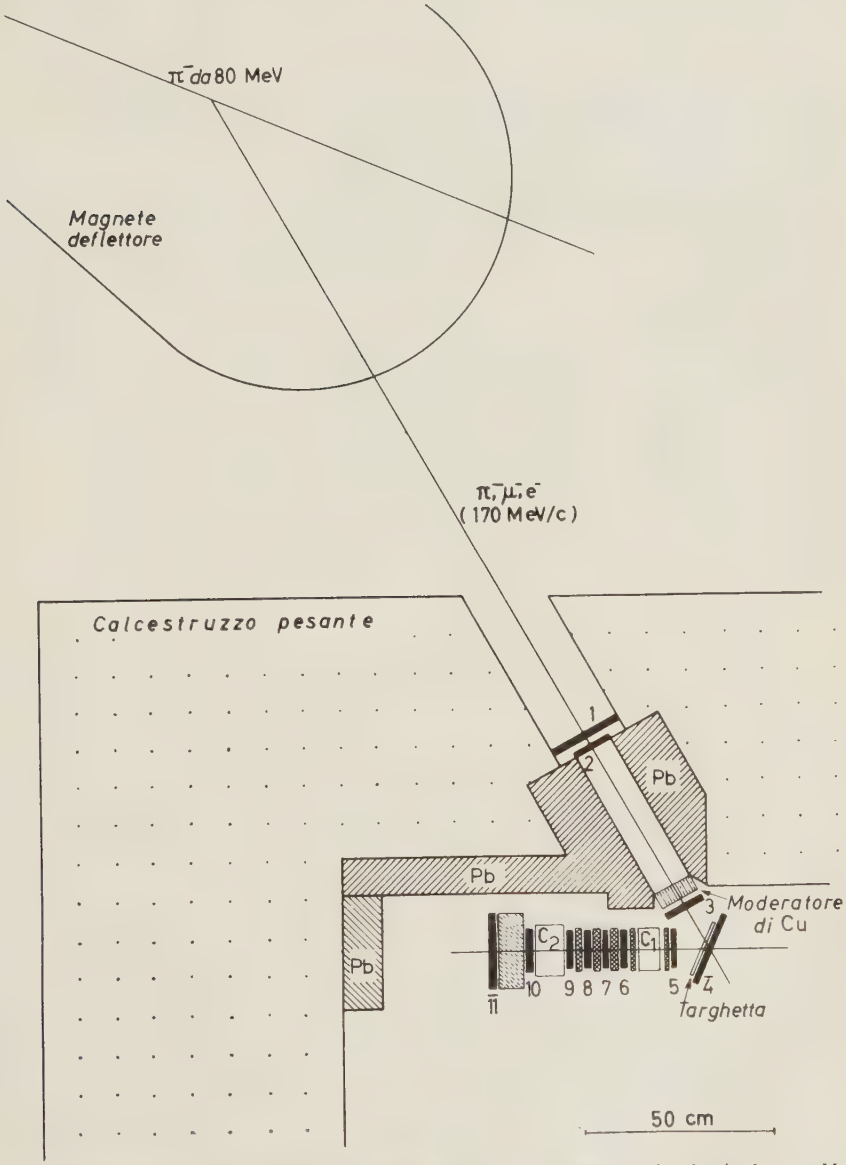

Fig. 2. – Esposizione dell'apparato sperimentale al fascio di pioni da 80 MeV del sincrociclotrone del CERN.

(*) In misure eseguite a Roma prima di trasferire l'apparato al CERN è stato controllato che il materiale impiegato nei due contatori di Čerenkov non possiede proprietà scintillanti.

tatori di Čerenkov (posti tutti in coincidenza tra di loro) sono alternati con spessori di grafite compressa (densità 2.04 g/cm²), dello spessore di 2 o di 1 cm, in ciascuno dei quali gli elettroni hanno una probabilità relativamente

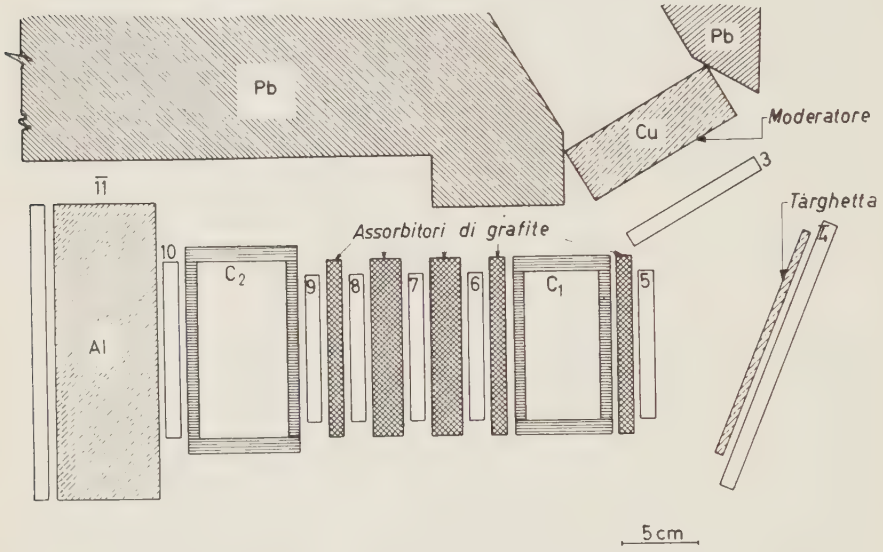

Fig. 3. – Apparato sperimentale. La targhetta usata nelle misure per la ricerca del processo (3) è una lastrina di Cu spessa 0.5 cm.

piccola di irraggiare, pur perdendovi per ionizzazione un'apprezzabile frazione della loro energia. L'uso di tanti contatori in coincidenza in TE ha lo scopo di minimizzare la probabilità di rivelare un elettrone di disintegrazione che attraversi parte del telescopio sotto forma di radiazione elettromagnetica non perdendo in tal caso energia per ionizzazione. Il contatore di anticoincidenza 11 posto in fondo al telescopio serve infine ad escludere dalla rivelazione eventuali elettroni che attraversino TE non provenendo dalla targhetta. D'altra parte un elettrone del processo ricercato non è di regola eliminato perchè si arresta nello spessore di 8 cm di Al che separa il contatore 11 dal resto del telescopio. L'angolo solido utile ω per gli elettroni di cattura emessi dalla targhetta in TE si ricava dalle caratteristiche geometriche dell'apparato e risulta $\omega/4\pi = 7.5 \cdot 10^{-3}$.

Da misure riportate nella successiva comunicazione si deduce che il rendimento ε di TE per gli elettroni del processo (3) è del 15% se la cattura coerente è sei volte più probabile di quella incoerente (Sezione 1). Il rendimento per gli elettroni di disintegrazione del mesone μ risulta invece inferiore a 10^{-5}

(cfr. Sezione 3). Il metodo permette dunque di conseguire una nettissima distinzione tra elettroni di cattura ed elettroni di decadimento (*).

Nella Fig. 4 è riportato uno schema a blocchi semplificato dell'apparato impiegato per la registrazione elettronica dei vari tipi di eventi definiti nella

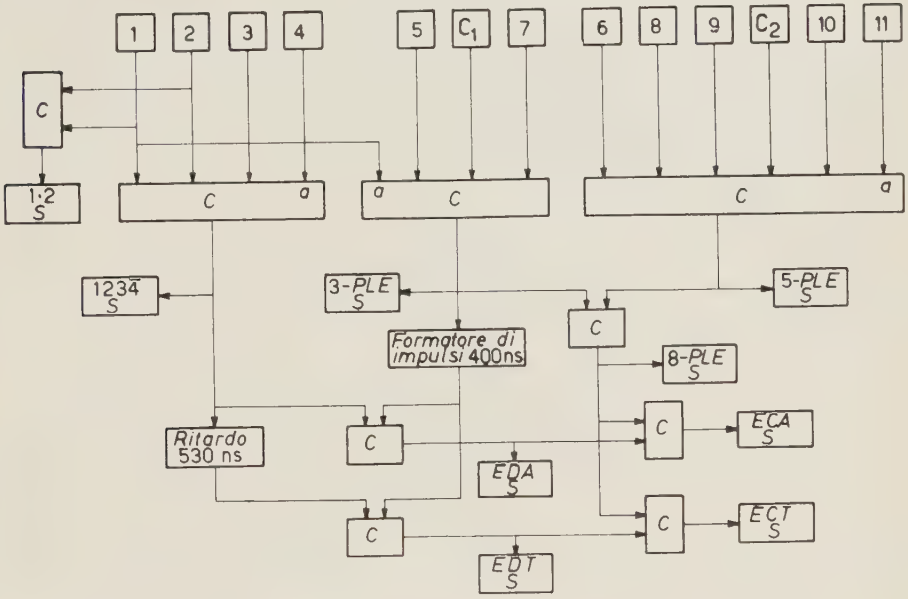

Fig. 4. – Schema logico dell'elettronica. Il circuito di anticoincidenze per le 3-ple ($5.C_1.7.\bar{1}$) è ad accoppiamento diretto. È stato controllato che questo circuito conserva una piena efficienza (99.99%) anche quando il canale di anticoincidenza *a* è sottoposto a fiotti di impulsi distribuiti casualmente con frequenze istantanee fino a $3 \cdot 10^6$ imp./s.

Tabella I. Le misure si sono svolte in successivi intervalli di tempo della durata di mezz'ora ciascuno e la registrazione di tanti diversi tipi di eventi si è rivelata di grande utilità avendo consentito di mantenere continuamente sotto controllo l'intero dispositivo sperimentale, e di determinare con accuratezza il numero medio totale di eventi ECA senza far ricorso al numero (affetto da un grosso errore statistico) registrato all'uscita ECA (**) di Fig. 4. Questo

(*) TE presenta sostanziali analogie con il telescopio elettronico impiegato al CERN nell'esperimento sul decadimento β del pione ([11]) dal quale differisce per la presenza dei due contatori di Čerenkov e del contatore di anticoincidenza 11.

([11]) J. Ashkin, T. Fazzini, G. Fidecaro, A. W. Merrison, H. Paul e A. W. Tollestrup: *Nuovo Cimento*, **13**, 1240 (1959).

(**) In tutto l'esperimento si è registrato un solo evento su questa uscita.

TABELLA I. – *Eventi registrati elettronicamente mediante le coincidenze e le anticoincidenze elencate nella* 1ª *colonna.* I numeri sovrasegnati sono relativi a contatori usati in anticoincidenza. Nella 2ª colonna sono utilizzate le abbreviazioni: E = elettroni; D = disintegrazione; C = cattura; T = « totali » (ossia genuini più « accidentali »); A = « accidentali ». La differenza tra i numeri di eventi EDT e EDA fornisce il numero di elettroni di disintegrazione genuini (in coincidenza ritardata con lo « stop » di un muone nella targhetta) capaci di raggiungere il contatore 7. A parte un possibile contributo « spurio » dovuto agli elettroni di disintegrazione, la differenza tra i numeri di eventi ECT e ECA dà (statisticamente) il numero di eventi dovuti al processo ricercato. Nell'intero esperimento sono stati registrati 3 eventi ECT ed 1 evento ECA.

Coincidenza o anticoincidenza	Simbolo usato	Spiegazioni
1.2	M	Registrate come « monitors »
$1.2.3.\overline{4}$	« stop »	Evento tipico: arresto di un μ^- nella targhetta
$5.C_1.7.\overline{1}$	3-pla	Evento tipico: elettrone di decadimento che penetra in TE almeno fino al contatore 7
$(5.C_1.7.\overline{1})(1.2.3.\overline{4})_{\text{ritard.}}$	EDT	Eventi tipici: *a*) processo $\mu^- = e^- + \nu + \bar{\nu}$; *b*) coincidenza accidentale tra uno « stop » ed una 3-pla
$(5.C_1.7.\overline{1})(1.2.3.\overline{4})$	EDA	Evento tipico: coincidenza accidentale tra uno « stop » ed una 3-pla
$5.C_1.6.7.8.9.C_2.10.\overline{11}.\overline{1}$	8-pla	Evento tipico: elettrone che penetra in TE arrestandosi nel blocco di Al tra i contatori 10 e 11.
$(8\text{-pla})(1.2.3.\overline{4})_{\text{ritard.}}$	ECT	Eventi tipici: *a*) processo $\mu^- + \mathcal{N} = \mathcal{N} + e^-$; *b*) coincidenza accidentale tra uno « stop » ed una 8-pla
$(8\text{-pla})(1.2.3.\overline{4})$	ECA	Evento tipico: coincidenza accidentale tra uno « stop » ed una 8-pla
$6.8.9.C_2.10.\overline{11}$	5-pla	Registrate per controllo

numero medio totale è stato determinato facendo uso, per ciascuna misura parziale, della relazione

$$\frac{\text{Numero di EDA}}{\text{Numero di 3-ple}} = \frac{\text{Numero di ECA}}{\text{Numero di 8-ple}}, \tag{5}$$

che permette tale determinazione prescindendo dalla conoscenza esatta della struttura temporale del fascio, soggetta a sensibili variazioni durante il funzionamento della macchina.

Gli eventi che si possono attribuire agli elettroni di cattura sono rappresentati da uno « stop » $1.2.3.\bar{4}$ seguito, entro l'intervallo $\Delta\theta = 410$ ns, compreso tra 20 e 430 ns, da una coincidenza ottupla tra i contatori di TE non accompagnata, entro 20 ns, da impulsi dei contatori 1 e 11. Con il contatore 1 posto in anticoincidenza rispetto alle coincidenze ottuple dette si esclude dalla registrazione ogni evento simultaneo con l'arrivo di una particella del fascio sul dispositivo sperimentale: in particolare restano esclusi eventuali elettroni del fascio che, per processi di « scattering » nella targhetta, vengano deviati in TE.

Poichè gli eventi ricercati sono caratterizzati dalla vita media dei mesoni μ^- nel Cu, che è di 160 ns ([12]), la selezione del detto intervallo temporale $\Delta\theta$ da 20 a 430 ns riduce ad una frazione $u = 0.84$ il numero degli eventi medesimi.

3. – Nel corso dell'intero esperimento, comprendente ~ 100 ore di tempo di misura, sono stati registrati tre eventi del tipo ECT (v. Tabella I). Corrispondentemente si sono avuti $N = 1.63 \cdot 10^8$ « stops » attribuiti a mesoni μ^- arrestati nella targhetta. Poichè non tutti gli « stops » $1.2.3.\bar{4}$ sono dovuti a mesoni μ, il numero N è stato dedotto dal numero dei « monitors » 1.2 registrati nel corso dell'esperimento e dal risultato di un'apposita misura delle coincidenze $5.6_1.7.\bar{1}$ registrate, in assenza di assorbitori di grafite in TE, utilizzando una targhetta di grafite equivalente a quella di Cu. In effetti, dato che in assenza di assorbitori in TE il rendimento del sistema dei primi quattro contatori di TE per gli elettroni di disintegrazione è deducibile con buona approssimazione da preesistenti misure ([13]), tale misura consente di normalizzare il numero degli « stops » effettivi al numero dei « monitors » 1.2.

Solo una frazione $f = 0.92$ dei mesoni μ^- subiscono la cattura nucleare nel rame ([12]). Il numero medio $m(R)$ di eventi del tipo ECT che ci si dovrebbe aspettare di registrare nell'intero esperimento per un valore R del « branching ratio » (4) è dunque:

$$m(R) = aR + b\,,$$

dove

$$a = N \cdot f \cdot u \cdot \frac{\omega}{4\pi} \cdot \varepsilon = 1.35 \cdot 10^5\,,$$

e b rappresenta il « fondo » di eventi spuri che simulano il processo ricercato.

([12]) J. C. Sens: *Phys. Rev.*, **113**, 679 (1959).
([13]) S. Lokanathan e J. Steinberger: *Suppl. Nuovo Cimento*, **2**, 151 (1955).

Al fondo b contribuiscono: 1) le coincidenze accidentali fra un'anticoincidenza $1.2.3.\bar{4}$ ed una « 8-pla » susseguentesi in posizione temporale relativa tale da simulare un elettrone di cattura; 2) gli elettroni di disintegrazione eccezionalmente capaci di produrre scintillazione in tutti i contatori di TE escluso il contatore 11.

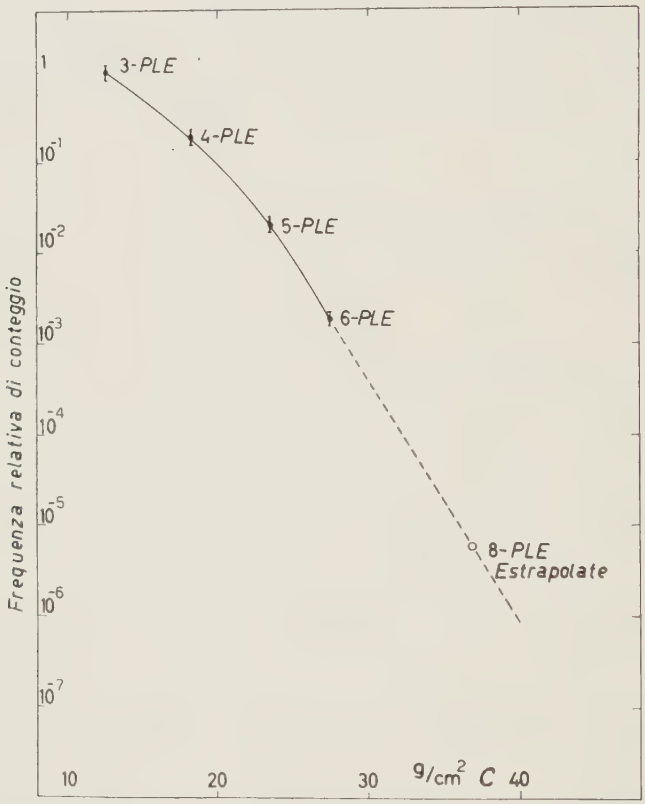

Fig. 5. - Frequenza di conteggio relativa delle coincidenze n-ple tra i primi n contatori di TE. L'estrapolazione (arbitraria) indicata dal segmento tratteggiato serve solo a mostrare che il contributo spurio agli eventi ECT proveniente dagli elettroni di decadimento di mesoni μ^- è presumibilmente trascurabile.

In Fig. 5 è mostrata, in unità arbitrarie, la frequenza di conteggio relativa per le coincidenze n-ple fra i primi n contatori del telescopio TE. Se si ammette che fino alle coincidenze 6-ple i conteggi registrati siano dovuti essenzialmente agli elettroni di decadimento e, nel modo indicato dal segmento tratteggiato della curva, si estrapola tale frequenza allo spessore corrispondente alle coincidenze 8-ple, si trova che il secondo dei due elencati contributi è trascurabile. Ammettendo di poterlo effettivamente trascurare (con il che

si tende a sovrastimare il « branching ratio » R) e valutando il primo dei due contributi in base alla (5), si ottiene

$$b = 1.53 \pm 0.27 .$$

La probabilità $P(R)$ di aver ottenuto il nostro risultato (3 eventi ECT, ossia del tipo attribuibile ad elettroni di cattura) è una funzione di R data dalla distribuzione poissoniana

$$P(R) = (aR + b)^3/3 ! \cdot \exp [- aR - b] ,$$

rappresentata graficamente nella Fig. 6. Questo grafico, che sarà ripreso in esame nella comunicazione successiva, contiene il risultato del nostro esperimento. La funzione $P(R)$ si riduce al di sotto di 1/10 del suo massimo valore per $R > 5 \cdot 10^{-5}$. Si è così portati a concludere che, se il modo coerente di cattura nel Cu è sei volte più probabile del modo incoerente (Sezione **1**) si ha

$$R < 5 \cdot 10^{-5} ,$$

con un livello di confidenza del 90%. Nel caso di cattura puramente incoerente il rendimento di TE si ridurrebbe dal valore del 15%, usato per calcolare il coefficiente a, al 5%; cosicchè risulterebbe $R < 1.5 \cdot 10^{-5}$ con lo stesso livello di confidenza.

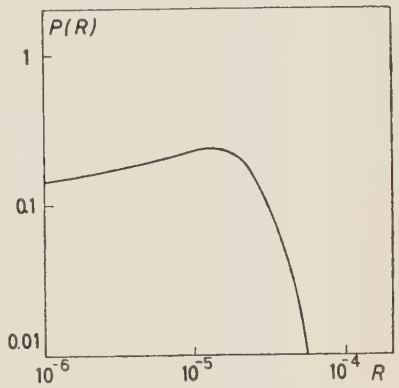

Fig. 6. – Probabilità che in un esperimento come quello descritto si ottengano 3 eventi del tipo ECT, espressa in funzione del « branching ratio » R del processo (3).

Per un confronto con il risultato riportato da STEINBERGER e WOLFE [5] occorre osservare che questi autori lo hanno dedotto dal rendimento del loro sistema calcolato nell'ipotesi che il processo di cattura sia puramente incoerente, mediante un metodo di Montecarlo basato su un'errata valutazione del cammino di radiazione di un elettrone in polietilene (essi hanno usato il valore 62.5 g/cm², mentre il valore corretto è di circa 45 g/cm²). L'effetto di questo errore numerico sul risultato da essi riportato non può essere valutato con esattezza senza ripetere il calcolo con il metodo di Montecarlo. Il valore r del rendimento del loro sistema di contatori si può nondimeno ricavare da misure da noi effettuate con elettroni di varie energie, riportate nella successiva comunicazione. Se si ammette che la cattura coerente sia 6 volte più probabile della cattura incoerente si trova in tal modo $r = 0.4$. Corrispondentemente il limite

superiore che può dedursi dal detto esperimento per il « branching ratio » del processo ricercato risulta uguale a $1.1 \cdot 10^{-3}$ con livello di confidenza del 90%. Si conclude perciò che il nostro esperimento è circa 22 volte più sensibile di quello di STEINBERGER e WOLFE.

SUMMARY

We refer on a first experimental search for neutrino less μ^- capture with electron emission. In this experiment μ^--mesons from the CERN 600 MeV synchrocyclotron are made to stop in a copper target. The upper limit for the branching ratio of the process searched for, relative to ordinary muon capture, has been improved by more than a factor 20 with respect to the most sensitive previous measurements.

Ricerca del processo $\mu^- + \mathcal{N} = e^- + \mathcal{N}$ (*).

M. Conversi, L. di Lella, A. Egidi, C. Rubbia e M. Toller

Istituto di Fisica dell'Università - Roma
Istituto Nazionale di Fisica Nucleare - Sezione di Roma

(ricevuto l'11 Novembre 1960)

Riassunto. — A continuazione della ricerca descritta nella precedente comunicazione, è stato eseguito al sincrociclotrone del CERN un secondo esperimento sul processo $\mu^- + \mathcal{N} = e^- + \mathcal{N}$ frenando in una targhetta di rame il fascio ad alta intensità di mesoni μ di bassa energia sviluppato ultimamente dal gruppo di Citron. Se, come previsto teoricamente, la cattura « coerente » è nel rame almeno 6 volte più probabile di quella « incoerente », il « branching ratio » del processo (1) rispetto alla cattura ordinaria risulta inferiore a $5.9 \cdot 10^{-6}$ con livello di confidenza del 90%. Questo risultato è posto in confronto con quello di un analogo esperimento eseguito a Berkeley contemporaneamente al nostro. Dalla discussione emerge l'importanza di effettuare un ulteriore esperimento di ancor più spinta sensibilità.

1. – Nella precedente comunicazione è stato descritto un esperimento che ha permesso di migliorare per oltre un fattore 20 il limite superiore precedentemente ottenuto, da Steinberger e Wolfe [1], per il « branching ratio » R del processo

$$\mu^- + \mathcal{N} = \mathcal{N} + e^- \tag{1}$$

rispetto alla cattura ordinaria. Nella presente comunicazione riferiremo su di un secondo esperimento che ha permesso di stabilire per R un limite superiore ancora ~ 10 volte più piccolo. Questo risultato — che sarà discusso nell'ultima parte della comunicazione — è stato reso possibile dall'uso del fascio

(*) Comunicato al XLVI Congresso della S.I.F. in una seduta del 3 Ottobre 1960.
(1) J. Steinberger e H. B. Wolfe: *Phys. Rev.*, **100**, 1490 (1955).

di mesoni μ^- ad alta intensità, recentemente sviluppato al sincrociclotrone del CERN(2). Tale fascio è ottenuto immettendo i pioni generati nella targhetta interna del sincrociclotrone in un canale magnetico composto di 24 lenti quadrupolari destinate a concentrare i mesoni μ^- provenienti dai pioni che decadono lungo il percorso. All'uscita del canale i mesoni μ^- di energia minore sono separati mediante un magnete deflettore e costituiscono un fascio che, nelle condizioni di operazione da noi usate, ha un'energia di circa 60 MeV, una contaminazione (di pioni e di elettroni) inferiore al 5% ed un'intensità tale da consentire il frenamento di circa 3700 mesoni μ^- al secondo su un'area di 100 cm^2, in una targhetta di rame spessa 0.5 cm, inclinata a 45° rispetto al fascio stesso, posta ad una distanza di 1.1 m dall'uscita del magnete deflettore.

2. – Il dispositivo sperimentale, riprodotto in Fig. 1, presenta alcune differenze rispetto a quello impiegato nell'esperimento descritto nella comunicazione precedente. Uno dei due contatori di Čerenkov è stato eliminato, mentre è stato aumentato il numero degli scintillatori plastici del telescopio per elettroni (TE) al fine di ridurre ulteriormente la probabilità che gli elettroni originati dal decadimento dei muoni, incapaci di raggiungere gli ultimi contatori di TE, vi producano indirettamente scintillazione attraverso i fotoni di « Bremsstrahlung » da essi emessi nella prima parte di TE. Per conseguire un'ancora più drastica riduzione del fondo (specialmente la parte di esso dovuta alla radiazione cosmica) si sono inoltre aggiunti due scintillatori plastici, 11 e 12, in anticoincidenza rispetto agli altri contatori di TE. Il contatore 12, non disegnato in Fig. 1, era posto orizzontalmente al di sopra di TE (in modo da proteggerlo dagli sciami dei raggi cosmici), separato da questo da una lastra di piombo spessa 2 cm.

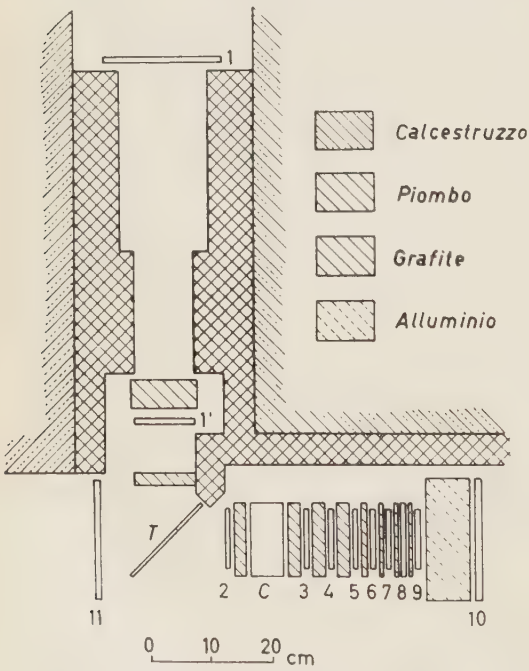

Fig. 1. – Dispositivo sperimentale.

(2) Comunicazione presentata da A. Citron al Berkeley Meeting, Sept. 1960.

L'apparato elettronico di registrazione associato al dispositivo di Fig. 1 è schematicamente rappresentato nella Fig 2. Data la purezza e la buona definizione in energia del fascio una coincidenza doppia (1.1′) tra i contatori 1 e 1′

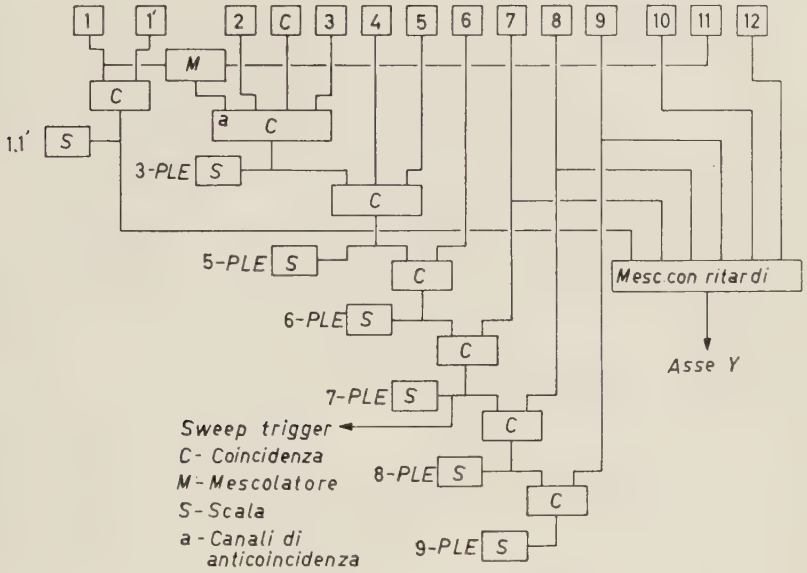

Fig. 2. – Schema logico dell'elettronica.

rappresenta in generale l'arresto di un mesone μ^- nella targhetta. La coincidenza 1.1′ ha al tempo stesso la funzione di « monitor ». Dal numero di tali coincidenze registrate nel corso dell'intero esperimento si risale al numero totale dei mesoni μ^- effettivamente frenati nella targhetta facendo uso, per la

Tabella I. – *Risultati di misure fatte senza assorbitori in TE e con targhetta di grafite equivalente alla targhetta di rame.* In assenza di assorbitori il rendimento del sistema di contatori 2, C, 3 si può dedurre da preesistenti misure [3] e risulta del 64%. Dato che per il detto sistema l'angolo solido di accettazione degli elettroni è di circa 0.19 sr, dai dati delle prime due colonne si conclude che per ogni « monitor » 1.1′ si hanno 0.4 mesoni μ^- frenati nella targhetta.

	Tipo di evento	1.1′	3-ple	5-ple	6-ple	7-ple	8-ple	9-ple
Numero di eventi	con targhetta di carbonio	$1238 \cdot 10^3$	5192	1679	1053	514	377	288
	senza targhetta	$2881 \cdot 10^3$	841	214	140	80	57	37

[3] S. Lokanathan e J. Steinberger: *Suppl. Nuovo Cimento*, **2**, 151 (1955).

normalizzazione, di misure appositamente eseguite escludendo gli assorbitori da TE ed usando una targhetta di grafite equivalente a quella di rame. I risultati di queste misure sono contenuti nella Tabella I.

L'apparato elettronico consente in particolare di registrare (mediante scale e contatori meccanici) le coincidenze tra i primi n contatori di TE, a partire da $n = 3$, con la condizione che esse non siano accompagnate entro 20 ns da impulsi dei contatori 1 e 11 e che il corrispondente evento abbia avuto luogo durante l'impulso del sincrociclotrone (la cui durata si aggira intorno a 400 μs). Agli eventi che soddisfano queste condizioni ci riferimento per brevità, nel seguito, parlando di 3-ple, 4-ple, ..., 9-ple.

Le informazioni fondamentali fornite dall'apparato sono registrate fotografando lo schermo di un tubo oscillografico. Più precisamente gli impulsi di uscita delle coincidenze 7-ple comandano la « sweep » di un oscilloscopio (Tektronix 545) sul cui asse y sono inviati, attraverso opportuni ritardi che permettono di separarli in modo soddisfacente, gli impulsi (negativi) dei contatori 7, 8, 9, 10, 12 e quelli (positivi) corrispondenti alle coincidenze 1.1′. Un fotogramma in cui compaiono tutti gli impulsi appare come quello disegnato nella Fig. 3.

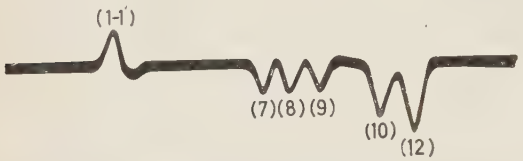

Fig. 3. Riproduzione schematica di un oscillogramma contenente gli impulsi di tutti i contatori.

Il fotogramma caratteristico di un elettrone del processo (1) non dovrebbe contenere gli impulsi dei contatori 10 e 12, mentre vi dovrebbero figurare gli impulsi dei tre contatori 7, 8 e 9 nonchè l'impulso 1.1′ in posizione tale da indicare l'arresto di un mesone μ^- nella targhetta seguito, entro un intervallo di tempo compreso tra ~ 20 e 500 ns, dal corrispondente elettrone di cattura.

Nel corso dell'intero esperimento, eseguito in circa 47 ore di tempo effettivo di misura, si sono ottenuti i risultati riportati nella Tabella II. Notiamo

Tabella II. – *Risultati di circa* 47 h *di misure eseguite esponendo il dispositivo di Fig.* 1, *con targhetta di rame spessa* 0.5 cm, *al fascio intenso di mesoni* μ^- *da* ~ 60 MeV. Dal numero dei « monitors » 1.1′ (1ª colonna) e dai risultati della Tabella I si deduce il numero totale di mesoni μ^- frenati nella targhetta ($6.26 \cdot 10^8$). Le n-ple « buone » sono caratterizzate dall'assenza degli impulsi dei contatori 10 e 12 e dalla presenza di un impulso 1.1′ in posizione tale da indicare l'arresto di un mesone μ^- seguito dall'emissione del corrispondente elettrone tra ~ 20 e 500 ns.

Tipo di evento	11′	3-ple	5-ple	6-ple	7-ple	8-ple	9-ple
numero totale	$1.56 \cdot 10^9$	$207 \cdot 10^3$	695	62	33	18	7
n-ple « buone »	—	—	—	—	5	0	0

esplicitamente che in corrispondenza di

$$N = 6.26 \cdot 10^8$$

mesoni μ^- frenati nella targhetta non solo non è stata registrata alcuna 9-pla, ma neppure alcuna 8-pla attribuibile ad elettroni di cattura. Questa circostanza ci consente di ricavare un limite superiore per il « branching ratio » R ignorando l'esistenza del contatore 9, ossia considerando TE come composto soltanto dei primi otto contatori. Dalla geometria del dispositivo sperimentale si riconosce allora che la frazione di elettroni accettata in TE (relativamente alle 8-ple) è $\omega/4\pi = 5.5 \cdot 10^{-3}$,essendo ω l'angolo solido utile di accettazione. D'altra parte soltanto una frazione $f = 0.92$ dei mesoni μ^- frenati nel rame subiscono la cattura nucleare e, tenuto conto che la vita media dei mesoni μ^- in Cu è di 160 ns, si riconosce subito che solo una frazione $u = 0.87$ di questi possono dar luogo ad emissione di elettroni entro l'intervallo temporale compreso tra 20 e 500 ns. Pertanto, se si indica con b il valore di aspettazione dell'eventuale fondo (eventi di carattere spurio che simulano elettroni di cattura) il numero di 8-ple che in media ci si dovrebbe aspettare di registrare nel corso dell'intero esperimento in corrispondenza di un dato valore di R è

$$m(R) = Nfu\left(\frac{\omega}{4\pi}\varepsilon R\right) + b = aR + b\,, \tag{2}$$

dove ε rappresenta il rendimento di TE per gli elettroni di cattura (relativamente, al solito, alle 8-ple).

3. – Piuttosto che calcolare ε con un metodo di Montecarlo, abbiamo preferito effettuare una determinazione sperimentale diretta del rendimento di TE per elettroni di varie energie, relativamente alle coincidenze 7-ple, 8-ple, e 9-ple. Per far ciò è stato necessario preparare un fascio di elettroni sensibilmente monoenergetici. Questo si è ottenuto facendo incidere i protoni estratti dal sincrociclotrone su una targhetta di Pb e selezionando, mediante due magneti analizzatori, le particelle in essa prodotte con impulso definito entro un piccolo intervallo. La calibrazione dell'impulso selezionato in corrispondenza di dati valori delle correnti dei magneti analizzatori, è stata effettuata in base a misure di percorso residuo dei mesoni di quell'impulso, misure che venivano eseguite con lo stesso telescopio TE.

Le determinazioni del rendimento di TE sono state ripetute, per ciascuna energia selezionata, interponendo sul fascio elettronico incidente in TE lastrine di Cu di vario spessore, atte a simulare le perdite di energia subite dagli elettroni nella targhetta di Cu.

I risultati di queste misure di rendimento di TE sono contenuti nella Tabella III. I rendimenti relativi alle coincidenze 3-ple sono stati calcolati trascurando il fatto che le perdite di energia per ionizzazione, riducendo l'energia dell'elettrone, ne influenzano le perdite per irraggiamento (*). Questa approssimazione appare legittima dalla consistenza dei rendimenti calcolati con quelli misurati alla stessa energia di 100 MeV (v. Tabella III) per quattro diversi spessori di rame.

TABELLA III. – *Risultati delle misure di rendimento del telescopio T.E., eseguite senza contatori di anticoincidenza, per elettroni monocromatici di varie energie filtrati attraverso fogli di rame di vario spessore.* L'errore indicato è puramente statistico. I numeri di coincidenze 3-ple sono stati calcolati con il procedimento indicato nel testo.

E (MeV)	spessore rame (mm)	rendimento percentuale					
		3-ple	5-ple	6-ple	7-ple	8-ple	9-ple
70	4	67	15±1	5.3±0.6	2.2±0.4	0.6±0.2	0.17±0.09
80	4	71	24±1	11.8±0.9	6.3±0.6	2.7±0.4	1.1±0.2
90	4	75	32±2	19 ±2	12.6±1.2	7.8±0.9	4 ±0.6
100	0	91	61±2	46 ±2	35 ±2	29 ±1	20.5 ±1.0
100	2	86	52±2	38 ±2	28 ±1	18.6±1.	13.8 ±0.8
100	4	78	39±2	26 ±1	19.1±0.9	12.9±0.7	8.4 ±0.5
100	7	70	29±1	18 ±1	11.1±0.6	7.1±0.5	4.2 ±0.3
110	4	81	45±2	32 ±2	24.7±1.2	18.2±1.	11.9 ±0.7

Le curve di Fig. 4 mostrano come il rendimento delle 7-ple, 8-ple e 9-ple di TE misurate senza i contatori di anticoincidenza, dipendono dall'energia degli elettroni incidenti, nel caso in cui il fascio di elettroni monocromatici

(*) L'espressione del rendimento delle 3-ple si identifica in questa approssimazione con la probabilità che un elettrone di energia E, perdendo in X cammini di radiazione energia solo per irraggiamento, resti con una energia maggiore di quella, E_i, che esso perde per sola ionizzazione attraversando lo stesso spessore. Tale probabilità vale [1]

$$\frac{(X-1,\ln(E/E_i))!}{\Gamma(X)}.$$

[1] W. HEITLER: *Quantum Theory of Radiation* (Oxford, 1954).

attraversa uno spessore di Cu equivalente a metà della targhetta usata (~ 4 mm, tenuto conto dell'inclinazione della targhetta). Il contatore di anticoincidenza 10 riduce ulteriormente tale rendimento a causa dello sviluppo della cascata elettrofotonica che, per fluttuazione, può penetrare l'intero assorbitore di Al. Per elettroni da 100 MeV filtrati attraverso 4 mm di Cu la riduzione del rendimento nel caso delle coincidenze 8-ple è risultata (da una misura della percentuale delle coincidenze stesse accompagnate da un impulso del contatore 10) di circa il 10%. Tenuto conto di questa riduzione, dalla curva di Fig. 4 relativa alle 8-ple si deduce che il rendimento di TE relativo ad elettroni prodotti nella targhetta con uno spettro di energia quale risulta dalla mescolanza di un processo di cattura coerente sei volte più probabile del processo incoerente, ha il valore $\varepsilon = 0.14$. Si trova così $a = 3.98 \cdot 10^5$.

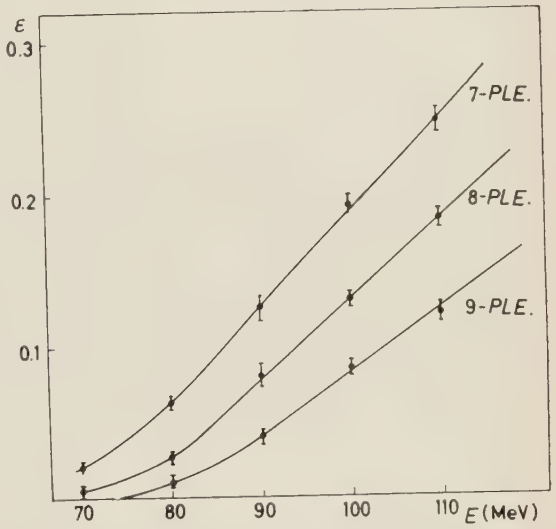

Fig. 4. – Curve di rendimento relativo al telescopio TE, senza il contatore 10 di anticoincidenza, per elettroni dell'energia indicata in ascissa, filtrati attraverso 4 mm di rame.

4. – Poichè nell'intero esperimento non è stata registrata alcuna coincidenza 8-pla, la probabilità di questo risultato è rappresentata, per una statistica poissoniana, dalla funzione

$$P(R) = \exp\left[-(aR + b)\right],$$

che come si vede è il prodotto della probabilità $Q(R) = \exp\left[-aR\right]$ che non si registri nessun evento genuino (mentre il valore di aspettazione è aR) per la probabilità $\exp\left[-b\right]$ che non si registri nessun evento spurio (mentre il valore di aspettazione è b). Perciò le informazioni che si possono ricavare da questo esperimento sono indipendenti dal valore di aspettazione b del fondo.

Inserendo il valore numerico di a si ottiene

$$Q(R) = \exp\left[-3.98 \cdot 10^5 R\right].$$

Questa funzione si riduce al di sotto di 1/10 per $R > 5.9 \cdot 10^{-6}$. Se ne deduce che nel caso di cattura coerente sei volte più probabile della cattura incoerente il processo (1) ha rispetto alla cattura ordinaria un « branching ratio »

$$R < 5.9 \cdot 10^{-6} ,$$

con un livello di confidenza del 90%.

Osserviamo esplicitamente che il non aver registrato in tutto l'esperimento neppure una coincidenza 8-pla è probabilisticamente consistente con il valore di aspettazione b del fondo. Come si è detto nella precedente comunicazione quest'ultimo trae origine da eventi di natura accidentale e da elettroni di disintegrazione eccezionalmente capaci di produrre, direttamente o indirettamente, scintillazione in tutti i contatori di Te che precedono il contatore 9. Ora da un'analisi più dettagliata dei nostri dati si può stimare che il contributo a b proveniente da queste due cause è complessivamente dell'ordine dell'unità, in accordo con il risultato negativo dell'esperimento.

5. – Volendo ora discutere brevemente il nostro risultato, incominciamo col confrontarlo con quelli di altri esperimenti sullo stesso processo. Nella Fig. 5

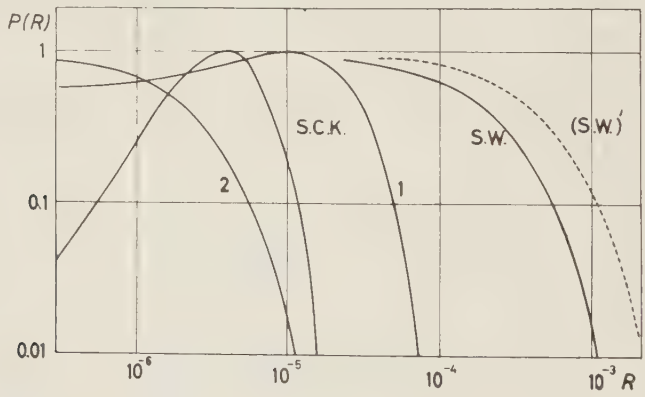

Fig. 5. – Probabilità in funzione di R, dei risultati ottenuti negli esperimenti: (S.W.)': esperimento di Steinberger e Wolfe, rielaborato nel modo precisato nella comunicazione precedente; S.W.: curva riportata da Steinberger e Wolfe (per cattura incoerente); 1: esperimento descritto nella comunicazione precedente; S.C.K.: esperimento di Sard, Crowe e Kruger; 2: presente esperimento.

sono disegnati i grafici che, a meno di una costante, rappresentano in funzione di R la probabilità di ottenere i risultati effettivamente trovati negli esperimenti indicati. Le curve sono normalizzate in modo da essere tutte eguali a 1

nel loro massimo. Dalla figura si riconosce in particolare che il nostro esperimento fornisce per R un limite superiore oltre 180 volte più piccolo di quello deducibile dall'esperimento di STEINBERGER e WOLFE. Esso ha invece una sensibilità confrontabile a quella dell'esperimento di SARD, CROWE e KRUGER di cui si è avuta notizia al recente Congresso di Rochester [5]. In tale esperimento di fa uso di un magnete a deflessione di 180° e di un grande scintillatore proporzionale posto in fondo al magnete stesso. Selezionati dal magnete ed analizzati dallo scintillatore, gli eventuali elettroni di alta energia emessi nel processo (1) di cattura coerente difficilmente possono essere simulati da elettroni di disintegrazione o da altri possibili processi più complessi. In una recente esposizione al ciclotrone di Berkeley sono stati osservati con questo dispositivo 3 eventi attribuibili ad elettroni di cattura coerente, nonostante il valore di aspettazione del fondo sia secondo gli autori di soli 0.23 eventi. Il risultato di SARD e dei suoi collaboratori indicherebbe dunque l'esistenza del processo (1) con un « branching ratio » $R = (4 \pm 3) \cdot 10^{-6}$, non incompatibile con il nostro limite superiore. La compatibilità dei due risultati si vede anche dalle curve della Fig. 5, le quali mostrano che entrambi i risultati hanno una buona probabilità di essere verificati se $R \approx 2 \cdot 10^{-6}$. Da quanto precede appare comunque evidente l'opportunità di effettuare un esperimento di sensibilità ancor più spinta, tale da poter mettere in evidenza il processo (1) qualora esso esista con una « branching ratio » dell'ordine di 10^{-6} rispetto alla cattura ordinaria.

Il risultato ottenuto ci permette di stabilire un estremo superiore per i coefficienti che compaiono nell'elemento di matrice fenomenologico ricavato da WEINBERG e FEINBERG [6] e da CABIBBO e GATTO [7] relativamente all'interazione rappresentata dal diagramma di Fig. 1 della comunicazione precedente. In questo elemento di matrice compaiono i quattro fattori di forma adimensionali $f_{E0}(q^2)$, $f_{M0}(q^2)$, $f_{E1}(q^2)$, $f_{M1}(q^2)$ relativi alle transizioni di monopolo e di dipolo elettrico e magnetico, dipendenti dal quadrato del modulo del quadrimpulso q del fotone. Essi permettono di esprimere la probabilità di transizione per il processo da noi ricercato: per la cattura coerente q^2 coincide con il quadrato dell'energia totale m_μ del muone nell'orbita K di un nucleo di Cu ($m_\mu = 103.8$ MeV). Per un tale nucleo questa probabilità è data da [6]

$$W = 56\, m_\mu (Z_{\text{eff}})^4 \alpha^5 [\xi_0(m_\mu^2)]^2 , \tag{2}$$

dove $[\xi_0(m_\mu^2)]^2 = |f_{E0}(m_\mu^2) - f_{M1}(m_\mu^2)|^2 + |f_{E1}(m_\mu^2) + f_{M0}(m_\mu^2)|^2$; α è la costante della struttura fine e Z_{eff} è la ben nota « carica efficace », che tiene conto della struttura non puntiforme del nucleo.

[5] R. D. SARD, K. M. CROWE e H. W. KRUGER: *Rochester Conference* (Sett. 1960).
[6] S. WEINBERG e G. FEINBERG: *Phys. Rev. Lett.*, **3**, 111, 244 (1959).
[7] N. CABIBBO e R. GATTO: *Phys. Rev.*, **116**, 1334 (1959).

La probabilità di cattura ordinaria è invece data dalla formula di Primakoff [8]

$$W(\mu^- + \mathrm{Cu} \to (\mathrm{Ni})^* + \nu) = 220\ \mathrm{s}^{-1} \cdot (Z_{\mathrm{eff}})^4 \left[1 - \delta \frac{A - Z}{2A}\right], \tag{3}$$

che assume questa forma se si ammette la validità dell'interazione universale di Fermi nel descrivere il processo elementare $\mu^- + \mathrm{p} \to \mathrm{n} + \nu$.

Dalle (2) e (3) segue che il valore teorico del « branching ratio » del processo da noi ricercato è dato da

$$\frac{8.5 \cdot 10^{11} [\xi_0(m_\mu^2)]^2}{[1 - \delta(A - Z)/2A]} = R\,. \tag{4}$$

Notando che per il Cu si ha $1 - \delta((A - Z)/2A) \simeq 0.25$, dal nostro risultato si ricava in base alle (4):

$$[\xi_0(m_\mu^2)]^2 < 2 \cdot 10^{-18}\,. \tag{5}$$

Il limite superiore di circa 10^{-6} ottenuto sperimentalmente [9] per il « branching ratio » del processo $\mu^+ \to e^+ + \gamma$ rispetto al decadimento ordinario permette di stabilire in modo analogo che $|f_{E1}(0)|^2 + |f_{M1}(0)|^2 < 10^{-21}$. ammettendo in base a questa diseguaglianza di poter trascurare f_{E1} e f_{M1} rispetto a f_{E0} e f_{M0} anche per $q^2 = m_\mu^2$, si ottiene dalla (5)

$$|f_{E0}(m_\mu^2)|^2 + |f_{M0}(m_\mu^2)|^2 < 2 \cdot 10^{-18}\,.$$

* * *

Ci è gradito ringraziare il Prof. R. Gatto ed il Dr. N. Cabibbo per molte utilissime discussioni sugli aspetti teorici di questa ricerca. Siamo grati al Prof. G. Fidecaro per numerose informazioni e per l'aiuto prestatoci specialmente nella fase iniziale del nostro lavoro al CERN. Al Dr. A. Citron, al Dr. E. G. Michaelis ed agli altri membri del loro gruppo desideriamo infine esprimere la nostra riconoscenza per l'uso del fascio di mesoni μ^- ad alta intensità e per consigli vari.

[8] H. Primakoff: *Proc. of the 5th Ann. Rochester Conf.* (1955).

[9] D. Berley, J. Lee e M. Bardon: *Phys. Rev. Lett.*, **2**, 357 (1959); J. Ashkin, T. Fazzini, G. Fidecaro, N. H. Lipman, A. W. Merrison e J. Paul: *Nuovo Cimento*, **14**, 1266 (1959).

SUMMARY

A second experiment has been performed on the process $\mu^- + \mathcal{N} \rightarrow \mathcal{N} + e$ making use of the low energy high intensity μ^- beam recently developed at CERN. If, as expected on theoretical ground, coherent neutrinoless capture of muons in copper is at least 6 times more probable than the corresponding incoherent process, the branching ratio relative to ordinary muon capture turns out to be less than $5.9 \cdot 10^{-6}$, with 90% confidence level. This result is compared with that independently obtained in an experiment of similar sensitivity carried out at the Berkeley synchrocyclotron.

IL NUOVO CIMENTO Vol. XIX, N. 5 1° Marzo 1961

On Radiative Corrections due to Soft Photons.

K. E. Eriksson

CERN - Geneva

(ricevuto il 2 Dicembre 1960)

Summary. — It is shown how the infra-red divergent part, due to soft virtual photons, of any scattering amplitude can be factorized in a Lorentz invariant manner. It is further shown that if the energy resolution for a process is negligible compared to the electron rest mass then the whole soft photon contribution to the transition probability density can be factorized leaving a Lorentz-invariant remainder. This factorization is then extended to the more realistic case of an energy resolution which is of the same order of magnitude as the electron rest mass, or larger. Finally, the magnitudes of radiative corrections are discussed.

1. – Introduction.

It has been known for a long time that the so-called infra-red divergences encountered in quantum electrodynamics are connected with the fact that the number of soft photons is not an observable. It is also well-known that the infra-red divergences cancel exactly when soft photons are treated collectively. A proof of this cancellation to all orders of perturbation theory was given by Nakanishi [1].

In their work on infra-red divergences Jauch and Rohrlich [2] introduced a low energy cut-off equal to the energy resolution ΔE and then succeded

[1] N. Nakanishi: *Prog. Theor. Phys.*, **19**, 159 (1958).

[2] J. M. Jauch and F. Rohrlich: *Helv. Phys. Acta*, **27**, 613 (1954). This paper contains further references to the earlier literature. See also ref. [6], pp. 390-405.

in expressing the soft photon contributions in closed form as a factor in the scattering cross-section. Since the appearence of their paper the factorization of the soft photon contributions has been accomplished in different ways by several authors ([3]) with the use of an infra-red cut-off.

In a recent paper YENNIE, FRAUTSCHI and SUURA ([4]) find that the soft photon contributions to a scattering cross-section can be factorized in such a way that the remainder is cut-off independent and can be calculated with the usual methods of perturbation theory.

The same result has been obtained independently by the present author, and a proof of the cut-off independent factorization in perturbation theory is given in this paper. The difficulties that occur in the paper of YENNIE, FRAUTSCHI and SUURA in connection with what they call « overlapping infra-red divergences » will not appear in the following treatment. They are avoided by a splitting of the electromagnetic field into two « components », one for soft photons and one for hard photons, similar to the method of MUROTA ([5]).

In high energy electromagnetic processes only part of the low energy radiation can be factorized; the rest is left to be handled by perturbation theory. A discussion of this is contained in the last part of the paper.

With regard to metric, normalization factors etc. we shall follow the conventions used in the text-book of JAUCH and ROHRLICH ([6]).

We shall consider a process

$$|i\rangle \to |f\rangle \tag{1}$$

in which r particles with momenta $p_1, \ldots, p_r$ and charges $Q_1, \ldots, Q_r$ take part. With this process there is connected a (Lorentz-) *invariant amplitude*, M, defined in terms of the S-matrix element by

$$\langle f|S-1|i\rangle = \delta(P_f - P_i)\, M\,. \tag{2}$$

Here P_i and P_f are the total momenta of the states $|i\rangle$ and $|f\rangle$ respectively.

In general M is infra-red divergent. However, as is well known — and as is shown below — the infra-red divergences deriving from M cancel with the infra-red divergences deriving from soft photon emission accompanying

---

([3]) E. L. LOMON: *Nucl. Phys.*, **1**, 101 (1956); *Phys. Rev.*, **113**, 726 (1959); D. R. YENNIE and H. SUURA: *Phys. Rev.*, **105**, 1378 (1957); E. R. CAIANIELLO and S. OKUBO: *Nuovo Cimento*, **17**, 355 (1960); S. OKUBO: *Nuovo Cimento*, **18**, 70 (1960).

([4]) D. R. YENNIE, S. C. FRAUTSCHI and H. SUURA: to be published.

([5]) T. MUROTA: preprint.

([6]) J. M. JAUCH and F. ROHRLICH: *Theory of Photons and Electrons* (Cambridge, Mass., 1955).

the process (1). Since « soft » is not an invariant concept, the discussion, of soft photons must be restricted to a specific Lorentz-frame L. We assume that in L the energy loss due to soft photon emission does not exceed ΔE, with

$$\Delta E \ll m\,, \qquad (m = \text{electron rest mass}), \tag{3}$$

In Section 2 an investigation is made of the origin of the infra-red divergences, and a preliminary separation of the infra-red contributions is performed. In Section 3 the infra-red divergent part of M is factorized in a Lorentz-invariant manner, and a « non-infra-red invariant amplitude », $\overline{M}$, is defined. In Section 4 the transition probability density for process (1) with energy resolution ΔE, is derived in the form $F(\Delta E)\,|\overline{M}\,|^2$ and the infra-red factor $F(\Delta E)$ is studied in detail. In Section 5, finally, some questions are discussed that are of interest for practical calculations on electrodynamic processes at high energies. Then we omit restriction (3).

2. – Preliminary discussion.

Throughout the following we shall make all considerations with reference to the Lorentz-frame L, mentioned above.

We define a region R_ε of the 4-dimensional k-space by

$$k \in R_\varepsilon \quad \text{if and only if} \quad \begin{cases} |\boldsymbol{k}| \leqslant \varepsilon \\ k_0 \leqslant \varepsilon \end{cases} \qquad \varepsilon \ll m\,. \tag{4}$$

To the division of k-space into R_ε an dits complementary region there corresponds a separation of the free electromagnetic field into two parts (like in ref. [5])

$$a_\mu(x) = a_{s\mu}(x) + a_{h\mu}(x) \tag{5}$$

where

$$\begin{cases} a_{s\mu}(x) = \dfrac{1}{(2\pi)^{\frac{3}{2}}} \displaystyle\int\limits_{k_0 = |\boldsymbol{k}| \leq \varepsilon} \frac{\mathrm{d}^3 k}{\sqrt{2k_0}} \left[a_\mu(\boldsymbol{k}) \exp\left[ikx\right] + a_\mu^*(\boldsymbol{k}) \exp\left[-ikx\right]\right], \\ a_{h\mu}(x) = \dfrac{1}{(2\pi)^{\frac{3}{2}}} \displaystyle\int\limits_{k_0 = |\boldsymbol{k}| > \varepsilon} \frac{\mathrm{d}^3 k}{\sqrt{2k_0}} \left[a_\mu(\boldsymbol{k}) \exp\left[ikx\right] + a_\mu^*(\boldsymbol{k}) \exp\left[-ikx\right]\right]. \end{cases} \tag{6}$$

As a consequence of the commutation relations

$$(7)\qquad \begin{cases} [a_\mu(\boldsymbol{k}), a_\nu(\boldsymbol{k}')] = [a^*_\mu(\boldsymbol{k}), a^*_\nu(\boldsymbol{k}')] = 0\,; \\ [a_\mu(\boldsymbol{k}), a^*_\nu(\boldsymbol{k}')] = g_{\mu\nu}\delta(\boldsymbol{k}-\boldsymbol{k}')\,, \end{cases}$$

we then have the new relations

$$(8)\qquad [a_{s\mu}(x), a_{h\nu}(x')] = [a_{s\mu}(x), a^*_{h\nu}(x')] = [a^*_{s\mu}(x), a_{h\nu}(x')] = [a^*_{s\mu}(x), a^*_{h\nu}(x')] = 0\,,$$

showing that soft photons (those described by the field $a_{s\mu}(x)$) and hard photons (those described by the field $a_{h\mu}(x)$) can be treated as different particles with different graphical representations in perturbation theory (Fig. 1).

To see this more explicitly let

$$(9)\qquad S = \sum_{n=0}^{\infty} S^{(n)}$$

Fig. 1.

be an expansion of the S-operator in powers of the coupling constant e. Then the n-th term of the expansion is

$$(10)\qquad S^{(n)} = \frac{e^n}{n!}\int\!\!\ldots\!\!\int \mathrm{d}x_n \ldots \mathrm{d}x_1\, O^{\mu_1\ldots\mu_n}(x_1, \ldots, x_n)\, T\big(a_{\mu_1}(x_1) \ldots a_{\mu_n}(x_n)\big)\,,$$

where $O^{\mu_1\ldots\mu_n}(x_1, \ldots, x_n)$ is an operator which is symmetric in $x_1, \ldots, x_n$ and is composed of all fields except the electromagnetic field, and T means time-ordered product. According to (8) the expression (10) can be split into

$$(11)\qquad \begin{aligned} S^{(n)} = \frac{e^n}{n!}\sum_{n'=0}^{n}\binom{n}{n'}\int\!\!\ldots\!\!\int \mathrm{d}x_n \ldots \mathrm{d}x_1\, O^{\mu_1\ldots\mu_n}(x_1, \ldots, x_n)\, T\big(a_{h\mu_1}(x_1) \ldots a_{h\mu_{n'}}(x_{n'})\big)\cdot \\ \cdot T\big(a_{s\mu_{n'+1}}(x_{n'+1}) \ldots a_{s\mu_n}(x_n)\big) = \sum_{n'=0}^{n}\frac{e^{n'}}{n'!}\,\frac{e^{n-n'}}{(n-n')!}\int\!\!\ldots\!\!\int \mathrm{d}x_n \ldots \mathrm{d}x_1\cdot \\ \cdot O^{\mu_1\ldots\mu_n}(x_1, \ldots, x_n)\, T\big(a_{h\mu_1}(x_1) \ldots a_{h\mu_{n'}}(x_{n'})\big)\, T\big(a_{s\mu_{n'+1}}(x_{n'+1}) \ldots a_{s\mu_n}(x_n)\big)\,. \end{aligned}$$

Let the « black box », $\widehat{M}$, in Fig. 2 represent the sum over all diagrams for the process (1) that do not include any soft photons. The corresponding transition amplitude will also be denoted by « $\widehat{M}$ ». Then $\widehat{M}$ must be corrected for virtual and real soft photon interactions. Only soft photons giving rise to infra-red divergences, *i.e.* to logarithmic momentum dependences need to be considered, since terms which are linear in soft photon momenta, are smaller by a factor $\Delta E/m$ and can be neg-

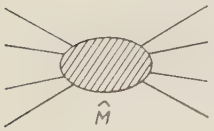

Fig. 2.

lected because of (3). It appears that a soft photon gives rise to an infra-red divergence only if it is attached at a «single photon corner» to an external line of $\hat{M}$ (*). Thus the only corrections to $\hat{M}$ that one needs to consider are those due to interchange of soft photons between external lines and emission of soft photons (with a total energy $\leqslant \Delta E$) from the external lines (see Fig. 3).

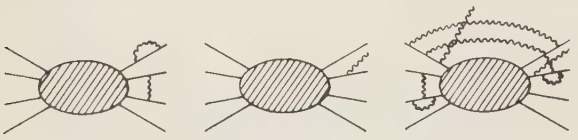

Fig. 3.

Consider first one of the external lines of $\hat{M}$, say the i-th line. Assume that it represents an outgoing particle. Then we can write

$$\hat{M} = \beta^*(p_i)\,\hat{M}_i \qquad (\beta^*(p_i) = \text{boson emission factor}), \tag{12-b}$$

if that line represents a boson, and

$$\hat{M} = \overline{u}(p_i)\,\hat{M}_i\,, \qquad (\overline{u}(p_i) \text{ is a spinor}), \tag{12-f}$$

if it represents a fermion. If $Q_i = 0$, no soft photons can be attached to the i-th line. Assume $Q_i \neq 0$. Let us attach n soft photons with momenta $k_1, \ldots, k_n$ (counted as outgoing) to that line. If we suppress photon factors and neglect terms in the numerators that are linear in soft photon momenta, the added soft photons change $\hat{M}$ into

$$(eQ_i)^n \sum_{(j_1,\ldots,j_n)} \beta^*(p_i)\, \frac{2ip_i^{\mu_{j_1}} \cdot 2ip_i^{\mu_{j_2}} \ldots 2ip_i^{\mu_{j_n}}}{2k_{j_1}\cdot p_i\,[2(k_{j_1}+k_{j_2})\cdot p_i] \ldots [2(k_{j_1}+\ldots+k_{j_n})\cdot p_i]}\, \hat{M}_i \tag{13-b}$$

(boson case),

(*) This is a well-known fact. It can easily be proved that a soft photon which is attached to

a) the interior of $\hat{M}$ (Fig. 4*a*) or

b) a closed loop (Fig. 4*b*) or

c) a boson line at a «two-photon corner» (Fig. 4*c*)

gives a contribution which is not infra-red divergent but vanishes when the photon momentum goes to zero.

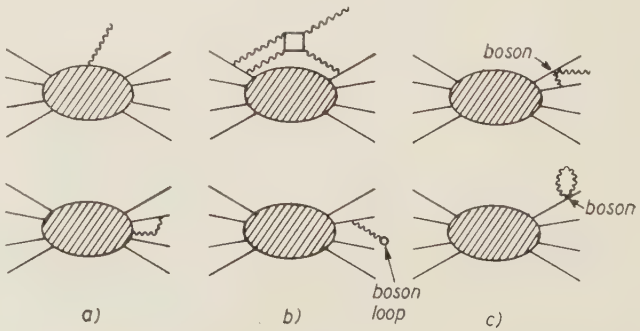

Fig. 4.

(13-f) $$(eQ_i)^n \sum_{(j_1,\ldots,j_n)} \bar{u}(p_i)\, \frac{\gamma^{\mu_{j_1}}(ip_i - m)\,\gamma^{\mu_{j_2}}(ip_i - m)\ldots\gamma^{\mu_{j_n}}(ip_i - m)}{2k_{j_1}\cdot p_i[2(k_{j_1}+k_{j_2})\cdot p_i]\ldots[2(k_{j_1}+\ldots+k_{j_n})\cdot p_i]}\,\hat{M}_i$$

$(p_i = p_i^\mu \gamma_\mu)$ (fermion case).

The summations are over all permutations of $j_1, \ldots, j_n$ among $1, \ldots, n$. Rearranging the factors in (13*b*, *f*) (with the use of the Dirac equation for (13*f*)) and inserting (12*b*, *f*) we get for bosons and fermions the identical result

(14) $$\prod_{i=1}^{n}(ieQ_i p_i^{\mu_j}) \sum_{(j_1,\ldots,j_n)} \frac{1}{(k_{j_1}\cdot p_i)[(k_{j_1}+k_{j_2})\cdot p_i]\ldots[(k_{j_1}+\ldots+k_{j_n})\cdot p_i]}\,\hat{M} = \prod_{j=1}^{n}\left(\frac{ieQ_j p_i^{\mu_j}}{k_j\cdot p_i}\right)\hat{M}.$$

If the i-th particle were incoming rather than outgoing, every factor in the denominator of (14) should include a minus sign. Thus the contribution from the diagrams with n soft photons attached to the i-th external line (representing an in- or out-going, charged or uncharged particle) of $\hat{M}$ is, apart from photon factors, given by

(15) $$\prod_{j=1}^{n}\left(\frac{ieQ_i p_i^{\mu_j}}{k_j\cdot\varepsilon_i p_i}\right)\hat{M},$$

where

(16) $$\varepsilon_i = \begin{cases} +1 \\ -1 \end{cases} \text{ if the } i\text{-th particle is } \begin{cases} \text{incoming} \\ \text{outgoing} \end{cases}.$$

Consider next a diagram with m emitted and l internal soft photons. Assume that the m'-th emitted photon has a momentum $\boldsymbol{k}_{m'}$ and polarization $e_{m'}$ and is emitted from the $i_{m'}$-th external line of $\hat{M}$. The l'-th internal photon is assumed to have a momentum $k'_{l'}$ and to join the $i_{l'1}$-th and the $i_{l'2}$-th external lines of $\hat{M}$. The generalized quantity corresponding to (15) — including photon factors $(i(2\pi)^{-\frac{3}{2}}\cdot(2k_{m'0})^{-\frac{1}{2}}e_{m'\mu_{m'}}$ for emitted and $i(2\pi)^{-1}(k'^2_{l'})^{-1}$ for internal soft photons), and also including integrations over internal momenta — is now

(17) $$\prod_{m'=1}^{m}\left(\frac{i}{(2\pi)^{\frac{3}{2}}}\,\frac{ieQ_{im'}p_{im'}\cdot e_{m'}}{\sqrt{2k_{m'0}}(k_{m'}\cdot\varepsilon_{i_{m'}}p_{i_{m'}})}\right)\cdot$$

$$\cdot\prod_{l'=1}^{l}\left(\frac{-i}{(2\pi)^4}\int_{(R_\varepsilon)}\frac{\mathrm{d}^4k'_{l'}e^2Q_{i_{l'1}}Q_{i_{l'2}}p_{i_{l'1}}\cdot p_{i_{l'2}}}{(k'^2_{l'}+\lambda^2)(k'_{l'}\cdot\varepsilon_{i_{l'1}}p_{i_{l'1}})(-k'_{l'}\cdot\varepsilon_{i_{l'2}}p_{i_{l'2}})}\right)\hat{M};\quad (k_{m'0}=\sqrt{\boldsymbol{k}^2_{m'}+\lambda^2}),$$

(λ = fictious photon mass; $\lambda \ll \varepsilon,\ \Delta E$).

We introduce now the following definitions which will prove useful.

$$s^{\mu}(k) = \frac{ie}{(2\pi)^{\frac{3}{2}}} \sum_{i=1}^{r} \frac{2Q_i p_i^{\mu}}{k^2 + 2k \cdot \varepsilon_i p_i}, \tag{18}$$

and

$$\hat{A} = \frac{1}{2\pi i} \int_{(R_\varepsilon)} \frac{\mathrm{d}^4 k}{k^2 + \lambda^2} \, s_{\mu}(k) \, s^{\mu}(-k) \,. \tag{19}$$

The expression (17) must be summed over all diagrams in which soft photons are emitted. This means

(i) a summation over each of the $m + 2l$ indices $i_1, \ldots, i_m, i_{11}, \ldots, i_{l2}$ from 1 to r.

(ii) division by a factor

$$l!\, 2^l \tag{20}$$

since each diagram has been counted $l!2^l$ times.

(iii) a summation over l from 0 to ∞.

So using the definitions (18) and (19) we get (since $k^2 \cong 0$ for soft photons)

$$\sum_{l=0}^{\infty} \frac{1}{l!\, 2^l} \sum_{\substack{i_1, \ldots, i_m, \\ i_{11}, \ldots, i_{l2} = 1}}^{r} \prod_{m'=1}^{m} \left(\frac{i}{(2\pi)^{\frac{3}{2}}} \frac{ieQ_{i_{m'}} p_{i_{m'}} \cdot e_{m'}}{\sqrt{2k_{m'0}} (k_{m'} \cdot \varepsilon_{i_{m'}} p_{i_{m'}})} \right) \cdot \tag{21}$$

$$\cdot \prod_{l'=1}^{l} \left(\frac{-i}{(2\pi)^4} \int_{(R_\varepsilon)} \frac{\mathrm{d}^4 k'_{l'} e^2 Q_{i_{l'1}} Q_{i_{l'2}} p_{i_{l'1}} \cdot p_{i_{l'2}}}{(k'^2_{l'} + \lambda^2)(k'_{l'} \cdot \varepsilon_{i_{l'1}} p_{i_{l'1}})(-k'_{l'} \cdot \varepsilon_{i_{l'2}} p_{i_{l'2}})} \right) \widehat{M} =$$

$$= \sum_{l=0}^{\infty} \frac{1}{l!\, 2^l} \prod_{j=1}^{m} \left(\frac{is(k_j) \cdot e_j}{\sqrt{2k_{j0}}} \right) (-\hat{A})^l \widehat{M} = \prod_{j=1}^{m} \left(\frac{is(k_j) \cdot e_j}{\sqrt{2k_{j0}}} \right) \exp\left[-\tfrac{1}{2} \hat{A} \right] \widehat{M} \,.$$

Thus the result we have obtained in this Section is that the transition amplitude $M(\boldsymbol{k}_1, e_1; \ldots; \boldsymbol{k}_m, e_m)$ for emission of m soft photons with momenta $\boldsymbol{k}_1, \ldots, \boldsymbol{k}_m$ and polarizations $e_1, \ldots, e_m$ accompanying the process (1) is given by

$$M(\boldsymbol{k}_1, e_1; \ldots; \boldsymbol{k}_m, e_m) = \prod_{j=1}^{m} \left(\frac{is(k_j) \cdot e_j}{\sqrt{2k_{j0}}} \right) \exp\left[-\tfrac{1}{2} \hat{A} \right] \widehat{M} \,; \quad (k_{j0} = \sqrt{\boldsymbol{k}_j^2 + \lambda^2}), \tag{22}$$

with the natural convention that if $m = 0$, the product reduces to unity.

3. – The infra-red contribution from internal photons.

When no soft photons are emitted, *i.e.* when $m = 0$ in (22) we have simply the invariant amplitude M, that is

$$M = \exp[-\tfrac{1}{2}\hat{A}]\,\hat{M}\,. \tag{23}$$

We define

$$A = \frac{1}{2\pi i}\int \frac{\mathrm{d}^4k}{k^2+\lambda^2}\, s_\mu(k)s^\mu(-k)\,, \tag{24}$$

and

$$\bar{M} = \exp[\tfrac{1}{2}(A-\hat{A})]\,\hat{M}\,. \tag{25}$$

By definition $\hat{M}$ is non-infra-red. From (19) and (24) it follows that $A-\hat{A}$ is non-infra-red. Hence $\bar{M}$ is non-infra-red. From (23) and (25) we conclude that

$$M = \exp[-\tfrac{1}{2}A]\bar{M}\,. \tag{26}$$

Since M and A are Lorentz-invariant, so is $\bar{M}$. With (26) we have accomplished a Lorentz-invariant and cut-off independent separation of M into an infra-red part, $\exp[-\frac{1}{2}A]$, and a non-infra-red part $\bar{M}$. We shall call $\bar{M}$ the « *non-infra-red invariant amplitude* », and from now on consider (26) as the (exact) definition of $\bar{M}$.

If M and $\bar{M}$ are expressed by perturbation expansions in α,

$$M = \sum_{n=0}^{\infty} M^{(n)} \tag{27}$$

$$\bar{M} = \sum_{n=0}^{\infty} \bar{M}^{(n)} \tag{28}$$

then $\bar{M}^{(n)}$ can be obtained from $M^{(0)}$, $M^{(1)}$, ..., $M^{(n)}$ by

$$\bar{M}^{(n)} = \sum_{n'=0}^{n} \frac{1}{(n-n')!}(\tfrac{1}{2}A)^{n-n'}M^{(n')}\,. \tag{29}$$

This follows from (26). The terms $M^{(0)}$, $M^{(1)}$, ..., $M^{(n)}$ are to be calculated according to the usual recipe (*) (with the same photon mass, λ, as that occurring in A).

(*) See for instance ref. (6), Table 8-2.

4. – The total infra-red contribution.

By means of (25), the amplitude for photon emission given by (22) can be expressed in terms of the non-infra-red invariant amplitude $\bar{M}$, as follows

$$M(\boldsymbol{k}_1, e_1; \ldots; \boldsymbol{k}_m, e_m) = \prod_{j=1}^{m}\left(\frac{is(k_j)\cdot e_j}{\sqrt{2k_{j0}}}\right)\exp\left[-\tfrac{1}{2}A\right]\bar{M}; \qquad (k_{j0}=\sqrt{\boldsymbol{k}_j^2+\lambda^2}) \,. \tag{30}$$

Using the rule for summation over polarizations

$$\sum_{\text{pol}} e^{\mu} e^{\nu} = g^{\mu\nu} \tag{31}$$

we then obtain the following probability density

$$P(\boldsymbol{k}_1, \ldots, \boldsymbol{k}_m) = \sum_{\text{pol}} |\, M(\boldsymbol{k}_1, e_1; \ldots; \boldsymbol{k}_m, e_m)\,|^2 = \tag{32}$$

$$= \prod_{j=1}^{m}\left[\frac{1}{2k_{j0}}\, s^{\mu}(k_j) s^{*}_{\mu}(k_j)\right] \exp\left[-\operatorname{Re}\{A\}\right] |\,\bar{M}\,|^2 \,.$$

The restriction on the total energy of the emitted soft photons

$$\sum_{j=1}^{m} k_{j0} \leqslant \Delta E \tag{33}$$

is now introduced through the function

$$I(k_{10}, \ldots, k_{m0}) = \begin{cases} 1\,, \text{ for } \sum_{j=1}^{m} k_{j0} \leqslant \Delta E, \\ 0\,, \text{ for } \sum_{j=1}^{m} k_{j0} > \Delta E, \end{cases} \tag{34}$$

which will be used in the form

$$I(k_{10}, \ldots, k_{m0}) = \int_0^{\Delta E} \mathrm{d}x\, \delta\Big(\sum_{j=1}^{m} k_{j0} - x\Big) = \frac{1}{2\pi}\int_0^{\Delta E}\mathrm{d}x \int_{-\infty}^{\infty}\mathrm{d}y \exp\Big[i\Big(\sum_{j=1}^{m} k_{j0} - x\Big) y\Big]. \tag{35}$$

We are now prepared to write down an expression for the probability density (*), $P(\Delta E)$, for the process (1) with an energy loss due to soft photon

(*) Here and in the following we omit a factor $(2\pi)^{-4}\delta(P_f - P_i)$. See ref. (6) eq. (8-34).

emission not exceeding ΔE. The natural value for the limit between soft and hard photon energies ε (see eq. (6)) is then just $\varepsilon = \Delta E$.

Using (32) and (35) we get

$$(36)\qquad P(\Delta E) = \sum_{m=0}^{\infty} \frac{1}{m!} \int\limits_{\substack{|\boldsymbol{k}_j| \leq \Delta E \\ k_{j0} = \sqrt{\boldsymbol{k}_j^2 + \lambda^2}}} \mathrm{d}^3k_1 \ldots \mathrm{d}^3k_m \, I(k_{10}, \ldots, k_{m0}) P(\boldsymbol{k}_1, \ldots, \boldsymbol{k}_m) =$$

$$= \frac{1}{2\pi} \int_0^{\Delta E} \mathrm{d}x \int_{-\infty}^{\infty} \mathrm{d}y \exp[-ixy] \sum_{m=0}^{\infty} \frac{1}{m!} \left[\int\limits_{\substack{|\boldsymbol{k}| \leq \Delta E \\ k_0 = \sqrt{\boldsymbol{k}^2 + \lambda^2}}} \frac{\mathrm{d}^3k}{2k_0} s^{\mu}(k) s_{\mu}^*(k) \exp[ik_0 y] \right]^m \cdot$$

$$\cdot \exp[-\mathrm{Re}\{A\}] |\bar{M}|^2 = \frac{1}{2\pi} \int_0^{\Delta E} \mathrm{d}x \int_{-\infty}^{\infty} \mathrm{d}y \exp[-ixy] \cdot$$

$$\cdot \exp\left[\int\limits_{\substack{|\boldsymbol{k}| \leq \Delta E \\ k_0 = \sqrt{\boldsymbol{k}^2 + \lambda^2}}} \frac{\mathrm{d}^3k}{2k_0} s^{\mu}(k) s_{\mu}^*(k) \exp[ik_0 y] \right] \exp[-\mathrm{Re}\{A\}] |\bar{M}|^2 .$$

We can write $P(\Delta E)$ on the form

$$(37)\qquad P(\Delta E) = b \exp[\mathrm{G}(\Delta E)] |\bar{M}|^2$$

with

$$(38)\qquad b = \frac{1}{2\pi} \int_0^{\Delta E} \mathrm{d}x \int_{-\infty}^{\infty} \mathrm{d}y \exp[-ixy] \exp\left[\int\limits_{\substack{|\boldsymbol{k}| \leq \Delta E \\ k_0 = \sqrt{\boldsymbol{k}^2 + \lambda^2}}} \frac{\mathrm{d}^3k}{2k_0} s^{\mu}(k) s_{\mu}^*(k) (\exp[ik_0 y] - 1) \right],$$

$$(39)\qquad G(\Delta E) = -\mathrm{Re}\{A\} + \int\limits_{\substack{|\boldsymbol{k}| \leq \Delta E \\ k_0 = \sqrt{\boldsymbol{k}^2 + \lambda^2}}} \frac{\mathrm{d}^3k}{2k_0} s^{\mu}(k) s_{\mu}^*(k) .$$

The functions b and $G(\Delta E)$ are to be transformed into more useful forms. Introducing into (38) and (39) the definitions of A and $s^{\mu}(k)$, eq. (24) and (18), we get (*)

$$(40)\qquad b = \frac{1}{2\pi} \int_0^{\Delta E} \mathrm{d}x \int_{-\infty}^{\infty} \mathrm{d}y \exp[-ixy] \exp\left[C \int_0^{\Delta E} \frac{\mathrm{d}k}{k} (\exp[iky] - 1) \right],$$

(*) Because of the factor $(\exp[ik_0 y] - 1)$ in the k-integral of (38) b is not infra-red divergent so we can at once put $\lambda = 0$ in the expression for b.

with

$$C=\frac{\alpha}{\pi}\sum_{i,j=1}^{r}Q_iQ_j(-p_i\cdot p_j)\frac{1}{4\pi}\int_{l_\nu=|\boldsymbol{l}|=1}\frac{\mathrm{d}\Omega_l}{(l\cdot\varepsilon_ip_i)(-l\cdot\varepsilon_jp_j)}\,, \tag{41}$$

and

$$G(\Delta E)=\frac{\alpha}{\pi}\sum_{i,j=1}^{r}Q_iQ_j(-p_i\cdot p_j)\,\mathrm{Re}\left\{\frac{1}{4\pi}\int_{\substack{|\boldsymbol{k}|\leq\Delta E\\ k_0=\sqrt{\boldsymbol{k}^2+\lambda^2}}}\frac{\mathrm{d}^3k}{k_0(k\cdot\varepsilon_ip_i)(-k\cdot\varepsilon_jp_j)}-\right. \tag{42}$$

$$\left.-\frac{1}{i\pi^2}\int\frac{\mathrm{d}^4k}{(k^2+\lambda^2)(k^2+2k\cdot\varepsilon_ip_i)(k^2-2k\cdot\varepsilon_jp_j)}\right\}.$$

By a change of the names of the integration variables ($x\to x\Delta E$, $y\to y/\Delta E$, $k\to k\Delta E$), (40) transforms into

$$b=\frac{1}{2\pi}\int_0^1\mathrm{d}x\int_{-\infty}^{\infty}\mathrm{d}y\,\exp\left[-ixy\right]\exp\left[C\int_0^1\frac{\mathrm{d}k}{k}\left(\exp\left[iky\right]-1\right)\right], \tag{43}$$

which shows that b is independent of ΔE. To simplify (43) we start with the integral occurring in the exponential (*)

$$\int_0^1\frac{\mathrm{d}k}{k}\left(\exp\left[iky\right]-1\right)= \tag{44}$$

$$=\int_0^{1/y}\frac{\mathrm{d}k}{k}\left(\exp\left[iky\right]-1\right)+\int_{1/y}^{\infty}\frac{\mathrm{d}k}{k}\exp\left[iky\right]-\int_{1/y}^{1}\frac{\mathrm{d}k}{k}-\int_1^{\infty}\frac{\mathrm{d}k}{k}\exp\left[iky\right]=$$

$$=\int_0^1\frac{\mathrm{d}k}{k}\left(\exp\left[ik\right]-1\right)+\int_1^{\infty}\frac{\mathrm{d}k}{k}\exp\left[ik\right]-\ln y-\int_1^{\infty}\frac{\mathrm{d}k}{k}\exp\left[iky\right]=$$

$$=\int_0^1\frac{\mathrm{d}k}{k}\left(\cos k-1\right)+\int_1^{\infty}\frac{\mathrm{d}k}{k}\cos k+i\int_0^{\infty}\frac{\mathrm{d}k}{k}\sin k-\ln y-\int_1^{\infty}\frac{\mathrm{d}k}{k}\exp\left[iky\right]=$$

$$=-\gamma+\tfrac{1}{2}\pi i-\ln y-\int_1^{\infty}\frac{\mathrm{d}k}{k}\exp\left[iky\right]. \qquad (\gamma=\text{Euler's constant}).$$

(*) We have adopted the method of ref. [4] for the calculation of b. Originally this method is due to E. L. Lomon and A. Shaw.

From this we get the y-integral of (43)

$$(45)\qquad \exp\left[-C(\gamma-\tfrac{1}{2}\pi i)\right]\int_{-\infty}^{\infty}\frac{\mathrm{d}y}{y^{c}}\exp\left[-ixy\right]\exp\left[-C\int_{1}^{\infty}\frac{\mathrm{d}k}{k}\exp\left[iky\right]\right]=$$

$$=\exp\left[-C(\gamma-\tfrac{1}{2}\pi i)\right]\int_{-\infty}^{\infty}\frac{\mathrm{d}y}{y^{c}}\exp\left[-ixy\right]+$$

$$+\exp\left[-C(\gamma-\tfrac{1}{2}\pi i)\right]\int_{-\infty}^{\infty}\frac{\mathrm{d}y}{y^{c}}\exp\left[-ixy\right]\left\{\exp\left[-C\int_{1}^{\infty}\frac{\mathrm{d}k}{k}\exp\left[iky\right]\right]-1\right\}.$$

The integrand in the last term of (45) is analytic for $\mathrm{Im}\,\{y\}>0$. When $x\leqslant 1$ its norm decreases sufficiently rapidly for $\mathrm{Im}\,\{y\}>0$, $|y|\to\infty$ that the contour can be closed by a semicircle in the upper half-plane. Thus the last term of (45) vanishes and b reduces to

$$(46)\qquad b=\frac{1}{2\pi}\exp\left[-C(\gamma-\tfrac{1}{2}\pi i)\right]\int_{0}^{1}\mathrm{d}x\int_{-\infty}^{\infty}\frac{\mathrm{d}y}{y^{c}}\exp\left[-ixy\right]=$$

$$=\frac{1}{2\pi i}\exp\left[-C(\gamma-\pi i)\right]\int_{0}^{1}\mathrm{d}x\,x^{c-1}\int_{-i\infty}^{i\infty}\frac{\mathrm{d}y}{y^{c}}\exp\left[-y\right]=$$

$$=\frac{\exp\left[-C\gamma\right]}{C}\,\frac{\exp\left[C\pi i\right]}{2\pi i}\int_{-i\infty}^{i\infty}\frac{\mathrm{d}y}{y^{c}}\exp\left[-y\right].$$

By cutting the y-plane along the positive real axis, and using formulae for the Γ-function, we can solve the integral in the last member of (46) and obtain

$$(47)\qquad b=\frac{\exp\left[-C\gamma\right]}{C}\cdot\frac{\exp\left[C\pi i\right]}{2\pi i}\int_{0}^{\infty}\frac{\mathrm{d}y}{y^{c}}\exp\left[-y\right](1-\exp\left[-2C\pi i\right])=$$

$$=\frac{\exp\left[-C\gamma\right]}{C}\cdot\frac{\sin\left(C\pi\right)}{\pi}\,\Gamma(1-C)=\frac{\exp\left[-C\gamma\right]}{C}\cdot\frac{1}{\Gamma(C)}=\frac{\exp\left[-\gamma C\right]}{\Gamma(1+C)}.$$

This is our final expression for b (*).

We now turn to C and $G(\Delta E)$. By the use of Feynman's method of inte-

(*) A series expansion in C of $b=\exp\left[-\gamma C\right]/\Gamma(1+C)$ starts with $b=1-(\pi^2/12)C^2+\ldots$.

gration, expressed by the formula

$$\frac{1}{ab} = \int_0^1 \frac{\mathrm{d}x}{[ax + b(1-x)]^2}, \tag{48}$$

with the prescription that an eventual singularity is avoided by a detour into the complex x-plane, (41) and (42) are transformed into

$$C = \frac{\alpha}{\pi} \sum_{i,j=1}^{r} Q_i Q_j (-p_i \cdot p_j) \int_0^1 \mathrm{d}x\, f(\varepsilon_i p_i x - \varepsilon_j p_j (1-x)), \tag{49}$$

$$f(p) = \frac{1}{4\pi} \int_{l_0 = |\boldsymbol{l}| = 1} \frac{\mathrm{d}\Omega_l}{(l \cdot p)^2}, \tag{50}$$

and

$$G(\Delta E) = \frac{\alpha}{\pi} \sum_{i,j=1}^{r} Q_i Q_j (-p_i \cdot p_j) \operatorname{Re} \left\{ \int_0^1 \mathrm{d}x\, g(\varepsilon_i p_i x - \varepsilon_j p_j (1-x); \Delta E) \right\}, \tag{51}$$

$$g(p; \Delta E) = \frac{1}{4\pi} \int_{\substack{|\boldsymbol{k}| \le \Delta E \\ k_0 = \sqrt{\boldsymbol{k}^2 + \lambda^2}}} \frac{\mathrm{d}^3 k}{k_0 (k \cdot p)^2} - \frac{1}{i\pi^2} \int \frac{\mathrm{d}^4 k}{(k^2 + \lambda^2)(k^2 + 2k \cdot p)^2}. \tag{52}$$

From (50) we get simply

$$f(p) = \frac{1}{2} \int_{-1}^{1} \frac{\mathrm{d}z}{(|\boldsymbol{p}|z - p_0)^2} = \frac{1}{-p^2}. \tag{53}$$

Inserting (53) into (49) and performing the x-integration we obtain the final expression for C

$$\left| \begin{array}{l} C = \dfrac{\alpha}{\pi} \left[-\sum_{i=1}^{r} Q_i^2 - \sum_{1 \le i < j \le r} \dfrac{\varepsilon_i Q_i \varepsilon_j Q_j}{C_{ij}} \ln \left(\dfrac{1 + C_{ij}}{1 - C_{ij}} \right) \right], \\ C_{ij} = \left[1 - \dfrac{p_i^2 p_j^2}{(p_i \cdot p_j)^2} \right]^{\frac{1}{2}}. \end{array} \right. \tag{54}$$

Clearly, C is Lorentz-invariant.

The evaluation of the integrals in (52) is not very complicated and yields

$$\frac{1}{i\pi^2} \int \frac{\mathrm{d}^4 k}{(k^2 + \lambda^2)(k^2 + 2k \cdot p)^2} = \frac{1}{-2p^2} \ln \left(\frac{-p^2}{\lambda^2} \right), \tag{55}$$

$$(56)\qquad \frac{1}{4\pi}\int\limits_{\substack{|\boldsymbol{k}|\leq\Delta E\\ k_0=\sqrt{\boldsymbol{k}^2+\lambda^2}}} \frac{\mathrm{d}^3k}{k_0(k\cdot p)^2} = \frac{1}{-2p^2}\ln\left(\frac{-p^2}{\lambda^2}\right)+\frac{1}{-p^2}\ln\left(\frac{\Delta E}{E}\right)+$$
$$+\frac{1}{-p^2}\left[\frac{1}{2}\ln\left(\frac{4E^2}{-p^2}\right)-\int\limits_0^1 \mathrm{d}y\,\frac{p_0^2}{p_0^2-\boldsymbol{p}^2y^2}\right].$$

Here the total energy $E=P_{i0}=P_{f0}$ has been introduced. Clearly the λ-dependence of (52) vanishes and we get

$$(57)\qquad g(p;\Delta E)=\frac{1}{-p^2}\ln\left(\frac{\Delta E}{E}\right)+\frac{1}{-p^2}\left[\frac{1}{2}\ln\left(\frac{4E^2}{-p^2}\right)-\int\limits_0^1 \mathrm{d}y\,\frac{p_0^2}{p_0^2-\boldsymbol{p}^2y^2}\right].$$

Insertion of (57) into (51) and use of (49) and (53) then yield

$$(58)\qquad G(\Delta E)=C\ln\left(\frac{\Delta E}{E}\right)+B,$$

where

$$(59)\qquad \begin{cases} B=\dfrac{\alpha}{\pi}\left\{\sum\limits_{i=1}^{r}Q_i^2\left[1+\dfrac{p_i^2}{E^2}\,h\left(\dfrac{p_i}{E}\right)\right]-\right.\\ \qquad\qquad -2\sum\limits_{1\leq i<j\leq r}Q_iQ_j\,\dfrac{p_i\cdot p_j}{E^2}\,\mathrm{Re}\left\{\int\limits_0^1\mathrm{d}x\,h\left(\dfrac{\varepsilon_ip_ix-\varepsilon_jp_j(1-x)}{E}\right)\right\}\Bigg\}, \\ h(p)=\dfrac{1}{p^2}\left[\dfrac{1}{2}\ln\left(\dfrac{-p^2}{4}\right)+\int\limits_0^1\mathrm{d}y\,\dfrac{p_0^2}{p_0^2-\boldsymbol{p}^2y^2}\right]. \end{cases}$$

From (37), (47) and (58) we now collect the following result which contains no divergences

$$(60)\qquad P(\Delta E)=\left(\frac{\Delta E}{E}\right)^C e^B\,\frac{\exp\left[-\gamma C\right]}{\Gamma(1+C)}\,|\bar{M}|^2,$$

where C is given, by (54) B by (59) and $\bar{M}$ by (26), (24) and (18). In perturbation theory $\bar{M}$ is given by (29).

The whole ΔE-dependence in (60) is contained in the first factor and B is a quantity that depends on the components of the momenta $p_1,\ldots,p_r$ in the Lorentz-frame L. The quantity C depends also on these momenta but in an invariant manner. Finally, the non-infra-red invariant amplitude $\bar{M}$ contains all non-infra-red interactions between the r particles.

5. – High energy processes.

Through the preceding sections the mechanism of collective soft photon effects was treated in a simple but general way. Two results were obtained, (i) the invariant factorization of the infra-red part of the invariant amplitude M, achieved in Section **3**, and (ii) the closed expression (60) for $P(\Delta E)$ which is correct when the energy resolution is restricted by (3). The result (ii) is, however, only of academic interest so far, because the restriction (3) can be satisfied only in experiments performed at very low energies, and we know beforehand that radiative corrections are unimportant at low energies.

In this Section we shall try to extend the discussion to high energy processes. Then we abandon restriction (3).

Take L to be the c.m.-system and assume an isotropic energy resolution, wich satisfies

$$\Delta E \ll \mathrm{p}_{i0}, \text{ for each } i \text{ such that } Q_i \neq 0 . \tag{61}$$

This restriction allows us to neglect the « recoil » terms as we did above in (13*b*, *f*), because those terms are small of the order $\Delta E/p_{i0}$. But we can no longer neglect those diagrams for photon emission that do not give rise to infra-red divergences. In Sections **2** and **4** these diagrams could be neglected because they gave contributions that were linear in soft photon momenta and thus bounded by quantities of magnitude $\simeq \Delta E/m$ (*), which were negligibly small because of (3). In high energy processes, however, it usually happens that a ΔE satisfying (61) still is considerably larger than m.

We can generalize (36) so as to include also emission of soft photons through diagrams not giving rise to infra-red divergences. Let the index n refer to the number of emitted photons of this kind and m, as before, to the number of emitted photons giving infra-red divergences. We do not put $\varepsilon = \Delta E$ here but keep $\varepsilon \ll m$. Then the generalization of (36) is

$$P(\Delta E) = \frac{1}{2\pi}\int_0^{\Delta E} \mathrm{d}x \int_{-\infty}^{\infty} \mathrm{d}y \, \exp\left[-ixy\right] \sum_{m=0}^{\infty} \frac{1}{m!} \left[\int\limits_{\substack{|\boldsymbol{k}|\leq\varepsilon \\ k_0=\sqrt{\boldsymbol{k}^2+\lambda^2}}} \frac{\mathrm{d}^3k}{2k_0} \, s^{\mu}(k) s^{*}_{\mu}(k) \exp\left[ik_0 y\right] \right]^m \cdot \tag{62}$$

$$\cdot \exp\left[-\mathrm{Re}\,\{A\}\right] \sum_{n=0}^{\infty} \hat{P}_n(y),$$

(*) *Note added in proof*: There are some indications that these contributions are of the order $\Delta E/P_{i0}$. If that is true and if the contributions from pair emission also are of the order $\Delta E/P_{i0}$ then (60) holds also for high energy processes as long as (61) is fulfilled.

with

$$\hat{P}_n(y) = \int\!\!\cdots\!\!\int_{\varepsilon \le k_{j0} = |\boldsymbol{k}|_j \le \Delta E} \mathrm{d}^3k_1 \ldots \mathrm{d}^3k_n \exp\left[iy \sum_{j=1}^{n} k_{j0}\right] \hat{R}(\boldsymbol{k}_1, \ldots, \boldsymbol{k}_n) , \tag{63}$$

$$\hat{R}(\boldsymbol{k}_1, \ldots, \boldsymbol{k}_n) = \sum_{\substack{\text{diagrams} \\ i_1, i_2}} \bar{M}_{i_1}(\boldsymbol{k}_1, \ldots, \boldsymbol{k}_n) \bar{M}^*_{i_2}(\boldsymbol{k}_1, \ldots, \boldsymbol{k}_n) , \tag{64}$$

where $\bar{M}_i(\boldsymbol{k}_1, \ldots, \boldsymbol{k}_n)$ is the term in the non-infra-red amplitude (for emission of n photons with momenta $\boldsymbol{k}_1, \ldots, \boldsymbol{k}_n$ along the process (1)) that corresponds to the i-th diagram. In (63) a summation over all polarizations is understood.

Now if a collection of terms $\bar{M}_{i_1} \bar{M}^*_{i_2}$ in the sum (64) can be written in the form (apart from numerical factors)

$$N(\boldsymbol{k}_1, \ldots, \boldsymbol{k}_{n'}) \bar{M}_{i'_1}(\boldsymbol{k}_{n'+1}, \ldots, \boldsymbol{k}_n) \bar{M}^*_{i'_2}(\boldsymbol{k}_{n'+1}, \ldots, \boldsymbol{k}_n) , \tag{65}$$

with

$$N(\boldsymbol{k}_1, \ldots, \boldsymbol{k}_{n'}) = \prod_{j=1}^{n'} \frac{s^\mu(k_j) s^*_\mu(k_j)}{2k_{j0}} , \tag{66}$$

then the contribution from the factor $N(\boldsymbol{k}_1, \ldots, \boldsymbol{k}_{n'})$ can be removed to the soft photon ($|\boldsymbol{k}| \le \varepsilon$) integral in (62). If this is done for each term $\bar{M}_{i_1} \bar{M}^*_{i_2}$ in (64) and for each $\hat{P}_n(y)$, then (62), (63) and (64) transform into

$$P(\Delta E) = \frac{1}{2\pi} \int_0^{\Delta E} \mathrm{d}x \int_{-\infty}^{\infty} \mathrm{d}y \exp[-ixy] \sum_{m=0}^{\infty} \frac{1}{m!} \left[\int_{\substack{|\boldsymbol{k}| \le \Delta E \\ k_0 = \sqrt{\boldsymbol{k}^2 + \lambda^2}}} \frac{\mathrm{d}^3k}{2k_0} s^\mu(k) s^*_\mu(k) \exp[ixk_0 y] \right]^m \cdot \exp[-\mathrm{Re}\{A\}] \sum_{n=0}^{\infty} P_n(y) , \tag{67}$$

with

$$P_n(y) = \int\!\!\cdots\!\!\int_{k_{j0} = |\boldsymbol{k}_j| \le \Delta E} \mathrm{d}^3k_1 \ldots \mathrm{d}^3k_n \exp\left[iy \sum_{j=1}^{n} k_{j0}\right] R(\boldsymbol{k}_1, \ldots, \boldsymbol{k}_n) , \tag{68}$$

$$R(\boldsymbol{k}_1, \ldots, \boldsymbol{k}_n) = \sum'_{\substack{\text{diagrams} \\ i_1, i_2}} \bar{M}_{i_1}(\boldsymbol{k}_1, \ldots, \boldsymbol{k}_n) \bar{M}^*_{i_2}(\boldsymbol{k}_1, \ldots, \boldsymbol{k}_n) . \tag{69}$$

In (69) « $\sum'$ » means that the summation goes only over such pairs of diagrams that do not give contributions containing factors of the type (66) with logarithmic singularities at $k_{j0} = |\boldsymbol{k}_j| = 0$. Summation over m in (67) leads to an exponential. Using the definitions (39) and (41) and the result (58) we can

rewrite (67) as

$$(70)\quad P(\Delta E) = \left(\frac{\Delta E}{E}\right)^{C} e^{B} \frac{1}{2\pi} \sum_{n=0}^{\infty} \int\!\!\dots\!\!\int_{k_{j0}=|\boldsymbol{k}_j|\leq \Delta E} \mathrm{d}^3 k_1 \dots d^3 k_n \int_{-\sum_{j=1}^{n} k_{j0}}^{\Delta E - \sum_{j=1}^{n} k_{j0}} \mathrm{d}x \int_{-\infty}^{\infty} \mathrm{d}y \exp\left[-ixy\right] \cdot$$

$$\cdot \exp\left[C \int_0^{\Delta E} \frac{\mathrm{d}k}{k} \left(\exp\left[iky\right] - 1\right)\right] R(\boldsymbol{k}_1, \dots, \boldsymbol{k}_n) .$$

After a calculation similar to that for b in Section **4**, one is led to the following result for the transition probability density

$$(71)\qquad P(\Delta E) = e^{B} \frac{\exp\left[-\gamma C\right]}{\Gamma(1+C)} \int_0^{\Delta E} \mathrm{d}x \left(\frac{x}{E}\right)^{C} \sum_{n=0}^{\infty} \int\!\!\dots\!\!\int_{k_{j0}=|\boldsymbol{k}_j|\leq \Delta E} \mathrm{d}^3 k_1 \dots \mathrm{d}^3 k_n \cdot$$

$$\cdot R(\boldsymbol{k}_1, \dots, \boldsymbol{k}_n) \delta\left(\Delta E - x - \sum_{j=1}^{n} k_{j0}\right) .$$

Actually if one compares the formulae (60) and (71) one sees that the latter is a natural generalization of the former to the case when part of the energy loss goes through « non-infra-red photons ».

Emission of electron pairs, which may occur if $\Delta E > 2m$ can easily be included in (71) simply by defining $R(\boldsymbol{k}_1, \dots, \boldsymbol{k}_n)$ (eq. (69)) to include also pair emission.

The quantities B and C occurring in (60) and (71) are expressed in terms of the external momenta by (59) and (54) respectively. In electron scattering processes at high energies and high momentum transfers B and C will both be of the order of magnitude

$$(72)\qquad \frac{2\alpha}{\pi} \ln\left(\frac{q^2}{m^2}\right); \qquad \left(q^2 = \mathrm{Max}\left[(p_i - p_j)^2\right]\right) .$$

So if (60) or (71) is expressed as a perturbation series in α, the effective expansion parameter as far as the soft photon factors are concerned is at most

$$(73)\qquad \frac{2\alpha}{\pi} \ln\left(\frac{q^2}{m^2}\right) \mathrm{Max}\left[1, \ln\left(\frac{E}{\Delta E}\right)\right] .$$

In realistic experiments, though (61) holds with reasonable accuracy one has a $\ln(E/\Delta E)$ which is only of the order of a few units. Thus the effective

expansion parameter for the soft photon part is of the order of magnitude

$$\frac{2\alpha}{\pi}\ln\left(\frac{q^2}{m^2}\right). \tag{74}$$

The « structure » of the probability density (71) can be visualized in a very schematic way by the formula

$$P(\Delta E) = \int\ldots\int F \sum{}' \bar{M}\bar{M}^* . \tag{75}$$

Here F is the soft photon part. It can be expanded in powers of the effective parameter (74). The $\bar{M}$'s are terms of non-infra-red invariant amplitudes, and $\sum'$ has the same meaning as in (69).

In actual high energy experiments one generally has — beside the isotropic energy loss ΔE — a certain amount of photons and pairs with an energy $> \Delta E$ emitted, mainly along the incoming and outgoing particle momenta. When this emission is taken into account the recoil effects can no longer be neglected. The integrals over the momenta of the emitted particles are limited by complicated surfaces. It would be meaningless to try to write down a formula like (71) for a general energy resolution. However the « structure » indicated by (75) (with the general effective expansion parameter (74) for F) is still obtained in the general case.

The invariance of $\bar{M}$ means that $\bar{M}$ depends on its momentum variables only through the scalar products that can be formed by them. That $\bar{M}$ is non-infra-red means that inside the integral over internal photon momenta k_1', k_2', ... there are enough k's in the numerator to make the integral convergent when any of the k's goes to zero with all its components.

In a later publication ([7]) it will be shown that if $\bar{M}$ is expressed in a perturbation series in α, its effective expansion parameter is at most

$$\frac{\alpha}{\pi}\ln^{\frac{4}{3}}\left(\frac{q^2}{m^2}\right) \tag{76}$$

Comparison between (76) and the effective expansion parameter for F, (74), then shows that *the effective expansion parameter for the transition probability density of an electromagnetic scattering process is at most* $\alpha/\pi \ln^{\frac{4}{3}}(q^2/m^2)$.

This result and its implications for the reliability of radiative correction calculations was stated in a note by PETERMAN and the author ([8]).

([7]) K. E. ERIKSON: *Nuovo Cimento*, **19**, 1044 (1961). *Note added in proof*: In this paper it is shown that in perturbation theory $P(\Delta E)$ is expanded in terms of the effective parameter $(\alpha/\pi)\ln(q^2/m^2)$.

([8]) K. E. ERIKSSON and A. PETERMAN: *Phys. Rev. Lett.*, **5**, 444 (1960).

One implication mentioned in ref. ([8]) was that at energies which are used in present experiments, calculations of first order radiative corrections to scattering cross-sections give a sufficient accuracy. To first order in α (71) and (60) are identical and we have

$$P(\Delta E) = |M^{(0)}|^2 \left[1 + C \ln\left(\frac{\Delta E}{E}\right) + B\right] + 2 \operatorname{Re}\{M^{(0)*} \overline{M}^{(1)}\}. \tag{77}$$

One must then add to (77) the probability density for emission of one photon with an energy $> \Delta E$.

* * *

I wish to thank Dr. A. PETERMAN for many discussions and for valuable comments on the manuscript.

RIASSUNTO (*)

Si mostra come la parte divergente infrarossa, dovuta a fotoni virtuali molli, di qualunque ampiezza di scattering può essere sviluppata in fattori in forma invariante secondo Lorentz. Si mostra inoltre che se la risoluzione dell'energia per un processo è trascurabile in confronto alla massa di riposo dell'elettrone, in tal caso tutto il contributo del fotone molle alla densità di probabilità della transizione può essere fattorizzato lasciando un resto invariante secondo Lorentz. La fattorizzazione viene estesa poi al caso più realistico in cui la risoluzione dell'energia è dello stesso ordine di grandezza della massa di riposo dell'elettrone, o maggiore. Infine si discute la grandezza delle correzioni radiative.

(*) *Traduzione a cura della Redazione.*

IL NUOVO CIMENTO Vol. XIX, N. 5 1° Marzo 1961

Radiative Corrections to Muon-Electron Scattering.

K. E. Eriksson
CERN - Geneva

(ricevuto il 2 Dicembre 1960)

Summary. — The differential cross-section for μ-e scattering is calculated to order e^6.

1. – Introduction.

Scattering of muons by electrons at high energies has been planned [1] as an experiment for testing the validity of quantum electrodynamics at small distances. In order to interpret the results obtained in such an experiment one must know, of course, to a good accuracy, what is really predicted by quantum electrodynamics. In a recent note it was pointed out by Peterman and the author [2] that for experiments performed or planned nowadays, it is quite sufficient to calculate first order radiative corrections to scattering cross sections.

The present paper reports on such a calculation on μ^- -e$^-$ scattering with an energy resolution which is assumed to be isotropic in the c.m. system and much smaller than the c.m. energies of the muon and the electron (*). From the result of this calculation we conclude that the formula derived by Schwinger for scattering of an electron by a potential [4] holds with a

(*) A similar calculation has recently been performed independently by Nikishov [3].

[1] W. K. H. Panofsky: S. C. Internal Report 59-5, (CERN, 1959); see also S. D. Drell: *Ann. Phys.*, **4**, 75 (1958)

[2] K. E. Eriksson and A. Peterman: *Phys. Rev. Lett.*, **5**, 444 (1960).

[3] A. I. Nikishov: *Žurn. Èksp. Teor. Fiz.*, **39**, 757 (1960) (In Russian).

[4] J. Schwinger: *Phys. Rev.*, **76**, 790 (1949).

good accuracy also for μ-e scattering at the energies one is planning with at present. Some numerical results for the radiative corrections at different energies and angles are given in a Table.

The inelastic process of soft photon emission that accompanies the basic process is here taken into account by the application of a general formula derived by the present author in another publication ([5]) (*).

The result obtained here is not yet complete enough to be directly compared to experiments. A certain amount of hard photon emission will be permitted by the experimental geometry and the cross section for that process must be calculated separately for every particular experimental design. Good examples of how this can be done are found in the work of TSAI ([7]) on electron-electron scattering.

In Section 2 the differential cross section is expressed in terms of the matrix elements corresponding to different diagrams. These matrix elements are calculated in Section 3. The final formulae are then collected in Section 4, where also the Table with numerical results is presented.

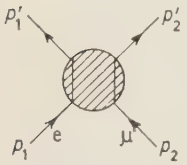

Fig. 1.

2. – The cross section.

The kinematics for elastic scattering of muons by electrons are given in the c.m. system by the following equations (see Fig. 1)

$$(1)\qquad \begin{cases} p_1 = (E_1,\, q,\, 0,\, 0)\,, \\ p_2 = (E_2,\, -q,\, 0,\, 0)\,, \end{cases} \qquad \begin{cases} p_1' = (E_1,\, q\cos\theta,\, q\sin\theta,\, 0)\,, \\ p_2' = (E_2,\, -q\cos\theta,\, -q\sin\theta,\, 0)\,, \end{cases}$$

$$(2)\qquad E_i^2 = m_i^2 + q^2, \qquad (i = 1,\, 2),$$

where we can choose $q > 0$. The following definitions will be useful:

$$(3)\qquad \begin{cases} W^2 = -(p_1 + p_2)^2 = (E_1 + E_2)^2, \\ p_3 = p_1' - p_1 = p_2 - p_2', \\ \Delta^2 = p_3^2 = 2q^2(1 - \cos\theta)\,, \end{cases}$$

(*) In the following this paper will be referred to as I. As in I we shall follow the conventions used in the text-book of J. M. JAUCH and F. ROHRLICH ([6]) as regards metric normalization factors, etc..

([5]) K. E. ERIKSSON: *Nuovo Cimento*, **19**, 1010 (1961).

([6]) J. M. JAUCH and F. ROHRLICH: *Theory of Photons and Electrons* (Cambridge, Mass., 1955).

([7]) Y. S. TSAI: *Nuovo Cimento*, **16**, 370 (1960); *Phys. Rev.*, **120**, 269 (1960).

$$\text{(4)} \qquad \begin{cases} t_i &= \dfrac{4m^2}{\Delta^2}\,, \\ T &= \tfrac{1}{4}(t_1 + t_2)\,, \end{cases}$$

$$\text{(5)} \qquad \Delta^2 u = -2p_1\cdot p_2\,.$$

Thus W is the total c.m. energy and Δ is the invariant momentum transfer. The definitions (3), (4) and (5) imply the relations

$$\text{(6)} \qquad \begin{cases} -2p_1\cdot p_3 = 2p_2\cdot p_3 = \Delta^2\,, \\ -2p_i\cdot p_i' = \Delta^2(1 + \tfrac{1}{2}t_i)\,, \\ 2p_1\cdot p_2' = \Delta^2(1-u). \end{cases}$$

If we include the emission of one soft photon with an energy not exceeding ΔE, where

$$\text{(7)} \qquad \Delta E \ll q\,,$$

then the transition probability density can be written

$$\text{(8)} \qquad (2\pi)^{-4}\delta(p_1' + p_2' - p_1 - p_2)\,\tfrac{1}{4}\sum_{\text{spins}} P(\Delta E)\,.$$

Here we have averaged over initial spins and summed over final spins. The differential cross section is given by the following equation

$$\text{(9)} \qquad \frac{\mathrm{d}\sigma}{\mathrm{d}\Omega} = (2\pi)^2\,\frac{E_1 E_2}{\sqrt{(p_1\cdot p_2)^2 - m_1^2 m_2^2}}\iint \mathrm{d}^3p_1'\,\mathrm{d}\,|\boldsymbol{p}_2'|\,|\boldsymbol{p}_2'|^2\,\delta(p_1' + p_2' - p_1 - p_2)\,\tfrac{1}{4}\sum_{\text{spins}} P(\Delta E),$$

which can be simplified to

$$\text{(10)} \qquad \frac{\mathrm{d}\sigma}{\mathrm{d}\Omega} = (2\pi)^2\,\frac{(E_1E_2)^2}{W^2}\,\tfrac{1}{4}\sum_{\text{spins}} P(\Delta E)\,.$$

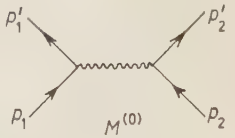

Fig. 2.

We now take from I (eq. (I.77)) the following formula for $P(\Delta E)$:

$$\text{(11)} \qquad P(\Delta E) = |M^{(0)}|^2\left[1 + C\ln\left(\frac{\Delta E}{E}\right) + B\right] + 2\,\mathrm{Re}\,\{M^{(0)*}\bar{M}^{(1)}\}\,.$$

Here $M^{(0)}$ is the lowest order (e^2) matrix element, corresponding to the diagram in Fig. 2; $\bar{M}^{(1)}$ is the non-infra-red part of the next order (e^4) matrix

element, $M^{(1)} = \sum_{i=1}^{6} M_i^{(1)}$, corresponding to the six diagrams in Fig. 3. The quantities C and B are connected with the emission of one soft photon (see

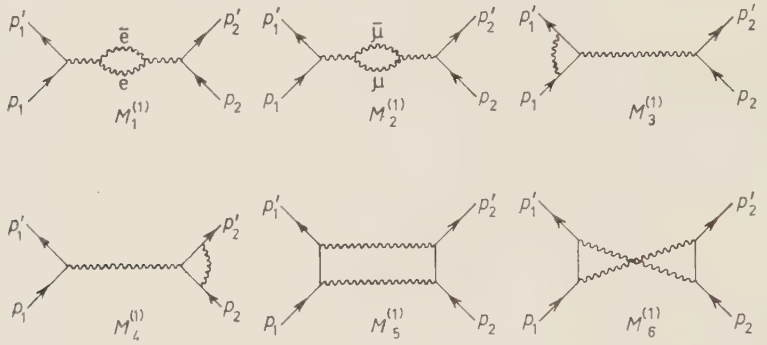

Fig. 3.

Fig. 4). They are given by formulae (I.54) and (I.59). According to (I.29) $\bar{M}^{(1)}$ can be expressed in terms of $M^{(0)}$ and $M^{(1)}$ by the relation

$$\bar{M}^{(1)} = M^{(1)} + \tfrac{1}{2} A M^{(0)} . \tag{12}$$

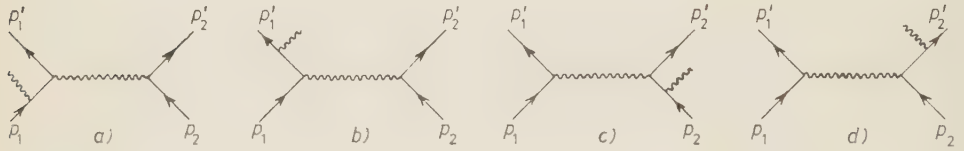

Fig. 4.

Here A contains the whole infra-red divergent contribution to $M^{(1)}$. From (I.24) and (I.18) we conclude that

$$A = -\frac{\alpha}{\pi} \cdot \frac{1}{i\pi^2} \int \frac{\mathrm{d}^4 l}{l^2 + \lambda^2} \left\{ \sum_{i=1}^{2} \left[\frac{2p_i^2}{(l^2 + 2l\cdot p_i)(l^2 - 2l\cdot p_i)} + \frac{2p_i \cdot p_i'}{(l^2 + 2l\cdot p_i)(l^2 + 2l\cdot p_i')} \right] - \right.$$
$$\left. - Q \left[\frac{4p_1 \cdot p_2}{(l^2 - 2l\cdot p_1)(l^2 + 2l\cdot p_2)} + \frac{4p_1 \cdot p_2'}{(l^2 + 2l\cdot p_1)(l^2 + 2l\cdot p_2')} \right] \right\}, \tag{13}$$

where λ is the fictitious photon mass and Q is the product of the two charges ($Q = +1$, if the muon and the electron have equal charges, and $Q = -1$ if they have different charges).

In the next section it will be shown that the terms of $M^{(1)}$ corresponding to the diagrams in Fig. 3 can be written in the form

$$
(14)\quad \begin{cases} M_1^{(1)} + M_2^{(1)} = -\dfrac{\alpha}{2\pi} l M^{(0)}, \\ M_3^{(1)} + M_4^{(1)} = -\dfrac{\alpha}{2\pi}\left\{-\dfrac{1}{i\pi^2}\displaystyle\int \frac{\mathrm{d}^4 l}{(l^2+\lambda^2)} \sum_{i=1}^{2}\left[\frac{2p_i^2}{(l^2+2l\cdot p_i)(l^2-2l\cdot p_i)} + \right.\right. \\ \qquad\qquad \left.\left. + \dfrac{2p_i\cdot p_i'}{(l^2+2l\cdot p_i)(l^2+2l\cdot p_i')}\right] + l'\right\} M^{(0)} + \bar{M}_3^{(1)} + \bar{M}_4^{(1)}, \\ M_5^{(1)} = \dfrac{\alpha}{2\pi} Q \dfrac{1}{i\pi^2}\displaystyle\int \frac{\mathrm{d}^4 l}{(l^2+\lambda^2)} \frac{4p_1\cdot p_2}{(l^2-2l\cdot p_1)(l^2+2l\cdot p_2)} \cdot M^{(0)} + \bar{M}_5^{(1)}, \\ M_6^{(1)} = \dfrac{\alpha}{2\pi} Q \dfrac{1}{i\pi^2}\displaystyle\int \frac{\mathrm{d}^4 l}{(l^2+\lambda^2)} \frac{4p_1\cdot p_2'}{(l^2-2l\cdot p_1)(l^2+2l\cdot p_2')} \cdot M^{(0)} + \bar{M}_6^{(1)}. \end{cases}
$$

If we use now eq. (10) to (14), the infra-red divergences cancel, and we get the following expression for the cross section

$$
(15)\quad \frac{\mathrm{d}\sigma}{\mathrm{d}\Omega} = \left(\frac{\mathrm{d}\sigma}{\mathrm{d}\Omega}\right)^{(0)}\left[1 + C\ln\left(\frac{\Delta E}{E}\right) + B - \frac{\alpha}{\pi}(l+l')\right] - \frac{\alpha^3}{\pi}\frac{1}{W^2}(R_3+R_4+R_5+R_6),
$$

where $(\mathrm{d}\sigma/\mathrm{d}\Omega)^{(0)}$ is the lowest order cross section,

$$
(16)\quad \left(\frac{\mathrm{d}\sigma}{\mathrm{d}\Omega}\right)^{(0)} = (2\pi)^2 \frac{(E_1E_2)^2}{W^2}\cdot\tfrac{1}{4}\sum_{\text{spins}} |M^{(0)}|^2,
$$

and R_j is defined by

$$
(17)\quad -\frac{\alpha^3}{\pi}\frac{R_j}{W^2} = (2\pi)^2\frac{(E_1E_2)^2}{W^2}\cdot\tfrac{1}{4}\sum_{\text{spins}} 2\,\mathrm{Re}\,\{M^{(0)*}\bar{M}_j^{(1)}\} \qquad (j=3,4,5,6).
$$

3. – Calculations of the contributions from the diagrams $M^{(0)}, \ldots, M_6^{(1)}$.

3·1. *The lowest order diagram* $M^{(0)}$. – Following the usual techniques for evaluation of diagrams, we obtain the contribution from the lowest order diagram (Fig. 2)

$$
(18)\quad \tfrac{1}{4}\sum_{\text{spins}} |M^{(0)}|^2 = \frac{\alpha^2}{(2\pi)^2}\cdot\frac{1}{(E_1E_2)^2}\cdot\frac{1}{\Delta^4} F_{1\mu\nu}F_2^{\mu\nu},
$$

with

$$
(19)\quad F_{i\mu\nu} = m_i^2 \sum_{\text{spins}} (\bar{u}_i(p_i')\gamma_\mu u_i(p_i))^* (\bar{u}_i(p_i')\gamma_\nu u_i(p_i)) .
$$

A simple trace calculation gives

$$F_{i\mu\nu} = p'_{i\mu} p_{i\nu} + p'_{i\nu} p_{i\mu} + \tfrac{1}{2} \Delta^2 g_{\mu\nu} \,. \tag{20}$$

Inserting this into (18) and using the definitions (4) and (5) we get

$$\tfrac{1}{4} \sum_{\text{spins}} |M^{(0)}|^2 = \frac{\alpha^2}{(2\pi)^2} \frac{1}{(E_1 E_2)^2} (u^2 - u - T + \tfrac{1}{2}) \,. \tag{21}$$

Thus, the lowest order cross section given by eq. (16) becomes

$$\left(\frac{\mathrm{d}\sigma}{\mathrm{d}\Omega}\right)^{(0)} = \frac{\alpha^2}{W^2} (u^2 - u - T + \tfrac{1}{2}) \,. \tag{22}$$

3·2. *The vacuum polarization diagrams, $M_1^{(1)}$ and $M_2^{(1)}$.* – From ref. (6) eq. (9.66) and (9.71) it is immediately seen that the contribution from the diagrams $M_1^{(1)}$ and $M_2^{(1)}$ in Fig. 3 is of the form indicated in (14) and that

$$l = \frac{2}{3} \sum_{i=1}^{2} \left(\frac{5}{3} - t_i - (1 - \tfrac{1}{2} t_i) \sqrt{1 + t_i} \, \ln \frac{\sqrt{1 + t_i} + 1}{\sqrt{1 + t_i} - 1} \right) . \tag{23}$$

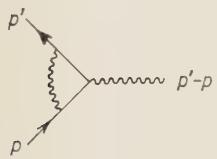

Fig. 5.

3·3. *The vertex diagrams, $M_3^{(1)}$ and $M_4^{(1)}$.* – We start with a general vertex diagram of order e^3 with free external fermion lines (Fig. 5). The renormalized vertex function $\Lambda_{f\mu}(p', p)$ is given by

$$\begin{cases} \Lambda_{f\mu}(p', p) = \Lambda_\mu(p', p) - \Lambda_\mu(p, p) \,, \\ \Lambda_\mu(p', p) = -\dfrac{\alpha}{2\pi} \cdot \dfrac{1}{i\pi^2} \displaystyle\int \frac{\mathrm{d}^4 l}{(l^2 + \lambda^2)} \frac{N_\mu(p', p)}{(l^2 - 2l \cdot p')(l^2 - 2l \cdot p)} \,, \end{cases} \tag{24}$$

where (with the notation $k = k_\mu \gamma^\mu$)

$$N_\mu = \tfrac{1}{2} \gamma_\nu (ip' - il - m) \gamma_\mu (ip - il - m) \gamma^\nu = \tag{25}$$

$$= -2p' \cdot p \gamma_\mu + l^\nu (\gamma_\mu \gamma_\nu p' + p \gamma_\nu \gamma_\mu) - l^\nu l^\varrho (\tfrac{1}{2} g_{\nu\varrho} \gamma_\mu - 2 g_{\mu\nu} \gamma_\varrho) - \tfrac{1}{2} l^2 \gamma_\mu \,.$$

Separating out the infra-red divergent terms we get

$$\Lambda_{f\mu}(p', p) = \frac{\alpha}{2\pi} \cdot \frac{1}{i\pi^2} \int \frac{\mathrm{d}^4 l}{(l^2 + \lambda^2)} \left(\frac{2p^2}{(l^2 + 2l \cdot p)(l^2 - 2l \cdot p)} + \right. \tag{26}$$

$$\left. + \frac{2p \cdot p'}{(l^2 + 2l \cdot p)(l^2 + 2l \cdot p')} \right) \gamma_\mu + \bar{\Lambda}_{f\mu}(p', p) \,,$$

where $\bar{\Lambda}_{f\mu}(p', p)$ is the non-infra-red part of the vertex function.

$$(27)\quad \bar{\Lambda}_{f\mu}(p', p) = -\frac{\alpha}{2\pi}\frac{1}{i\pi^2}\int d^4l \left\{\frac{l^\nu(\gamma_\mu\gamma_\nu p' + p\gamma_\nu\gamma_\mu) - l^\nu l^\varrho(\frac{1}{2}g_{\nu\varrho}\gamma_\mu - 2g_{\mu\nu}\gamma_\varrho)}{l^2(l^2 - 2l\cdot p)(l^2 - 2l\cdot p')} - \right.$$
$$- \frac{2i\,ml_\mu - l^\nu l^\varrho(\frac{1}{2}g_{\nu\varrho}\gamma_\mu - 2g_{\mu\nu}\gamma_\varrho)}{l^2(l^2 - 2l\cdot p)^2} - \gamma_\mu\left(\frac{l\cdot(p' - p)}{(l^2 - 2l\cdot p)^2(l^2 - 2l\cdot p')} - \right.$$
$$\left.\left. - \frac{4p^2}{(l^2 - 2l\cdot p)^2(l^2 + 2l\cdot p)}\right)\right\}.$$

It can be evaluated with Feynman's integral techniques (*) and the result is

$$(28)\quad \bar{\Lambda}_{f\mu}(p', p) = -\frac{\alpha}{2\pi}\left|\gamma_\mu\left(4 - \frac{3}{2}\sqrt{1+t}\ln\frac{\sqrt{1+t}+1}{\sqrt{1+t}-1}\right) - \right.$$
$$\left. - \frac{im(p'_\mu + p_\mu)}{(p' - p)^2}\frac{1}{\sqrt{1+t}}\ln\frac{\sqrt{1+t}+1}{\sqrt{1+t}-1}\right|. \qquad t = \frac{4m^2}{(p' - p)^2}.$$

From (26) and (28) it follows that $M_3^{(1)} + M_4^{(1)}$ (Fig. 3) is of the form indicated in (14) and that

$$(29)\quad l' = \sum_{i=1}^{2}\left(4 - \frac{3}{2}\sqrt{1+t_i}\ln\frac{\sqrt{1+t_i}+1}{\sqrt{1+t_i}-1}\right).$$

For the magnetic contribution $R_3 + R_4$, defined by (17), we get

$$(30)\quad R_3 + R_4 = \frac{2m_1^2 m_2^2}{\Delta^6}\,\mathrm{Re}\,\{F_{1\mu}F_2{}^\mu\}\sum_{i=1}^{2}\frac{1}{\sqrt{1+t_i}}\ln\frac{\sqrt{1+t_i}+1}{\sqrt{1+t_i}-1},$$

with

$$(31)\quad F_{i\mu} = m_i\sum_{\text{spins}}\bar{u}_i(p'_i)\gamma_\mu u_i(p_i)(\bar{u}_i(p'_i)u_i(p_i))^*.$$

A simple calculation gives

$$(32)\quad F_{i\mu} = -i(p_{i\mu} + p'_{i\mu})$$

which inserted into (30) yields

$$(33)\quad R_3 + R_4 = \frac{1}{8}t_1t_2(2u - 1)\sum_{i=1}^{2}\frac{1}{\sqrt{1+t_i}}\ln\frac{\sqrt{1+t_i}+1}{\sqrt{1+t_i}-1}.$$

(*) See ref. (6) Sect. A 5-1.

3·4. *The two photon exchange diagrams, $M_5^{(1)}$ and $M_6^{(1)}$.* – The contributions from the diagrams $M_5^{(1)}$ and $M_6^{(1)}$ in Fig. 3 can be expressed in terms of each other by changing particle 2 into its antiparticle and reversing the signs of its momenta (q_2 is the charge)

$$\text{(34)} \qquad \begin{cases} (2) \to (\bar{2}) , \\ q_2 \to -q_2 , \end{cases} \qquad \begin{cases} p_2 \to -p_2 , \\ p_2' \to -p_2' . \end{cases}$$

The cross section terms are invariant under the transformation (34). This fact is used in Fig. 6 to show that

$$\text{(35)} \qquad \mathrm{Re}\,\{M^{(0)*} M_6^{(1)}\} = -\,\mathrm{Re}\,\{M^{(0)*} M_5^{(1)}\}_{(p_2 \leftrightarrow -p_2')} .$$

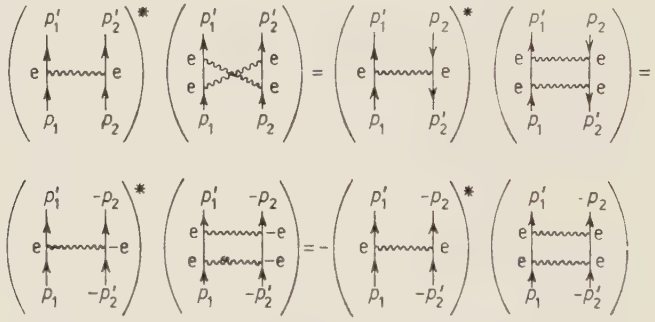

Fig. 6.

Therefore, it is sufficient to consider only the diagram $M_5^{(1)}$. The corresponding matrix element is given by

$$\text{(36)} \qquad Q M_5^{(1)} = -\frac{\alpha}{2\pi}\left(\frac{\alpha}{i\pi}\frac{m_1 m_2}{E_1 E_2}\right)\cdot\frac{1}{2}\frac{1}{i\pi^2}\int \mathrm{d}^4k\, \bar{u}_1(p_1')\gamma_\nu \frac{2ip_{1\mu} - ik\gamma_\mu}{k^2 - 2k\cdot p_1} u_1(p_1)\cdot$$

$$\cdot\frac{1}{k^2+\lambda^2}\frac{1}{(p_3+k)^2+\lambda^2}\bar{u}_2(p_2')\gamma^\nu\frac{2ip_2{}^\mu + ik\gamma^\mu}{k^2+2k\cdot p_2}u_2(p_2) =$$

$$= -\frac{\alpha}{2\pi}\frac{1}{i\pi^2}\int\frac{\mathrm{d}^4k}{(k^2-2k\cdot p_1)(k^2+2k\cdot p_2)}\cdot$$

$$\cdot\left\{-2p_1\cdot p_2\left(\frac{1}{k^2+\lambda^2}+\frac{1}{(p_3+k)^2+\lambda^2}-\frac{2k\cdot(k+p_3)}{k^2(p_3+k)^2}\right)M^{(0)}+\left(\frac{\alpha}{i\pi}\frac{m_1 m_2}{E_1 E_2}\right)\frac{1}{k^2(p_3-k)^2}\cdot\right.$$

$$\cdot\left[k^\sigma(\bar{u}_1(p_1')\gamma_\nu\gamma_\sigma p_2 u_1(p_1)\bar{u}_2(p_2')\gamma^\nu u_2(p_2) - \bar{u}_1(p_1')\gamma^\nu u_1(p_1)\bar{u}_2(p_2')\gamma_\nu\gamma_\sigma p_1 u_2(p_2)) + \right.$$

$$\left.\left. + \tfrac{1}{2}k^\sigma k_\tau\bar{u}_1(p_1')\gamma_\nu\gamma_\sigma\gamma_\mu u_1(p_1)\bar{u}_2(p_2')\gamma^\nu\gamma^\tau\gamma^\mu u_2(p_2)\right]\right\}.$$

The infra-red contribution here is easily transformed into that of eq. (14). For R_5, defined by (17), we obtain

$$QR_5 = -2u(u^2 - u - T + \tfrac{1}{2})I + \\ + \mathrm{Re}\left\{\frac{1}{i\pi^2}\int \mathrm{d}^4k \, \frac{k^\sigma N_\sigma + \frac{1}{2}k^\sigma k_\tau N_\sigma{}^\tau}{(k^2 - 2k\cdot p_1)(k^2 + 2k\cdot p_2)k^2(k+p_3)^2}\right\}, \tag{37}$$

where

$$I = \mathrm{Re}\left\{\Delta^2 \frac{1}{i\pi^2}\int \frac{\mathrm{d}^4k\, k\cdot(k+p_3)}{(k^2 - 2k\cdot p_1)(k^2+2k\cdot p_2)k^2(k+p_3)^2}\right\}, \tag{38}$$

and

$$\begin{cases} N_\sigma = \dfrac{1}{\Delta^2}(p_2{}^\mu F_{1\varrho\nu\sigma\mu}F_2{}^{\varrho\nu} - p_1{}^\mu F_1{}^{\varrho\nu}F_{2\varrho\nu\sigma\mu}), \\ N_\sigma{}^\tau = \dfrac{1}{\Delta^2}F_{1\varrho\nu\sigma\mu}F_2{}^{\varrho\nu\tau\mu}. \end{cases} \tag{39}$$

The second rank tensor $F_{i\mu\nu}$ appearing in (39) is given by (19) and (20) and the fourth rank tensor is defined by

$$F_{i\varrho\nu\sigma\mu} = m_i^2 \sum_{\text{spins}} (\overline{u}_i(p_i')\gamma_\varrho u_i(p_i))^*(\overline{u}_i(p_i')\gamma_\nu\gamma_\sigma\gamma_\mu u_i(p_i)). \tag{40}$$

Trace calculations give

$$F_{i\varrho\nu\sigma\mu} = F_{i\varrho\nu}g_{\sigma\mu} + p_{i\varrho}'(p_{i\mu}g_{\nu\sigma} - p_{i\sigma}g_{\nu\mu}) + p_{i\nu}'(p_{i\mu}g_{\varrho\sigma} - p_{i\sigma}g_{\varrho\mu}) + \\ + (p_{i\sigma}p_{i\mu}' - p_{i\mu}p_{i\sigma}')g_{\nu\varrho} + \tfrac{1}{2}\Delta^2(g_{\varrho\mu}g_{\nu\sigma} - g_{\varrho\sigma}g_{\nu\mu}) + \\ + p_{i\varrho}(p_{i\mu}'g_{\nu\sigma} - p_{i\sigma}'g_{\nu\mu}) - p_{i\nu}(p_{i\mu}'g_{\varrho\sigma} - p_{i\sigma}g_{\varrho\mu}). \tag{41}$$

After calculating the tensor products in (39) we get

$$\Delta^2(k^\sigma N_\sigma + \tfrac{1}{2}k^\sigma k_\tau N_\sigma{}^\tau) = (4(p_1\cdot p_2)^2 - \tfrac{1}{2}\Delta^2 W^2)((k^2 - 2k\cdot p_1) + (k^2 + 2k\cdot p_2)) - \\ - 2p_1\cdot p_2(m_2^2(k^2 - 2k\cdot p_1) + m_1^2(k^2 + 2k\cdot p_2) + (\Delta^2 - W^2)k\cdot(k+p_3)) + \\ + k^2\Delta^2(p_1\cdot p_2 + \tfrac{1}{2}\Delta^2) + k_\sigma k_\tau(\Delta^2(p_1{}^\sigma p_1{}^\tau + p_2{}^\sigma p_2{}^\tau) + 4p_1\cdot p_2 p_1{}^\sigma p_2{}^\tau + \\ + 2(p_1\cdot p_2 - \tfrac{1}{2}\Delta^2)(p_2{}^\sigma - p_1{}^\sigma)p_3{}^\tau - 2p_1\cdot p_2 p_3{}^\sigma p_3{}^\tau). \tag{42}$$

This inserted into (37) gives us

$$QR_5 = -u(2u^2 - u - T)I + \sum_{i=1}^{2}(u^2 - \tfrac{1}{2}u - \tfrac{1}{2}T + \tfrac{1}{4}ut_i)I_i + \left\{\tfrac{1}{2}(1-u)g^{\mu\nu} + \right. \\ \left. + \frac{1}{\Delta^2}(p_1{}^\mu p_1{}^\nu + p_2{}^\mu p_2{}^\nu + u(p_3{}^\mu p_3{}^\nu - 2p_1{}^\mu p_2{}^\nu) + (1+u)(p_1{}^\mu - p_2{}^\mu)p_3{}^\nu)\right\} I_{\mu\nu}, \tag{43}$$

where

$$I_i = \mathrm{Re}\left\{\Delta^2 \frac{1}{i\pi^2}\int \frac{\mathrm{d}^4k}{(0)(i)(3)}\right\}, \qquad (i=1,2), \tag{44}$$

and

$$I_{\mu\nu} = \mathrm{Re}\left\{\Delta^2 \frac{1}{i\pi^2}\int \frac{\mathrm{d}^4k\, k_\mu k_\nu}{(0)(1)(2)(3)}\right\}. \tag{45}$$

Here we have used the abbreviations

$$\begin{cases} (0) = k^2, & \\ (3) = (p_3 + k)^2, & \end{cases} \qquad \begin{cases} (1) = k^2 - 2k\cdot p_1, & \\ (2) = k^2 + 2k\cdot p_2. & \end{cases} \tag{46}$$

The quantities

$$T_{ij} = \frac{1}{\Delta^2}\, p_i^{\mu} p_j^{\nu} I_{\mu\nu}, \qquad (i,j=1,2,3), \tag{47}$$

can be expressed in terms of I, I_i and the integrals

$$X = g^{\mu\nu} I_{\mu\nu} = \mathrm{Re}\left\{\Delta^2 \frac{1}{i\pi^2}\int \frac{\mathrm{d}^4k}{(1)(2)(3)}\right\}, \tag{48}$$

$$\begin{cases} a = \mathrm{Re}\left\{\dfrac{1}{i\pi^2}\displaystyle\int \mathrm{d}^4k\, \frac{(3)-(0)+\Delta^2}{(1)(2)(3)}\right\}, \\ a' = \mathrm{Re}\left\{\dfrac{1}{i\pi^2}\displaystyle\int \mathrm{d}^4k\, \frac{(0)(3)-(1)(2)}{(0)(1)(2)(3)}\right\}, \\ a_i = \mathrm{Re}\left\{\dfrac{1}{i\pi^2}\displaystyle\int \mathrm{d}^4k\, \frac{(3)-(i)}{(0)(i)(3)}\right\}, \end{cases} \tag{49}$$

in the following way

$$\begin{cases} T_{11} = -\tfrac{1}{4}(a_2 + a - a' - X) + \dfrac{1}{4(t_2+1)}\left((2u-1)a_2 - (u+\tfrac{1}{2}t_2)I_2\right), \\ T_{33} = \tfrac{1}{4}(4X - 2I - a) + \dfrac{1}{4u^2 - t_1t_2}\left((u+\tfrac{1}{2}t_1)a_1 + (u+\tfrac{1}{2}t_2)a_2 - 2(u+T)a'\right), \\ T_{12} = \tfrac{1}{4}(a_1 + a_2 + a - a' - X), \\ T_{13} = \tfrac{1}{4}(I_2 + a - 2X). \qquad \text{(similarly for } T_{22} \text{ and } T_{23}). \end{cases} \tag{50}$$

Now the expression for QR_5 (43) can be written in terms of I, I_i, a, a', a_i and X. It turns out that the coefficient for X vanishes (as it should do,

because X is infra-red divergent) and we arrive at

$$
\begin{aligned}
(51)\qquad QR_5 = &-(2u^2-u-T+\tfrac{1}{2})[uI-\tfrac{1}{2}(I_1+I_2)]- \\
&-\tfrac{1}{4}ua+\tfrac{1}{2}\left(1+u-\frac{u(u+T)}{u^2-\tfrac{1}{4}t_1t_2}\right)a'+ \\
&+\tfrac{1}{4}\sum_{i=1}^{2}\left[t_iI_i\left(u-\frac{\tfrac{1}{2}-u}{1+t_i}\right)-a_i\left(1+2u+\frac{1-2u}{1+t_i}-\frac{u(u+\tfrac{1}{2}t_i)}{u^2-\tfrac{1}{4}t_1t_2}\right)\right].
\end{aligned}
$$

Evaluation of the remaining integrals gives the result

$$
(52)\qquad \begin{cases}
I=\dfrac{1}{4\sqrt{u^2-\tfrac{1}{4}t_1t_2}}\displaystyle\sum_{i=1}^{2}\left[\ln^2\frac{t_i}{4}-\ln\frac{(u+\tfrac{1}{2}t_i+\sqrt{u^2-\tfrac{1}{4}t_1t_2})^2}{4(u^2-\tfrac{1}{4}t_1t_2)}\ln\frac{t_i}{4}+\right. \\
\left.+\ln\dfrac{u+T}{u^2-\tfrac{1}{4}t_1t_2}\ln\dfrac{(u+\tfrac{1}{2}t_i+\sqrt{u^2-\tfrac{1}{4}t_1t_2})^2}{4(u+T)}+2\Phi\left(\frac{1}{2}\left(1-\frac{u+\tfrac{1}{2}t_i}{\sqrt{u^2-\tfrac{1}{4}t_1t_2}}\right)\right)-\right. \\
\left.-2\Phi\left(\frac{1}{2}\left(1+\frac{u+\tfrac{1}{2}t_i}{\sqrt{u^2-\tfrac{1}{4}t_1t_2}}\right)\right)-\pi^2\theta\left(u+\frac{t_1}{2}\right)\theta\left(u+\frac{t_2}{2}\right)\right];\quad \theta(x)=\begin{cases}0, & x\leqslant 0,\\ 1, & x>0,\end{cases} \\
I_i=-\dfrac{1}{\sqrt{1+t_i}}\left[\Phi(z_i^+)-\Phi(z_i^-)+2\Phi\left(\frac{1}{z_i^+}\right)-2\Phi\left(\frac{1}{z_i^-}\right)\right]; \\
\quad z_i^{\pm}=\dfrac{2}{t_i}(-1\pm\sqrt{1+t_i}), \\
a=-\dfrac{1}{\sqrt{u^2-\tfrac{1}{4}t_1t_2}}\displaystyle\sum_{i=1}^{2}\left[\ln\frac{(u+\tfrac{1}{2}t_i+\sqrt{u^2-\tfrac{1}{4}t_1t_2})^2}{(u+T)}-\ln\frac{t_i}{4}\right], \\
a'=-\dfrac{\sqrt{u^2-\tfrac{1}{4}t_1t_2}}{2(u+T)}\displaystyle\sum_{i=1}^{2}\left[\ln\frac{(u+\tfrac{1}{2}t_i+\sqrt{u^2-\tfrac{1}{4}t_1t_2})^2}{4(u+T)}-\right. \\
\qquad\qquad\left.-\left(1-\frac{u+\tfrac{1}{2}t_i}{\sqrt{u^2-\tfrac{1}{4}t_1t_2}}\right)\ln\frac{t_i}{4}\right], \\
a_i=-\ln\dfrac{t_i}{4}.
\end{cases}
$$

Here $\Phi(x)$ is a so-called Spence function defined by

$$
(53)\qquad \Phi(x)=\int_0^x\frac{\mathrm{d}y}{y}\ln|1-y|.
$$

Because of (35) we may write

$$
(54)\qquad R_5+R_6=(u^2-u-T+\tfrac{1}{2})\sum_{i=1}^{2}(R_i(u)-R_i(1-u))
$$

since the interchange $p_2 \leftrightarrow -p_2'$ is equivalent to $u \leftrightarrow (1-u)$ as follows from (5) and (6). We combine (51) and (52) and approximate $\sqrt{u^2 - \frac{1}{4}t_1 t_2}$ with u, which is correct when $(E_{\mu\,\mathrm{lab}})^2 \gg m_\mu^2$. ($E_{\mu\,\mathrm{lab}}$ = muon energy in the rest frame of the electron.) Then we obtain the following expression for $R_i(u)$

$$
\left\{
\begin{aligned}
R_i(u) = {} & \tfrac{1}{4}Q(u^2 - u - T + \tfrac{1}{2})^{-1}\Big\{-(2u^2 - u - T + \tfrac{1}{2})\cdot \\
& \cdot\Big[\ln^2\frac{t_i}{4} - 2I_i - 2\ln\frac{t_i}{4}\ln\Big(1+\frac{t_i}{4u}\Big) - \ln\frac{u^2}{u+T}\ln\frac{(u+t_i/4)^2}{u+T} + \\
& + 2\Phi\Big(-\frac{t_i}{4u}\Big) - 2\Phi\Big(1+\frac{t_i}{4u}\Big) - \pi^2\theta\Big(u+\frac{t_1}{2}\Big)\theta\Big(u+\frac{t_2}{2}\Big)\Big] + \\
& + t_i\Big[-\tfrac{1}{2}\Big(\ln\frac{t_i}{4}\Big)\Big(\frac{1+u}{u+T} + \frac{2-4u}{1+t_i}\Big) + I_i\Big(u - \frac{\frac{1}{2}-u}{1+t_i}\Big)\Big] + \\
& + \Big[2 - \frac{u(1+u)}{u+T}\Big]\ln\frac{(u+t_i/4)^2}{u+T}\Big\}, \\
I_i = {} & -\frac{1}{\sqrt{1+t_i}}\Big[\Phi(z_i^+) - \Phi(z_i^-) + 2\Phi\Big(\frac{1}{z_i^+}\Big) - 2\Phi\Big(\frac{1}{z_i^-}\Big)\Big]; \\
z_i^\pm = {} & \frac{2}{t_i}(-1 \pm \sqrt{1+t_i})\,.
\end{aligned}
\right. \tag{55}
$$

4. – Results.

We can now add the contributions from the different diagrams. Neglecting the magnetic contribution (33) which involves the small factor $1/8t_1t_2$, we obtain from (15), (I.54), (I.59), (23), (29) and (54), after some calculations

$$
\frac{\mathrm{d}\sigma}{\mathrm{d}\Omega} = \Big(\frac{\mathrm{d}\sigma}{\mathrm{d}\Omega}\Big)^{(0)}\Big[1 - \frac{\alpha}{\pi}(\delta_1 + \delta_2)\Big], \tag{56}
$$

$$
\delta_i = L_i + K_i(u)\ln\frac{q}{\Delta E} + H_i(u) + \tfrac{1}{2}H'(u) + R_i(u) - R_i(1-u)\,, \tag{57}
$$

$$
\left\{
\begin{aligned}
L_i = {} & \frac{28}{9} - \frac{2}{3}t_i - \Big(\frac{13}{6} - \frac{1}{3}t_i\Big)\sqrt{1+t_i}\ln\frac{\sqrt{1+t_i}+1}{\sqrt{1+t_i}-1}\,, \\
K_i(u) = {} & 2\Big[\frac{1+\frac{1}{2}t_i}{\sqrt{1+t_i}}\ln\frac{\sqrt{1+t_i}+1}{\sqrt{1+t_i}-1} - \\
& - 1 + \ln\Big|\frac{u+T}{1-u+T}\Big| - 2\ln\Big|\frac{u+\frac{1}{4}t_i}{1-u+\frac{1}{4}t_i}\Big|\Big],
\end{aligned}
\right. \tag{58}
$$

$$
\left\{
\begin{aligned}
&H_1(u) + H_2(u) + H'(u) = -\left(\frac{\alpha}{\pi}\right)^{-1} B + 4 = \\
&\qquad = 2\sum_{i=1}^{2}\left|\frac{p_i\cdot p_i'}{q^2}\,\mathrm{Re}\left\{\int_0^1 \mathrm{d}x\, h\left(\frac{p_i x - p_i'(1-x)}{q}\right)\right\} - \frac{p_i^2}{q^2}\,h\left(\frac{p_i}{q}\right)\right| + \\
&\qquad + 4Q\left[\frac{p_1\cdot p_2}{q^2}\,\mathrm{Re}\left\{\int_0^1 \mathrm{d}x\, h\left(\frac{p_1 x - p_2(1-x)}{q}\right)\right\} + \right. \\
&\qquad \left. + \frac{p_1\cdot p_2'}{q^2}\,\mathrm{Re}\left\{\int_0^1 \mathrm{d}x\, h\left(\frac{p_1 x + p_2'(1-x)}{q}\right)\right\}\right]; \\
&h(p) = -\frac{1}{p^2}\left[\tfrac{1}{2}\ln\frac{-p^2}{4} - \int_0^1 \mathrm{d}y\,\frac{p_0^2}{p_0^2 - \boldsymbol{p}^2 y^2}\right].
\end{aligned}
\right. \tag{59}
$$

(Poles are avoided by detours into the upper half-plane).

The zero order cross section is given above in (22). The function $R_i(u)$ is expressed in (55). From (59) we separate out the more explicit formulae

$$
\begin{aligned}
H_i(u) = {} & \frac{E_i - q}{q}\ln\frac{E_i - q}{2q} - \frac{E_i + q}{q}\ln\frac{E_i + q}{2q} + 2\sin^2\frac{\theta}{2}\,(1 + \tfrac{1}{2}t_i)\cdot \\
& \cdot\int_0^1 \frac{\mathrm{d}x}{\varphi(x)}\left[\frac{q}{E_i - q\varphi(x)}\ln\frac{E_i + q\varphi(x)}{2q} - \frac{q}{E_i + q\varphi(x)}\ln\frac{E_i - q\varphi(x)}{2q}\right];
\end{aligned} \tag{60}
$$

$$
\begin{aligned}
H'(u) = {} & 2Q\left\{\sum_{i=1}^{2}\left|\Phi\left(\frac{E_i - q}{2q}\right) - \Phi\left(\frac{E_i + q}{2q}\right)\right| \cdot\right. \\
& + 2\sin^2\frac{\theta}{2}\,(1-u)\int_0^1 \frac{\mathrm{d}x}{\psi(x)}\left[\frac{q}{E_1 + (E_2 - E_1)x + q\psi(x)}\cdot\ln\frac{E_1 + (E_2 - E_1)x - q\psi(x)}{2q} - \right. \\
& \left.\left. - \frac{q}{E_1 + (E_2 - E_1)x - q\psi(x)}\ln\frac{E_1 + (E_2 - E_1)x + q\psi(x)}{2q}\right]\right\};
\end{aligned} \tag{61}
$$

$$
\left\{
\begin{aligned}
\varphi(x) &= \left[1 - 4\sin^2\frac{\theta}{2}\,x(1-x)\right]^{\frac{1}{2}}, \\
\psi(x) &= \left[1 - 4\cos^2\frac{\theta}{2}\,x(1-x)\right]^{\frac{1}{2}}.
\end{aligned}
\right. \tag{62}
$$

By examining the result stated in equations (55) to (62) one can see that when $\Lambda \gg m$ — as is the case in high energy experiments — the predominant terms of the radiative corrections are those proportional to $\ln(\Lambda^2/m_e^2)$. ($m_{e,\mu}$ = electron (muon) rest mass.) This is true until the momentum transfer becomes so large that the $\ln(\Lambda^2/m_\mu^2)$-terms are also important.

It appears that the $\ln(\Delta^2/m_e^2)$-terms derive extensively from the « electron diagrams » $M_1^{(1)}$ and $M_3^{(1)}$ in Fig. 3 and *a* and *b* in Fig. 4. Similarly, the $\ln(\Delta^2/m_\mu{}^2)$-terms derive extensively from the « muon diagrams », $M_2^{(1)}$ and $M_4^{(1)}$ in Fig. 3 and *c* and *d* in Fig. 4. The two-photon exchange diagrams $M_5^{(1)}$ and $M_6^{(1)}$, on the other hand, do not contribute any terms that become large with large Δ.

The momentum transfers that occur in experiments planned at present are such that the $\ln(\Delta^2/m_e^2)$-terms will dominate the radiative corrections. If we take into account only the « electron diagrams », $M_1^{(1)}$, $M_3^{(1)}$ (Fig. 3) and *a*, *b* (Fig. 4) we get (56) and (57) replaced by the simpler formulae

$$\frac{\mathrm{d}\sigma}{\mathrm{d}\Omega} = \left(\frac{\mathrm{d}\sigma}{\mathrm{d}\Omega}\right)^{(0)}\left[1 - \frac{\alpha}{\pi}\delta\right], \tag{63}$$

$$\delta = L_1 + K_1(u)\ln\frac{q}{\Delta E} + H_1(u)\,, \tag{64}$$

where L_1 and $K_1(u)$ are given by (58) and $H_1(u)$ by (60) and (62). Neglecting terms that are linear in m_e/Δ we then obtain the following simple expression for δ:

$$\left\{\begin{aligned} &\delta = \frac{28}{9} - \frac{13}{6}\ln\left(\frac{\Delta^2}{m_e^2}\right) + 2\left[\ln\left(\frac{\Delta^2}{m_e^2}\right) - 1\right]\ln\left(\frac{q}{\Delta E}\right) + J\,; \\ &J = 2\sin\frac{\theta}{2}\int_{\cos(\theta/2)}^{1}\frac{\mathrm{d}x}{\sqrt{x^2 - \cos^2(\theta/2)}}\left[\frac{1}{1-x}\ln\left(\frac{1+x}{2}\right) - \frac{1}{1+x}\ln\left(\frac{1-x}{2}\right)\right] = \\ &\qquad = \ln\left(\sin^2\frac{\theta}{2}\right)\ln\left(\cos^2\frac{\theta}{2}\right) - \Phi\left(\sin^2\frac{\theta}{2}\right). \end{aligned}\right. \tag{65}$$

As one could expect this is precisely the result obtained by SCHWINGER (ref. (4), eq. (2.105) and (2.97)) for the radiative corrections to the scattering of an electron by a potential (*). A similar result was obtained by TSAI (7) for electron-electron scattering.

The muon diagrams and the two-photon exchange diagrams — which are neglected when δ is approximated by the formula (65) — give corrections to δ of the order

$$\frac{\Delta}{m_\mu}\,. \tag{66}$$

So (65) is obtained in the « static limit » when $m_\mu \to \infty$.

(*) The author is indebted to Professor G. KÄLLÉN who kindly drew his attention to the evaluated form of the integral J in (65) which is given in ref. (8) eq. (35), (24), (25). The definition of $\Phi(x)$ in ref. (8) is different from the definition (53).

When $\Delta \gg m_\mu$, the expression (65) has to be extended by a muon term similar to the electron term.

Numerical results based on (65) are shown in Table I for some energies and angles at which this formula is expected to give a reasonable approximation. The error due to the neglection of « muon diagrams » is certainly very small. The error due to the neglection of two-photon-exchange diagrams is probably less than 2% of the cross section, but before the theory is compared to actual experiments, the contributions from these diagrams should be estimated more carefully from the general formulae given above.

TABLE I. – *First order radiative corrections to* μ-e *scattering in per cent* $(100\,(\alpha/\pi)\delta)$.

		c.m. scattering angle, θ		
$E_{\mu\text{lab}}$	q/m_e	45°	90°	180°
2 GeV	17.7	$1.9 \ln(q/\Delta E) - 1.8$	$2.5 \ln(q/\Delta E) - 2.2$	$2.8 \ln(q/\Delta E) - 2.5$
10 GeV	68.3	$3.2 \ln(q/\Delta E) - 3.2$	$3.8 \ln(q/\Delta E) - 3.6$	$4.1 \ln(q/\Delta E) - 3.8$
50 GeV	202	$4.2 \ln(q/\Delta E) - 4.3$	$4.8 \ln(q/\Delta E) - 4.7$	$5.1 \ln(q/\Delta E) - 4.9$

As mentioned in the introduction, the cross section for the hard photon emission, permitted by the experimental geometry has also to be calculated before the radiative corrections can be compared to experimental results.

* * *

I wish to thank Dr. A. PETERMAN for suggesting this problem and for many helpful discussions. I also thank Dr. S. M. BERMAN for some discussions.

(8) G. KÄLLÉN: *Handb. d. Phys.*, **5/1**, 169 (1958).

RIASSUNTO (*)

Si calcola sino all'ordine e^6 la sezione d'urto differenziale per lo scattering μ-e.

(*) *Traduzione a cura della Redazione.*

IL NUOVO CIMENTO Vol. XIX, N. 5 1° Marzo 1961

High-Energy Behaviour of Electromagnetic Scattering Cross-Sections.

K. E. Eriksson

CERN - Geneva

(ricevuto il 12 Dicembre 1960)

Summary. — The theory of the renormalization group is used in order to show that for large momentum transfer the perturbation expansion in α of the differential cross-section for the scatteringo f an electron by a potential in first order Born approximation is expanded in terms of the effective parameter $(\alpha/\pi)\ln(q^2/m^2)$. (q = invariant momentum transfer, m = electron rest mass; $q/m \gg 1$.)

1. – Introduction.

In a recent note it was pointed out by Peterman and the author [1] that the effective perturbation expansion parameter for cross-sections for electromagnetic processes at high energies and momentum transfers is at most

$$\frac{\alpha}{\pi}\ln^{\frac{4}{3}}\left(\frac{q^2}{m^2}\right), \tag{1}$$

where q is the invariant momentum transfer in the process and m is the electron rest mass.

This result was obtained from considerations of Feynman diagrams and though we conjectured that the effective expansion parameter should in fact be

$$\frac{\alpha}{\pi}\ln\frac{q^2}{m^2}, \tag{2}$$

[1] K. E. Eriksson and A. Peterman: *Phys. Rev. Lett.*, **5**, 444 (1960).

we could not prove this due to difficulties in handling diagrams containing closed electron loops.

By use of the properties of the renormalization group (*) it has now been possibile to show that (2) *is indeed the effective perturbation expansion parameter for electromagnetic scattering cross-sections at high energies and momentum transfers.*

Here this theorem will be proved for the scattering of an electron by a potential in first order Born approximation. Since that process involves all features that are characteristic for electromagnetic processes this is not a severe limitation, and it will be quite straightforward to extend the proof to more complicated scattering processes.

2. – Preliminary discussion.

Consider an electron with initial momentum p that is scattered by an external electromagnetic field A_μ and thereby obtains the final momentum p'. The kinematics are given by

$$\begin{cases} p = (\sqrt{\tfrac{1}{4}q^2 + m^2}, \quad \tfrac{1}{2}q, 0, 0) , \\ p' = (\sqrt{\tfrac{1}{4}q^2 + m^2}, -\tfrac{1}{2}q, 0, 0) , \end{cases} \tag{3}$$

where q is the invariant momentum transfer. We assume that

$$q^2 \gg m^2 . \tag{4}$$

Let the energy resolution ΔE be isotropic in the Lorentz-frame determined by (3). Assume further that

$$\Delta E \ll q , \qquad \text{but} \qquad \left| \ln \frac{\Delta E}{q} \right| = O(1) . \tag{5}$$

We write down the probability density $P(q^2/m^2, \Delta E/q)$ for the process

(*) The existence of this group was first noticed by STUECKELBERG and PETERMAN [2]. Further developments were made by BOGOLIUBOV and SHIRKOV [3], who used the properties of the group to investigate the asymptotic behaviour of Green's functions.

[2] E. C. G. STUECKELBERG and A. PETERMAN: *Helv. Phys. Acta*, **24**, 317 (1951); *Helv. Phys. Acta*, **26**, 499 (1953).

[3] N. N. BOGOLIUBOV and D. V. SHIRKOV: *Introduction to the Theory of Quantized Fields* (New York, London, 1959), Sect. **42-44**. This book contains further references.

in the form

$$(6)\qquad P\left(\frac{q^2}{m^2},\frac{\Delta E}{q}\right)=\sum_{m=0}^{\infty}\sum_{n=0}^{\infty}\int\!\!\ldots\!\int \mathrm{d}^3\boldsymbol{k}_1\ldots\mathrm{d}^3\boldsymbol{k}_m\,\mathrm{d}^3\boldsymbol{p}_{11}\,\mathrm{d}^3\boldsymbol{p}_{12}\ldots\mathrm{d}^3\boldsymbol{p}_{n1}\,\mathrm{d}^3\boldsymbol{p}_{n2}\cdot$$

$$\cdot\theta\Big(\Delta E-\sum_{i=1}^{m}|\boldsymbol{k}_i|-\sum_{j=1}^{n}(E_{j1}+E_{j2})\Big)\cdot$$

$$\cdot\sum_{\substack{\text{spins}\\ \text{polarizations}}}\left|M_{mn}\left(\frac{q^2}{m^2};\boldsymbol{k}_1,e_1;\ldots\boldsymbol{k}_m,e_m;\boldsymbol{p}_{11},s_{11};\ldots;\boldsymbol{p}_{n2},s_{n2}\right)\right|^2,$$

$$E_{jk}=\sqrt{\boldsymbol{p}_{jk}^2+m^2};\qquad \theta(x)=\begin{cases}0, & x<0,\\ 1, & x\geqslant 0,\end{cases}$$

where

$$M_{mn}\left(\frac{q^2}{m^2};\boldsymbol{k}_1,e_1;\ldots;\boldsymbol{k}_m,e_m;\boldsymbol{p}_{11},s_{11};\ldots;\boldsymbol{p}_{n2},s_{n2}\right)$$

is the invariant amplitude when the scattering process is accompanied by emission of m low energy photons with momenta $\boldsymbol{k}_1,\ldots,\boldsymbol{k}_m$ and polarizations $e_1,\ldots,e_m$ and n electron pairs with momenta $p_{11},\ldots,p_{n2}$ and spins $s_{11},\ldots,s_{n2}$. In general M_{mn} is infra-red divergent. However, the infra-red divergences inside the sum cancel and $P(q^2/m^2,\Delta E/q)$ is not infra-red divergent.

We define $X(q^2/m^2,\Delta E/q)$ by the equation

$$(7)\qquad P\left(\frac{q^2}{m^2},\frac{\Delta E}{q}\right)=X\left(\frac{q^2}{m^2},\frac{\Delta E}{q}\right)P^{(0)}\left(\frac{q^2}{m^2}\right),$$

where

$$(8)\qquad P^{(0)}\left(\frac{q^2}{m^2}\right)=\frac{\alpha}{\pi}\,|\,\overline{u}(p')\gamma_\mu A^\mu u(p)\,|^2$$

is the lowest order (in α) invariant amplitude for the elastic process. The function $X(q^2/m^2,\Delta E/q)$ now contains all radiative corrections.

Since we are interested in the q^2/m^2-dependence of X, we suppress the dependence on $\Delta E/q$ and write

$$(9)\qquad X\left(\frac{q^2}{m^2},\frac{\Delta E}{q}\right)=X\left(\frac{q^2}{m^2}\right).$$

In the next section the renormalization group will be used to get information about how X depends on q^2/m^2. When dealing with the renormalization group it is most natural to work in a gauge where the photon

propagator $D_{\mu\nu}(k)$ contains only transverse components

$$D_{\mu\nu}(k) = \frac{\mathrm{d}(k^2/m^2)}{k^2}\left(g_{\mu\nu} - \frac{k_\mu k_\nu}{k^2}\right). \tag{10}$$

In order to study the renormalization properties of the dimensionless functions $d(q^2/m^2)$ and $X(q^2/m^2)$, we follow the methods of ref. [3] and introduce the more general functions

$$d\left(\frac{q^2}{\lambda^2}, \frac{m^2}{\lambda^2}, e^2\right) \quad \text{and} \quad X\left(\frac{q^2}{\lambda^2}, \frac{m^2}{\lambda^2}, e^2\right), \quad \lambda^2 > 0 \text{ (space-like)}, \tag{11}$$

with the normalization

$$\begin{cases} d\left(1, \frac{m^2}{\lambda^2}, e^2\right) = 1\,, \\ X\left(1, \frac{m^2}{\lambda^2}, e^2\right) = 1\,. \end{cases} \tag{12}$$

Here e is the electric charge and λ^2 is a squared normalization momentum.

With $e_0 =$ the physical electron charge, we define also

$$\begin{cases} d_0\left(\frac{q^2}{m^2}, e_0^2\right) = d\left(\frac{q^2}{m^2}\right), \\ X_0\left(\frac{q^2}{m^2}, e_0^2\right) = X\left(\frac{q^2}{m^2}\right), \end{cases} \tag{13}$$

which have the following normalization

$$\begin{cases} d_0(0, e_0^2) = 1\,, \\ X_0(0, e_0^2) = 1\,, \end{cases} \tag{14}$$

and thus correspond to the case that $\lambda^2 = 0$ in (11) and (12).

3. – Proof of the theorem.

Under multiplicative renormalization each $|M_{mn}|^2$ occurring in (6), and hence also $P(q^2/m^2, \Delta E/q)$, transforms like $|\bar{\psi} e \Gamma \psi|^2$, where ψ is the electron field, and Γ is the vertex function. From (8) is seen that $P^{(0)}(q^2/m^2)$ transforms like $|\bar{\psi} e \psi|^2$. Because of (7) this implies that X transforms like

$$|\Gamma|^2. \tag{15}$$

We consider the following renormalization

$$
(16)\qquad \begin{cases} d\left(\dfrac{q^2}{\lambda_2^2}, \dfrac{m^2}{\lambda_2^2}, e_2^2\right) = z_3\, d\left(\dfrac{q^2}{\lambda_1^2}, \dfrac{m^2}{\lambda_1^2}, e_1^2\right), \\ X\left(\dfrac{q^2}{\lambda_2^2}, \dfrac{m^2}{\lambda_2^2}, e_2^2\right) = z^2 X\left(\dfrac{q^2}{\lambda_1^2}, \dfrac{m^2}{\lambda_1^2}, e_1^2\right), \\ e_2^2 = z_3^{-1} e_1^2 . \end{cases}
$$

The renormalization constants z and z_3 can be eliminated, and using (12) we are led to the following functional equations (see ref. [3], Section **42**·3)

$$
(17)\qquad \begin{cases} d\left(\dfrac{q^2}{\lambda_2^2}, \dfrac{m^2}{\lambda_2^2}, e_2^2\right) = \dfrac{d(q^2/\lambda_1^2,\ m^2/\lambda_1^2,\ e_1^2)}{d(\lambda_2^2/\lambda_1^2,\ m^2/\lambda_1^2,\ e_1^2)}, \\ X\left(\dfrac{q^2}{\lambda_2^2}, \dfrac{m^2}{\lambda_2^2}, e_2^2\right) = \dfrac{X(q^2/\lambda_1^2,\ m^2/\lambda_1^2,\ e_1^2)}{X(\lambda_2^2/\lambda_1^2,\ m^2/\lambda_1^2,\ e_1^2)}, \\ e_2^2 = e_1^2 d\left(\dfrac{\lambda_2^2}{\lambda_1^2}, \dfrac{m^2}{\lambda_1^2}, e_1^2\right). \end{cases}
$$

Taking $\lambda_1^2 = 0$, $\lambda_2^2 = \lambda^2$ and using the functions defined by (13), we then have as a special case of (17)

$$
(18)\qquad \begin{cases} d\left(\dfrac{q^2}{\lambda^2}, \dfrac{m^2}{\lambda^2}, e^2\right) = \dfrac{d_0(q^2/m^2,\ e_0^2)}{d_0(\lambda^2/m^2,\ e_0^2)}, \\ X\left(\dfrac{q^2}{\lambda^2}, \dfrac{m^2}{\lambda^2}, e^2\right) = \dfrac{X_0(q^2/m^2,\ e_0^2)}{X_0(\lambda^2/m^2,\ e_0^2)}, \\ e^2 = e_0^2 d_0\left(\dfrac{\lambda^2}{m^2}, e_0^2\right). \end{cases}
$$

With

$$
(19)\qquad x = \frac{q^2}{\lambda^2}; \qquad y = \frac{m^2}{\lambda^2}; \qquad \lambda^2 = \lambda_2^2 ,
$$

the following Lie differential equations can be derived from the eq. (17) (see ref. [3], Section **42**·4)

$$
(20)\qquad \begin{cases} \dfrac{\partial e^2 d(x, y, e^2)}{\partial x} = \dfrac{e^2 d(x, y, e^2)}{x} \varphi\left(\dfrac{y}{x}, e^2 d(x, y, e^2)\right), \\ \dfrac{\partial \ln X(x, y, e^2)}{\partial x} = \dfrac{1}{x} \psi\left(\dfrac{y}{x}, e^2 d(x, y, e^2)\right), \end{cases}
$$

where

$$\text{(21)} \qquad \begin{cases} \varphi(y, e^2) = \left[\dfrac{\partial}{\partial \xi} d(\xi, y, e^2)\right]_{\xi=1}, \\ \psi(y, e^2) = \left[\dfrac{\partial}{\partial \xi} \ln X(\xi, y, e^2)\right]_{\xi=1}. \end{cases}$$

We are interested in the case when $q^2 \gg m^2$, *i.e.* when $x \gg y$. If we choose $\lambda^2 = O(q^2)$, we have $y \ll 1$. Putting $y = 0$ in (20) and (21) we then get

$$\text{(22)} \qquad \begin{cases} \dfrac{\partial e^2 d(x, e^2)}{\partial x} = \dfrac{e^2 d(x, e^2)}{x} \varphi(e^2 d(x, e^2)), \\ \dfrac{\partial \ln X(x, e^2)}{\partial x} = \dfrac{1}{x} \psi(e^2 d(x, e^2)), \end{cases}$$

and

$$\text{(23)} \qquad \begin{cases} \varphi(e^2) = \left[\dfrac{\partial}{\partial \xi} d(\xi, e^2)\right]_{\xi=1}, \\ \psi(e^2) = \left[\dfrac{\partial}{\partial \xi} \ln X(\xi, e^2)\right]_{\xi=1}, \end{cases}$$

with the definitions

$$\text{(24)} \qquad \begin{cases} d(x, e^2) = d(x, 0, e^2), \\ X(x, e^2) = X(x, 0, e^2). \end{cases}$$

Integration of the eq. (22) gives with use of (12)

$$\text{(25)} \qquad \begin{cases} \ln x = \displaystyle\int_{e^2}^{e^2 d(x, e^2)} \frac{\mathrm{d}z}{z\varphi(z)}, \\ \ln X(x, e^2) = \displaystyle\int_{e^2}^{e^2 d(x, e^2)} \frac{\mathrm{d}z}{z\varphi(z)} \psi(z). \end{cases}$$

In perturbation theory $d(x, e^2)$ and $X(x, e^2)$ can be expanded in the following way

$$\text{(26)} \qquad \begin{cases} d(x, e^2) = 1 + \displaystyle\sum_{i,j=1}^{\infty} a_{ij} e^{2i} (\ln x)^j, \\ X(x, e^2) = 1 + \displaystyle\sum_{i,j=1}^{\infty} b_{ij} e^{2i} (\ln x)^j, \end{cases}$$

where b_{ij} are functions of $\Delta E/q$. Because of the condition on $\ln \Delta E/q$ in (5) the effective expansion parameter does not depend appreciably on $\Delta E/q$ (see ref. (4) Section **5**).

Insertion of (26) into (23) gives

$$\begin{cases} \varphi(e^2) = \sum_{i=1}^{\infty} a_i e^{2i}, \\ \psi(e^2) = \sum_{i=1}^{\infty} b_i e^{2i}, \end{cases} \tag{27}$$

where

$$\begin{cases} a_i = a_{i1}, \\ b_i = b_{i1}. \end{cases} \tag{28}$$

If

$$e^2 d(x, e^2) \ll 1, \tag{29}$$

then $z \ll 1$ in (25) and the following expansions obtainable from (27) are useful

$$\begin{cases} \dfrac{1}{z\varphi(z)} = \dfrac{1}{z^2} \sum_{i=0}^{\infty} \alpha_i z^i, \\ \dfrac{\psi(z)}{z\varphi(z)} = \dfrac{1}{z} \sum_{i=0}^{\infty} \beta_i z^i. \end{cases} \tag{30}$$

The coefficients α_i and β_i can be determined from a_i, b_i by the recurrence formulae

$$\begin{cases} \alpha_0 a_1 = 1, \\ \sum_{i=0}^{n-1} \alpha_i a_{n-i} = 0, \quad n > 1, \\ \sum_{i=0}^{n-1} \beta_i a_{n-i} = b_n. \end{cases} \tag{31}$$

We now insert the expansions (30) obtained from perturbation theory into the integral equations (25). This gives

$$\begin{cases} (\alpha_0 - e^2 \ln x) d(x, e^2) - \alpha_0 + \alpha_1 e^2 d(x, e^2) \ln d(x, e^2) + \\ \qquad + e^2 d(x, e^2) \sum_{n=1}^{\infty} \dfrac{\alpha_{n+1}}{n} e^{2n} \left[(d(x, e^2))^n - 1 \right] = 0, \\ X(x, e^2) - [d(x, e^2)]^{\beta_0} \exp\left[\sum_{n=1}^{\infty} \dfrac{\beta_n}{n} e^{2n} \left[(d(x, e^2))^n - 1 \right] \right] = 0. \end{cases} \tag{32}$$

(4) K. E. ERIKSSON: *Nuovo Cimento*, **19**, 1010 (1961).

To solve the equations (32) we make the following ansatz

$$\begin{cases} d(x, e^2) = \sum_{n=0}^{\infty} e^{2n} d^{(n)}(\eta) , \\ X(x, e^2) = \sum_{n=0}^{\infty} e^{2n} X^{(n)}(\eta) , \end{cases} \tag{33}$$

with

$$\eta = e^2 \ln x \tag{34}$$

which we introduce into (32). The condition that all coefficients for different powers of e^2 vanish gives then the solutions for $d^{(0)}(\eta), d^{(1)}(\eta), \ldots, X^{(0)}(\eta), X^{(1)}(\eta), \ldots$ So the ansatz is correct, and if we expand also in powers of η we see that the expansions (26) are unnecessarily general. In fact we have that

$$a_{ij} = b_{ij} = 0 , \qquad \text{if } i < j . \tag{35}$$

Recalling the definitions (19) and (24) and using (18) we then conclude that in the expansions of

$$\begin{cases} d\left(\frac{q^2}{m^2}\right) = d_0\left(\frac{q^2}{m^2}, e_0^2\right), \\ X\left(\frac{q^2}{m^2}\right) = X_0\left(\frac{q^2}{m^2}, e_0^2\right), \end{cases} \tag{13}$$

in powers of $\alpha = e_0^2/4\pi$ the terms with the highest power of $\ln (q^2/m^2)$ are of the form

$$\left(\frac{\alpha}{\pi} \ln \frac{q^2}{m^2}\right)^n . \tag{36}$$

Hence (2) is the effective expansion parameter of $X(q^2/m^2)$ and our theorem is proved.

4. – Concluding remark.

The above treatment indicates that the use of the renormalization group is a good method to improve the results calculated by ordinary perturbation methods. If the $2n$ coefficients $a_1, \ldots, a_n, b_1, \ldots, b_n$ in the perturbation expansions of $d(x, e^2)$ and $X(x, e^2)$ (see (26) and (28)) are known, then by (31) they determine $\alpha_0, \ldots, \alpha_{n-1}, \beta_0, \ldots, \beta_{n-1}$, and by (32) and

(33) these latter coefficients determine the $2n$ functions $d^{(0)}(\eta)$, ..., $d^{(n-1)}(\eta)$, $X^{(0)}(\eta)$, ..., $X^{(n-1)}(\eta)$. In ref. [3] it is shown how this works in calculations of Green's functions.

* * *

I am indebted to Dr. A. PETERMAN for many stimulating discussions from which the basic idea of the proof originates. His helpful criticism of the manuscript is also gratefully acknowledged.

RIASSUNTO (*)

Si fa uso della teoria del gruppo di rinormalizzazione allo scopo di mostrare come per grandi trasferimenti di impulso lo sviluppo in α della perturbazione della sezione d'urto differenziale per lo scattering di un elettrone da parte di un potenziale nella approssimazione di Born di primo ordine si effettui in termini del parametro effettivo $(\alpha/\pi)\ln(q^2/m^2)$ (q=trasferimento invariabile dell'impulso, m=massa di riposo dell'elettrone; $q/m \approx 1$).

(*) *Traduzione a cura della Redazione.*

Magnetism of a Small Particle as Revealed by an Electron Beam.

S. YAMAGUCHI

Institute of Physical and Chemical Research - Tokyo

(ricevuto il 7 Settembre 1960)

The rather soft electrons (voltage: about 50 kV) are suitable for studying the surface of matter by the aid of diffraction. The rather hard electrons (about 200 kV) are able to reveal the interior of a particle (grain size: about 3000 Å) [1].

The path of an electron beam is deflected by a magnetic field as the result of the Lorentz effect. This phenomenon is observable in the diffraction diagram from a ferromagnetic substance [2]. According to these two experiences, the electron penetration process with the variable accelerating voltage was used for studying whether the magnetic induction was higher or lower, at the surface of a small particle, (grain size: about 3000 Å) than in the interior of it.

Nickel powder was employed here as the sample for the experiment. The particles of nickel were attracted to the sharp edge of a razor blade of hard steel as a permanent magnet (remanence: about 10000 G). In this way these nickel particles were kept at saturation magnetization. An electron beam grazed these magnetized particles. The three electron beams were received on a dry plate fixed nearly perpendicular to the incident direction. The photograph obtained is shown in Fig. 1. Here, Z_1 and Z_2 correspond to the soft (wave

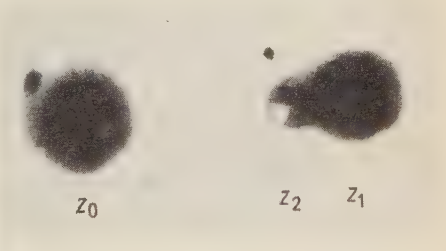

Fig. 1. - The incident beams under the magnetic influences. Z_0: the intact incident beam without magnetic effect. Z_1: the beam influenced by the surface induction. Z_2: the beam influenced by the interior induction.

lenght λ_1: 0.0462 Å) and hard electrons (λ_2: 0.0292 Å) subjected respectively to the magnetic field of the specimen, Z_0 is the original position of the incident

(1) S. YAMAGUCHI: *Journ. Chem. Phys.*, **27**, 1114 (1957).

(2) S. YAMAGUCHI: *Nuovo Cimento*, **12**, 286 (1959).

beam subjected to no magnetic field. We have a relation between the deflection of the beam and the magnetic induction:

$$\frac{Z_0 Z_1}{Z_0 Z_2} = \frac{\lambda_1 B_s}{\lambda_2 B_i}, \tag{1}$$

where B_s and B_1 mean respectively the induction at the surface of the particle and the one in the interior of it. On Fig. 1 we measure $\overline{Z_0 Z_1}/\overline{Z_0 Z_2} = 1.39$. Therefore, we obtain $B_s/B_1 = 0.88$. That is $B_s < B_i$. It is, therefore, concluded that the induction is lower at the surface than in the interior of the nickel particles in question. As a matter of fact the diffraction rings from the oxide (NiO) are found, *i.e.* the nickel particles are covered with the thin layer of this non-ferromagnetic oxide. These circumstances are illustrated in Fig. 2. Thus it is possible to reveal with the soft and hard electrons that the magnetic induction at the surface of a particle differs from that in the interior of it.

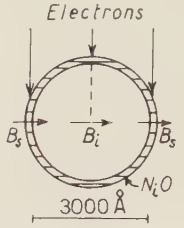

Fig. 2. – Ni—NiO particle. B_s: the surface induction. B_i: the interior induction. $B_s < B_i$.

There was found another case, *i.e.* $B_s > B_i$. The particles of this character were prepared by grinding a piece of non-ferromagnetic austenitic stainless steel. It is known that the ground surface of this steel becomes ferromagnetic as the result of the strain-induced transformation from austenite to martensite [2].

IL NUOVO CIMENTO Vol. XIX, N. 5 1° Marzo 1961

On the Polarization of Protons in (d, p) Stripping Reactions.

E. Coffou

Institute « Rudjer Bošković » - Zagreb

(ricevuto il 24 Ottobre 1960)

The polarization of outgoing protons in stripping nuclear reactions with unpolarized target nuclei and an arbitrary polarized incident deuteron beam is considered (*).

To get the quantities $\langle T^{\mathrm{p}}_{\lambda'\varkappa'}\rangle \lambda' = 0.1;\ -\lambda' \leqslant \varkappa' \leqslant \lambda'$ ($\langle T_{\lambda\varkappa}\rangle$ is the average of the $T_{\lambda\varkappa}$ component of a tensor operator in the system of particles with a given spin) defining the polarization of protons in the exit channel we use the known formula

$$\langle T^{\mathrm{p}}_{\lambda'\varkappa'}\rangle = \frac{\mathrm{Tr}\,(T^{\mathrm{p}}_{\lambda'\varkappa'} F \varrho_{\mathrm{in}} F^{+})}{\mathrm{d}\sigma/\mathrm{d}\Omega}\,, \tag{1}$$

where ϱ_{in} is the density operator of the entrance channel, F the scattering amplitude for the process, and $\mathrm{d}\sigma/\mathrm{d}\Omega$ the angular distribution of protons given by

$$\frac{\mathrm{d}\sigma}{\mathrm{d}\Omega} = \mathrm{Tr}\,(F \varrho_{\mathrm{in}} F^{+}) = \mathrm{Tr}\,(T^{\mathrm{p}}_{00} F \varrho_{\mathrm{in}} F^{+})\,. \tag{2}$$

As we consider the reaction with unpolarized target nuclei, ϱ_{in} is given by

$$\varrho_{\mathrm{in}} = \frac{1}{\widehat{I}_i^2}\,\varrho_{\mathrm{d}}\ (**)\,,$$

where ϱ_{d} is the density operator of deuterons for which we use the expansion:

$$\varrho_{\mathrm{d}} = \frac{1}{\widehat{s}_{\mathrm{d}}^2} \sum_{\lambda=0}^{2} \sum_{\varkappa=-\lambda}^{\lambda} \langle T^{\mathrm{d}}_{\lambda\varkappa}\rangle T^{\mathrm{d}+}_{\lambda\varkappa}\,. \tag{3}$$

(*) The work was reported at the Congress of Mathematicians and Physicists of Yugoslavia, 19-24 September 1960, Belgrade.

(**) We use the abbreviation $\widehat{x} = (2x+1)^{\frac{1}{2}}$.

For the scattering amplitude F we take the scattering amplitude obtained by the distorted-wave Born approximation with zero-rang approximation for the V_{NP} interaction.

We suppose that the V_{FP} interaction contains a polarizing, l-s coupling term, but for the sake of simplicity we take only the spherically symmetric potential for the V_{TD} interaction.

For the trace appearing in the expression (1) we get the following results:

$$(4)\qquad \mathrm{Tr}\,(T^{p}_{\lambda'\varkappa}\,F\varrho_{\mathrm{in}}F^{+}) = N^2\frac{\hat{I}_f^2}{\hat{I}_i^2}\hat{s}_{\mathrm{d}}\hat{s}_{\mathrm{p}}\hat{\lambda}'\sum_{\lambda\varkappa}\hat{\lambda}\sum\exp\left[i(\sigma_{l_{\mathrm{d}}}+\sigma_{l_{\mathrm{p}}}-\sigma_{l'_{\mathrm{d}}}-\sigma_{l'_{\mathrm{p}}})\right]\cdot$$

$$\cdot i^{l_{\mathrm{p}}-l_{\mathrm{d}}-l'_{\mathrm{p}}-l'_{\mathrm{d}}}\hat{l}_{\mathrm{n}}^2\hat{l}_{\mathrm{p}}^2\hat{l}_{\mathrm{p}}^2\hat{l}_{\mathrm{d}}\hat{l}'_{\mathrm{d}}\hat{j}_{\mathrm{p}}^2\hat{j}_{\mathrm{p}}'^2\hat{e}^2\hat{f}^2\hat{g}^2\hat{a}^2|\gamma_{l_{\mathrm{n}}j_{\mathrm{n}}}|^2\cdot$$

$$\cdot A(l_{\mathrm{n}},l_{\mathrm{p}},j_{\mathrm{p}},l_{\mathrm{d}})A^{*}(l_{\mathrm{n}},l'_{\mathrm{p}},j'_{\mathrm{p}},l'_{\mathrm{d}})\langle T^{\mathrm{d}}_{\lambda\varkappa}\rangle(l_{\mathrm{n}}0l_{\mathrm{p}}0\,|\,l_{\mathrm{d}}0)\cdot$$

$$\cdot(l_{\mathrm{n}}0l'_{\mathrm{p}}0\,|\,l'_{\mathrm{d}}0)(l_{\mathrm{p}}0l'_{\mathrm{p}}0\,|\,p0)(l_{\mathrm{d}}0l'_{\mathrm{d}}0\,|\,d0)(\lambda'\varkappa' g-\varkappa'\,|\,p0)(\lambda\varkappa g-\varkappa\,|\,d0)(-1)^{\lambda'+\varkappa'+\varkappa}\mathscr{D}^{g}_{\varkappa\varkappa'}(\Phi,\Theta,0)\cdot$$

$$\cdot(-1)^{s_{\mathrm{n}}+l_{\mathrm{n}}-j_{\mathrm{n}}}W(l_{\mathrm{n}}s_{\mathrm{n}}l_{\mathrm{n}}s_{\mathrm{n}};j_{\mathrm{n}}e)(-1)^{e+g+d}W(gdfe;\lambda a)\cdot$$

$$\cdot\begin{Bmatrix} l'_{\mathrm{p}} & l_{\mathrm{p}} & p\\ s_{\mathrm{p}} & s_{\mathrm{p}} & \lambda'\\ j'_{\mathrm{p}} & j_{\mathrm{p}} & g\end{Bmatrix}\begin{Bmatrix} l'_{\mathrm{p}} & l_{\mathrm{p}} & a\\ s_{\mathrm{p}} & s_{\mathrm{p}} & f\\ j'_{\mathrm{p}} & j_{\mathrm{p}} & g\end{Bmatrix}\begin{Bmatrix} s_{\mathrm{n}} & s_{\mathrm{n}} & e\\ s_{\mathrm{p}} & s_{\mathrm{p}} & f\\ s_{\mathrm{d}} & s_{\mathrm{d}} & \lambda\end{Bmatrix}\begin{Bmatrix} l'_{\mathrm{p}} & l_{\mathrm{p}} & a\\ l'_{\mathrm{d}} & l_{\mathrm{d}} & d\\ l_{\mathrm{n}} & l_{\mathrm{n}} & e\end{Bmatrix},$$

where the second sum runs over l_{n}, j_{n}, l_{p}, j_{p}, l'_{p}, j'_{p}, l_{d}, l'_{d}, a, e, f, p, d and g with these restrictions on the sum over l_{n}, j_{n}:

$$(5)\qquad \begin{cases} |I_f-I_i|\leqslant j_{\mathrm{n}}\leqslant I_f+I_i\,,\\ (-1)^{l_{\mathrm{n}}}=\Pi_i\Pi_f\,,\end{cases}$$

following from the conservation laws for angular momenta and parities.

The quantities $A(l_{\mathrm{n}},l_{\mathrm{p}},j_{\mathrm{p}},l_{\mathrm{d}})$ are given by

$$(6)\qquad A(l_{\mathrm{n}},l_{\mathrm{p}},j_{\mathrm{p}},l_{\mathrm{d}})=\varkappa_{\mathrm{n}}k_{\mathrm{p}}k_{\mathrm{d}}\int_{R}^{\infty}\frac{h^{(1)}_{l_{\mathrm{n}}}(i\varkappa_{\mathrm{n}}r)}{h^{(1)}_{l_{\mathrm{n}}}(i\varkappa_{\mathrm{n}}R)}\,u_{l_{\mathrm{p}},j_{\mathrm{p}}}\left(k_{\mathrm{p}};\frac{M_i}{M_f}\,r\right)u_{l_{\mathrm{d}}}(k_{\mathrm{d}};r)\,r^2\,\mathrm{d}r\,,$$

where k_{p} and k_{d} are proton and deuteron wave numbers, respectively, for the corresponding relative motions in the c.m. system. $\varkappa_{\mathrm{n}}$ is given by $\varkappa_{\mathrm{n}}^2=2M_{\mathrm{n}}^{*}\varepsilon_{\mathrm{n}}/\hbar^2$, where ε_{n} is the binding energy for the captured neutron. $u_{l_{\mathrm{p}},j_{\mathrm{p}}}(k_{\mathrm{p}};r_{\mathrm{p}})$ and $u_{l_{\mathrm{d}}}(k_{\mathrm{d}};r_{\mathrm{d}})$ are solutions of the radial Schrödinger equation containing the appropriate potential for the V_{FP} or V_{TD} interactions, respectively (including the Coulomb interaction). $T^{\mathrm{d}}_{\lambda\varkappa}$ are components of the tensor operator in the co-ordinate system in which the z axis lies along the vector $\boldsymbol{k}_{\mathrm{d}}$. $T^{\mathrm{p}}_{\lambda'\varkappa'}$, however, are components in the co-ordinate system in which the z axis lies along the vector $\boldsymbol{k}_{\mathrm{p}}$ and the y axis along the vector $\boldsymbol{k}_{\mathrm{d}}\times\boldsymbol{k}_{\mathrm{p}}$. These two co-ordinate systems are connected by Eulerian angles $(\Phi,\Theta,0)$ where Φ and Θ are scattering angles.

Putting $\lambda'=\varkappa'=0$ in the formula (4) we obtain the angular distribution for protons (arbitrary polarized deuterons) [1].

[1] These two particular cases are treated in the article by L. J. B. Goldfarb and R. C. Johnson: *Nucl. Phys.*, **18**, 353 (1960).

The formula contains the polarization and angular distribution of protons when incident deuterons are unpolarized. In this case we have $\langle T^{\mathrm{d}}_{\lambda\varkappa}\rangle = 0$ for $\lambda \neq 0$ so that only one term remains from the sum over λ and $\varkappa$, *i.e.* the term with $\lambda = \varkappa = 0$ in which $\langle T^{\mathrm{d}}_{00}\rangle = 1$ [1].

From the formula (4) one can come to some conclusions without performing any calculations. For example:

1) if the polarizing term in the V_{FP} interaction is neglected, it will follow that: *a*) there are no contribution from $\langle T^{\mathrm{d}}_{2\varkappa}\rangle$ in the angular distribution for protons, *b*) there are no polarization effects if the condition

$$\frac{|\gamma_{l_{\mathrm{n}}, l_{\mathrm{n}}+\frac{1}{2}}|^2}{|\gamma_{l_{\mathrm{n}}, l_{\mathrm{n}}-\frac{1}{2}}|^2} = \frac{l_{\mathrm{n}}+1}{l_{\mathrm{n}}}, \tag{7}$$

is fulfilled.

2) To get the polarization effects under the condition (7) we must suppose the polarizing term in the V_{FP} interaction. It is easy to see that in this case neither the polarization nor angular distribution of protons depends on $\langle T^{\mathrm{d}}_{2\varkappa}\rangle$.

One now concludes that the information about the quantities $\langle T^{\mathrm{d}}_{1\varkappa}\rangle$ in both extreme cases mentioned above can be obtained by measuring only the angular distribution of outgoing protons. However, both polarization effects must be present if one wishes to get any information about $\langle T^{\mathrm{d}}_{2\varkappa}\rangle$ in the same way.

A Search for the Decay $\Sigma^+ \to p + \gamma$ (*).

R. G. Glasser and N. Seeman
U. S. Naval Research Laboratory - Washington, D. C.

Y. Prakash, G. A. Snow and P. Steinberg
University of Maryland - College Park, Md.

(ricevuto il 31 Ottobre 1960)

A search for the decay $\Sigma^+ \to p + \gamma$ was carried out in two emulsion stacks exposed to 300 MeV/c K^--mesons at the Bevatron of the Lawrence Radiation Laboratory.

Two somewhat different methods were employed. The Naval Research Laboratory group followed out all grey and black tracks from 3 037 K^--stars [1]. The Maryland group followed out all secondary tracks from 13 290 K^--stars until they either left the pellicle of the parent star or came to rest in that pellicle. All secondary tracks that apparently came to rest and gave rise to a *single* grey or black prong were examined. The ranges of these prongs were carefully measured.

This sample of events consists primarily of $\Sigma^+ \to p + \pi^0$ decays at rest and Σ^- one prong capture stars. The disintegration of the Σ^+ at rest into a proton and a γ-ray gives rise to a proton of unique range of the order of 3 000 μm.

No events having protons of this range were observed. In this sample, 144 events consistent with $\Sigma^+ \to p + \pi^0$ were found (NRL 70, Maryland 74).

Two definite examples and one possible example of $\Sigma^+ \to p + \gamma$ have been reported by Quareni *et al.* [2]. They estimate a branching ratio $(p+\gamma)/(p+\pi^0)$ of the order of 1%.

Clearly negative results such as the one reported here should be combined with the one reported positive result in order to obtain a more accurate value for the $(p+\gamma)/(p+\pi^0)$ branching ratio.

(*) This work supported in part by the U. S. Atomic Energy Commission.

(1) A preliminary report of this work appeared in N.R.L. *Quart. on Nucl. Sci. and Techn.* (April, 1960).

(2) G. Quareni, A. Quareni Vignudelli, G. Dascola and S. Mora: *Nuovo Cimento*, **14**, 1179 (1959).

IL NUOVO CIMENTO Vol. XIX, N. 5 1° Marzo 1961

Covariant Quantization of the Gravitational Field.

J. R. Klauder

Bell Telephone Laboratories, Incorporated - Murray Hill, N. J.

(ricevuto il 21 Novembre 1960)

It is expected that the familiar factor-ordering problem will be encountered when the Einstein gravitational field is quantized [1]. However, at least one additional problem will be encountered, special to the gravitational field, which does not occur in the quantization of either a Lorentz invariant field or any generally-covariant field when the metric tensor is assumed fixed. The additional problem in quantized general relativity is created by the necessity to specify the initial data of the metric field $g_{\mu\nu}(x)$ on a space-like surface — a three-surface in the four-manifold — on which, prior to the solution of the problem, the metric cannot be defined. Consequently, without a solution of the entire problem at hand, it is not possible to select an appropriate initial surface that is manifestly space-like. Several recent proposals to quantize the gravitational field have been based on sacrificing complete covariance and have concentrated on expressing the Hamiltonian in terms of « basic » gravitational variables [2]. All of these quantization techniques essentially ignore the conceptual problem encountered in selecting an initial space-like surface in a manifold with no metric.

Our purpose is to point out that this conceptual problem can be eliminated and the quantization accomplished in a completely covariant manner. The necessary mathematical formalism is akin to the external-field formalism introduced by Schwinger [3]. More recently, a reinterpretation of the external-field formalism has been proposed which provides a completely covariant, self-contained quantization procedure [4]. Novizolov and Tulub, for example, present an excellent review of this covariant point of view [5]. The application of this so-called four-dimensional quantization (or hyperquantization) technique to the gravitational field is briefly discussed below.

---

[1] The factor-ordering problem has been discussed, for example, by C. W. Misner: *Rev. Mod. Phys.*, **29**, 497 (1957); and by R. Arnowitt and S. Deser: *Phys. Rev.*, **113**, 745 (1959).

[2] P. A. M. Dirac: *Proc. Roy. Soc.*, A **246**, 333 (1958); R. Arnowitt and S. Deser: *Phys. Rev.*, **113**, 745 (1959); R. Arnowitt, S. Deser and C. W. Misner: *Phys. Rev.*, **116**, 1322 (1959).

[3] J. Schwinger: *Proc. Nat. Acad. Sci.*, **37**, 452 (1951).

[4] F. Coester: *Phys. Tev.*, **95**, 1318 (1954); J. M. Jauch: *Helv. Phys. Acta*, **29**, 287 (1954); J. G. Valatin: *Nuovo Cimento*, **4**, 726 (1956).

[5] J. V. Novozilov and A. V. Tulub: *Fortschr. d. Phys.*, **6**, 50 (1958).

In order to characterize the pure gravitational field, the integral of the contracted Ricci curvature is chosen to represent the classical action functional (units: $c = 16\pi G = \hbar = 1$; the summation convention for Greek indices, equal to 0, 1, 2, or 3, is employed).

$$I = \int R_{\mu\nu} g^{\mu\nu} (-g)^{\frac{1}{2}} \, \mathrm{d}x \, . \tag{1}$$

The Ricci curvature tensor $R_{\mu\nu}$ is obtained by one contraction of the four-index Riemann curvature tensor, and $R_{\mu\nu}$ is a function of the metric and its derivatives up to second order (6).

In the covariant four-dimensional quantization procedure all components of the metric tensor commute with each other at any two space-time points x and y, *i.e.*,

$$[g_{\mu\nu}(x), g_{\sigma\tau}(y)] = 0 \, . \tag{2}$$

Besides the metric tensor, a symmetric tensor $v_{\mu\nu}(x)$ is introduced whose components, while commuting among themselves, obey the following commutation rules with the metric tensor:

$$[(-g)^{\frac{1}{2}} g^{\sigma\tau}(x), v_{\mu\nu}(y)] = -\frac{i}{2} (\delta^{\sigma}_{\mu}\delta^{\tau}_{\nu} + \delta^{\tau}_{\mu}\delta^{\sigma}_{\nu}) \, \delta(x - y) \, , \tag{3}$$

as well as

$$[g^{\sigma\tau}(x), v_{\mu\nu}(y)] = -\frac{i}{2} (-g)^{-\frac{1}{2}} [\delta^{\sigma}_{\mu}\delta^{\tau}_{\nu} + \delta^{\tau}_{\mu}\delta^{\sigma}_{\nu} - g_{\mu\nu}(x) \, g^{\sigma\tau}(y)] \, \delta(x - y) \, , \tag{4}$$

where $\delta(x - y)$ denotes the invariant four-dimensional δ-function. In addition to $v_{\mu\nu}$ a tensor $\mathfrak{V}_{\mu\nu}$ exists, which satisfies

$$[g^{\sigma\tau}(x), \mathfrak{V}_{\mu\nu}(y)] = -\frac{i}{2} (\delta^{\sigma}_{\mu}\delta^{\tau}_{\nu} + \delta^{\tau}_{\mu}\delta^{\sigma}_{\nu}) \, \delta(x - y) \, , \tag{5}$$

and is defined in terms of $v_{\sigma\tau}$ and $g^{\sigma\tau}$ as follows:

$$\mathfrak{V}_{\sigma\tau} = \tfrac{1}{2} [(v_{\sigma\tau} - \tfrac{1}{2} v_{\alpha\beta} g^{\alpha\beta} g_{\sigma\tau})(-g)^{\frac{1}{2}} + \text{H.c.}] \, , \tag{6}$$

where H. c. denotes the Hermitian conjugate expression. Let $\bar{g}^{\mu\nu}$ given by

$$\bar{g}^{\mu\nu} = -i[-\det (\delta/\delta v_{\sigma\tau})]^{-\frac{1}{2}} (\delta/\delta v_{\mu\nu}) \, , \tag{7}$$

denote the functional differential form for $g^{\mu\nu}$ that satisfies eqs. (3) and (4). Then, the functional differential equation,

$$\left\{(-\bar{g})^{\frac{1}{2}} [R_{\mu\nu}(\bar{g}^{\tau\lambda}) - \tfrac{1}{2} R(\bar{g}^{\tau\lambda}) \bar{g}_{\mu\nu}] + \mathfrak{V}_{\mu\nu}(\bar{g}^{\tau\lambda})\right\} \Omega(v_{\mu\nu}) = 0 \, , \tag{8}$$

(6) Our notation follows that of L. LANDAU and E. LIFSHITZ: *Classical Theory of Fields* (Cambridge, 1951).

where the dependence of various terms on $\bar{g}^{\tau\lambda}$ has been indicated, represents the « four-dimensional » counterpart of the Tomonaga-Schwinger equation, and of course, Ω is the appropriately generalized « wave vector ». One formal solution to eq. (8) can readily be expressed as a functional integral over metrics:

$$\Omega_3(v_{\mu\nu}) = \int \exp\left[i \int (v_{\mu\nu} + R_{\mu\nu}) g^{\mu\nu} (-g)^{\frac{1}{2}} \, \mathrm{d}x\right] \mathscr{D}g \ , \tag{9}$$

where the symbol $\int \ldots \mathscr{D}g$ instructs one to carry out an equally weighted summation over all permissible metrics in the entire manifold. The choice for $\mathfrak{R}_{\mu\nu}$ given by eq. (6) restricts the measure on metrics $\mathscr{D}g$ to be identical with that found by MISNER (7), namely,

$$\mathscr{D}g \propto \Pi_x [-g(x)]^{-\frac{5}{2}} \Pi_{\mu \leq \nu} \, \mathrm{d}g_{\mu\nu}(x) \ . \tag{10}$$

As usual the product over points is best interpreted as the limit of a denumerable product over a space-time lattice of points. It is the ambiguity in defining functional integrals such as eq. (9) - an ambiguity so apparent in the case of a denumerable number of points — that is the analog of the factor-ordering ambiguity in quantum mechanics.

The field $v_{\mu\nu}$ has little connection with the representation of the wave function Ω_0 in the traditional sense. In fact, in the four-dimensional formalism, the traditional representation is already largely preselected: the functional Ω_0 is a generating functional for « outgoing » eigenstates expressed in the representation of the « incoming » eigenstates (8). In familiar scattering problems the « incoming » and « outgoing » states generally consist of a collection of isolated stable particles, which are either elementary particles or bound combinations thereof. One possible analog in the gravitational case consists of « incoming » and « outgoing » states that are collections of isolated « wormholes » (9), each of which is essentially a stable concentration of gravitational energy. Of course, interesting questions are not confined to scattering problems. The « incoming » and « outgoing » states may even belong to spaces of differing topological character (10).

Instead of solving eq. (8) for each example, a particular « transition element » $\Omega_{\mathcal{A}}(v_{\mu\nu})$ can also be obtained by applying $\mathcal{A}(v_{\mu\nu}, \delta/\delta v_{\mu\nu})$, one of a class of appropriate covariant functional differential operators, to the functional Ω_0. In this sense Ω_0 may be viewed as a cyclic vector (11). In principle, a knowledge of Ω_0 and the various operators $\mathcal{A}$ would enable a determination of all the transition elements of physical interest without regard to the space-like character of any particular surface.

(7) C. W. MISNER: *Rev. Mod. Phys.*, **29**, 497 (1957).

(8) C. N. YANG and O. FELDMAN: *Phys. Rev.*, **79**, 972 (1950).

(9) Wormhole, is the picturesque name for a multiple connected region of space-time whose importance has been stressed by J. A. WHEELER: *Phys. Rev.*, **97**, 511 (1955).

(10) Several discussions with Dr. J. G. FLETCHER have helped clarify the role of topology in quantized relativity, as well as the intrinsic difficulty in selecting an initial space-like surface.

(11) R. HAAG and F. COESTER: *Phys. Rev.*, **117**, 1137 (1960); H. ARAKI: *Thesis* (Princeton University, 1960); compare an analogous generating functional discussed, for example, by J. L. ANDERSON: *Phys. Rev.*, **94**, 703 (1954).

Recoil Proton Polarization in π^--p Elastic Scattering at 600 MeV (*).

P. Franzini (**) and J.-M. Gaillard (***)
Columbia University - New York, N. Y.

(ricevuto il 9 Dicembre 1960)

The purpose of the present letter is to show what information on the phase shifts of the π-nucleon system can be obtained from the angular distribution of the recoil proton polarization in π^--p elastic scattering at 600 MeV.

It is now well established that the total π^--p cross section has a peak around 600 MeV ([1-4]). The first evidence was found in photoproduction experiments ([5-7]). Since no increase was observed in π^+-p total cross section ([1,3]), it is assumed that the observed effect is due to a $T=\frac{1}{2}$ state. Those experiments have shown also that the increase of the total cross section is mainly due to the elastic process. Different interpretations have been given in terms of a P_{13} resonant state by Wilson ([8]), and in terms of a D_{13} resonant state by Peierls ( ). The total angular momentum was assumed to be $J=\frac{3}{2}$ in both cases.

For the case of photoproduction, Sakurai ([10]) predicted a large polarization of the recoil proton of $\gamma+p\to\pi^0+p$ in the D_{13} case; if the resonant state were P_{13}, the polarization should be small. A large polarization was found by several authors ([11]), but it has since been pointed out by Landovitz and Marshall ([12]) that all the results of the

(*) Partially supported by the United States Atomic Energy Commission.

(**) Fulbright Fellow. On leave from the University of Pisa (Italy).

(***) On leave from the CEN of Saclay (France).

([1]) H. C. Burrowes, D. O. Caldwell, D. H. Frisch, D. A. Hill, D. M. Ritson, R. A. Schluter and M. A. Wahlig: *Phys. Rev. Lett.*, **2**, 119 (1959).

([2]) R. R. Crittenden, J. H. Scandrett, W. D. Shephard, W. D. Walker and J. Ballam: *Phys. Rev. Lett.*, **2**, 121 (1959).

([3]) J. C. Brisson, J. Detoef, P. Falk-Vairant, L. van Rossum, G. Valladas and L. C. L. Yuan: *Phys. Rev. Lett.*, **3**, 561 (1959).

([4]) J.-M. Gaillard, P. Lehmann, A. Lèvêque, J. Meyer, D. Revel and J. Sacton: *Compt. Rend.*, **249**, 1497 (1959).

([5]) J. W. DeWire, H. E. Jackson and R. Littauer: *Phys. Rev.*, **110**, 1208 (1958).

([6]) P. C. Stein and K. C. Rogers: *Phys. Rev.*, **110**, 1209 (1958).

([7]) M. Heinberg, W. M. McClelland, F. Turkot, W. M. Woodward, R. R. Wilson and D. M. Zipoy: *Phys. Rev.*, **110**, 1211 (1958).

([8]) R. R. Wilson: *Phys. Rev.*, **110**, 1212 (1958).

([9]) R. F. Peierls: *Phys. Rev. Lett.*, **1**, 174 (1958).

([10]) J. J. Sakurai: *Phys. Rev. Lett.*, **1**, 258 (1958).

([11]) P. C. Stein: *Phys. Rev. Lett.*, **2**, 173 (1959); L. Bertanza, P. Franzini, I. Mannelli, G. V. Silvestrini and V. Z. Peterson: on *Nuovo Cimento*, **19**, 467 (1961); R. Querzoli *et al.*: private communication.

([12]) L. F. Landovitz and L. Marshall: *Phys. Rev. Lett.*, **3**, 190 (1959).

photoproduction, including the high polarization, can be explained by an interference between a second P_{13} resonance and a third resonance of proper parity. At the present time, although there is good evidence in favor of a D_{13} resonance, it seems difficult to make any definite conclusion before a complete analysis in terms of *SPD* phase shifts is done.

The actual experimental results are not sufficient to permit such an analysis. Although it is possible, as has been shown by WALKER ([13]), to get a unique set of phase shifts which satisfy continuity conditions with respect to the energy, this kind of analysis does not give any evidence that one of the phase shifts for P_{13} or for D_{13} is equal to 90°.

An *SPD* analysis implies the determination of 20—1=19 parameters (*). By measuring angular distributions for $\pi^{\pm}$+p elastic scattering, total cross sections for $\pi^{\pm}$+p, and total cross sections for the following reactions,

$$\pi^- + p \to \pi^- + \pi^+ + n\,,$$
$$\pi^- + p \to \pi^- + \pi^0 + p\,,$$
$$\pi^+ + p \to \pi^+ + \pi^+ + n\,,$$

one obtains 15 independent pieces of information (**). Five more numbers could be obtained by the angular distribution of π^-+p $\to \pi^0$+n; however, it is difficult to obtain accurate data for this last reaction.

Measurements of the recoil proton polarization in π^-+p are useful for two reasons:

1) They give four more independent pieces of information;

2) There will probably be ambiguities if the phase shifts are determined from the cross sections alone; the polarization angular distribution will permit the elimination of some sets. In the case of the 600 MeV π^-+p resonance, this difference should provide a means of deciding between D_{13} and P_{13}.

For computing the polarization, we have first analyzed, in terms of phase shifts, the angular distribution for the π^--p elastic scattering from Saclay ([4]) (*). We did three different analyses of this distribution starting from the set of phase shifts given by WALKER ([13]) and assuming:

1) No resonance;
2) $\delta_{13} = 90°$;
3) $\alpha_{13} = 90°$.

The analysis has been done looking for the best fit to the experimental

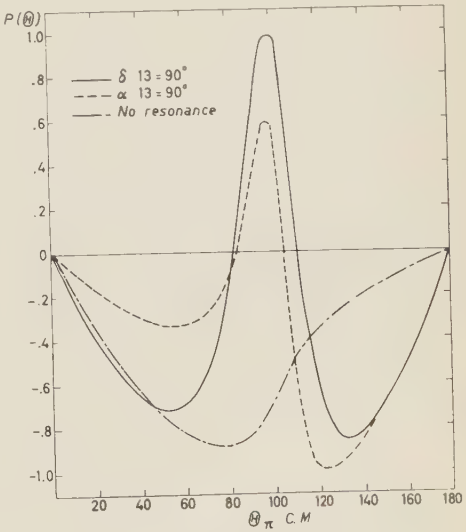

Fig. 1.

([13]) W. D. WALKER, J. DAVIS and W. D. SHEPHARD: *Phys. Rev.*, **118**, 1612 (1961).

(*) The notation is $L_{2T,2J}$ for the states. The real parts of the phase shifts will be denoted by $\alpha_{2T,2J}$ for *S* and *P* waves, and by $\delta_{2T,2J}$ for the *D* waves. The η's are equal to $\exp[-2\,\mathrm{Im}\,\alpha]$.

(**) Data for those processes will be available soon from Saclay with very good statistics ($\sim$1500 events for the angular distributions).

(*) This angular distribution, based on 300 events, has been obtained in a hydrogen chamber with an energy definition of 15 MeV and is slightly different from the distribution found by CRITTENDEN *et al.* ([2]) at the same energy in a propane chamber.

distribution. The results given by a least square analysis show a good fit for the three cases. Two additional checks have been done by computing the total cross sections for π^-+p and π^++p. The results are within the experimental errors. All the computations have been done with the IBM 650 at Nevis. The values obtained for the phase shifts are given by Table I. We have then computed the polarization angular distribution for the three sets. Results are shown in Fig. 1. The difference between the curves is less pronounced than that predicted in the case of the photoproduction. However, it is still possible to distinguish experimentally between the three cases.

Using carbon as an analyzer, kinematics of π-p scattering will allow the measurement of the polarization between 60° and 120° in the c.m.

An experiment in which 2000 scatterings of the recoil proton on a carbon analyser are observed will give the polarization with an absolute error of about 10%.

In conclusion, even if the sets of phase shifts which will be finally determined with a greater amount of data prove to be different, one can hope that a similar qualitative difference will remain between the three cases, and that a selection of the correct set of phase shifts will still be possible from polarization measurements.

TABLE I.

No resonance		$\delta_{13} = 90°$		$\alpha_{13} = 90°$	
$\alpha_1 = 65°$	$\eta_1 = 0.8$	$\alpha_1 = 30°$	$\eta_1 = 0.6$	$\alpha_1 = 40°$	$\eta_1 = 0.6$
$\alpha_3 = -50°$	$\eta_3 = 0.6$	$\alpha_3 = -35°$	$\eta_3 = 1$	$\alpha_3 = -35°$	$\eta_3 = 1$
$\alpha_{11} = 18°$	$\eta_{11} = 0.6$	$\alpha_{11} = 35°$	$\eta_{11} = 0.4$	$\alpha_{11} = 10°$	$\eta_{11} = 0.2$
$\alpha_{31} = -20°$	$\eta_{31} = 1$	$\alpha_{31} = -20°$	$\eta_{31} = 0.8$	$\alpha_{31} = -30°$	$\eta_{31} = 1$
$\alpha_{13} = -14°$	$\eta_{13} = 0.6$	$\alpha_{13} = -15°$	$\eta_{13} = 1$	$\alpha_{13} = 90°$	$\eta_{13} = 0.4$
$\alpha_{33} = 155°$	$\eta_{33} = 1$	$\alpha_{33} = 160°$	$\eta_{33} = 1$	$\alpha_{33} = 162.5°$	$\eta_{33} = 1$
$\delta_{13} = 20°$	$\eta'_{13} = 0.5$	$\delta_{13} = 90°$	$\eta'_{13} = 0.5$	$\delta_{13} = 10°$	$\eta'_{13} = 0.85$
$\delta_{33} = 8°$	$\eta'_{33} = 1$	$\delta_{33} = 10°$	$\eta'_{33} = 1$	$\delta_{33} = 8°$	$\eta'_{33} = 1$
$\delta_{15} = -5°$	$\eta'_{15} = 1$	$\delta_{15} = -2.1°$	$\eta'_{15} = 1$	$\delta_{15} = -2°$	$\eta'_{15} = 1$
$\delta_{35} = -3.3°$	$\eta'_{35} = 0.8$	$\delta_{35} = -2.3°$	$\eta'_{35} = 1$	$\delta_{35} = -1.3°$	$\eta'_{35} = 1$

A Network Approach to the Analysis of Čerenkov Radiation Problems.

Comment on the paper «On the Theory of some Čerenkovian Effects» by G. Toraldo di Francia.

L. B. Felsen (*)

Office of Naval Research - London

A. Hessel (**)

Microwave Research Institute - Brooklyn

(ricevuto il 5 Gennaio 1961)

In a recent paper (1), Toraldo di Francia has studied certain Čerenkov radiation effects arising from the motion of a charged particle in the vicinity of plane stratified dielectric media and plane diffraction gratings. Basic to the analysis is the decomposition of the field in vacuum generated by a charged particle in uniform straight motion along the x-axis of a chosen co-ordinate system into a set of waves which decay exponentially away from a fictitious reference plane containing the particle trajectory (x-y plane). The use of these waves, which separate into TE and TM modes relative to the (z) direction perpendicular to the reference plane, facilitates the matching of the electromagnetic field components required in the presence of obstacle configurations whose planar interfaces are parallel to the x-y plane. Toraldo di Francia obtains his formulation by representing the known closed form expression for the vector electromagnetic fields associated with the moving charge in terms of a double Fourier integral, and determines the TE and TM mode amplitudes by utilizing the inverse Fourier transform. The rather complicated evaluation of the *vector* mode amplitudes, requiring the calculation of various integrals, comprises a major portion of Toraldo di Francia's paper.

It is the purpose of this note to present an alternative procedure which, through the utilization of network concepts, leads more directly to the modal representation derived by Toraldo di Francia, and which permits one to account for the presence of perturbing objects near the particle trajectory in a straightforward manner. While a network approach to the analysis of the fields radiated by arbitrary electro-

(*) Office of Naval Research, Branch Office London, on leave of absence from the Microwave Research Institute, Polytechnic Institute of Brooklyn.

(**) Microwave Research Institute, Polytechnic Institute of Brooklyn.

(1) G. Toraldo di Francia: *Nuovo Cimento*, **16**, 61 (1960).

magnetic sources in isotropic regions has received attention in the literature [5], it does not appear to have been utilized systematically in the study of Čerenkov type radiation problems. The authors are currently engaged in an investigation of network methods for the analysis of the electromagnetic fields caused by a particle in uniform straight motion in the vicinity of certain classes of planar and cylindrical isotropic and anisotropic configurations. However, at this time we recall only the network derivation of the modal representation of the particle field in plane stratified isotropic regions, from which the free space formulas derived by Toraldo di Francia emerge as a special case.

The aim of the network procedure utilizing a modal decomposition with respect to a certain preferred co-ordinate, the transmission co-ordinate, is the reduction of the vector electromagnetic field problem to a *scalar* network problem involving transmission lines, one for each mode. The effects of the current source (and of any perturbing objects along the transmission co-ordinate) are represented as active (and passive) loadings on the various transmission lines, and the desired modal amplitudes, *i.e.*, the transmission line voltages and currents, are determined by a conventional network calculation. A given mode is identified by fixed wavenumbers descriptive of its temporal and transverse spatial periodicities whence, for the representation of a field depending on both space and time, one requires a spatial and temporal superposition of modes. Since the temporal dependence of a typical mode is expressed by the function $\exp[\pm i\omega t]$, $\omega > 0$, while its detailed spatial variation depends upon the choice of a particular co-ordinate system, it is convenient and conventional to eliminate the time dependence at the outset. If $\hat{\boldsymbol{E}}(\boldsymbol{r}, t)$, $\hat{\boldsymbol{H}}(\boldsymbol{r}, t)$, $\hat{\boldsymbol{J}}(\boldsymbol{r}, t)$ denote the space-time dependent vector electric field, magnetic field, and electric source current, respectively, the Fourier integral representation

$$\hat{\boldsymbol{Q}}(\boldsymbol{r}, t) = \frac{1}{2\pi}\int_{-\infty}^{\infty} \boldsymbol{Q}(\boldsymbol{r}, \omega) \exp[-i\omega t]\, \mathrm{d}\omega \,, \tag{1}$$

implies that the spectrum function $\boldsymbol{Q}(\boldsymbol{r}, \omega)$ is given by

$$\boldsymbol{Q}(\boldsymbol{r}, \omega) = \int_{-\infty}^{\infty} \hat{\boldsymbol{Q}}(\boldsymbol{r}, t) \exp[i\omega t]\, \mathrm{d}t \,, \tag{2}$$

where $\hat{\boldsymbol{Q}}$ stands for either $\hat{\boldsymbol{E}}$, $\hat{\boldsymbol{H}}$ or $\hat{\boldsymbol{J}}$.

For the case of a particle with charge q moving parallel to the x-co-ordinate with constant speed v, one has [6]

$$\hat{\boldsymbol{J}}(\boldsymbol{r}, t) = \boldsymbol{x}_0 q v\, \delta(x - vt)\, \delta(y)\, \delta(z - z') \,, \tag{3}$$

where $\boldsymbol{x}_0$ is a unit vector along the positive x direction. From eq. (2) one obtains for the current spectrum function

$$\boldsymbol{J}(\boldsymbol{r}, \omega) = \boldsymbol{x}_0 q \exp[ikx/\beta]\, \delta(y)\, \delta(z - z') \,, \qquad k = \frac{\omega}{c} \,, \quad \beta = \frac{v}{c} < 1 \,. \tag{4}$$

[5] N. Marcuvitz and J. Schwinger: *Journ. Appl. Phys.*, **22**, 806 (1951).
[6] MKS units employed throughout.

i.e., the corresponding steady-state problem has for its excitation an infinite line source of electric current having a linearly varying phase, located at co-ordinates $y=0$, $z=z'$. In regions which are homogeneous along the x co-ordinate, such a source will excite waves whose phase velocity along x is given by v. Since $v<c$, where c is the speed of light in vacuum, these waves are « slow » waves in vacuum, whence one recognizes from the analogy with the propagation of surface waves that the associated fields decay exponentially away from the source and there is no radiation in the transverse direction. In the corresponding network picture the transmission line, representative of propagation along a transverse (z) co-ordinate, is below cut-off (*).

To obtain Toraldo di Francia's representation we choose a rectangular waveguide description for the infinite cross-section in the x-y plane, with z as the transmission co-ordinate. A network analysis of the fields radiated by arbitrary prescribed source distributions in uniform waveguides has been presented previously [4] and is summarized below. As is well known, the electromagnetic fields are expressible in terms of two scalar (hertzian) potential functions $\pi'(\boldsymbol{r}, \omega)$ and $\pi''(\boldsymbol{r}, \omega)$ comprising TM mode and TE mode contributions, respectively, with respect to the z direction (**):

— *TM modes*

$$(5a) \qquad \boldsymbol{E}'(\boldsymbol{r}, \omega) = \nabla \times \nabla \times [\boldsymbol{z}_0 \pi'(\boldsymbol{r}, \omega)], \qquad \boldsymbol{H}'(\boldsymbol{r}, \omega) = -i\omega\varepsilon \nabla \times [\boldsymbol{z}_0 \pi'(\boldsymbol{r}, \omega)],$$

— *TE modes*

$$(5b) \qquad \boldsymbol{E}''(\boldsymbol{r}, \omega) = i\omega\mu \nabla \times [\boldsymbol{z}_0 \pi''(\boldsymbol{r}, \omega)], \qquad \boldsymbol{H}''(\boldsymbol{r}, \omega) = \nabla \times \nabla \times [\boldsymbol{z}_0 \pi''(\boldsymbol{r}, \omega)],$$

$\boldsymbol{z}_0$ is a unit vector along the z direction and ε and μ are the dielectric constant and permeability of the medium, respectively. Modal representations for the potential functions are given formally by:

$$(6a) \qquad \pi'(\boldsymbol{r}, \omega) = \frac{1}{-i\omega\varepsilon} \sum_i I'_i(z, \omega) \frac{\varphi_i(x, y)}{k'_{ti}},$$

$$(6b) \qquad \pi''(\boldsymbol{r}, \omega) = \frac{1}{-i\omega\mu} \sum_i V''_i(z, \omega) \frac{\psi_i(x, y)}{k''_{ti}},$$

I'_i, φ_i, k'_{ti} are the transmission line current, scalar mode function, and transverse wavenumber, respectively, for the i-th TM mode, while V''_i, ψ_i, k''_{ti} are the transmission line voltage, scalar mode function and transverse wavenumber, respectively, for the i-th TE mode. For the present case of an infinite waveguide cross section,

(*) However, as noted by Toraldo di Francia [see also Pierce (3)] radiation occurs in the presence of media or geometrical configurations which either can support suitable transversely propagating modes (*e.g.*, a medium with relative dielectric constant $\varepsilon' > c^2/v^2$) or provide coupling to such modes (*e.g.*, a periodic structure such as a grating).

(**) All the formulas listed herein are appropriate to a time factor $\exp[-i\omega t]$ corresponding to the range $0<\omega<\infty$ in eq. (1). For the range $-\infty<\omega<0$, equivalent to an $\exp[i\omega t]$ dependence, $0<\omega<\infty$, all $i=\sqrt{-1}$ should be replaced by $(-i)$, except for the factor $\exp[ikx/\beta]$ which retains this form for all ω [see eq. (4)].

(3) J. R. Pierce: *Journ. Appl. Phys.*, **26**, 627 (1955).

(4) L. B. Felsen and N. Marcuvitz: Polytechnic Institute of Brooklyn, Microwave Research Institute, R-446-55 *a*) and *b*). *Modal Analysis and Synthesis of Electromagnetic Fields* (1956).

the mode set is continuous so that the summations in eqs. (6) are replaced by integrals and the scalar mode functions φ_i, ψ_i and the transverse wavenumbers k'_{ti}, k''_{ti} are identical. Moreover, the fields excited by the line source in eq. (4) in a plane stratified region (along z) have, from symmetry considerations,[1] an x-dependence $\exp[ikx/\beta]$. Hence,

$$\varphi_\eta(x, y) = \psi_\eta(x, y) = \varphi_\eta(y) \exp[ikx/\beta], \qquad \varphi_\eta(y) = \frac{\exp[i\eta y]}{\sqrt{2\pi}}, \qquad -\infty < \eta < \infty, \tag{7a}$$

$$\sum_i \to \int_{-\infty}^{\infty} \mathrm{d}\eta, \qquad k'_{t\eta} = k''_{t\eta} = \left(\frac{k^2}{\beta^2} + \eta^2\right)^{\frac{1}{2}}, \tag{7b}$$

where the discrete index i has been replaced by the continuous variable η. Hence, eq. (6) are written as

$$\pi'(\boldsymbol{r}, \omega) = \frac{\exp[ikx/\beta]}{-i\omega\varepsilon\sqrt{2\pi}} \int_{-\infty}^{\infty} I'_\eta(z, \omega) \frac{\exp[i\eta y]}{(k^2/\beta^2 + \eta^2)^{\frac{1}{4}}} \mathrm{d}\eta, \tag{8a}$$

$$\pi''(\boldsymbol{r}, \omega) = \frac{\exp[ikx/\beta]}{-i\omega\mu\sqrt{2\pi}} \int_{-\infty}^{\infty} V''_\eta(z, \omega) \frac{\exp[i\eta y]}{(k^2/\beta^2 + \eta^2)^{\frac{1}{4}}} \mathrm{d}\eta. \tag{8b}$$

Eq. (5) and (6) can also be written in the frequently more convenient form [2,4] for the TM mode fields

$$\begin{cases} \boldsymbol{E}'_t(\boldsymbol{r}, \omega) = \sum_i V'_i(z, \omega) \boldsymbol{e}'_i(\boldsymbol{\rho}), & -i\omega\varepsilon E'_z(\boldsymbol{r}, \omega) = \sum_i I'_i(z) \nabla_t \cdot \boldsymbol{e}'_i(\boldsymbol{\rho}), \\ \boldsymbol{H}'_t(\boldsymbol{r}, \omega) \times \boldsymbol{z}_0 = \sum_i I'_i(z, \omega) \boldsymbol{e}'_i(\boldsymbol{\rho}), & H''_z(\boldsymbol{r}, \omega) = 0, \qquad \boldsymbol{\rho} = (x, y), \end{cases} \tag{9a}$$

while for the TE modes

$$\begin{cases} \boldsymbol{E}''_t(\boldsymbol{r}, \omega) = \sum_i V''_i(z, \omega) \boldsymbol{e}''_i(\boldsymbol{\rho}), & E''_z(\boldsymbol{r}, \omega) = 0, \\ \boldsymbol{H}''_t(\boldsymbol{r}, \omega) \times \boldsymbol{z}_0 = \sum_i I''_i(z, \omega) \boldsymbol{e}''_i(\boldsymbol{\rho}), & -i\omega\mu H''_z(\boldsymbol{r}, \omega) = \sum_i V''_i(z) \nabla_t \cdot \boldsymbol{z}_0 \times \boldsymbol{e}''_i(\boldsymbol{\rho}). \end{cases} \tag{9b}$$

The subscripts t and z denote transverse (to z) and z-vector components, respectively, and the transverse vector mode functions $\boldsymbol{e}_i$ are defined in terms of the scalar mode functions as

$$\boldsymbol{e}'_i(\boldsymbol{\rho}) = -\nabla_t \varphi_\eta(\boldsymbol{\rho})/k'_{t\eta}, \qquad \boldsymbol{e}''_i(\boldsymbol{\rho}) = \boldsymbol{z}_0 \times \nabla_t \psi_\eta(\boldsymbol{\rho})/k''_{t\eta}. \tag{9c}$$

The voltage V_η and current I_η on the i-th mode transmission line are determined via a conventional network calculation. The effect of the line current source in eq. (4) is represented by a point current generator whose strenght i_η is given in

the present instance by ([2,4])

$$(10a) \qquad i_\eta \delta(z-z') = \int_{-\infty}^{\infty} \boldsymbol{J}(\boldsymbol{r}, \omega)\cdot \boldsymbol{e}_\eta^*(x, y)\, dy = q \exp[ikx/\beta]\, \boldsymbol{x}_0 \cdot \boldsymbol{e}_\eta^*(x, 0)\, \delta(z-z'),$$

where the asterisk denotes the complex conjugate, whence via eqs. (9c)

$$(10b) \qquad i'_\eta = \frac{qik/\beta}{\sqrt{2\pi}\sqrt{(k/\beta)^2+\eta^2}}, \qquad i''_\eta = \frac{qi\eta}{\sqrt{2\pi}\sqrt{(k/\beta)^2+\eta^2}}.$$

The network problem for the evaluation of V_η and I_η has the general form shown in Fig. 1, wherein the current generator i_η at z' feeds a transmission line with propagation constant $\varkappa_\eta = (k^2 - k_{t\eta}^2)^{\frac{1}{2}}$ and characteristic impedance Z_η [$Z'_\eta = (\varkappa'_\eta/\omega\varepsilon)$ for TM modes, $Z''_\eta = (\omega\mu/\varkappa''_\eta)$ for TE modes] terminated at z_1 and z_2 in load impedances $Z_\eta(z_1)$ and $Z_\eta(z_2)$, respectively, whose detailed form depends on the nature of the medium stratification along the z-co-ordinate. Since

$$\varkappa_\eta^2 = (k^2 - k_{t\eta}^2) = -k^2[(1/\beta^2) - 1] - \eta^2,$$

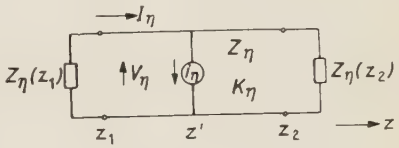

Fig. 1. – Modal network problem.

in vacuum is negative for all η, all the modal transmission lines are non-propagating and the voltage and current amplitudes decay away from the source. In a dielectric medium having a relative dielectric constant $\varepsilon' > 1$, however, $\varkappa_\eta^2 - \varkappa_{\eta\varepsilon}^2 = (k^2\varepsilon' - k_{t\eta}^2)$ may be positive for a certain range of η and hence permit propagation. (Note: when $\varkappa_\eta^2 < 0$, one defines $\varkappa_\eta = i|\varkappa_\eta|$).

While solutions of the network problem in Fig. 1 are available for a variety of specific situations, we mention here only the particularly simple case wherein $Z_\eta(z_1) = Z_\eta$, *i.e.*, the medium in the region $z < z'$ continues undisturbed to $z = -\infty$. In this instance, reflected waves can arise only from the termination at z_2 and one finds for observation points $z < z_2$ (for convenience we choose $z_2 = 0$)

$$(11a) \qquad V_\eta(z, \omega) = -\frac{Z_\eta i_\eta}{2}\left[\exp[i\varkappa_\eta|z-z'|] + \Gamma_\eta(0)\exp[-i\varkappa_\eta(z+z')]\right],$$

$$(11b) \qquad I_\eta(z, \omega) = \frac{-i_\eta}{2}\left[\varepsilon(z, z')\exp[i\varkappa_\eta|z-z'|] - \Gamma_\eta(0)\exp[-i\varkappa_\eta(z+z')]\right],$$

where $\varepsilon(z, z') = \pm 1$, $z \gtrless z'$, and $\Gamma_\eta(0)$ is the reflection coefficient seen looking to the right at $z = 0$:

$$(11c) \qquad \Gamma_\eta(0) = \frac{Z_\eta(0) - Z_\eta}{Z_\eta(0) + Z_\eta}.$$

If the medium continues undisturbed to the right of z', *i.e.*, in free space, one has $\Gamma_\eta = 0$. Substitution of the resulting V_η and I_η into eqs. (9) yields the modal repre-

sentation of Toraldo di Francia. It is to be emphasized that the result has been obtained here from direct substitution into known formulas, without need of intermediate steps involving non-trivial integrations. If a dielectric medium characterized by ε' occupies the half space $z > 0$, one has $Z_\eta(0) = Z_{\eta\varepsilon}$, with $\varkappa_{\eta\varepsilon}$ given as above. For a dielectric slab of thickness d occupying the region $0 < z < d$ and terminated by a perfectly conducting plane at $z = d$, one obtains

$$Z(0) = -iZ_{\eta\varepsilon} \operatorname{tg} \varkappa_{\eta\varepsilon} d\,, \quad \text{etc.}\,.$$

In the presence of a periodic structure, such as a grating, having a spatial period h along the x direction (see Fig. 2*a*), the transverse mode functions no longer have the simple form in eq. (7*a*). Instead of the fixed x dependence characterized by

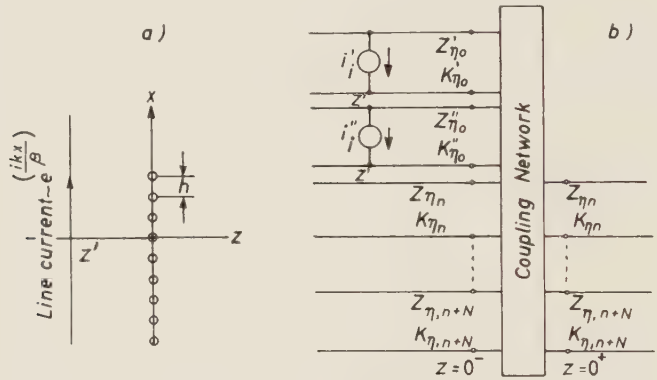

Physical configuration Equivalent network

Fig. 2. – Network problem for the evaluation of V_η and I_η in the presence of a periodic structu.

the wavenumber $k_x = k/\beta$, there now exists in addition the infinite discrete set of grating modes with $k_{xm} = k_x \pm (2m\pi/h)$, $m = 1, 2, \ldots$ In this instance, as pointed out by Toraldo di Francia, it may be possible for large enough h to have $k_{xm} < k$ whence, for a restricted range of η and m, $\varkappa_{\eta m}^2 = k^2 - k_{xm}^2 - \eta^2$ can be positive and the associated mode will propagate. If in the most favorable case, $\eta = 0$, there are N such propagating modes lying in the interval $m = n$ and $m = n + N$, the associated network problem is shown in Fig. 2*b* wherein it has been assumed that the observation point lies far enough from the discontinuity region $z \approx 0$ as to render negligible the effect of non-propagating modes. The coupling between the pertinent modes arising in the discontinuity region is represented schematically by a coupling network, and the structure is excited by the current sources in the non-propagating TE and TM mode transmission lines with $m = 0$. In the potential representations in eqs. (6), one then includes the sum over m between the limits $m = n$ and $m = n + N$.

It might also be remarked that the calculation of the total energy W radiated at a great distance through a unit area perpendicular to the z-axis is likewise simplified by the network procedure. In view of the formula [5]

$$\boldsymbol{W}(\boldsymbol{r}) = \int_{-\infty}^{\infty} \hat{\boldsymbol{P}}(\boldsymbol{r}, t)\, \mathrm{d}t = 4\pi \operatorname{Re} \int_0^{\infty} \boldsymbol{P}(\boldsymbol{r}, \omega)\, \mathrm{d}\omega\,, \tag{12}$$

[5] L. I. SCHIFF: *Quantum Mechanics* (New York, 1949), p. 263.

where $\hat{\boldsymbol{P}}$ and $\boldsymbol{P}$ are, respectively, the real and complex Poynting vectors

$$\hat{\boldsymbol{P}}(\boldsymbol{r}, t) = \hat{\boldsymbol{E}}(\boldsymbol{r}, t) \times \hat{\boldsymbol{H}}(\boldsymbol{r}, t) , \qquad \boldsymbol{P}(\boldsymbol{r}, \omega) = \boldsymbol{E}(\boldsymbol{r}, \omega \times \boldsymbol{H}^*(\boldsymbol{r}, \omega) ,$$

it is unnecessary to evaluate the real time dependent fields for a calculation of W. For $|z| > |z'|$, one recognizes from eq. (11) that one may write

$$(13) \qquad \bar{V}_\eta(z, \omega) = \bar{V}_\eta(\omega) \exp[i\varkappa_\eta |z|] , \qquad I_\eta(z, \omega) = \bar{I}_\eta(\omega) \exp[i\varkappa_\eta |z|] ,$$

so that, from a stationary phase evaluation of eq. (9a) for $|z| \gg |z'|$,

$$(14) \qquad \boldsymbol{E}_t'(\boldsymbol{r}, \omega) = -\frac{i \exp[ik_x x]}{\sqrt{2\pi}} \int_{-\infty}^{\infty} \bar{V}_\eta(\omega) \exp[i\eta y + i\varkappa_\eta |z|] \frac{(\boldsymbol{x}_0 k_x + \boldsymbol{y}_0 \eta)}{\sqrt{k_x^2 + \eta^2}} \, d\eta$$

$$\sim \sqrt{\frac{i\varkappa \cos^3\theta}{|z|}} \frac{\exp\left[i[k_x x + \varkappa y \sin\theta + \varkappa \cos\theta |z|]\right]}{\sqrt{k^2 \sin^2\theta + k_x^2 \cos^2\theta}} \bar{V}_\tau(\omega)(\boldsymbol{x}_0 k_x + \boldsymbol{y}_0 \tau) ,$$

where $\varkappa = (k^2 - k_x^2)^{\frac{1}{2}}$ is assumed real, $\theta = \mathrm{tg}^{-1}(y/|z|)$, and $\eta = \tau = \varkappa \sin\theta$ is the stationary phase point. A similar expression is derived for $\boldsymbol{H}_t'$ and also for $\boldsymbol{E}_t''$, $\boldsymbol{H}_t''$. Hence the calculation of $W(\boldsymbol{r})$, for large values of $|z|$, can be carried out directly in terms of $\bar{V}_\tau(\omega)$ and $\bar{I}_\tau(\omega)$.

A network procedure of the type sketched above, currently being investigated by the authors, can also be employed in the presence of anisotropic media, and also for circular cylindrical configurations (radial transmission line analysis).

* * *

The work reported in this paper was performed in connection with Contract no. AF-19(604)-4143 with the U. S. Air Force Command and Control Development Division.

LIBRI RICEVUTI E RECENSIONI

H. A. Liebhafsky, H. G. Pfeiffer, E. H. Winslow and P. D. Zemany – *X-ray Absorption and Emission in Analytical Chemistry*, x+357 pag., J. Wiley and Sons, New York, 1960. $ 13,50

Gli Autori di questo nuovo libro, tutti appartenenti al gruppo di ricerca del General Electric Laboratory, hanno voluto presentare, in una forma semplice e scorrevole, i metodi e le tecniche più moderne dell'analisi spettrochimica che impiegano i fenomeni di assorbimento e di emissione dei raggi X.

I primi capitoli sono dedicati ad una rassegna abbastanza completa delle proprietà generali dei raggi X, alle tecniche di misura della loro intensità, agli effetti di assorbimento con raggi policromatici e con raggi monocromatici, ed ai metodi più comunemente usati per la determinazione di spessori molto piccoli (films).

La spettrografia a raggi X, argomento che attualmente si va sviluppando molto rapidamente specialmente per i successi ottenuti nell'analisi qualitativa e quantitativa di elementi così importanti come i metalli di transizione e le terre rare, viene ampiamente trattata poichè, come gli Autori vogliono dimostrare, questo mezzo di indagine è ormai divenuto indispensabile all'analisi chimica, qualitativa e quantitativa. Dopo alcuni cenni storici e un'ampia rassegna delle possibilità future di questa tecnica, seguono un capitolo interamente dedicato agli strumenti ed alle apparecchiature più comunemente utilizzate ed un capitolo dedicato alla discussione dei limiti e delle possibilità attualmente offerte dall'analisi spettrografica a raggi X.

L'ultima parte del libro presenta una rassegna di alcuni argomenti speciali connessi con gli effetti di assorbimento e di emissione dei raggi X, come lo studio delle sorgenti puntiformi, il microscopio a raggi X, le sue applicazioni all'analisi dei tessuti animali ed alla biologia in generale, nonchè l'emissione e l'assorbimento dei raggi γ. In Appendice trovano posto numerose tabelle di utile ed immediato inpiego nella pratica.

Il libro, che è particolarmente dedicato al chimico analista desideroso di applicare i più moderni metodi dell'analisi spettrografica a raggi X, può essere apprezzato anche da coloro che sono interessati solo ad alcuni aspetti di questo vasto argomento.

L. Verdini

Proceedings of the 1960 Annual International Conference on High Energy Physics at Rochester; pubblicato dalla Università di Rochester, Rochester, N. Y., distribuito dalla Intersience Publishers, Inc., 1960; pp. xxv-890; prezzo non indicato.

I resoconti della Conferenza di Rochester dello scorso Agosto formano un volume di circa 900 pagine, pubblicato

con ammirevole solerzia dalla Università di Rochester, alla breve distanza di quattro-cinque mesi dalla fine della conferenza. Il volume è stato edito da SUDARSHAN, TINLOT e MELISSINOS, che con l'aiuto di 36 segretari scientifici sotto la direzione di J. S. TOLL sono riusciti abilmente ad includere nel volume i testi delle comunicazioni su invito fatte durante le sessioni simultanee, ed a riprodurre, per quanto possibile fedelmente, le discussioni. Si trovano anche inclusi nei *Proceedings* riassunti delle comunicazioni presentate alle sessioni simultanee. I testi delle relazioni generali presentate dai « rapporteur » e le discussioni relative sono riportate in forma completa. Il volume è stato stampato a Ginevra e distribuito dalla Interscience.

Come è già ormai ogni anno successo per le corrispondenti edizioni dei *Proceedings* di questa Conferenza Internazionale di Fisica di Alta Energia è da prevedere che anche questa volta il volume dei *Proceedings* sarà un importante testo di riferimento per il lavoro in corso e futuro nei varii laboratori di fisica delle particelle elementari. In particolare la pratica impossibilità di disporre di libri di testo aggiornati sino ad includere gli ultimi sviluppi rende questi volumi di *Proceedings* utili anche agli studenti e giovani ricercatori che si trovano ad iniziare il loro lavoro di ricerca.

R. GATTO

G. K. T. CONN, Editor – *Semiconductor Technology*. Butterworths Scientific Publications. London, 1960; pp. v-74; prezzo 10 s. e 6 p.

Questo volumetto raccoglie dodici articoli recentemente apparsi sulla rivista *Research*, dedicati ad alcuni aspetti della tecnologia dei semiconduttori: metodi di preparazione e purificazione dei materiali, proprietà di taluni semiconduttori, produzione di transistors, applicazioni di alcuni tipi di questi.

Gli articoli, dovuti a ricercatori dell'industria inglese, indubbiamente specialisti nel loro campo, si distinguono per la chiarezza e la praticità dell'esposizione e riescono di facile lettura essendo a carattere piuttosto divulgativo. Non tutti riusciranno in egual misura interessanti per ogni lettore, perchè alcuni riguardano la chimica del germanio e del silicio, altri la produzione e il controllo su scala industriale dei prodotti finiti. Tre o quattro articoli sono dedicati alla descrizione delle prestazioni di certi tipi di transistors e alcuni discutono proprietà fisiche fondamentali dei semiconduttori: questi ultimi sono probabilmente quelli a carattere più elementare.

Nell'insieme è chiaro che il volumetto è dedicato essenzialmente a chi lavora alla tecnologia dei transistors, con l'aggiunta di alcuni articoli destinati a illustrare qualche aspetto fisico dell'argomento. Ogni articolo cerca di mettere in rilievo la direzione verso cui gli sforzi futuri saranno presumibilmente orientati, e ciò è quanto mai conveniente in un campo di così rapido e promettente sviluppo.

Naturalmente il complesso dei dodici articoli non va riguardato come un libro in quanto non esaurisce affatto l'argomento e neppure ne tenta un'esposizione sistematica: questo era a priori ovvio e sarebbe stato difficile pretenderlo. Sarebbe forse stato consigliabile invece qualche rimaneggiamento al testo originale degli articoli per togliere ripetizioni e frasi che una volta giunto alla fine il lettore è portato a considerare alla stregua di luoghi comuni: per esempio si poteva premettere una breve introduzione storica all'argomento e sopprimere i cenni di natura storica che iniziano ogni articolo e le frasi che illustrano ogni tanto la rapidità dei progressi acquisiti nel campo dei transistors.

A parte facili appunti, questo volume

appare utile e interessante, sia perchè presenta in modo facile alcuni aspetti della fisica e della tecnologia dei semiconduttori, sia perchè fornisce un'idea generale del livello raggiunto dall'industria inglese in questo difficile campo.

E. GERMAGNOLI

Theoretical Physics in the Twentieth Century. A memorial Volume to Wolfgang Pauli. Edited by M. FIERZ, ZUERICH and V. F. WEISSKOPF, Cambridge, Mass. Interscience Publishers, New York, London, 1960; pp. 328; prezzo non indicato.

The present volume was planned several years ago to celebrate Pauli's 60th birthday on 25th April 1960. According to the editors the principal aim of this collection of articles is twofold: « ... to summarize briefly the progress made in some topics of physics which were closest to Pauli's interests ... » and to report in the « heroic period of physics during the 1930's ».

There is a foreword by Niels Bohr followed by twelve monographs by R. Kronig, W. Heisenberg, G. Wentzel, F. Villars, R. Jost, H. B. G. Casimir R. E. Peierls, M. Fierz, V. Bargmann, B. L. van der Waerden, L. D. Landau and Miss C. S. Wu. The book also contains a bibliography of Pauli's published works compiled by C. P. Enz.

The first monograph *The Turning Point* by R. Kronig is a masterly account of the development of the ideas of quantum physics during the middle twenties, a period which — in contrast to the editors — one would be inclined to term heroic. A quotation from a letter written by Heisenberg in June 1925 offers a particularly revealing insight in the genesis of modern quantum theory. Kronig's article together with the first part of van der Waerden's close what appears to the reviewer a painful gap in the existing literature, which tends to represent quantum mechanics as a deductive science depriving the student of the enjoyment of the beauty and boldness of its actual development.

Field theory is treated in 4 articles: a historical account by G. Wentzel leading up to the renormalization movement, a discussion of renormalization methods by F. Villars, R. Jost's article illustrating the interrelation between relativistic invariance and commutation relations and a brief outline of « fundamental problems » by L. D. Landau.

Pauli's interest in statistical mechanics is reflected in a paper by Fierz, which contains an outstandingly clear and brief outline of the development of the ergodic problem, the understanding of which was greatly advanced by recent work of van Hove in which an improved derivation of Pauli's so called « master equation » was given.

A short article by Casimir gives the background of Pauli's contribution to the theory of metals and Peierls' paper illustrates the consequences of Pauli's paper on the paramagnetism of an electron gas and continues with a discussion of the fundamental problem of solid state physics: the heat conduction of a perfect crystal.

Bargmann deals with Pauli's work on the special and general theory of relativity.

The neutrino and recent developments in the theory of β-decay are discussed in an article by Miss Wu.

This book most strikingly illustrates Pauli's outstanding and fundamental share in the development of modern physics. Nearly every turn in its path is marked by a paper by Pauli, who in the period of 40 years represents the element of continuity: the conscience of theoretical physics in the words of Niels Bohr.

The editors must be thanked for

their work in the selection of the contributions and for their decision to give this collection a time-like dimension by laying the stress on the development rather than on the state of our ideas in theoretical physics. The title of the book may sound pretentious, but it expresses what many of us then felt: that theoretical physics had come to an end on the 15th Dicember 1959.

B. Touschek

J. R. Reitz and F. J. Milford – *Foundation of Electromagnetic Theory*. Addison-Wesley Publ. Co. Inc., Reading, Mass., U.S.A., London, England, 1960; pp. xi-387; $ 8.75.

Non si può dire che manchino oggi libri di testo sui fondamenti dell'elettricità e del magnetismo per corsi universitari a carattere introduttivo, in particolare nella letteratura americana. ma il fatto stesso che se ne continuino a pubblicare e che ciascuno di essi avanzi qualche pretesa di originalità nell'impostazione, fa pensare che questo campo non sia ancora da considerare del tutto sistemato dal punto di vista didattico. Ciò si comprende, del resto, se si considera che la decisione relativamente recente di adottare il sistema Giorgi razionalizzato, in luogo dei molteplici ed ibridi sistemi in uso, ha fatto sorgere dei problemi didattici e concettuali ben più delicati di quanto non si sarebbe forse previsto per un semplice cambiamento di unità di misura.

Il volume che abbiamo sotto gli occhi si rivolge ad « advanced undergraduate students in science », per i quali è presupposta una conoscenza qualitativa della fisica atomica, ed una preparazione matematica che si può ritenere corrispondente a quella del nostro primo biennio. Il cap. I richiama, del resto, in forma accessibile anche a chi non ne avesse precedente nozione, le principali operazioni dell'algebra e dell'analisi vettoriale.

Il cap. II, sull'elettrostatica, contiene, oltre alle relazioni usuali, uno sviluppo del potenziale di una distribuzione generica di cariche in termini di multipoli. Il cap. III tratta principalmente delle soluzioni dell'equazione di Laplace con diversi sistemi di coordinate e diverse condizioni al contorno: fornendo degli esempi di applicazione dei metodi della fisica matematica classica. Una trattazione relativamente ampia del campo elettrostatico nei mezzi dielettrici, e dei problemi connessi, nei cap. IV, V e VI, trattazione basata sulle conoscenze attuali della costituzione dei dielettrici, prepara il terreno al successivo studio delle proprietà magnetiche della materia.

Il vettore induzione magnetica $\boldsymbol{B}$ viene definito nel cap. VIII per mezzo dell'espressione della forza di Lorentz su una carica in moto. Da essa si risale, attraverso al teorema della circuitazione di Ampère, alla definizione di potenziale vettore. Dopo il cap. IX, sull'induzione elettromagnetica, seguono tre capitoli sulle proprietà magnetiche della materia, e problemi connessi. Il resto del volume tratta delle correnti variabili, equazioni di Maxwell ed applicazioni alla propagazione delle onde, per concludere con una breve introduzione allo studio dell'irraggiamento da una carica in moto accelerato. Un capitolo è pure inserito, che tratta, in modo necessariamente sommario, la fisica dei plasmi.

L'impostazione è nettamente matematica, senza riferimento diretto ad esperienze o dispositivi di misura. È fatto uso sistematico degli operatori e dei metodi dell'analisi vettoriale, in particolare per la dimostrazione dei teoremi. Le deduzioni sono per lo più complete e rigorose a partire dai principi fondamentali. La trattazione vettoriale consente tuttavia una notevole concisione

senza scapito della chiarezza. Solo qua e là la preoccupazione della brevità ha indotto gli AA. a contentarsi di affermazioni dogmatiche, o di cenni eccessivamente sommari: per es. nella trattazione del campo molecolare in un dielettrico, e più ancora in quella della conduzione metallica. Altri argomenti sono del tutto omessi: per es. i semiconduttori sono appena nominati, insieme con gli elettroliti.

In questo, come del resto anche in altri testi, la costante dielettrica del vuoto ε_0 viene introdotta nel paragrafo sulla legge di Coulomb, attraverso il valore numerico approssimato

$$8{,}854 \cdot 10^{-12} \text{ coul}^2/\text{n} \cdot \text{m}^2,$$

senza indicare che ciò corrisponde a $10^7/4\pi c^2 = 1/\mu_0 c^2$. La relazione di ε_0 con la velocità della luce c non appare chiara neppure nell'appendice I, che pure si propone esplicitamente la « definizione logica delle unità del sistema MKS ». Essa è citata soltanto nel paragrafo sulla propagazione delle onde. Sembra allo scrivente che il prezzo che si paga nel sistema Giorgi con la introduzione delle costanti ε_0 e μ_0 sia giustificato soltanto quando si faccia apparire chiaramente il significato fisico di esse, come costanti che insieme condizionano la propagazione delle perturbazioni elettromagnetiche attraverso lo spazio vuoto.

Ma, del resto, la caratteristica di questo libro è proprio quella di mirare ad una esposizione concisa e rigorosa, soddisfacente dal punto di vista logico, più che a mettere in chiaro l'aspetto fisico delle questioni. Come già abbiamo detto, esso realizza bene, in massima, questo scopo. Una buona scelta di problemi, alla fine di ogni capitolo, aiuta ad approfondire gli argomenti trattati nel testo.

A. Rostagni

Direttore responsabile: G. POLVANI Tipografia Compositori - Bologna

Questo Fascicolo è stato licenziato dai torchi il 7-III-1961